# Leveraging Structural Constraint for Lewis Superacidity and Element-Ligand-Cooperativity of p-Block Elements

———————————

# Dissertation

to obtain the academic degree
Doctor rerum naturalium (Dr. rer. nat.)

submitted to the Faculty of Mathematics,
Engineering Sciences and Natural Sciences
of Heidelberg University
by
Daniel Roth, M. Sc.
b. in Munich, Germany

Date of Defense: 18.12.2023

1st Reviewer: Prof. Dr. Lutz Greb
2nd Reviewer: PD Dr. Joachim Ballmann

# List of Publications:

I.   **D. Roth**, H. Wadepohl, L. Greb. Bis(perchlorocatecholato)germane: Hard and Soft Lewis Superacid with Unlimited Water Stability.
 *Angew. Chem. Int. Ed.* **2020**, *59*, 20930-20934.

II.   T. Thorwart, **D. Roth**, L. Greb. Bis(pertrifluoromethylcatecholato)silane: Extreme Lewis Acidity Broadens the Catalytic Portfolio of Silicon.
*Chem. Eur. J.* **2021**, *27*, 10422-10427.

III.   **D. Roth**, J. Stirn, D. W. Stephan, L. Greb. Lewis Superacidic Catecholato Phosphonium Ions: Phosphorus–Ligand Cooperative C–H Bond Activation.
*J. Am. Chem. Soc.* **2021**, *143*, 38, 15845-15851.

IV.   M. Schorpp, R. Yadav, **D. Roth**, L. Greb. Calix[4]pyrrolato Stibenium: Lewis Superacidity by Antimony(III)-Antimony(V) Electromerism.
*Angew. Chem. Int. Ed*. **2022**, *61*, e2022079.

V.   **D. Roth**, T. Thorwart, C. Douglas, L. Greb. Bis(amidophenolato)-phosphonium: Si-H Hydride Abstraction and Phosphorous-Ligand Cooperative Activation of C-C Multiple Bonds.
*Chem. Eur. J.* **2023**, *29*, e202203024.

VI.   **D. Roth**, A. T. Radosevich, L. Greb. Reversible Oxidative Addition of Non-Activated C-H bonds to Structurally Constrained Phosphenium Ions.
*J. Am. Chem. Soc.* **2023**, *145*, 44, 24184-241890.

VII.   **D. Roth**, L. Greb. Structural Variability and E-H bond activation of (Catecholato)(*N*-pyridylamidophenolato)phosphonium Ions.
Manuscript in preparation.

It's very nice to be right sometimes.

<div align="right">Peter Higgs</div>

# Abstract

The study of main-group species for catalysis has emerged in recent years as an active field of study, promising a sustainable alternative to the precious transition metals, whose use comes attached with concerns of toxicity, abundance and costs. Through strategic choice of substituents, typically inactive p-block elements may be activated for challenging bond activations.

Rigid, bidentate catecholate and amidophenolate scaffolds were identified as suitable ligands for this purpose, and their impact on germanium and phosphorus compounds studied in this work. In the first part, perhalogenated bis(catecholato)germanes were prepared, characterized and shown by theory and experiment to be the first neutral germanium Lewis superacids, entirely stable in water. Additionally, they are active catalysts for a wide variety of reactions.

At phosphorus, catecholates propelled the element typically used as Lewis base to new heights of Lewis acidity. Theoretical and experimental scaling methods ranked the newly prepared catecholato-phosphonium ions among the strongest, isolable Lewis acids. The high Lewis acidity was achieved even without requiring perhalogenation or multiple charges, and energy decomposition analysis assigned structural constraint as the key contributing factor. Aside from being highly active Lewis acid catalysts, the juxtaposition of electrophilic phosphorus and nucleophilic oxygen facilitated phosphorus-ligand cooperative bond activations. This way, inert $C(sp^2)$-H, as well as Si-H bonds were cleaved, and cooperative addition of alkynes and alkenes was observed.

Further control over the electronic and steric profiles of the spirophosphonium ions was asserted with amidophenolate substituents, which allowed isolation of the strongest, monocationic phosphonium ion yet, as well as ligand-cooperative activation of alkynes and alkenes following a different mechanism. Combination of both substituents gave phosphonium ions with Lewis acidity dependent structures, which could activate CH bonds by a frustrated Lewis pair-type mechanism.

Lastly, a series of structurally constrained phosphenium ions based on pyridylmethylamidophenolate ligands was prepared and characterized. Tuning the substituents of the ligand periphery enabled reversible oxidative addition of even unactivated arenes such as benzene, which was unprecedented reactivity for main-group compounds. The mechanism of the reaction was elucidated by computations and a cooperative C-H deprotonation identified as key step.

# Kurzzusammenfassung

Die Untersuchung von Hauptgruppenverbindung für die Katalyse hat sich in den letzten Jahren zu einem aktiven Forschungsgebiet entwickelt mit dem Versprechen eine nachhaltige Alternative zu den kostbaren Übergangsmetallen zu bieten, deren Verwendung mit Bedenken hinsichtlich Toxizität, Häufigkeit und Kosten verbunden ist. Durch die strategische Wahl von Substituenten können typischerweise inaktive p-Block-Elemente für anspruchsvolle Bindungsaktivierungen aktiviert werden.

Starre, bidentate Catecholat- und Amidophenolate wurden als geeignete Liganden für diesen Zweck identifiziert, und ihre Auswirkungen auf Germanium- und Phosphorverbindungen in dieser Arbeit untersucht. Im ersten Teil wurden perhalogenierte Bis(catecholato)germane hergestellt, und durch Rechnungen und Experimente als erste, neutrale Germanium-Lewis-Supersäuren charakterisiert, die wasserstabil sind. Außerdem wurde hohe katalytische Aktivität für eine Vielzahl von Reaktionen festgestellt.

Anbringung der Catecholate am Phosphor verleihen dem typischerweise als Lewis-Base verwendeten Element hohe Lewis-Acidität. Theoretische und experimentelle Skalierungsmethoden stuften die neu hergestellten Catecholato-Phosphonium-Ionen als Einige der stärksten, isolierbaren Lewis-Säuren ein. Die hohe Lewis-Acidität wurde auch ohne Perhalogenierung oder höhere Ladungszustände erreicht, und theoretische Untersuchen identifizierten strukturelle Einschränkungen als den entscheidenden Faktor ein. Abgesehen davon, dass es sich hierbei auch um hochaktive Lewis-Säure-Katalysatoren handelte, ermöglichte die Nähe von elektrophilem Phosphor und nukleophilem Sauerstoff die Bindungsaktivierung durch Phosphor-Ligand-Kooperativität. Auf diese Weise wurden sowohl inerte $C(sp^2)$-H-, als auch Si-H-Bindungen gespalten und eine kooperative Addition von Alkinen und Alkenen beobachtet.

Verbesserte Kontrolle über das elektronische und sterische Profil der Spirophosphonium-Ionen wurde über Amidophenolat-Substituenten erreicht, die die Isolierung des bisher stärksten monokationischen Phosphonium-Ions, sowie die ligand-kooperative Aktivierung von Alkinen und Alkenen über einen anderen Mechanismus ermöglichten. Die Kombination beider Substituentenklassen ergab Phosphonium-Ionen mit Lewis-Acidität-abhängigen Strukturen, die CH-Bindungen als intramolekulare frustrierte Lewis-Paare aktivieren konnten.

Schließlich wurde eine Reihe strukturell eingeschränkter Phosphenium-Ionen auf Basis von Pyridylmethylamidophenolat-Liganden hergestellt und charakterisiert. Veränderungen der Ligandenperipherie ermöglichten präzise Kontrolle über die reversible oxidative Addition sogar von nicht-aktivierten Arenen wie Benzol, was für Verbindungen der Hauptgruppe eine bisher unerreichte Reaktivität darstellte. Der Mechanismus der Reaktion wurde durch quantenmechanische Rechnungen aufgeklärt und eine kooperative C-H-Deprotonierung als Schlüsselschritt identifiziert.

# Table of Contents

# Chapter 1

# General Introduction

Catalysis is a vital tool for the production and synthesis of desirable materials and chemicals. Late transition metals of the second and third row have been established as key actors in these transformations, but their use often comes attached with concerns regarding abundance, costs, toxicity, and the ecological footprint for obtaining these metals. Efforts to circumvent these issues have been made by application of the more abundant first-row transition metals and the development of organocatalysis.[1] Given their abundance and accessibility, the use of main group species has also garnered increasing interest in the past decades.[2] However, in contrast to transition metal-based compounds, p-block elements in their normal valence states usually remain inactive in bond activation reactions.[3] The right choice of substituents may achieve the necessary enhancement of the reactivity of these elements, which is the central topic of this doctoral thesis.

## 1.1    Main-Group Elements as Transition Metals

A key factor to the efficacy of transition metals in bond activation reactions and catalysis is the presence of closely located and partially occupied d-orbitals, enabling kinetically and thermodynamically favorable switching between multiple stable oxidation states. Closed-shell main group elements in their native oxidation states generally have large frontier orbital gaps leading to canonical behavior as simple nucleo- or electrophiles. Several strategies to unlock increased reactivity centered at the main-group elements have emerged in the past decades, based on mimicking the electronic situation of transition metals by generating energetically close donor/acceptor frontier orbitals (i.e. small HOMO-LUMO gaps) in spacial

proximity (fig. 1-1). The electronic structure for example can be emulated by main-group elements in reactive, low-valent oxidation states or by structural constraint of the ligand framework (see chapter 1.4).[4] Using combinations of bulky Lewis acids and bases to prevent simple Lewis pair formation leads to frustrated Lewis pairs (FLPs) which possess 'unquenched' reactivity suitable for small molecule activation and have been used extensively in metal-free catalysis.[5]
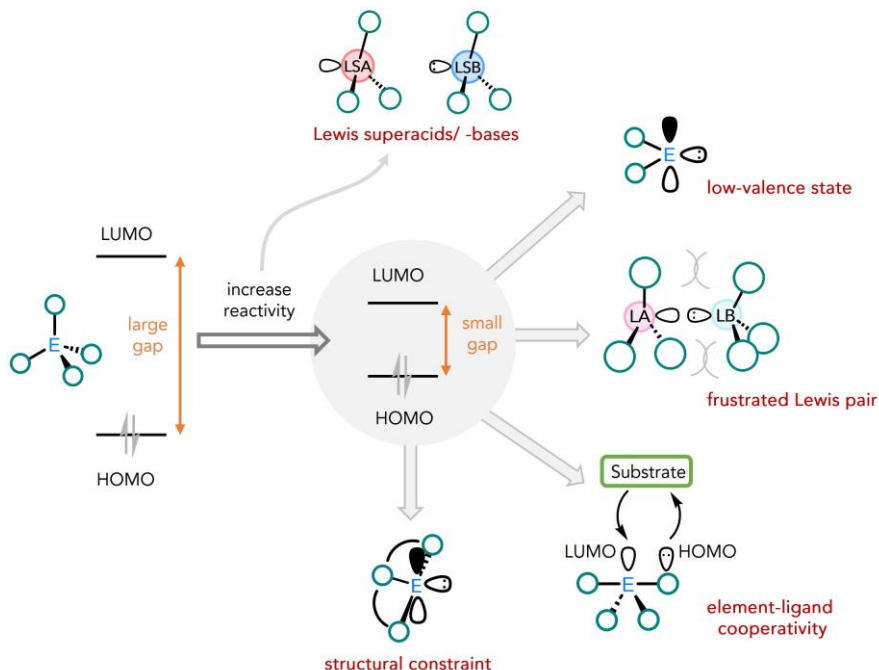


**Figure 1-1**: Strategies for increasing the reactivity of main-group elements towards small molecule activation and catalysis.

Finally, increased reactivity of main group compounds may also be achieved simply by elevating the fundamental nucleo- or electrophilicity to create Lewis superacids (LSA) or -bases (LSB) (see section 1.2.2 for LSA).[6]

## 1.2    Lewis Acids and Bases

Lewis acids (LA) and bases (LB) are ubiquitous and vital tools in all areas of chemistry.[7] The theory of Lewis acids and bases is a fundamental concept in

chemistry that guides our understanding of a wider range of reactions. Developed in 1923 by American Chemist Gilbert N. Lewis, a Lewis acid is defined as an electron-pair acceptor, while their counterparts, the Lewis bases, are considered electron-pair donors.[8] It is a generalization of the Brønsted acid-base theory, where Brønsted acids and bases are ascribed the ability to donate or accept protons, respectively.

### 1.2.1 Quantification of Lewis Acidity

The strength of a Brønsted acid is well defined through the $pK_a$ scale, quantifying its propensity to lose a proton, and can be easily determined through various methods in (aqueous) solution. On the other hand, the strength of a Lewis acid always depends on the Lewis base it interacts with, precluding the establishment of a generally valid, one-dimensional scale for Lewis acidity. The strength of the interaction can be predicted qualitatively using Pearsons' principle of hard and soft Lewis acids and bases (HSAB).[9] It categorizes Lewis acids and bases as hard, if high charge density and low polarizability are given or soft for Lewis acids and bases of low charge density and high polarizability. Lewis pairs of similar character are then predicted to interact more strongly. These interactions are based more on electrostatic interactions for hard Lewis pairs and covalent interactions for soft Lewis acids and bases, but exist on a continuum. The simple concept was later extended to the semi-quantitative ECW-scheme by Drago, introducing parameters for electrostatic ($E$) and covalent ($C$) contributions to the adduct strength for each Lewis acid and base.[10] These parameters have been derived empirically from experimental enthalpies. Together with a constant $W$ to factor in steric repulsion, it was formulated to give the reaction enthalpy ($\Delta H$) as:

$$-\Delta H = E_{LA}E_{LB} + C_{LA}C_{LB} + W$$

As the strength of a Lewis acid is an important predictor in determining its reactivity and application scope, a multitude of scaling methods have been developed. Depending on the specific quantity that is probed, the methods can generally be divided into three categories (fig. 1-2).[6a]

*Global* Lewis acidity (gLA) scales consider the overall thermodynamics of adduct formation (i.e. $\Delta G/\Delta H$), thereby being compliant with the IUPAC definition of Lewis

3

acidity.[11] The most prominent examples are the fluoride (FIA) or hydride ion affinity (HIA) scales (fig. 1-2A). As the experimental determination of these values is non-trivial, they are typically derived from computational methods.[6a, 12] Ion affinities are also often indirectly computed *via* isodesmic reactions, as the modelling of the electron affinity of a naked fluoride ion is difficult. The values are anchored for instance to the experimentally determined FIA of $COF_2$ or to the ion affinities of $Me_3Si^+$ calculated at a high level of theory.[13]

*Effective* Lewis acidity (eLA) scales assess the physicochemical changes to the Lewis base as it coordinates to the Lewis acid. Examples are the Gutmann-Beckett (GB) or the Childs method, where the changes to the $^{31}P$ or $^{1}H$ NMR signals of triethylphosphine oxide or the $H^3$ proton of crotonaldehyde are measured after adduct formation (fig. 1-1B).[14] Other scales based on changes to IR, UV-VIS or fluorescence responses of other Lewis basic probe molecules have also been reported.[15]

*Intrinsic* Lewis acidity (iLA) relates to properties of the free Lewis acid, such as the LUMO energy (E(LUMO)), the global electrophilicity index (GEI), the electron affinity (EA), or the NMR chemical shift of heteronuclei (especially for silylium ions).[16] These values can be obtained computationally at minimal cost, but do not account for
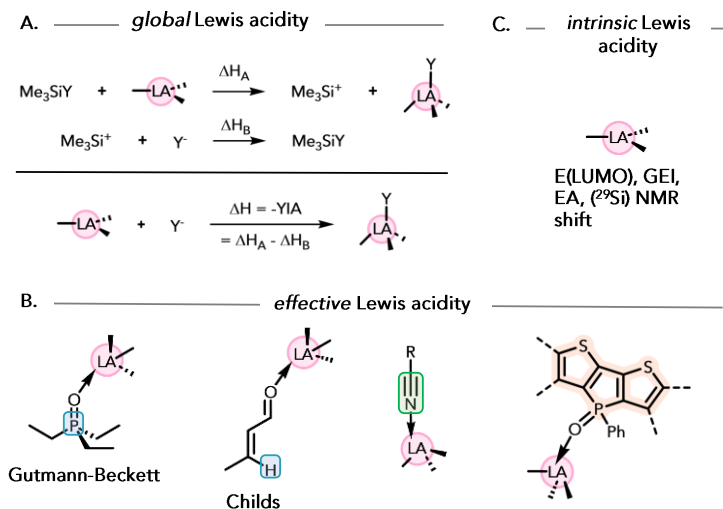


**Figure 1-2:** Schematic depiction of methods to determine **A.** global, **B.** effective and **C.** intrinsic Lewis acidity.

4

interactions arising from Lewis base coordination (i.e. deformation energy, steric repulsion).

## 1.2.2    Lewis Superacids

Lewis acids surpassing a certain threshold of Lewis acidity had been sporadically awarded the term Lewis superacids (LSA) in different contexts throughout the literature. A clear definition was given to the term in 2008, when Krossing defined Lewis superacids as molecular Lewis acids with a fluoride ion affinity higher than that of monomeric $SbF_5$ in the gas phase.[6b] Quite a few Lewis superacids have since then been reported, with better handleability and substantially higher Lewis acidities than the toxic and corrosive $SbF_5$ (selected examples are shown in fig. 1-3).[6a]
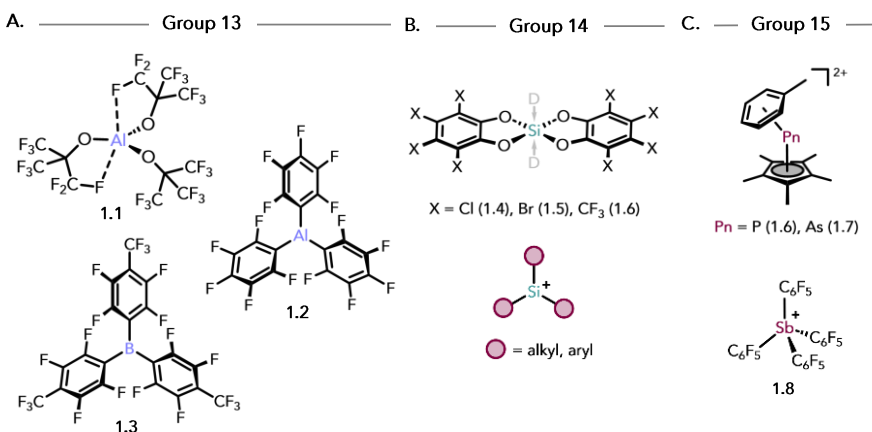


**Figure 1-3:** Selected examples of Lewis superacids of **A.** group 13, **B.** group 14, **C.** group 15. D = acetonitrile, sulfolane or other donor molecules.

To better account for strong Lewis acids with a softer character, the complementary definition of soft Lewis superacid (sLSA) was added in 2018 by Greb for Lewis acids with a higher hydride ion affinity than $B(C_6F_5)_3$. Most of the LSA contain naturally electron-deficient elements of group 13 such as aluminum and boron, where the Lewis acidity is derived from the presence of low-lying, vacant p-orbitals (fig. 1-3A). Further enhancements to the Lewis acidity are achieved through strongly electron-withdrawing substituents or addition of positive charges. Cationic silylium ions have long been considered to be among the strongest known Lewis acids in the

condensed phase and a truly free triorgano-substituted silylium ion could only be isolated by installing substantial steric bulk around the electrophilic silicon center (fig. 1-3B).[17] The first neutral group 14 Lewis superacids 1.4 – 1.6 were reported by Greb, relying on a combination of structural constraint and electron-withdrawing capabilities imparted by persubstituted catecholate ligands (fig. 1.3B).[18] However, the bis(catecholato)silanes were not stable against oligomerization without stabilization by a donor and engaged in low-barrier Si-O metathesis resulting in di-, oligo- or polymeric structures.[19] Lewis superacids based on group 15 elements all rely on positive charges to surpass the threshold, and neutral group 15 Lewis superacids have not been reported. Representative examples disclosed as Lewis superacids of group 15 are the tetrakis(pentafluorophenyl)stibenium ion 1.8 by Gabbai and co-workers or the pentacyclopentadienylphosphenium and -arsenium dications 1.6 and 1.7 by Stephan and co-workers, all cations are stabilized by weakly coordinating $[B(C_6F_5)_4]^-$ counterions (fig. 1-3C).[20]

### 1.2.3 Phosphorus Lewis Acids

Phosphorus compounds play an important role in homogenous organometallic chemistry and catalysis. They are typically employed as Lewis basic ligands and electron donors to stabilize transition metal fragments and enhance their reactivity. Although the electrophilic character of phosphorus had sporadically been exploited in the literature, most prominently with phosphorus ylides in the Wittig reaction, specific use of phosphorus in the design of Lewis acids has only recently come more into focus.[21]

#### 1.2.3.1 Phosphenium Ions

Phosphorus(III) compounds possess an accessible lone pair of electrons, generally making them Lewis bases. By introducing a cationic charge, examples of P(III) Lewis acids emerged in the form of phosphenium ion after their initial discovery in 1964.[22] Their interesting reactivity was demonstrated in an early example by Cowley, showing the insertion of the diamidophosphenium ion [($^i$Pr$_2$N)$_2$P][AlCl$_4$] (1.9) into the activated C(sp$^2$)-H bonds of stannocene and plumbocene (fig. 1-4A).[23] N-heterocyclic phosphenium ions (NHPs), the isoelectronic counterparts of widely used N-heterocyclic carbenes (NHCs), are a particularly well-studied class of phosphenium ions.[24] Formation of adducts with Lewis bases such as

trimethylphosphine or 4-*N,N*-dimethylaminopyridine (DMAP) was demonstrated as typical Lewis acid behavior (fig. 1-4B).[25] Electrophilic P(III) compounds could also be prepared by capitalizing on structurally constraining ligands (see chapter 1.4). Stephan and co-workers managed to achieve Lewis superacidity at P(III) by preparation of the pentamethylcyclopentadienyl phosphorus dication 1.6.[20b] Experimental fluoride abstraction from $SbF_6^-$, furnishing the product 1.14 after $\eta^5 - \eta^2$ ring slippage consolidated the Lewis superacidic nature. Furthermore, the dication also reacted with triethylsilylchloride and triethylsilane under chloride and hydride abstraction to afford the products 1.12 and 1.13. (fig. 1-3C). Lewis superacidity was also demonstrated for the higher homologue $\eta^5$-Cp*As(toluene)$^{2+}$ 1.7.[20c]
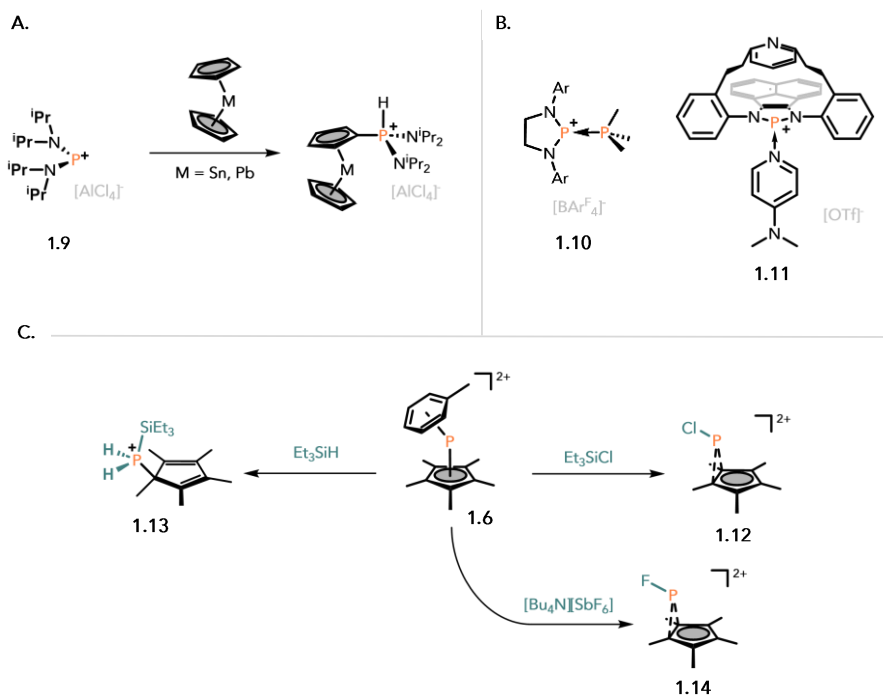


Figure 1-4: A. Insertion of a phosphenium Ion into C-H bonds, B. Lewis aducts of NHPs and C. Reactions of $\eta^5$-Cp*P(toluene)$^{2+}$ (counterion B(C$_6$F$_5$)$_4^-$ omitted for clarity).

## 1.2.3.2 Electrophilic Phosphonium Ions

P(V) compounds are naturally more Lewis acidic than P(III) compounds, and plenty of examples of both neutral phosphorane and cationic phosphonium Lewis acids exist in the literature. Simple $PF_5$ is already a Lewis acid of moderate strength that undergoes adduct formation with Lewis bases.[26] The Lewis acidity at P(V) is generally derived from the presence of a low-lying σ*-orbital opposite the electron-withdrawing group that functions as a Lewis pair acceptor. A 2006 study by Terada and Kouchi showed that alkoxyphosphonium ion based Lewis acids catalyze the Diels-Alder reaction of α,β-unsaturated amides with cyclopentadiene (fig. 1-5).[27] More specifically, only the catechol-bearing cations were active catalysts, while related biphenol-derived derivatives were not, illustrating the crucial effect of structural constraint by the smaller bite-angle catecholates. At the same time, oxygen-base substituents were much more effective than their structurally related carbon counterparts of similar bite-angles.



| Yield: | 41 - 91 % | 7 -34 % | no reaction |
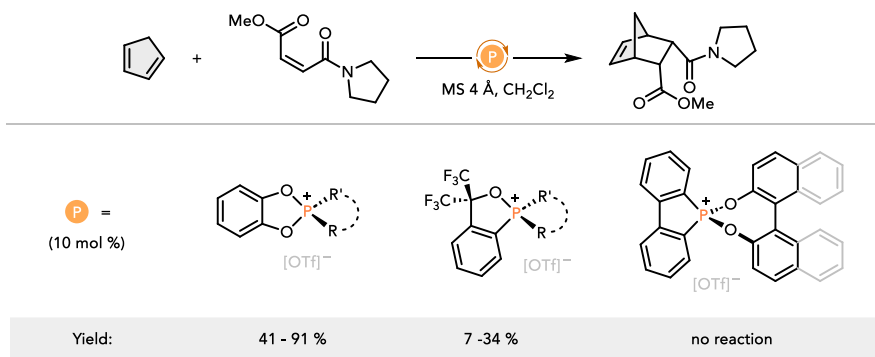
**Figure 1-5:** Comparison of different alkoxyphosphonium ions in the catalysis of a Diels-Alder reaction. R, R' = alkyl, aryl substituents, in some cases tethered together.

A highly electrophilic phosphonium ion was only introduced in 2013 with the fluorophosphonium salt $[FP(C_6F_5)_3][B(C_6F_5)_4]$ (1.15) in a seminal report by Stephan and co-workers (fig. 1-6A).[28] Fluorophilicity higher than the strong Lewis acid $B(C_6F_5)_3$ was already indicated by its failure in the attempted fluoride abstraction from the difluorophosphorane precursor $F_2FP(C_6F_5)_3$. A large Gutmann-Beckett shift ($\Delta^{31}P$ = 40.4 ppm versus free $OPEt_3$) and fluoride ion abstraction from $Ph_3CF$ corroborated the unprecedented Lewis acidity at phosphorus. For 1.15, the exceptionally low-lying σ*-orbital responsible for its acceptor properties lies

opposite the P-F bond and is accessible even to weak Lewis bases (fig. 1-6A).

In the presence of a hydrosilane, the phosphonium ion catalyzed the hydrodefluorination of a broad scope of fluoroalkanes (fig. 1-6B). The initial discovery was followed up with numerous reports of (fluoro)phosphonium ions all prepared by a general procedure. Oxidation of a phosphine with $XeF_2$ and subsequent fluoride abstraction with a suitable reagent such as $[Et_3Si][B(C_6F_5)_4]$ generated the target phosphonium salt (fig. 1-6A).[29] These cations proved to be effective catalysts for a broad spectrum of Lewis acid-catalyzed reactions, such as hydrosilylations, deoxygenations or dehydrocouplings (fig. 1-6B).[30]
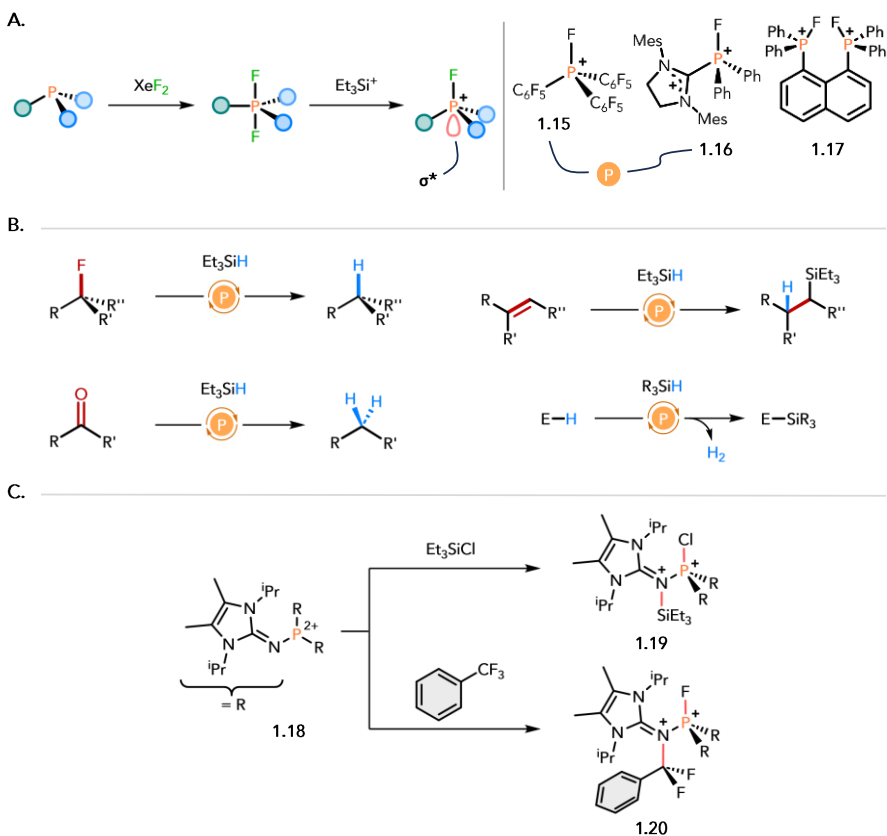


Figure 1-6: A. Examples of electrophilic fluorophosphonium cations and their general synthesis. B. Examples of reactions catalyzed by 1.15 and 1.16. C. Dielmanns' dication 1.18 and cooperative bond activations thereof. ($B(C_6F_5)_4^-$ counterions were omitted for clarity in all structures)

An alternate path to achieve high Lewis acidities aside from highly electron-withdrawing substituents was established by introducing multiple charges with synthesis of dications such as 1.16 and 1.17 (fig. 1-6A). 1.16 readily abstracts a fluoride from 1.15-F, thereby proving its superior fluorophilicity. The tricoordinate phosphorus dication 1.18 isoelectronic to silylium ions and boranes was reported by Dielmann and shown to activate inert σ-bonds.[31] With the presence of a nucleophilic nitrogen next to phosphorus, it did not react by simple abstraction but instead added Et₃SiCl and trifluorotoluene in cooperative fashion along the P-N bond after cleavage of the Si-Cl and C-F bonds (fig. 1-6C).

## 1.3    Element-Ligand Cooperation

Element-ligand cooperative bond activation has emerged in recent years as one of several powerful strategies to elevate the reactivity of main-group compounds (see chapter 1.1). It capitalizes on the direct involvement of ligands with suitable frontier orbitals in crucial bond activation steps and catalysis. The concept of ligand-cooperativity was originally established in transition-metal chemistry (termed metal-ligand cooperation, MLC), but had already long before been exploited in nature by enzymes to facilitate challenging reactions under mild conditions.[32] Seminal findings by Milstein and co-workers first demonstrated the utility of MLC in acceptorless dehydrogenation reactions with the ligand directly involved in bond cleavage, departing from its typical ancillary role as mere 'spectator'.[33] The catalytic turnover was achieved by re- and dearomatization cycles of the pyridine-based pincer ligand, liberating dihydrogen as sole byproduct (fig. 1-7).
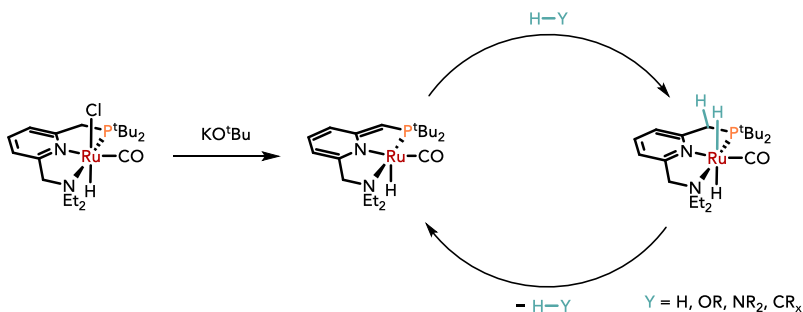


**Figure 1-7:** Metal-ligand cooperative bond activation by Milstein's ruthenium pincer complex.

It was later found that using slightly modified ligands, catalytic hydrogenations of alkynes, alkenes and aldimines were also possible with magnesium sitting at the ligand center instead of a transition metal.[34] The synergistic bond activation by p-block elements and suitable ligands, while still relatively underexplored, has also been achieved with other ligand systems and was more broadly coined element-ligand cooperation (ELC).[35]

Fedushkin and Abakumov found that the bis(imino)acenaphthalene (BIAN) ligated aluminum complex 1.24 underwent aluminum-ligand cooperative cycloaddition of diphenylacetylene at elevated temperatures to give 1.25, as well as cooperative N-H bond scission to give product 1.26 at room temperature (fig. 1-8A).[36]
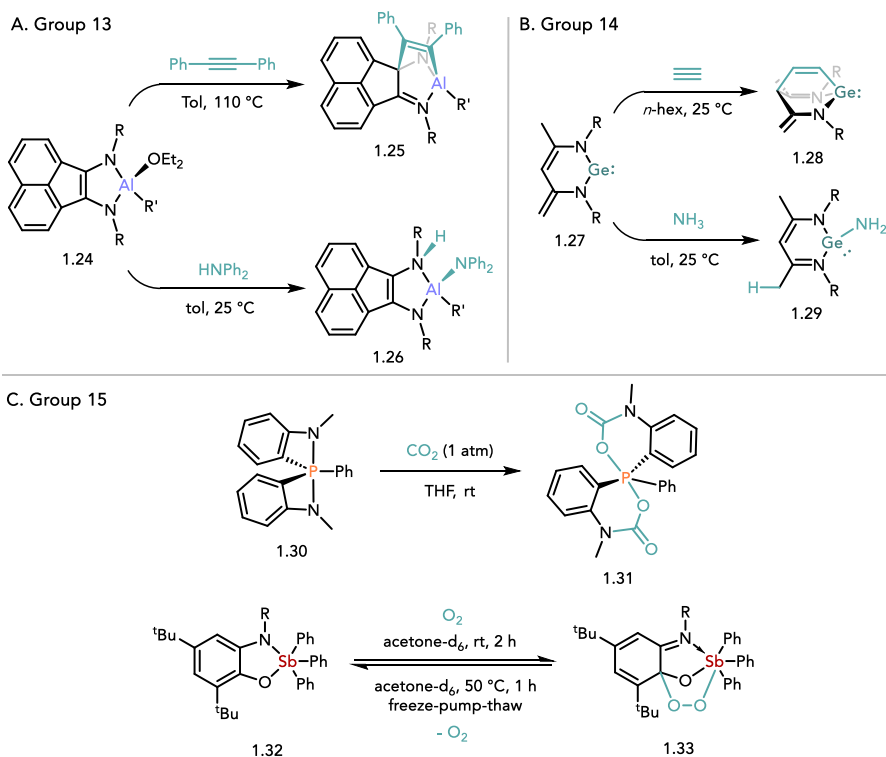


**Figure 1-8:** Examples of ELC bond activation by elements of groups 13, 14 and 15 (R = 2,6-diisopropyphenyl).

A prominent example of group 14 ELC reactivity was demonstrated with Driess' *N*-heterocyclic divalent germylene 1.27 embedded in a β-diketiminato ligand that is deprotonated in the backbone (fig. 1-8B). Upon treatment with ethyne, it underwent [4+2] cycloaddition to give the bicyclic product 1.28.[37] If phenylacetylene was employed instead, small amounts of C(sp)-H addition products were also observed. In similar fashion, the N-H bond of ammonia was cleaved at room temperature to afford the germanium amide 1.29 with a protonated ligand backbone.[38]

By capitalizing on the strain in the bicyclic amidophosphorane 1.30, the ligand-assisted capture of carbon dioxide was successfully shown by Stephan and co-workers (fig. 1-8C).[39] The addition of two units of $CO_2$ across the P-N bonds proceeded under mild conditions as the ring expansion alleviates the strain. The first reversible $O_2$ sequestration by a non-transition-metal complex was accomplished with antimony-ligand cooperation displayed by compound 1.32 (fig. 1-8C).[40] The dioxygen activation also relied on the redox-active nature of the amidophenolate ligand. The proposed addition mechanism was initiated by single electron-transfer (SET) from ligand to oxygen to give a triplet radical ion pair. Intersystem crossing (ISC) was then facilitated by the antimony atom and radical recombination gave the final product 1.33. The starting antimony complex 1.32 could then be regenerated by moderate heating and release of $O_2$.

## 1.4    Structurally Constrained P(III) Compounds

Tethered ligand systems can be used to lower the local symmetry at phosphorus(III) compounds, transitioning from archetypical tricoordinate phosphorus compounds of local, trigonal $C_{3v}$ symmetry to non-VSEPR (valence shell electron repulsion) structures of $C_s$, $C_{2v}$ or $C_1$ symmetry. The descent in symmetry lifts the degeneracy of the antibonding orbitals of 2e symmetry at phosphorus, while the lone pair ($2a_1$ symmetry) remains largely unaffected (fig. 1-9).[41] The consequence is a lowering of the energy for one of the antibonding orbitals, furnishing a more accessible LUMO and a lowered HOMO-LUMO gap.
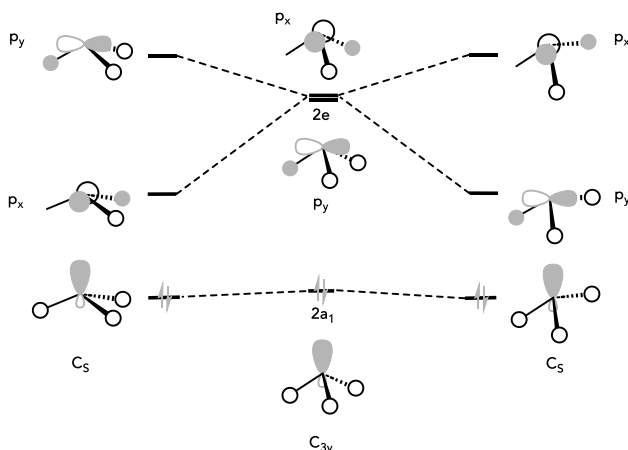


**Figure 1-9:** Qualitative correlation diagram for frontier orbitals of a $\sigma^3$-P compound upon non-trigonal perturbation.

These changes to the frontier orbitals energies were experimentally and computationally validated for phosphorus triamide compounds using K-edge XANES (X-ray absorption near-edge spectroscopy) and TDDFT (time-dependent density functional theory) calculations.[42] The electronic situation becomes reminiscent of transition metals or other low-valent main group compounds such as carbenes or silylenes and confers biphilic reactivity to typically nucleophilic phosphorus(III). The ordering of the orbitals can even be switched upon sufficient lowering of the LUMO by structural constraint. This was proposed for the $C_{2v}$ symmetric, T-shaped 10-P-3 species 1.34 prepared by Arduengo (fig. 1.10).[43]
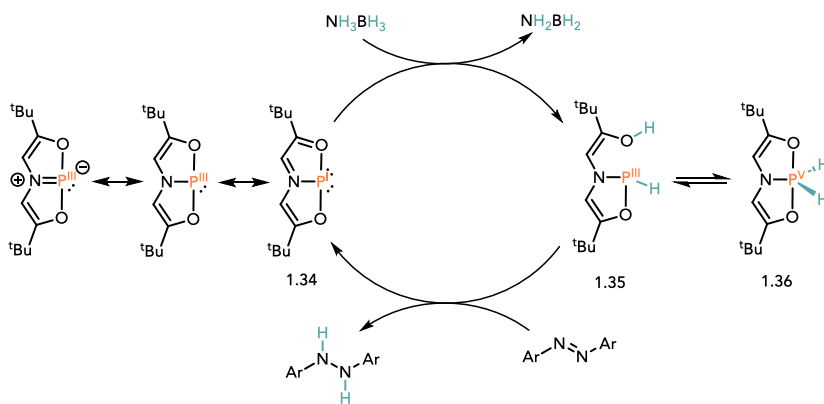
**Figure 1-10:** Limit resonance structures of 1.34 and catalytic cycle for the transfer hydrogenation of azobenzene.

The compound can be described by several resonance structures and DFT calculations predicted a P(I) oxidation state with two lone pairs of p-type and sp-hybrid character, respectively.[44] The T-shaped complex was proposed to serve as a model for the transition state in the edge-inversion of trigonal pnictogens. Radosevich and co-workers then showed in 2012 that 1.34 catalyzes the transfer hydrogenation of azobenzene to diphenylhydrazine using ammonia-borane as hydrogen surrogate (fig. 1-10).[45] They proposed a mechanism *via* a reversible P$^{III}$/P$^V$ redox cycle involving the dihydridophosphorane intermediate 1.36, but DFT calculations by Sakaki and co-workers suggested that the P(V) product 1.36 only constitutes a resting state. The catalysis instead proceeds via a P$^I$/P$^{III}$ redox cycle with phosphorus-ligand cooperative dehydrogenation of ammonia-borane to intermediate 1.35, followed by hydrogen transfer to azobenzene.[44]

Even preceding this seminal study, the strain-induced enhanced electrophilicity at phosphorus had been described in early examples with the reactivity of 1,3,2-diheterophospholanes towards polar E-H bonds.[46] For instance, the pinacol-based σ$^3$-P(III)-compounds of the general structure 1.37 by Barrans *et al.* reacted reversibly
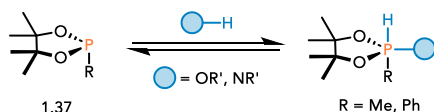


**Figure 1-11:** Oxidative addition of alcohols and amines to a cyclic phosphonite.

with alcohols and amines by oxidative addition to the respective $\sigma^5$-P phosphoranes (fig. 1-11).[47] The equilibrium position was determined by the nature of the alcohol, amine and phosphorus-substituent R.

Later studies showed enhanced competence in bond scission reactions of polar E-H bonds (E = O, N, S, B) by different bicyclic, structurally constrained P(III) compounds with aromatic pincer-type ligands, both neutral and cationic (fig. 1-12 and 1-13).[41]



$\Delta G^{\ddagger}_{exp}$ = 10.7(5) kcal/mol
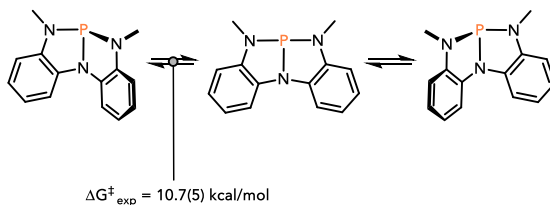
**Figure 1-12:** Interconversion of phosphorus triamide 1.38 enantiomers.

An example is the $C_S$ symmetric phosphorus triamide 1.38 by Radosevich *et al.*, which adopts a folded structure in the relaxed state and whose enantiomers readily interconvert *via* a T-shaped, $C_{2v}$ symmetric intermediate (fig. 1-12).[48] The barrier was determined by VT-NMR experiments to be around 10.7(5) kcal/mol.
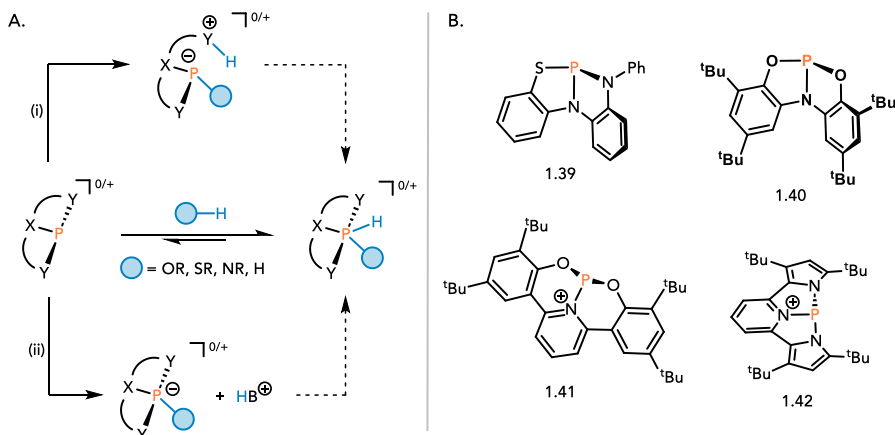


**Figure 1-13: A.** E-H oxidative addition to structurally constrained P(III) compounds via (i) internal or (ii) external base-assisted mechanisms. **B.** Examples of such P(III) compounds by Goicoechea (1.39 and 1.40) and Dobrovetrsky (1.41 and 1.42).

Compound 1.38 also selectively and reversibly reacted with alcohols and amines *via* oxidative addition. Several other phosphorus pincer compounds of similar reactivity both neutral (1.39 and 1.40 by Goicoechea) and cationic (1.41, 1.42 and 1.43 by Dobrovetsky) were reported, all relying on an internal (fig. 1-13A(i)) or external (fig. 1-13A(ii)) base-assisted deprotonation mechanisms for E-H bond cleavage (fig. 1-13A).[49] Depending on the substrate and P(III) compound, the equilibrium for $\sigma^3$-P/$\sigma^5$-P ring-chain tautomerization was on the side of either the $\sigma^3$-P compound or gave the respective $\sigma^5$-P products, completing the overall oxidative additions. Exceedingly high computed barriers for the concerted oxidative E-H addition pathways excluded this mechanistic possibility commonly observed in transition metal complex (see chapter 1.5).[49b, 50]

Concerted transition states for the oxidative addition of $Et_3SiH$ to 1.42 or dihydrogen to the highly Lewis acidic, carborane-based pincer compound 1.43 were proposed, their experimental verification or computations at a high level of theory however are still outstanding (fig. 1-14). Nonetheless, 1.43 was shown to be an active catalyst for the hydrogenation of activated alkenes and arenes following a $P^{III}/P^V$ redox cycle.[51]
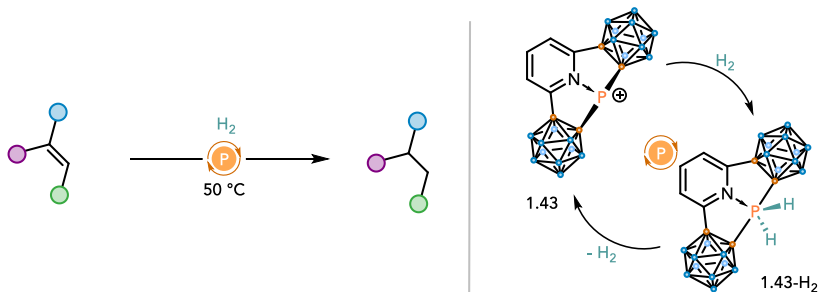


**Figure 1-14:** Hydrogenation of activated alkenes and arenes catalyzed by a structurally constrained phosphenium ion (10 mol% catalyst was used).

## 1.5 C-H Activation

The selective activation and functionalization of carbon-hydrogen bonds presents a long-standing challenge in organic chemistry but holds tremendous promise. The direct conversion of inert C-H bonds can expedite a given chemical synthesis through bypassing the need for prefunctionalization of substrates, improving the atom-economy and minimizing waste production on the way to more sustainability.[52] Since the 1980s, significant progress has been made in developing new methodologies, championed by the ability of precious transition metal catalysts to effect the various catalytic steps.[53] To lower the reliance on the costly and scarcely abundant precious metals, the use of cheaper 3d metals has proven to be a relatively fruitful approach.[52c, 54] A key step of the C-H functionalizations often is the C-H bond cleavage, and reactions may be differentiated by the mechanism by which it occurs. There are generally three primary categories of activation modes described in the literature.[52c, 53]
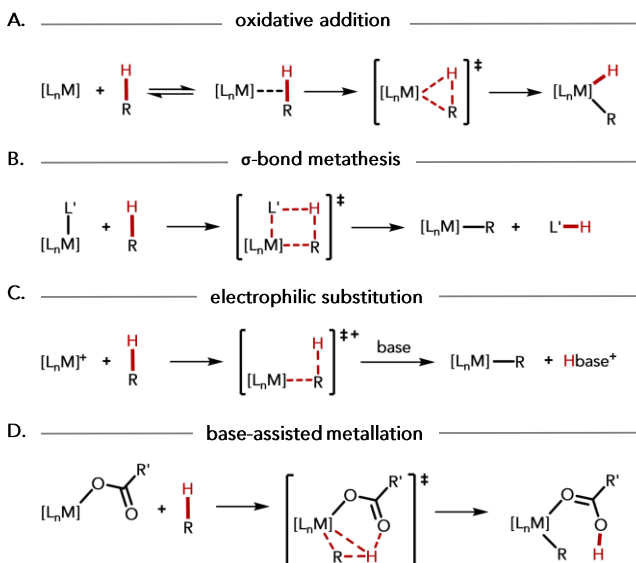


**Figure 1-15:** Mechanisms of C-H activation, including **A.** oxidative addition, **B.** σ-bond metathesis, **C.** electrophilic substitution and **D.** base-assisted metalation.

These include oxidative addition, σ-bond metathesis or electrophilic activation (fig. 1-15) and their occurrence depends on the combination of metal, ligand and substrate. However, the distinction between these mechanisms is not always unambiguous as the reactivities exist on a continuum. An increasingly important electrophilic substitution mechanism is the isohypsic (i.e. redox-neutral) base-assisted metalation (fig. 1-15D) typically operative with assistance of carboxylate ligands. The base-assisted metalation reactions can be further divided into concerted metalation deprotonation (CMD) or ambiphilic metal ligand activation (AMLA) depending on subtle differences in the mechanisms.[53-55]

## 1.5.1    C-H Activation and Functionalization by p-Block Elements

Although much less explored, the functionalization of C-H bonds through the use of main-group elements has garnered interest as another viable strategy.[34a] It has largely relied on electrophilic activation of arenes by Lewis acidic main-group compounds generating a Wheland-type complex, followed by deprotonation with a suitable Lewis base akin to the electrophilic substitution mechanism for transition metals (fig. 1-15C).

This mechanistic manifold was demonstrated in numerous examples of both stoichiometric and catalytic C-H activation using Lewis acidic boranes or borenium cations.[56] Frustrated Lewis pairs act similarly, with the distinction that C-H bond activation and deprotonation steps occur in concerted fashion in a single step.[34a] Seminal work by Fontaine and co-workers reported on the catalytic borylation of activated heteroarenes by borane FLP catalyst 1.44 (fig. 1-16).[34b] The reaction proceeded by initial concerted C-H bond cleavage *via* an FLP-type mechanism after the aminophenylborane dimer 1.44 dissociated in solution. Subsequent liberation of dihydrogen from 1.44 furnished the diarylborane 1.46. Sigma-bond metathesis with pinacol borane was then computed to yield the final product, regenerating the catalyst in the process. By modifying the borane and the adjacent amine, C(sp$^2$)-H bond cleavage of unactivated arenes and alkenes such as benzene or 1-hexene was achieved, albeit only stoichiometrically.[57]
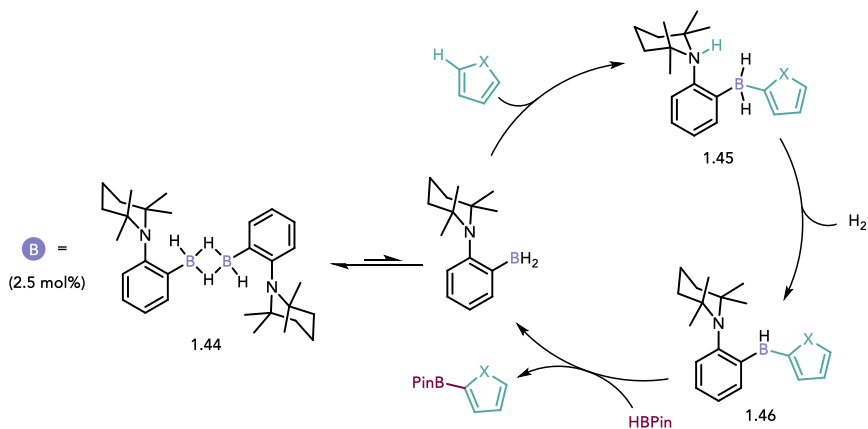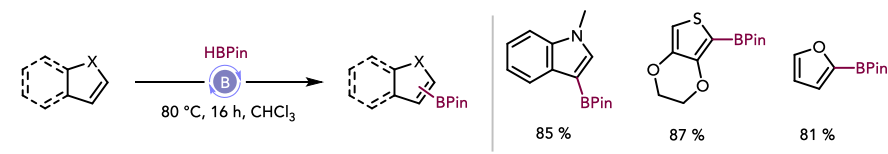
**Figure 1-16:** Catalytic borylation of heteroarenes by a borane FLP including the proposed mechanism.

## 1.5.2 Oxidative Addition

Fewer examples exist for the cleavage of C-H bonds by oxidative addition to main-group compounds and have been mostly limited to activated C-H bonds but could nonetheless also be demonstrated. Additionally, the strong thermodynamic driving forces to a significantly more stable oxidation state that facilitate these reactions have generally rendered them irreversible at main-group elements.[4a] The Al(I) compound NacNacAl 1.47 first introduced by Cimpoesu and co-workers in 2000 reacted with sterically encumbered pentamethylcyclopentadiene (Cp*) upon heating to 70 °C, furnishing the hydrido alkyl Al(III) compound 1.48 by C(sp³)-H oxidative addition (fig. 1-17A).[58] The group of Aldridge later reported in 2018 the synthesis of the first aluminyl anion 1.50, stabilized by a bulky xanthene-based diamido ligand.[59] Dissolution in benzene and heating to 80 °C led to cleavage of the unactivated C(sp²)-H bonds in benzene and formation of the oxidative addition product (fig. 1-17B). Interestingly, if the potassium counterion was sequestered by

[2.2.2]cryptand, reversible insertion of the 'naked' aluminyl anion into the aromatic C-C bond was observed instead.[60] The alkylsubstituted aluminyl compound 1.51 by Kurumada *et al.* reacted with benzene already at room temperature, also by oxidative addition.[61] The reactions were proposed to follow a nucleophilic aromatic substitution mechanism with exclusive *meta*-selectivity observed for the reactions of 1.50 with substituted arenes.[62] With a sufficiently lowered singlet-triplet gap, insertion of carbenes into nonacidic C-H bonds was reported for a broad range of different carbenes. For instance, the cyclic alkyl amino carbene (CAAC) 1.49 readily activated the sp-, sp$^2$- and sp$^3$-hybridized C-H bonds of phenylacetylene, 1-octyne, pentafluorobenzene and chloroform (fig. 1-17C).[63] In the absence of a suitable substrate, 1.49 also underwent intramolecular C-H activation of the diisopropylphenyl group at elevated temperatures.
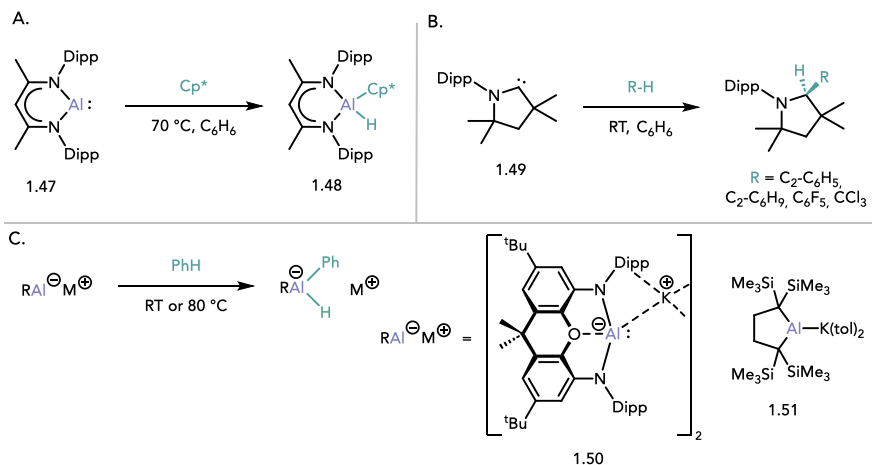


**Figure 1-17:** C-H oxidative addition reactions of **A.** NacNacAl, **B.** a CAAC and **C.** aluminyl salts.

Very few examples of group 15 compounds capable of C-H bond cleavage by oxidative addition currently exist in the literature. The early example of C-H insertion by the diamidophosphenium ion 1.9 (chapter 1.2.3.1, fig. 1-4A) reported by Cowley and co-workers was follow-up only by the carbodicarbene-supported phosphenium dication 1.52 by Vidovic, which inserted into the activated C(sp$^3$)-H bonds of xanthene and 1,3,5-cycloheptatriene, although for the latter the oxidative addition was only a minor reaction pathway (compound 1.55). Both products however were

not stable enough to be isolated.[23, 64]
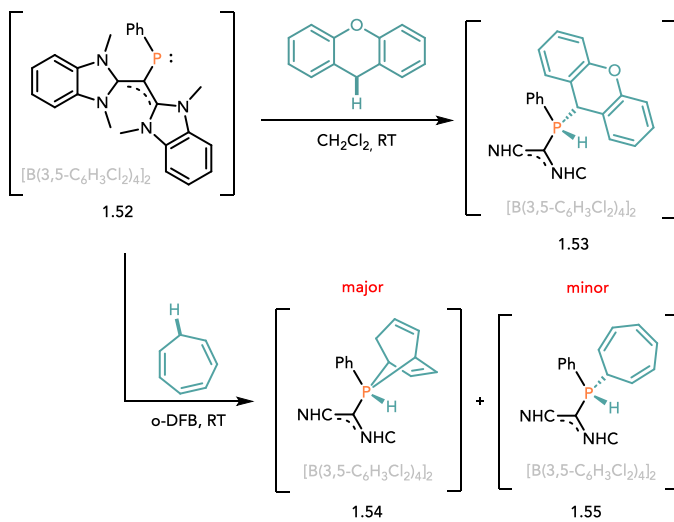


**Figure 1-18:** Reaction of phosphenium dication 1.52 with xanthene and 1,3,5-cycloheptatriene.

# Motivation and Aim of This Work

The overarching goal of this work was to explore new methodologies and ligand frameworks to expand the known reactivities and applications of p-block element compounds. In pursuit of this goal, catecholates were identified as a promising ligand class in earlier works by our group for their ability to increase reactivity at silicon(IV) and generate the first neutral silicon Lewis superacids.[18a] Still, several shortcomings of this class of compounds limited broad applicability, including instability under ambient conditions and without donor stabilization, as well as poor solubility.

To address the issue of stability, chapter 2 of this work was dedicated to the synthesis and characterization of the homologous perhalogenated bis(catecholato)germanes and their adducts, whose unsubstituted parent compound had long been known to be water-stable.[65] After in-depth characterization and assessment of their Lewis acidity by different experimental and theoretical methods was completed, applications as Lewis acid catalysts should be tested and if necessary, the compounds further optimized.

The other objective of this work, as shown in chapters 3 to 6, was to gauge the potential of the catecholates and related amidophenolates as ligands for group 15 elements, namely phosphorus. By introduction of a positive charge with the phosphonium ions isoelectric to the group 14 compounds, further increases to the Lewis acidity were anticipated, as well as stabilization of the monomeric species by charge repulsion. The preparation as salts of lipophilic, weakly coordinating anions should also confer higher solubility in non-polar solvent. Apart from high Lewis acidities, potential for the catecholate-based phosphorus compounds to engage in element-ligand cooperative bond activations was conjectured, facilitated by the proximity of electrophilic (P) and nucleophilic (O) sites.

The use of amidophenolates as substituents at P(V) should equally result in highly reactive phosphonium salts, with the added benefit of enhanced control over electronic and steric properties at phosphorus through an additional, tunable substituent at the nitrogen.

Installation of low-valent phosphorus(III) at an amidophenolate substituted with a methylene linked pyridyl group would further allow the preparation of structurally

constrained phosphenium ions. High Lewis acidity at phosphorus and a dative P-N bond should facilitate cooperative activation and oxidative addition of inert E-H bonds inaccessible by previous examples of constrained P(III) compounds (see chapter 1.4).

Overall, leveraging the structural constraint enforced by catechol- and amidophenolate-based ligands should lead to unprecedented properties and reactivities at phosphorus and germanium, including Lewis superacidity and element-ligand cooperativity.

# Chapter 2

# Bis(catecholato)germanes: Water-stable, Soft and Hard Lewis (Super)acids[a]

## 2.1    Introduction

As previously disclosed in chapter 1, numerous reports of new Lewis superacids have emerged in recent years with strengths greatly exceeding that of SbF$_5$.[6a] Despite this trend, applications have still remained somewhat limited due to shortcomings with regards to their thermal or hydrolytic instability, as well as their high oxophilicity. The Lewis superacidic bis(catecholato)silanes developed in our group were no different in this regard and highly sensitive towards moisture.[18]
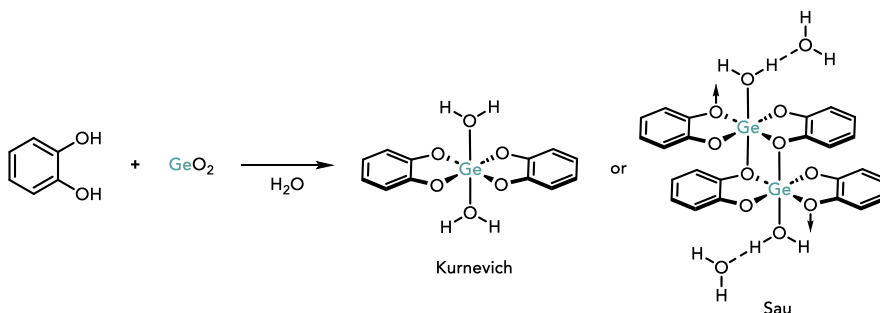


**Figure 2-1:** First preparation of Ge(cat$^H$)$_2$-(H$_2$O)$_2$ by Bevillard and proposed structures.

---

[a] Initial parts of this project were already part of my master's thesis. Corresponding parts are marked with the respective reference.[68]

Inspired by the first synthesis of bis(catecholato)germanes in water by Bevillard in 1954 from catechol and germanium dioxide (fig. 2-1), we surmised that the stability should also translate to the more electron-deficient bis(perhalocatecholato)-germanes, resulting in both stability and high Lewis acidity.[65] Although known for a prolonged period of time, the structure of the bis(catecholato)germane water adducts remained subject to discussion in the literature. A structure with *trans*-coordinated water molecules was proposed by Kurnevich and co-workers, while Sau and co-workers proposed a polymeric structure to better account for the insolubility (fig. 2-1).[66] Since then, a few reports of the bis(catecholato)germane structural motif have been made in the literature, e.g. as intermediates for the conversion of elemental germanium to organogermanes or to recover germanium from different waste systems, but their use as Lewis acids was not reported prior to this work.[67]

## 2.2    Synthesis and Characterization of Ge(cat$^{Cl}$)$_2$ and Lewis Adducts

The water-adduct of bis(perchlorocatecholato)germane was prepared in a single-step in near quantitative yield on a multi-gram scale by heating two equivalents of perchlorocatechol and germanium dioxide in water (fig. 2.2).[68] Depending on the workup and drying procedure, between four and six equivalents of water were present. Recrystallization from water afforded single crystals suitable for X-ray diffraction, confirming the molecular structure containing an octahedrally coordinated germanium atom (fig. 2.3A). The unit cell contains six equivalents of water arranged in two $(H_2O)_3$-cluster connected by hydrogen bonds above and below the Ge(cat$^{Cl}$)$_2$ plane. Starting from the water adduct, different donor-adducts of Ge(cat$^{Cl}$) were then prepared by either direct addition of donors stronger than water in acetonitrile (e.g. Cl$^-$, ($n$-BuO)$_3$PO), OPEt$_3$, EtOH or DMSO), or for weaker donors such as acetonitrile or acetone by storing 2.1-$(H_2O)_n$ in the respective solvent or a mixture thereof over several days.[68] Released water was removed by molecular sieves and 2.1-(CH$_3$CN)$_2$ and 2.1-(acetone)$_2$ could be isolated in 95 % and 91 % yield, respectively. IR spectroscopy showed the CN stretching bands of bound acetonitrile were blue-shifted relative to free acetonitrile by 69 cm$^{-1}$, indicating substantial Lewis acidity of the parent compound Ge(cat$^{Cl}$)$_2$.
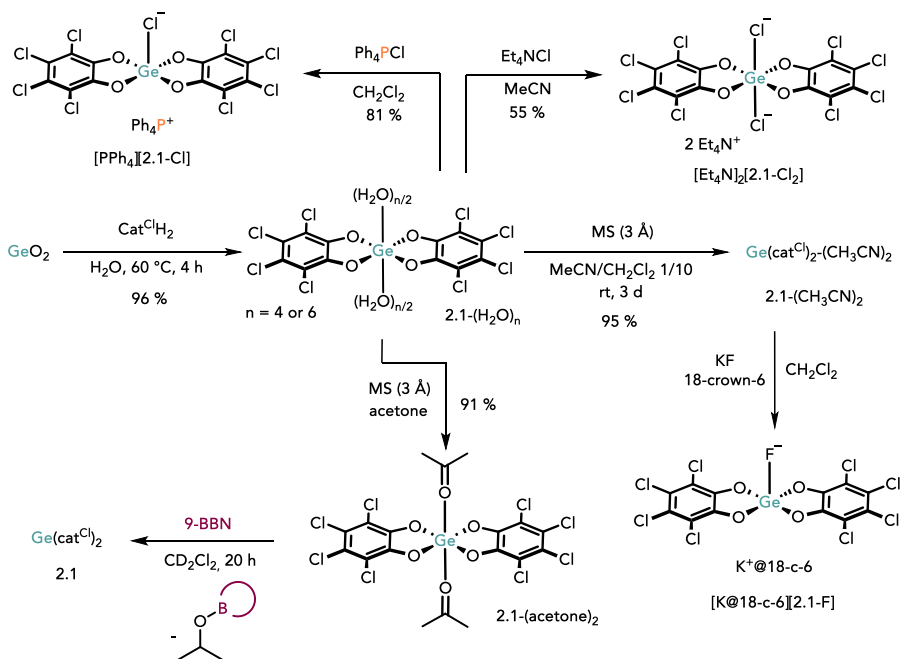
**Figure 2-2:** Synthesis of 2.1 and different Lewis adducts thereof.

Treatment of 2.1-(CH$_3$CN)$_2$ with KF and 18-crown-6 in dichloromethane under strictly anhydrous conditions furnished the fluorido-germanate [K@18-c-6][2.1-F], as corroborated by SCXRD showing the square-pyramidal fluoride-germanate (fig. 2.3C). Interestingly, after leaving the crystals under ambient conditions for several weeks, a single-crystal-to-single-crystal phase transition to the hexacoordinate water adduct [K@18-c-6] [H$_2$O-2.1-F] occurred (fig. 2.3D). The transition was accompanied by only minor changes to the unit cell dimensions and structural parameters. In line with expectations, the germanium water bond however was significantly elongated (d(Ge1-O5) = 2.249(3) Å) relative to the neutral water adduct 2.1-(H$_2$O)$_6$ (d(Ge1-O3) = 1.957(3) Å). Depending on the chosen reaction conditions, both mono- and dichloridogermanates [Ph$_4$P][2.1-Cl] and [Et$_4$N]$_2$ [2.1-Cl$_2$] could also be synthesized, and the structure of the latter could be corroborated by SXCRD of suitable single crystals grown from acetontrile, presenting the first example of a GeO$_4$Cl$_2$ structural motif (fig. 2.3B).
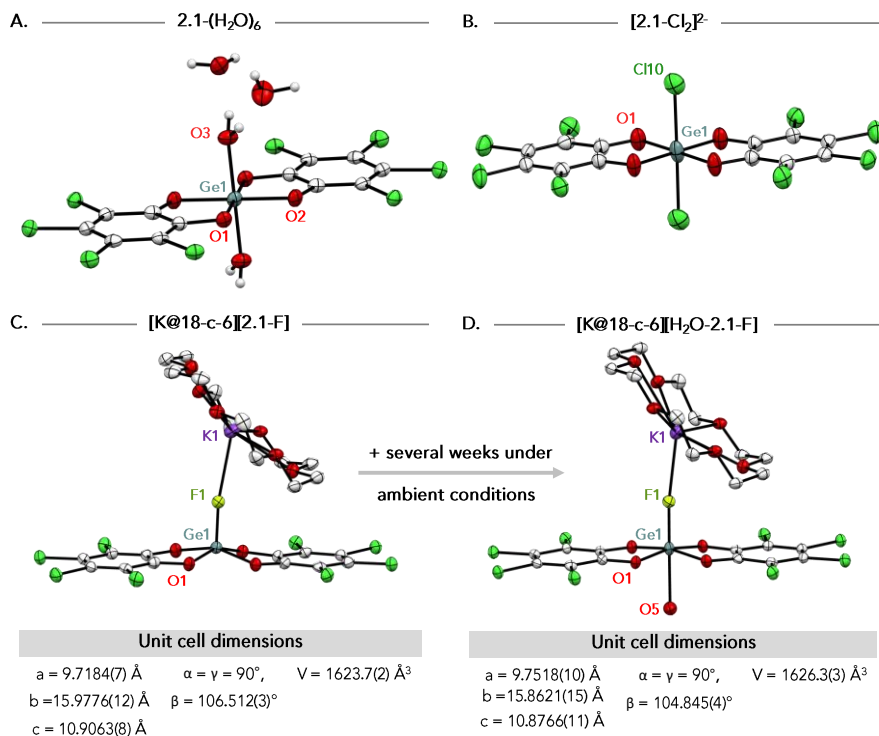
**Figure 2-3:** Solid-state structure of **A.** 2.1-(H₂O)₆ (only two water molecules of the second coordination sphere are depicted, d(Ge1-O1) = 1.845(3) Å, d(Ge1-O3) = 1.957(3) Å), **B.** [NEt₄]₂[2.1-Cl₂] (cations omitted for clarity), d(Ge1-O1) = 1.876(4) Å, d(Ge1-Cl) = 2.353(2) Å), **C.** [2.1-F][K@18-c-6], d(Ge1-O1) = 1.842(4) Å, d(Ge1-F1) = 1.735(3) Å, d(F1-K1) = 2.765(4) Å, **D.** [H₂O-2.1-F][K@18-c-6], d(Ge1-O1) = 1.857(3) Å, d(Ge1-O5) = 2.249(3) Å, d(Ge1-F1) = 1.768(2) Å, d(F1-K1) = 2.676(3) Å. Thermal ellipsoids are displayed at 30 % probability.

Subsequently, we initiated attempts to obtain the donor-free Lewis acid Ge(cat^Cl)₂. Hydroboration of the acetone molecules in 2.1-(acetone)₂ with 9-BBN turned them into donors weak enough to disfavor coordination to germanium, granting access to 2.1 as compound free of exogenous donors. However, we assumed that it possessed the same tendency to oligo- or polymerize as its silicon counterparts, for which the di-, deca- or tetradecamers were structurally characterized in our group.[18a, 19] Consequently, the compound was completely insoluble in non-donor solvents, but the composition could still be verified by elemental analysis and a clean spectrum of 2.1-(DMSO-d₆) after dissolution and depolymerization in DMSO-d₆.

## 2.3    Lewis Acidity Assessment of Ge(cat$^{Cl}$)$_2$

We then studied the *global* Lewis acidity of the theoretical donor-free Lewis acid Ge(cat$^{Cl}$)$_2$ by computations of the fluoride (FIA) and hydride ion affinities (HIA) both in the gas phase and within an implicit solvation sphere.[68] The results are summarized in figure 2-3A together with values of the silicon counterparts, other germanium-based Lewis acids, as well as examples of well-known Lewis acids computed at the same level of theory for comparison. The FIA closely resembles that of Si(cat$^{Cl}$)$_2$ and similarly surpasses the value computed for SbF$_5$, thus fulfilling the criterium for Lewis superacidity.[6b] In contrast to the silicon-based Lewis acid, the HIA also exceeds that of B(C$_6$F$_5$)$_3$, making 2.1 also a soft Lewis superacid.[6a]

**A.**

| Compound | FIA (solv) [kJmol$^{-1}$] | HIA (solv) [kJmol$^{-1}$] |
|---|---|---|
| GeF$_4$ | 360 (244) | 407 (427) |
| GeF(CF$_3$)$_3$ | 373 (224) | 437 (420) |
| Ge(CF$_3$)$_4$ | 355 (197) | 416 (387) |
| Ge(C(CF$_3$)$_2$OC$_6$H$_4$)$_2$ | 321 (148) | 458 (402) |
| Ge(cat$^{Cl}$)$_2$ | 504 (304) | 555 (485) |
| Si(cat$^{Cl}$)$_2$ | 507 (315) | 491 (429) |
| B(C$_6$F$_5$)$_3$ | 453 (259) | 515 (448) |
| SbF$_5$ | 501 | - |

**B.**



**C.**



| M = | ∡ C$_2$C$_1$O' [°] | d(M-O) [pm] |
|---|---|---|
| Ge | 116.41(9) | 186.47(9) |
| Si | 114.1(1) | 176.6 |

R = cat$^{Cl}$, (OPEt$_3$)$_2$

**D.** ———————————— Gutmann-Beckett ————————————
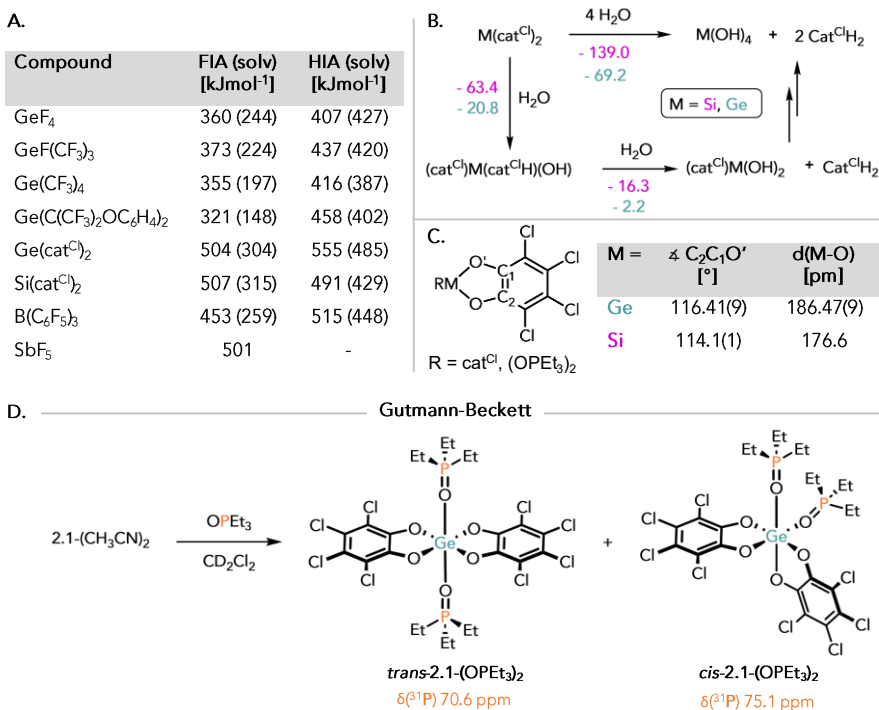


**Figure 2-4: A.** Computed FIA and HIA at the DLPNO-CCSD(T)/aug-cc-pVQZ+COSMO-RS(CH$_2$Cl$_2$)//PW6B95-D3(BJ)/def2-TZVPP level of theory. **B.** Computed reaction enthalpies in kJ mol$^{-1}$ of hydrolysis of 2.1 relative to Si(cat$^{Cl}$)$_2$ at the PW6B95-D3(BJ)/def2-TZVPP level of theory. **C.** Comparison of relevant bond lengths and angles in Si(cat$^{Cl}$)$_2$-(OPEt$_3$)$_2$ and 2.1-(OPEt$_3$)$_2$. **D.** Determination of Lewis acidity according to the Gutmann-Beckett method.

As the 'free' Lewis acid Ge(cat$^{Cl}$)$_2$ does not exist and instead polymeric structures were assumed, the predicted hard and soft Lewis superacidity was then verified experimentally using the acetonitrile adduct 2.1-(CH$_3$CN)$_2$. In the presence of [Ph$_4$P][SbF$_6$], rapid reaction and formation of the mono-fluoridogermanate [2.1-F]$^-$ was detected by $^{13}$C and $^{19}$F NMR spectroscopy signals consistent with previously prepared [2.1-F]$^-$, as well as by ESI mass spectrometry. Ensuing unselective reactions of the detected germanate with the strong oxidant SbF$_5$ prevented isolation of the reaction products. In similar fashion, hydride abstraction from [$^t$Bu$_3$PH][H-B(C$_6$F$_5$)$_3$] was observed with concomitant formation of the acetonitrile adduct MeCN-B(C$_6$F$_5$)$_3$, supporting the claim of 2.1 also as soft Lewis superacid.[68] Additionally, we assessed the *effective* Lewis acidity of 2.1 by monitoring the reaction of 2.1-(CH$_3$CN)$_2$ with OPEt$_3$ according to the Gutmann-Beckett method (fig. 2.4D).[14] Spectroscopic analysis of the reaction by $^{31}$P($^1$H) NMR revealed two new resonances at 70.6 and 75.1 ppm, which together with proton NMR data were assigned to the *trans*- and *cis*-bisadducts of 2.1 with OPEt$_3$.[68] The outcome was in line with the strong preference of hexa- over pentacoordination by Ge(cat$^{Cl}$)$_2$ as seen in previous experiments. Nevertheless, the shifts are comparable to those measured for the bisadduct of Si(cat$^{Cl}$)$_2$ and OPEt$_3$ and they easily surpass those measured for GeF$_4$-(OPEt$_3$)$_2$.[18a, 69] Comparison of the crystal structures of *trans*-2.1-(OPEt$_3$)$_2$ and *trans*-Si(cat$^{Cl}$)$_2$-(OPEt$_3$)$_2$ reveals diminished ring-strain of the five-membered ring enclosed by the catecholates and the central tetrel atom by virtue of the elongated tetrel-oxygen bonds resulting in smaller deviations of the preferred 120° O'-C-C angle at the catecholate (fig. 2.4C). The structural differences were considered as explanation of the greater hydrolytic stability of the germanium over the silicon compounds, which was further investigated by calculation of enthalpies for the stepwise hydrolysis of the M(cat$^{Cl}$)$_2$ (M = Si, Ge) species. Already the first hydrolytic ring-opening step is thermodynamically significantly more favorable for silicon by 43 kJ mol$^{-1}$, and the complete hydrolysis by over 70 kJ mol$^{-1}$.[68]

To investigate the acidification of water bound to 2.1, we computed the gas-phase Brønsted acidity (GA = standard Gibbs energy of deprotonation in the gas phase) of 2.1-(H$_2$O)$_2$. Calculations at the BP86/def2-TZVPP level of theory gave a GA value of 1168 kJ mol$^{-1}$, surpassing the values literature values of HSO$_3$F (1233 kJ mol$^{-1}$) and H$_2$SO$_4$ (1272 kJ mol$^{-1}$), making it a Brønsted superacid as well.[70] The value also approaches the one calculated for the Lewis superacid-water adduct

$H_2O$-$Al(OC(CF_3)_3)_3$ (1148 kJ mol$^{-1}$) by Krossing and co-workers at the same level of theory.[70c]

## 2.4    Catalysis

The efficacy of 2.1 and its adducts as Lewis acid catalysts was probed with a selected scope of reactions. In the presence of 0.5 to 5 mol% of 2.1-$(CH_3CN)_2$, clean reduction of aromatic and aliphatic aldehydes occurred with triethylsilane (fig. 2-5A).[68] The reaction was more tolerant towards electron-rich aldehydes than its silicon or phosphonium counterparts, which tended to overreduce the electron-rich substrates by deoxygenation of the aldehydes.[71] The robustness of the catalyst against trace impurities was demonstrated by rapid hydrodefluorination of 1-fluoroadamantane with catalyst loadings as low as 0.05 mol% and resulting turnover numbers (TON) up to 1900.[68] Detection of [2.1-F]$^-$ by $^{19}$F NMR spectroscopy during the course of the reaction indicated C-F over Si-H activation as the more likely reaction pathway. The substrate scope however was very limited, and less reactive 1-pentylfluoride could not be converted. The lack of reactivity was attributed to the inability of weak donors to displace coordinated acetonitrile to access the Lewis acidic germanium center.

Next, we sought to capitalize on the considerable computed HIA of 2.1 and applied it to transfer hydrogenations. 1,1-Diphenylethylene was readily reduced with 1,4-cyclohexadiene (1,4-CHD) as hydrogen surrogate in the presence of 10 mol% 2.1-$(CH_3CN)_2$ or with lower conversion rates in the presence of 2.1-$(H_2O)_4$. The reduction also worked with the hydrogen equivalent coming from triethylsilane and water bound to 2.1-$(H_2O)_6$. The origin of the transferred proton coming from water was confirmed by control experiments using $D_2O$. Using silanes and water to hydrogenate alkenes had not been reported for main group catalysts, but a precedent was set by an iridium catalyst.[72]  In the absence of a reductant, the Friedel-Crafts dimerization of 1,1-diphenylethylene was catalyzed by 2.1-$(CH_3CN)_2$, reaching 48 % conversion to the dimer after one day at 50 °C. The performance was about equal to the previously reported reaction under the same conditions with $B(C_6F_5)_3$ as catalyst.[73]

Going beyond the classical reduction chemistry, the performance of 2.1-$(CH_3CN)_2$ as catalyst for the intramolecular carbonyl-olefin metathesis of β-keto-esters was investigated.[74] With 5 mol% catalyst, full conversion was achieved after one day at

room temperature, performing similar to FeCl₃, as outlined in the original report by Schindler and co-workers. Interestingly, while the byproduct acetone did not inhibit the reaction, direct use of 2.1-(acetone)₂ was not productive.

A.



| R | x | t [h] | Conv. [%] |
|---|---|---|---|
| -C₆H₅F | 5 | 24 | >97 |
| -C₆H₅CH₃ | 5 | 24 | >97 |
| -C₆H₁₁ | 0.5 | 24 | >97 |

B.



| x | T [°C] | t [h] | Conv. [%] |
|---|---|---|---|
| 5 | 25 | 1 | >97 |
| 0.5 | 25 | 24 | >97 |
| 0.05 | 50 | 48 | 91 |

C.



| cat. | reagent | t [h] | Conv. [%] |
|---|---|---|---|
| 1-(CH₃CN)₂ | 1,4-CHD | 1 | >97 |
| 1-(H₂O)₄ | 1,4-CHD | 3 | 50 |
| 1-(H₂O)₆ | Et₃SiH | 1 | 93 |

D.



E.
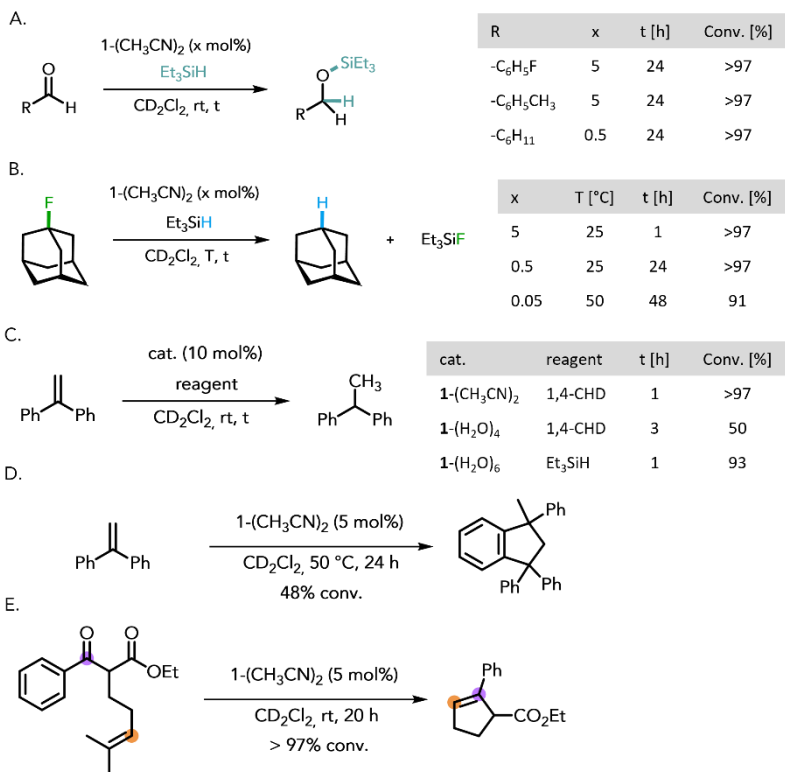


**Figure 2-5:** Selected catalytic applications of 2.1-(donor)₂ in **A.** the hydrosilylation of aldehydes, **B.** the hydrodefluorination of 1-adamantylfluoride, **C.** the transfer hydrogenation of 1,1-DPE, **D.** Friedel–Crafts dimerization of 1,1-DPE, and **E.** the intramolecular, ring-closing carbonyl–olefin metathesis. The conversions were determined by ¹H NMR integration against an internal standard.

## 2.5 Synthesis of Lewis Adducts of Ge(cat$^F$)$_2$

In an effort to obtain better insights into the reactivity of perhalogenated bis(catecholato)germanes, the synthesis of the perfluorinated derivative Ge(cat$^F$)$_2$ was targeted to facilitate NMR analysis in solution by adding nuclei with better receptivity than the $^{13}$C nuclei present in 2.1. The synthesis proceeded similar to that of 2.1-(H$_2$O)$_6$, and heating perfluorinated catechol with GeO$_2$ in water to 70 °C for three hours gave 2.2-(H$_2$O)$_6$ in excellent yield (fig. 2-6). Surprisingly, 2.2-(H$_2$O)$_6$ enjoys much greater solubility in water than 2.1-(H$_2$O)$_6$, possibly due to the ability of the organic fluorines to act as hydrogen bond acceptors.[75] The $^{19}$F NMR spectrum in D$_2$O displays two sets of signals, which were tentatively assigned to the *cis*- and *trans*-coordinated water-adducts similar to the observations made for 2.1-(OPEt$_3$)$_2$ in solution (fig. 2-6). The broad resonances are indicative of a dynamic equilibrium in solution interconverting the two isomeric forms.
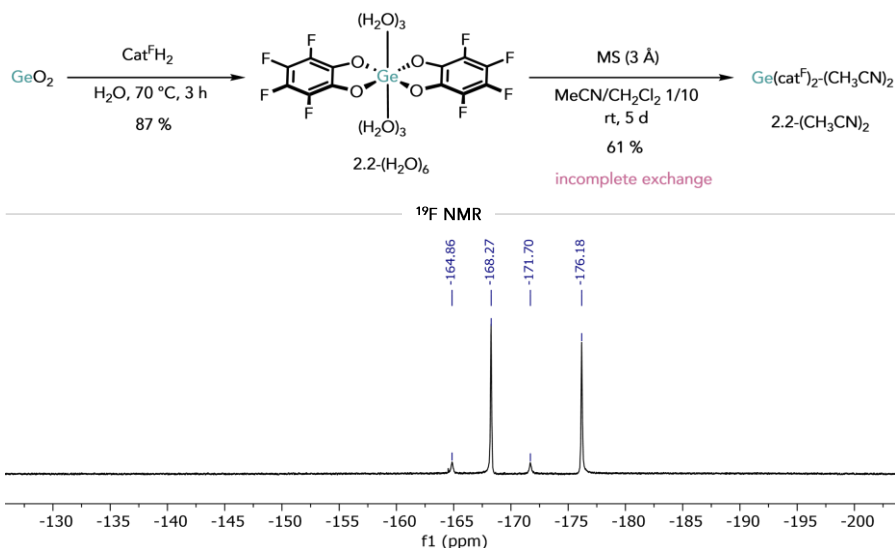


**Figure 2-6:** Synthesis of Ge(cat$^F$)$_2$-(H$_2$O)$_6$ and incomplete conversion to the acetonitrile adduct, as well as the abridged $^{19}$F NMR spectrum of 2.2-(H$_2$O)$_6$ in D$_2$O.

The exchange of water by acetonitrile was attempted under the same conditions as for 2.1. IR spectroscopy and the proton NMR in DMSO-d$_6$ revealed incomplete exchange as residual water was still present. Monitoring the exchange with DMSO-d$_6$ by $^{19}$F NMR further revealed a slow reaction that only ran to completion

over the course of a day. The higher difficulty to displace the water in 2.2-$(H_2O)_6$ compared to 2.1-$(H_2O)_6$ also manifested itself in complications trying to synthesize the adduct of 2.2 with OP(OBu)$_3$.

Despite the residual water in 2.2-$(CH_3CN)_2$, the effective Lewis acidity was gauged by treatment with triethylphosphine oxide in $CD_2Cl_2$. The emergence of three new $^{31}P$ NMR resonances was observed and the two singlets at 74.2 and 69.7 ppm were assigned to the *cis*- and *trans*-bis-adducts 2.2-$(OPEt_3)_2$. The remaining broad signal at 56.0 ppm (free OPEt$_3$: 50.5 ppm in $CD_2Cl_2$) was attributed to non-coordinated phosphine oxide engaged in a dynamic equilibrium with the two adducts.[18b] The peaks of coordinated OPEt$_3$ are shifted slightly upfield relative to the same peaks measured for 2.1-$(OPEt_3)_2$, suggesting slightly lower effective Lewis acidity. Similar observations were made previously for the corresponding bis(catecholato)silanes and explained by the diminished π-backbonding of chlorine compared to fluorine, which is also reflected by the greater Hammett parameter ($\sigma_p^{Cl}$ = 0.227, $\sigma_p^F$ = 0.962).[18a, 76]

## 2.6 Improving Catalyst Performance with Sulfone Adducts

### 2.6.1 Synthesis

As the Lewis base stabilizing the bis(catecholato)germanes plays an important role in their efficacy in Lewis acid catalysis, we surmised that exchange of acetonitrile by a more weakly bound donor could improve on the performance of 2.1 in Lewis acid catalysis. Sulfones were identified as suitable for this purpose, as they combine both low Lewis basicity with chemical robustness, as the stability in the presence of the bis(catecholato)silanes had already been established.[18c] The synthesis by water removal in the presence of the respective sulfone was ineffective, as residual water continued to be present in the final product under the tested reaction conditions for both 2.1 and 2.2. To circumvent this issue, other procedures starting from different germanium precursors such as elemental germanium, germanium(IV) chloride and germanium(II) iodide were thus considered. GeCl$_4$ was completely unreactive towards the perhalogenated catechols.
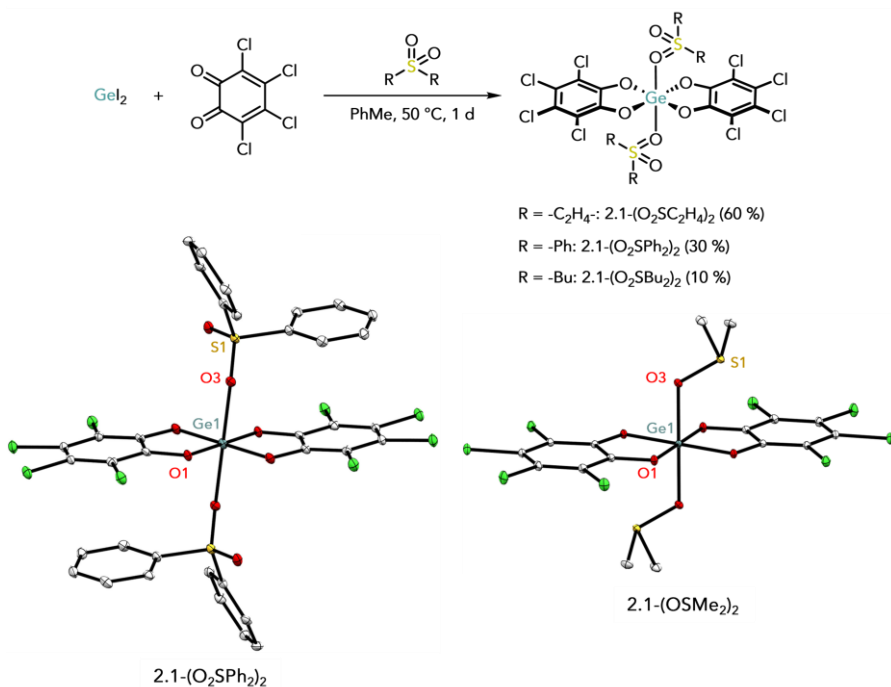
**Figure 2-7:** Synthesis of various sulfone adducts of Ge(cat$^{Cl}$)$_2$ starting from GeI$_2$, as well as solid-state structures of 2.1-(O$_2$SPh$_2$)$_2$ and 2.1-(SOMe$_2$)$_2$ for comparison. Thermal ellipsoids are displayed at 30 % probability, hydrogen atoms were omitted for clarity. Selected bond lengths (Å) and for 2.1-(O$_2$SPh$_2$)$_2$: d(Ge1−O1) = 1.830(3), d(Ge1−O3) = 2.082(3), d(S1−O3) = 1.474(3) and for 2.1-(OSMe$_2$)$_2$: d(Ge1−O1) = 1.8537(9), d(Ge1−O3) = 1.9790(9), d(S1−O3) = 1.5613(9).

The preparation of electron-rich bis(catecholato)germanes starting from elemental germanium and 3,5-di-tert-butyl-o-quinone in the presence of pyridine was reported by Lumb and co-workers.[67a] However, heating Ge and *ortho*-chloranil in toluene in the presence of sulfones only produced unidentified radical species, currently suspected to be the tris(dioxolane)germanium diradical.[77] In the end, treating GeI$_2$ with *o*-chloranil in the presence of sulfone, diphenylsulfone or dibutylsulfone was expedient and the reaction mixtures turned from red to brown over the course of the reaction as iodine was formed. The products could be isolated as colorless powders, although the yields were quite poor for the diphenyl- and dibutylsulfone adducts. Surprisingly, the solubility of the sulfone adducts was not high in non-polar solvents such as dichloromethane even with dibutylsulfone as

donor. Despite this, single crystals of 2.1-(O$_2$SPh$_2$)$_2$ suitable for X-ray diffraction deposited from a cooled-down reaction mixture with 1,1-diphenylethylene in dichloromethane. The structure shows the expected octahedrally coordinated germanium with the two diphenylsulfone molecules located in *trans*-orientation above and below the plane set by the Ge(cat$^{Cl}$)$_2$ unit. In comparison to both 2.1-(H$_2$O)$_6$ (d(Ge1-O3) = 1.957(3) Å) and 2.1-(OSMe$_2$)$_2$ (d(Ge1-O3) = 1.9790(9) Å), the germanium-oxygen bonds connecting the sulfone and Ge(cat$^{Cl}$)$_2$ fragments of 2.1-(O$_2$SPh$_2$)$_2$ are elongated (d(Ge1-O3) = 1.9790(9) Å), consistent with the lower Lewis basicity of the sulfone. The high degree of coplanarity between the catecholate and phenyl moieties indicate dispersive interactions between the two aromatic systems.

## 2.6.2    Catalysis

With the newly prepared adducts of 2.1 in hand, their potential as Lewis acid catalysts was evaluated in the Friedel-Crafts-dimerization of 1,1-diphenylethylene. As we had previously already shown, 2.1-(CH$_3$CN)$_2$ catalyzed the reaction and about 48 % conversion was achieved within one day at 50 °C and 5 mol% catalyst loading, similar to the results reported for BCF.[73] Compared to these results, the sulfone
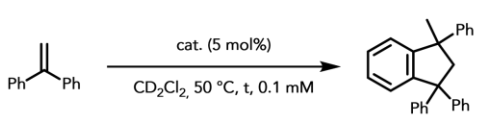


| entry | cat. | t [h] | Conv. [%] |
|---|---|---|---|
| 1 | 2.1-(CH$_3$CN)$_2$ | 24 | 48 |
| 2 | 2.1-(O$_2$SC$_2$H$_4$)$_2$ | 24/120 | 74/96 |
| 3 | 2.1-(O$_2$SPh$_2$)$_2$ | 15 | >97 |
| 4 | 2.1-(O$_2$SBu$_2$)$_2$ | 24 | 97 |
| 5 | 2.2-(CH$_3$CN)$_2$ | 24 | 0 |
| 6 | 2.1-(H$_2$O)$_6$ | 48/120 | 33/61 |

**Figure 2-8:** Friedel-Crafts dimerization of 1,1-diphenylethylene and results obtained for different adducts of 2.1 as catalysts. Conversions were determined by integration of suitable $^1$H NMR signals.

adducts yielded improvements across the board. The highest catalytic activity was measured for the adduct with diphenylsulfone, as full conversion to the dimer was achieved within 15 hours at 50 °C. The reaction with 2.1-(O$_2$SBu$_2$)$_2$ required slightly longer reaction times despite the expected higher solubility in non-polar solvents. We assumed that the weaker coordinating ability of diphenylsulfone was responsible here for the improved catalyst performance. Interestingly, no reaction was detected with the perfluorinated derivative 2.2-(CH$_3$CN)$_2$, which could be

attributed to the lower Lewis acidity or potentially worse solubility compared to 2.1-$(CH_3CN)_2$ (which might arise from the contamination with water).

We also applied these catalysts to other, more challenging reactions such as the deoxygenation of ketones or the hydrodefluorination of 1-pentylfluoride, but the performance was poor for all compounds.

## 2.7    Conclusion

To summarize, this chapter disclosed the preparation and characterization of perhalogenated bis(catecholato)germanes and their adducts. Computational assessment of their Lewis acidity revealed the elusive donor-free compound $Ge(cat^{Cl})_2$ as both soft and hard Lewis superacid, and the Lewis superacidic character was confirmed experimentally *via* its acetonitrile adduct. The stability in water was demonstrated by synthesis of the water adduct directly in water and rationalized by structural considerations and computations. With the perfluorinated complex $Ge(cat^{F})_2$, improved solubility in water was achieved, as well as access to analysis of solution phase processes by fluorine NMR. The utility as Lewis acid catalysts was shown by applications of 2.1-$(CH_3CN)_2$ as catalyst to a broad selection of reactions, including hydrosilylation, hydrodefluorination, transfer hydrogenation and Friedel-Crafts reactions, as well as the intramolecular carbonyl-olefin metathesis of a β-ketoester. Improvements to the catalytic efficacy could be made by synthesis of sulfone adducts, which deliver both enhanced chemical robustness and weaker coordination to 2.1.

# Chapter 3

## Lewis Superacidity and Phosphorus-Ligand Cooperativity of Catechecholato-Phosphonium Ions

### 3.1    Introduction

Compounds based on naturally electron-deficient boron and aluminium generally make up the bulk of strong main-group Lewis acids, but progress has been made in designing Lewis acids based on other p-block elements with increasing strength. Even for phosphorus compounds, typically employed as Lewis bases, highly Lewis acidic species could be prepared in the last decade using strongly electron-withdrawing substituents or by introduction of multiple charges.[21b] In this chapter, the bis(catecholato)-framework, which has been successful in creating the first neutral group 14 Lewis superacids, is transferred to group 15 as a new method to create highly electrophilic phosphonium ions.[18a, 78] The benefit of a single catecholate to the Lewis acidity at phosphorus was also already demonstrated by Terada and Kouchi, as previously disclosed in chapter 1.2.3.2.[27] The combination of catechols and phosphorus possesses rich historic precedent, as neutral bis(catecholato)phosphoranes have played important roles in understanding hypervalent phosphorus chemistry.[79] Additionally, anionic tris(catecholato)-phosphates (TRISPHAT) have been widely used as weakly coordinating anions, NMR-shift, or asymmetry inducing reagents.[80] Despite this, the tetracoordinate bis(catecholato)phosphonium ions had never been isolated. Although the formation of $P(cat^H)_2^+$ was reported in 1978, limited stability due to incompatibilities with the $SbCl_6^-$ counterion were noted (i.e. decomposition upon contact with a metal spatula)

and prevented complete characterization.[81]

## 3.2 Synthesis

Treating a solution of the respective catechol in dichloromethane with PCl$_5$ furnished the homoleptic bis(catecholato)chlorophosphoranes 3.1a and 3.1b in good yields of 70 and 75 % (fig. 3-1). At the same time, chlorophosphoranes containing two different ligands could be accessed by intermediate synthesis of compound 3.2 by oxidative addition of *ortho*-chloranil to phosphorus trichloride. Subsequent condensation of trichlorophosphorane 3.2 with the desired diol then gave the targeted, unsymmetrically substituted phosphoranes 3.1c – e in good to excellent yields. Depending on the starting 1,1'-bi-2-naphtol (binol), the binol-derived compounds were obtained either as racemic mixtures or enantiopure compounds. Subsequent chloride abstraction with a suitable reagent such as Na[B(C$_6$F$_5$)$_4$] or Li[Al(OR$^F$)$_4$] (R$^F$ = C(CF$_3$)$_3$) proceeded cleanly to the catecholato-phosphonium ions 3.3a – e as salts of the weakly coordinating anions (WCAs) in near quantitative yields (fig. 3-2). Only the chlorophosphorane 3.1c, the precursor to the putatively strongest Lewis acid did not react under these conditions.
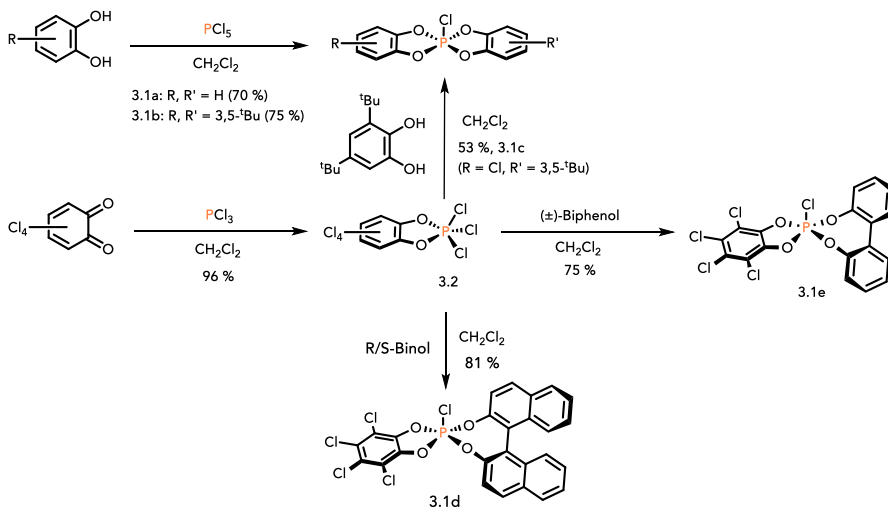


**Figure 3-1:** Synthesis of different homo- and heteroleptic catecholate-based chlorophosphoranes.
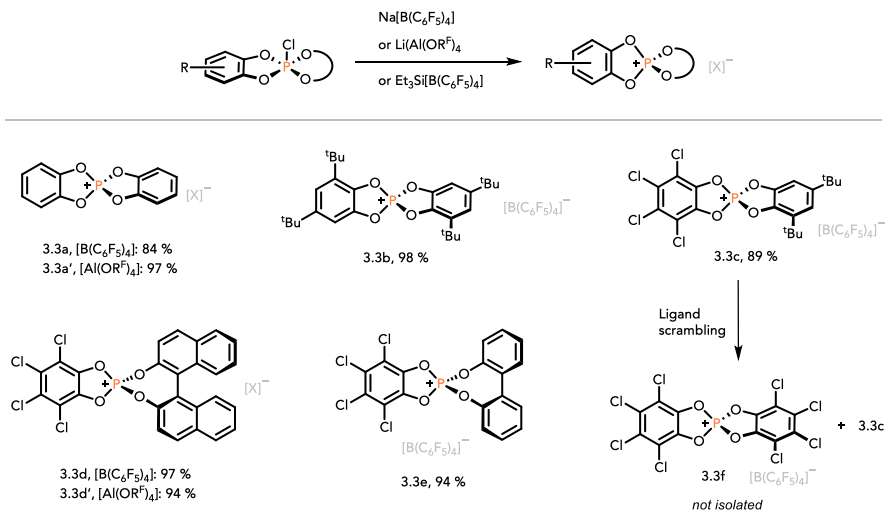
**Figure 3-2:** Synthesis of catecholato-phosphonium salts by chloride abstraction.

Nonetheless, it could also be prepared in excellent yields of 89 % by employing highly Lewis acidic silylium ions in benzene as stronger chloride abstraction reagent. All chlorophosphoranes 3.1a – e and phosphonium salts 3.3a – e syntheses could be executed easily on multi-gram scales. Solution-phase analysis by $^{31}$P NMR revealed significant downfield shifts of resonances from anywhere between -11.1 and -9.1 ppm for the chlorophosphoranes 3.1a – 3.1c to between 45.4 and 46.8 ppm for the bis(catecholato)phosphonium ions 3.3a – c. The shift was less pronounced for the mono-catecholato derivatives 3.3d and e, going from -13.0 and -15.5 to 27.5 and 25.3 ppm. Further comparison of the NMR chemical shifts to other known tetraoxo-phosphonium cations (< -17 ppm) highlights the pronounced deshielding effect by the catecholate-ligands.[14c, 82] Vapor diffusion of pentane into a concentrated solution of 3.3a in a toluene/chlorobenzene mixture led to deposition of singly crystals suitable for X-ray diffraction. As depicted in the thermal ellipsoid plot (fig. 3-3A), the spirophosphonium of 3.3a adopts a monomeric, donor-free structure with a tetrahedral arrangement around phosphorus that deviates slightly from ideality with a $\tau_4$-value of 0.92 (1 = ideal tetrahedron, 0 = square planar geometry).[83] A diffraction quality crystal could also be obtained for 3.3e (fig. 3-3B), and the refined molecular structure similarly contains a distorted tetrahedral phosphorus ($\tau_4$-value = 0.89).

41
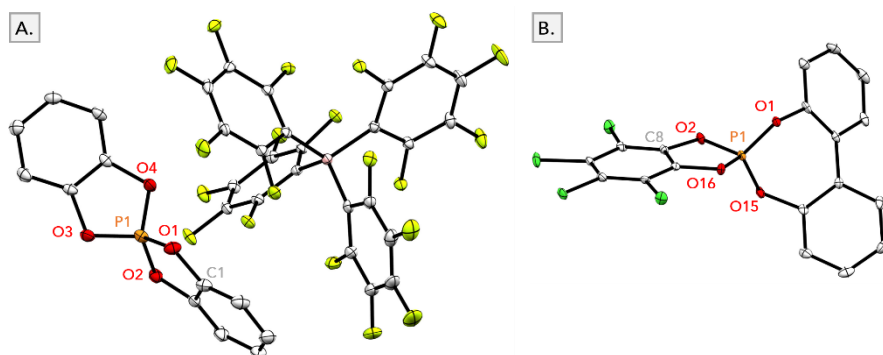
**Figure 3-3: A.** Solid-state structure of 3.3a and **B.** solid-state structure of 3.3e. Hydrogen atoms and the counteranion of 3.3e ($Al(OR^F)_4^-$) were omitted for clarity, ellipsoids are shown at the 30 % probability level. Selected bond lengths (Å) and angles (deg) for **3.3a**: d(P1−O1) = 1.5484(13), d(P1−O4) = 1.5563(12), d(C1−O1) = 1.430(2), ∠C1−O1−P1 = 108.05(11), ∠O1−P1−O2 = 101.4(7), ∠O1−P1−O4 = 114.94(7) and **3.3e**: d(P1−O1) = 1.527(4), d(P1−O2) = 1.569(4), d(C8−O2) = 1.416(6), ∠O1−P1−O15 = 111.1(2), ∠O2−P1−O16 = 101.00(19).

The most notable difference is the larger bite angle of the biphenolate substitutent (∠O1−P1−O15 = 111.1(2)°) compared to the catecholates (e.g. ∠O1−P1−O2 = 101.4(7)° for 3.3a). In contrast to the phosphonium ions, the isoelectronic group 14 congeners with silicon or germanium as central elements were not stable in the monomeric form in the absence of stabilization by donor molecules or sufficient steric shielding. The presence of both Lewis acidic central elements and Lewis basic oxygen atoms led to a strong tendency to di-, oligo- or polymerize.[19b] This tendency is largely suppressed by Coulombic repulsion of the positive charges for the phosphonium cations. Nonetheless, ligand scrambling could be observed for solutions of certain bis(catecholato)phosphonium salts. Over the course of several days, new products emerged after dissolution of 3.3c in $CD_2Cl_2$ with similar ^{31}P chemical shifts to 3.3c (fig. 3-4A). The major product was identified as the homoleptic bis(catecholato)phosphonium ion 3.3b. The minor products were putatively assigned as protode-*tert*-butylated products produced by retro-Friedel-Crafts alkylations under the highly acidic conditions. Concurrently, a colorless, crystalline solid precipitated slowly from the solution. The solid was tagged as $H(D)P(cat^{Cl})_2$ by X-ray diffraction (fig. 3-4C), the formal hydride(deuteride) abstraction product by 3.3f, indicating its intermediate formation as the other product of ligand scrambling that was not detected in solution. Monitoring the equimolar mixture of 3.3a and 3.3b by ^{31}P NMR showed the two discrete species
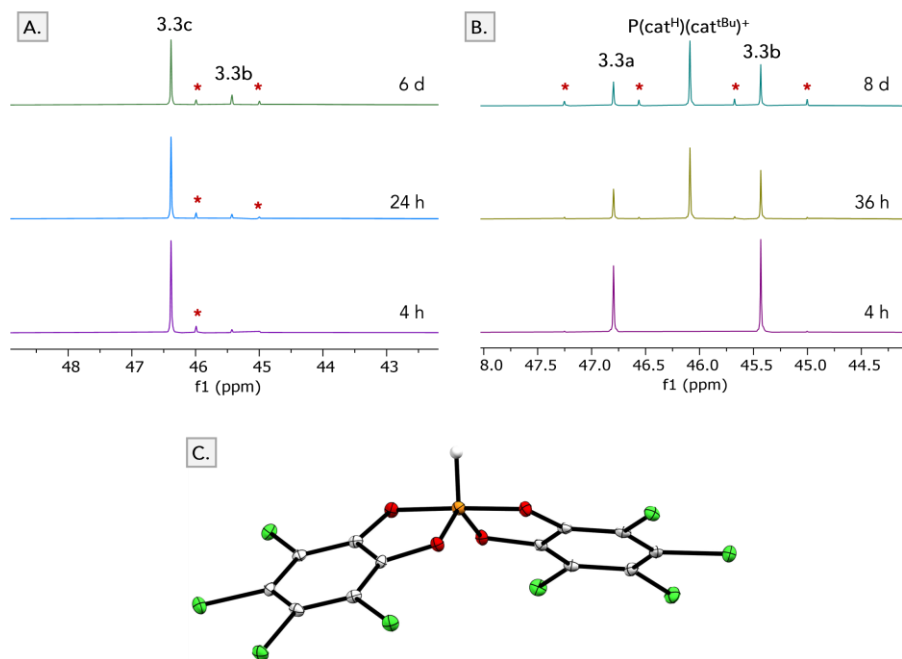
**Figure 3-4:** Stacked, abridged $^{31}P(^1H)$ NMR spectra at different time points in $CD_2Cl_2$ of **A.** a solution of 3.3c and **B.** an equimolar mixture of 3.3a and 3.3b. C. Solid-state structure of $H(D)P(cat^{Cl})_2$, ellipsoids shown at the 30 % probability level.

unreacted after one day at room temperature. After applying heat to the solution, however, resonances corresponding to the starting cations were slowly replaced by signals of several new tetracoordinate phosphonium species over the course of a few days (fig. 3-4B). Combined multinuclear NMR data were consistent with the formation of the unsymmetrical scrambling product $P(cat^H)(cat^{tBu})^+$ as the major component in solution. The reaction stabilized at a final 1:2:1 ratio matching a statistical distribution after approximately one and a half days. Further heating only increased the share of protode-*tert*-butylation side products. Single crystals obtained from the reaction mixture were analyzed by X-ray diffraction and revealed a mono-*tert*-butylated bis(catecholato)phosphonium ion, consolidating the hypothesis. Interestingly, no ligand scrambling was observed for 3.3d or 3.3e even at elevated temperature.

## 3.3 Assessment of Lewis Acidity

A measure of the effective Lewis acidity of the phosphonium cations was obtained by subjecting them to triethylphosphine oxide according to the Gutmann-Beckett (GB) method.[14] The emergence of two new doublets in the $^{31}P(^{1}H)$ NMR signaled the selective formation of the Lewis adducts in all cases. The relative phosphorus chemical shift of bound $OPEt_3$ followed the expected trend for compounds 3.3a – f, with a larger downfield shift correlating to the increasing electron-withdrawing nature of the substituents decorating the catecholate periphery. The catecholato-phosphonium ion compare favorably to other literature-known, strong Lewis acids, as they are ~1.3 to 1.4 times more Lewis acidic than Stephan's fluorophosphonium cation $[(C_6F_5)_3PF]^+$ and ~1.7 to 1.9 times more Lewis acidic than $B(C_6F_5)_3$ on the GB scale (fig. 3-5).[28, 84] The induced shifts also exceed those measured for silylium ions, Dielmanns' phosphorus dications or the borenium ion $[B(cat^H)]^+$, but are surpassed by the dication $[Cp^*P]^{2+}$.[20b, 31, 84] However, the values do forfeit some of their meaningfulness when comparing different classes of compounds as different steric and electronic effects come into play.[14c]
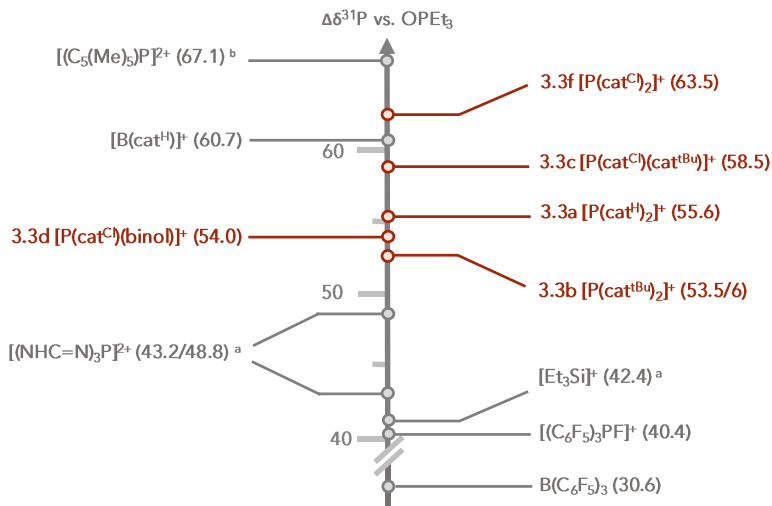


**Figure 3-5:** Scale of $^{31}P$ NMR chemical shifts of TEPO bound to various Lewis acids relative to free TEPO in $CD_2Cl_2$. [a] Measured in $C_6D_6$, [b] Measured in oDFB.

To augment the experimentally obtained effective Lewis acidities with global Lewis acidity values, fluoride (FIA) and hydride (HIA) ion affinities were computed isodesmically, both in the gas phase and with implicit solvation (table 3-1). The generated qualitative order for the Lewis acidities of catecholato-phosphonium ions generally agreed with the experimental one, except the order of 3.3d and 3.3b was switched depending on which ion affinity value was referenced. The predicted high anion affinities further underlined the extreme Lewis acidity at phosphorus bestowed by the catecholate ligands. All newly prepared compounds easily surpassed the Lewis acidity of the perfluorinated cation $[(C_6F_5)_3PF]^+$ without requiring any halogenation. The 'catecholate-effect' becomes obvious when comparing the anion affinities of 3.3c with 3.3d, exchanging the binaphthol ligand with another catecholate yields an increase of 62 and 46 kJ mol$^{-1}$ in FIA and HIA, respectively. Additionally, the benefits of oxygen-based ligands are emphasized by the significantly lowered affinity values of Teradas catecholato-phosphonium ion with a biphenyl ligand (entry 9).[27]

**Table 3-1:** Computed fluoride and hydride ion affinities at the DLPNO-CCSD(T)/def2-TZVPP//ωB97x-D3(BJ)/def2-TZVPP+COSMO-RS (CH₂Cl₂) level of theory corrected values are in parentheses). Values are given in kJ mol$^{-1}$. Values for entry 8 were obtained from the literature.[31]

| Entry | Compound | FIA (solv) | HIA (solv) |
|-------|----------|------------|------------|
| 1 | $[P(cat^H)_2]^+$ (**3.3a**) | 776 (303) | 825 (486) |
| 2 | $[P(cat^{tBu})_2]^+$ (**3.3b**) | 739 (292) | 787 (474) |
| 3 | $[P(cat^{tBu})(cat^{Cl})]^+$ (**3.3c**) | 792 (330) | 845 (517) |
| 4 | $[P(cat^{Cl})_2]^+$ (**3.3f**) | 845 (367) | 900 (559) |
| 5 | $[P(cat^{Cl})(binol)]^+$ (**3.3d**) | 734 (298) | 799 (487) |
| 6 | $[(C_6F_5)_3PF]^+$ | 717 (248) | 799 (461) |
| 7 | $[(SIMes)PFPh_2]^{2+}$ | 996 (314) | 1032 (485) |
| 8 | $[(NHC=N)_3P]^{2+}$ | 904 (318) | -- |
| 9 | $[(C_6H_4-C_6H_4)P(cat^H)]^+$ | 677 (222) | 725 (403) |
| 10 | $B(C_6F_5)_3$ | 445 (249) | 471 (401) |

To better compare Lewis acids of different charges, adding solvation corrections to the gas phase values is essential, as they dampen the effects of charge neutralization in the gas phase for Lewis acids of higher charges. This way, the cations 3.3c and 3.3f emerged as the strongest Lewis acids in terms of FIA and HIA and should rank among the strongest isolable phosphorus Lewis acids in the condensed phase.

Next, we sought to rationalize the extreme Lewis acidity of the bis(catecholato)phosphonium ions. Looking at the computed frontier orbitals of 3.3a, the lowest unoccupied molecular orbital (LUMO) has significant contributions at phosphorus and likely plays the role of acceptor orbital in interactions with Lewis bases (fig. 3-6). It can be viewed as the superposition of the antibonding P-O σ*-orbitals. By contrast, the highest occupied molecular orbital (HOMO) is mainly located on the two catecholates.



HOMO (-13.37 eV)   LUMO (-2.23 eV)
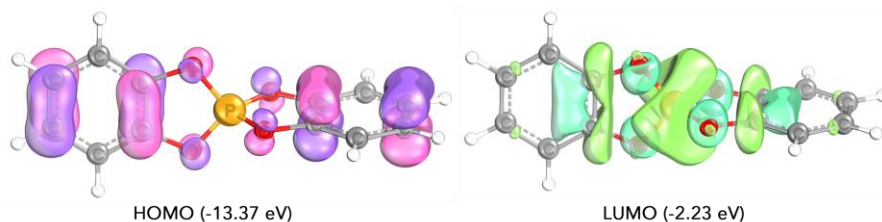
**Figure 3-6:** Frontier orbitals of 3.3a computed at the ωB97x-D3(BJ)/def2-TZVPP level of theory.

Fragmenting the fluoride adducts of 3.3a, $[P(OMe)_4]^+$ and $[P(OPh)_4]^+$ across the P-F bond and analyzing the interaction of the resulting parts by energy decomposition analysis (EDA) gave insights into the origins of the high Lewis acidities of catecholato-phosphonium ions (table 3-2).[85]

**Table 3-2:** Energy decomposition analysis results for phosphonium-fluoride interactions. [a] BP86-D3(BJ)/TZ2P, [b] interaction energy between the deformed fragments, [c] orbital energies of the parent cations and the GEI obtained at the ωB97x-D3(BJ)/def2-TZVPP level of theory.

| | $E_{Pauli}$ [a] | $E_{Coul}$ (%) [a] | $E_{Orb}$ (%) [a] | $E_{prep}$ [a] | $E_{int}$ [a/b] | $E_{LUMO}$ [eV] [c] | $\omega$ [eV] [c] |
|---|---|---|---|---|---|---|---|
| **FP(OMe)₄** | 1044 | -1235 (63) | 712 (36) | 265 | -910 | -1.40 | 2.63 |
| **FP(OPh)₄** | 1205 | -1230 (58) | 880 (42) | 256 | -914 | -1.69 | 2.32 |
| **FP(cat$^H$)₂** | 1593 | -1436 (57) | 1086 (43) | 129 | -937 | -2.23 | 2.73 |
| **F₂P(C₆F₅)₃** | 1156 | -1251 (61) | 799 (39) | 188 | -903 | -4.70 | 4.70 |

The total interaction energy ($E_{int}$) between the deformed cations (as in the adduct structure) and the fluoride ion increased continuously along the series [P(OMe)$_4$]$^+$ < [P(OPh)$_4$]$^+$ < 3.3a. The main contributor to this appeared to be the low preparation energy ($E_{prep}$) required to deform the cation [P(cat$^H$)]$^+$ to the structure it assumes in the adduct. This structural effect is brought about by the rigidity of the catecholate ligand and the 'angle strain' it enforces upon phosphorus by constraining the bond angles away from the ideal, 'relaxed' values. The strain is released upon coordination of a Lewis base, hence resulting in the substantial Lewis acidities of catecholate-based Lewis acids. This is likely why the Lewis acidities surpass those of the perfluorinated cation [(C$_6$F$_5$)$_3$PF]$^+$, despite its significantly lower LUMO energy and therefore higher GEI (tab. 3-2). The concept of 'strain-release' Lewis acidity was described by Denmark and mostly studied at silicon. It has resulted in several synthetic protocols for enantioselective reactions employing strained silanes as directing groups.[86] Enhanced electrophilicity was also reported for strained phosphate esters (see also chapter 1.4), as well as some germanium and aluminum compounds.[46, 82, 86b, 87]

The Lewis superacidity of herein prepared compounds was validated with competition experiments against SbF$_5$ and BCF. 3.3a, 3.3b, and 3.3d reacted rapidly in the presence of tetraphenylphosphonium hexafluoroantimonate under fluoride abstraction to the corresponding fluoride adducts and other byproducts due to follow-up reaction with generated SbF$_5$ (fig. 3-7(i)). Rapid hydride abstraction from [$^t$Bu$_3$PH][HB(C$_6$F$_5$)$_3$] by 3.3b to form HP(cat$^{tBu}$)$_2$ and BCF also confirmed the soft Lewis superacidity (HIA > BCF) (fig. 3-7(ii)).
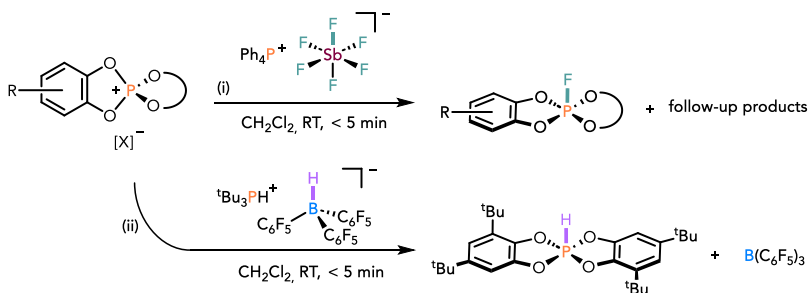


**Figure 3-7: (i)** Fluoride abstraction from [Ph$_4$P][SbF$_6$] by 3.3a, b and d. **(ii)** Hydride abstraction from [$^t$Bu$_3$P][HB(C$_6$F$_5$)$_3$] by 3.3b.

## 3.4 Catalysis

The serviceability of the phosphonium salts as catalysts was evaluated with several known Lewis acid-catalyzed reactions. Subjecting a solution of 1,1-diphenylethylene to 0.5 mol% of 3.3a led to rapid and selective Friedel-Crafts dimerization, with complete conversion (96 % isolated yield) to the dimer within 30 min reaction time (fig. 3-8A). By contrast, a close structural analog, the (perfluorophenoxy)-tris(pentafluorophenyl)phosphonium ion (containing 20 fluorides!) required 2.5 h (five-fold time) at 2 % (four-fold) catalyst loading for the same transformation.[88] The hydrosilylation of norbornene and hydrodeoxygenation of acetophenone using triethylsilane as reducing agent was catalyzed by 3.3a/b/d at low catalyst-loadings of 0.5 mol% within the time period it took to analyze the products by NMR (fig. 3-8B/C). Further lowering of catalyst loadings was not possible as catalyst decomposition through different pathways occurred under the reaction conditions (see chapter 3.5).
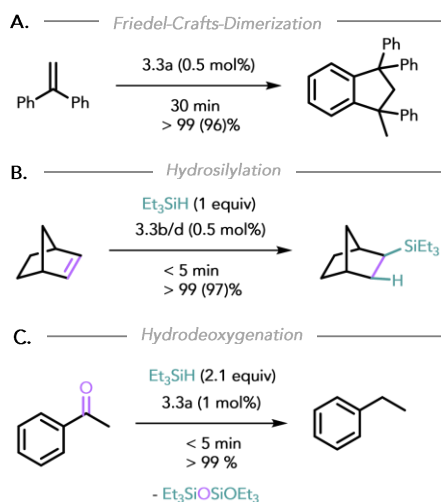


**Figure 3-8:** Examples of Lewis acid catalysis, including **A.** Friedel-Crafts dimerization of 1,1-diphenylethylene, **B.** hydrosilylation of norbornene and **C.** hydrodeoxygenation of acetophenone. NMR yields are given, with isolated yields in parentheses.

To broaden the catalytic portfolio of electrophilic phosphonium cations (EPCs) beyond the classical reduction chemistry, the application of 3.3a to the intramolecular carbonyl-olefin metathesis (COM) was probed, which critically

benefits from high Lewis acidity (fig. 3-9).[74, 89] Earlier seminal studies by Schindler and co-workers revealed iron(III)chloride as the best catalyst, leading to complete conversion of β-ketoester 3.4 to the cyclized product 3.5 in 24 h at 5 mol% catalyst loading. A few other Lewis acids have been identified as suitable catalysts since then, without any substantially improved performance compared to FeCl3.[90]
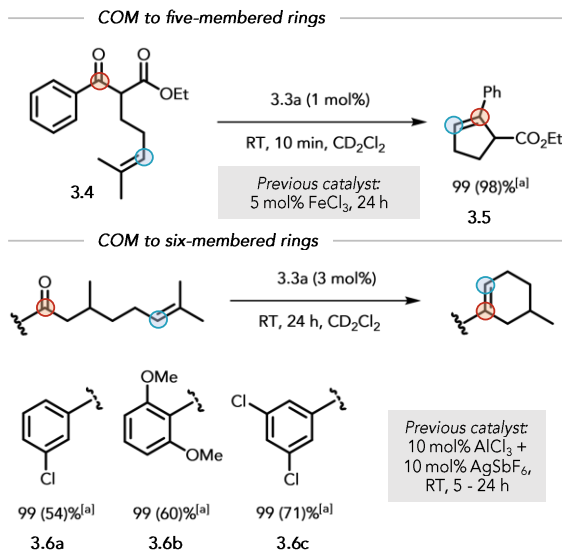


**Figure 3-9:** Examples of intramolecular carbonyl-olefin metathesis (COM) to five- and six-membered rings catalyzed by 3.3a. [a] Conversions (Yields) were determined by ^{1}H NMR spectroscopy against an internal standard.

Strikingly, utilizing 1 mol% of 3.3a, the ring-closing COM of 3.4 was complete within 10 min at room temperature. Even for the more challenging formation of six-membered rings, 3.3a showed good performance (fig. 3-9), and the presence of donating methoxy groups on the substrate was tolerated. Complete conversion of the substrate was observed, but the yields were limited due to competing pathways such as the carbonyl-ene reaction. The same observations were made in the initial report by Schindler *et al.*, which used a combination of 10 mol% AlCl3 and AgSbF6 to *in situ* generate the putative bimetallic ion pair 'AlCl2+SbF6-' to catalyze this reaction.[89b] Noteworthily, with the substance class of catecholato-phosphonium salts, a properly defined Lewis superacidic system is now at hand that permits well-defined ligand modifications to address selectivity and potential desymmetrization

reactions with chiral derivatives in the future.

## 3.5 Phosphorus-Ligand Cooperative Reactivity

### 3.5.1 Reaction with Silanes

To better understand the catalyst deactivation pathways that placed limits on the catalyst loadings despite the high turnover frequencies, stoichiometric reactions with different reagents were studied. The reaction of the phosphonium salt 3.3a with different tertiary silanes rapidly produced new P(V)-H species with decent selectivities (fig. 3-10). For instance, the reaction with $^tBuMe_2SiH$ afforded a major product at $\delta(^{31}P) = 35.9$ ppm ($J_{PH} = 945.7$ Hz). The combined multinuclear NMR data identified it as product 3.7a of the silane addition across one of the P-O bonds. The transformation is reminiscent of the B-H bond activation of HBPin by the NNN-P(III) chelate from Radosevich.[91]
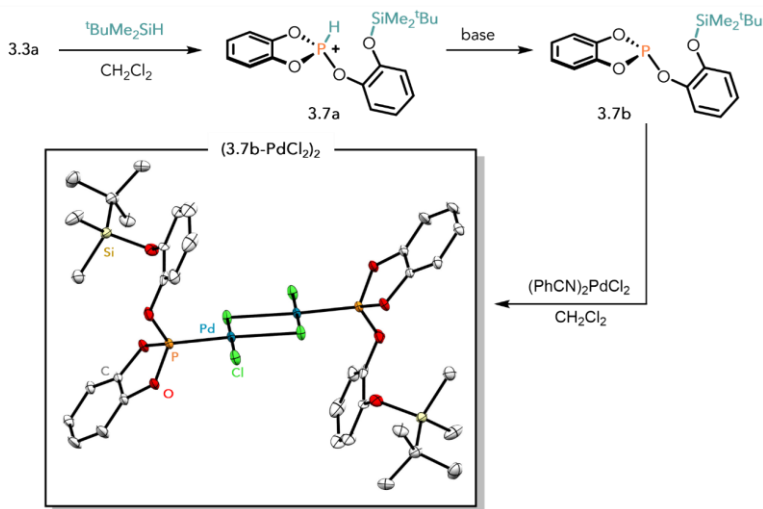


**Figure 3-10:** Reaction of 3.3a with silane, as well as follow-up reactivity to the Pd-complex (3.7b-PdCl$_2$)$_2$ (The solid-state structure is shown with ellipsoids at the 30 % level, hydrogen atoms were omitted for clarity).

The silane hydrogen umpolung to an acidic proton facilitated deprotonation with a suitable base such as 2,6-di-*tert*-butylpyridine to furnish phosphite 3.7b, which was isolated as a colorless oil. The solid-state structure to corroborate the proposed

path to 3.7b was obtained after complexation with (PhCN)$_2$PdCl$_2$ and crystallization of the dinuclear palladium-phosphite complex (3.7b-PdCl$_2$)$_2$ (fig. 3-10).

The mechanism of the phosphorus-ligand cooperative Si-H bond cleavage was interrogated using density functional theory (DFT) at the DSD-BLYP-D3(BJ)/def2-QZVPP+SMD(CH$_2$Cl$_2$)//r$^2$-SCAN-3c level of theory.[70b, 92] Upon approach of 3.3a by trimethylsilane as model substrate, one catecholate moiety twisted away so that the silane could be accommodated to form the square-pyramidal, intermediate σ-complex IM-I (fig. 3-11). Ensuing silylium ion transfer to a catecholate oxygen proceeded through the low-lying transition state TS-II to deliver the final product. The partial alleviation of ring-strain through opening of the phosphorus-catecholate pentacycle, combined with the formation of a strong Si-O bond confers high thermodynamic stability of the adduct relative to the reactants.
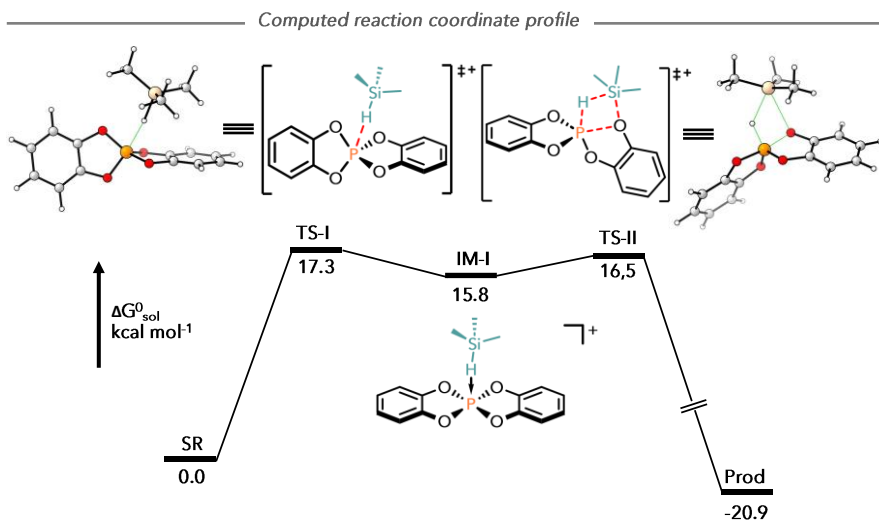


Figure 3-11: Computed reaction coordinate profile for the addition of trimethylsilane to 3.3a.

## 3.5.2    Reaction with Heteroarenes

Encouraged by the high reactivity towards Si-H bonds, we investigated the potential of the phosphonium ions for the activation of more inert C-H bonds. Consequently, the addition of 2-methylthiophene to phosphonium salt 3.3d in CD$_2$Cl$_2$ was

monitored by $^{31}$P NMR spectroscopy at ambient temperature. Over the course of one day, the signal of 3.3d was consumed and replaced by a doublet of a doublet
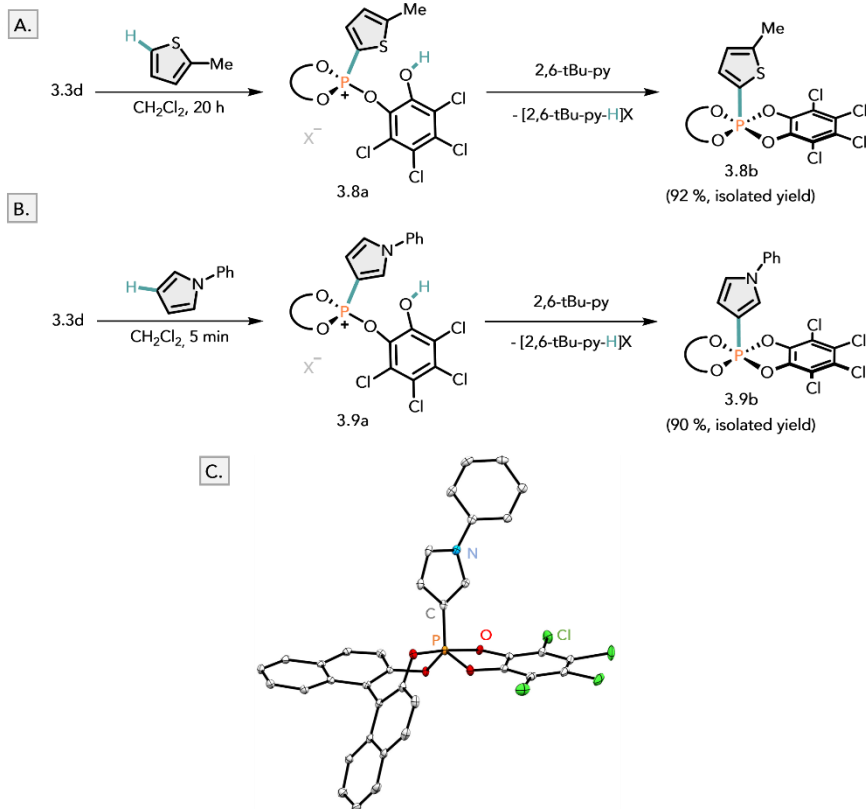


**Figure 3-12:** Phosphorylation of **A.** 2-methylthiophene and **B.** 1-phenylpyrrole by C-H activation with 3.3d. **C.** Solid-state structure of the reaction product 3.9b, thermal ellipsoids are displayed at 30 % probability, hydrogen atoms were omitted for clarity.

at 35.3 ppm, still within the region corresponding to tetracoordinate phosphonium ions. Correlations of this signal to all thiophene protons were detected in the $^{1}$H-$^{31}$P HMBC experiment, as well as a new $^{13}$C NMR doublet with a large coupling constant ($^{1}J_{PC}$ = 235.4 Hz). Additionally, a new singlet appeared in the proton NMR at 6.36 ppm without $^{13}$C HSQC or $^{31}$P HMBC correlations. Together with the broad vibrational band that emerged in the IR spectrum around 3504 cm$^{-1}$, the presence of a hydroxy-group was inferred.

Overall, the spectral data were consistent with the product 3.8a that resulted from C(sp$^2$)-H bond cleavage of 2-methylthiophene and addition across the P-O bond of 3.3d (fig. 3-12A). An analogous product was observed in the reaction with 1-phenylpyrrole, but in a much shorter time frame and with C-H activation at the 3-position to give 3.9a (fig. 3-12B). The reaction transformed the non-acidic CH bonds in the heteroarenes into highly acidic OH bonds that could be deprotonated with bases as weak as 2,6-di-*tert*-butylpyridine, *N,N*-diisopropylbenzamide or even a chloride ion to give the phosphorylated heteroarenes in high isolated yields.
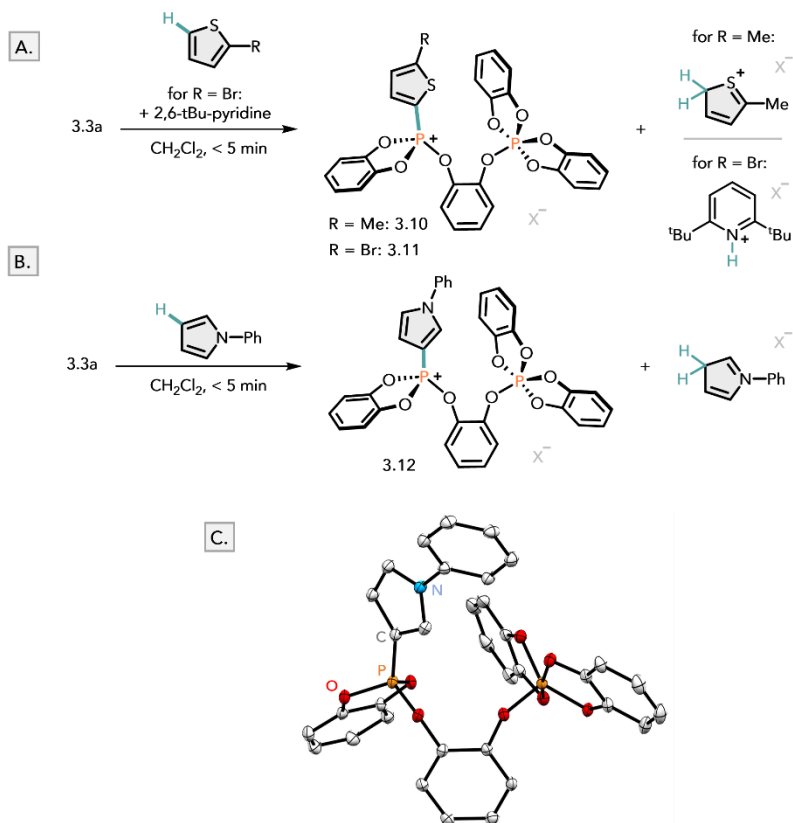


**Figure 3-13:** Reactions of 3.3a with **A.** 2-methylthiophene and 2-bromothiophene and **B.** 1-phenylpyrrole. **C.** Solid-state structure of the reaction product 3.12, thermal ellipsoids are displayed at 30 % probability, hydrogen atoms and the counterion were omitted for clarity.

Divergent outcomes were detected after mixing the heteroarenes with 3.3a, as

clean formation of two new resonances were observed in the $^{31}P(^{1}H)$ NMR in a 1:1 ratio. The chemical shifts appeared around 50 ppm and -30 ppm, in the regions for tetracoordinate phosphonium ions and pentacoordinate phosphorus species, respectively. The spectral data was in line with products 3.10 and 3.12 (fig. 3-13). The $^{1}H$ NMR spectrum also showed signals consistent with the protonated heteroarenes.[14c]

The molecular structures insinuated by the combined multinuclear NMR data were confirmed by the solid-state structure of the reaction product of 3.3a and 1-phenylpyrrole (fig. 3-13C). The divergent outcomes with 3.3a and 3.3d were attributed to differences in steric bulk and Lewis acidity, enabling a second unit of 3.3a to coordinate to an intermediately formed C-H activation product of the type 3.8a or 3.9a. The generated hydroxy group becomes a Brønsted acid of sufficient strength to be deprotonated by the remaining heteroarene in solution to give products 3.10 and 3.12. With less nucleophilic 2-bromothiophene, a selective reaction was only achieved in the presence of an exogenous base.

### 3.5.2.1 Mechanism

The mechanism for the inceptive $C(sp^2)$-H deprotonation step was then analyzed computationally at the DLPNO-CCSD(T)/def2-TZVPP+SMD(CH$_2$Cl$_2$)//PBEh-3c level of theory (fig. 3-14).[70b, 92c, 93] The sequence is initiated by electrophilic addition of the phosphonium ion to the arene, forming a Wheland-type intermediate INT-I via the transition state TS-I. A subsequent intramolecular deprotonation step transferring the acidified proton to one of the catecholate-oxygen atoms gives the reaction products identified in the experiment (e.g. 3.8b, fig. 3-12). However, the calculated barrier heights of TS-II (31.8 and 36.3 kcal mol$^{-1}$ for 1-phenylpyrrole and 2-methylthiophene, respectively) do not agree well with the observed reactivity at room temperature. Potential involvement of a second heteroarene molecule to lower TS-II would be conceivable. Another explanation for the disagreement between experimental and theoretical reaction kinetics could involve tunneling of the transferred proton through the barrier. Qualitatively, the lower barriers for the deprotonation of pyrrole compared to thiophene agreed with experimental observations.
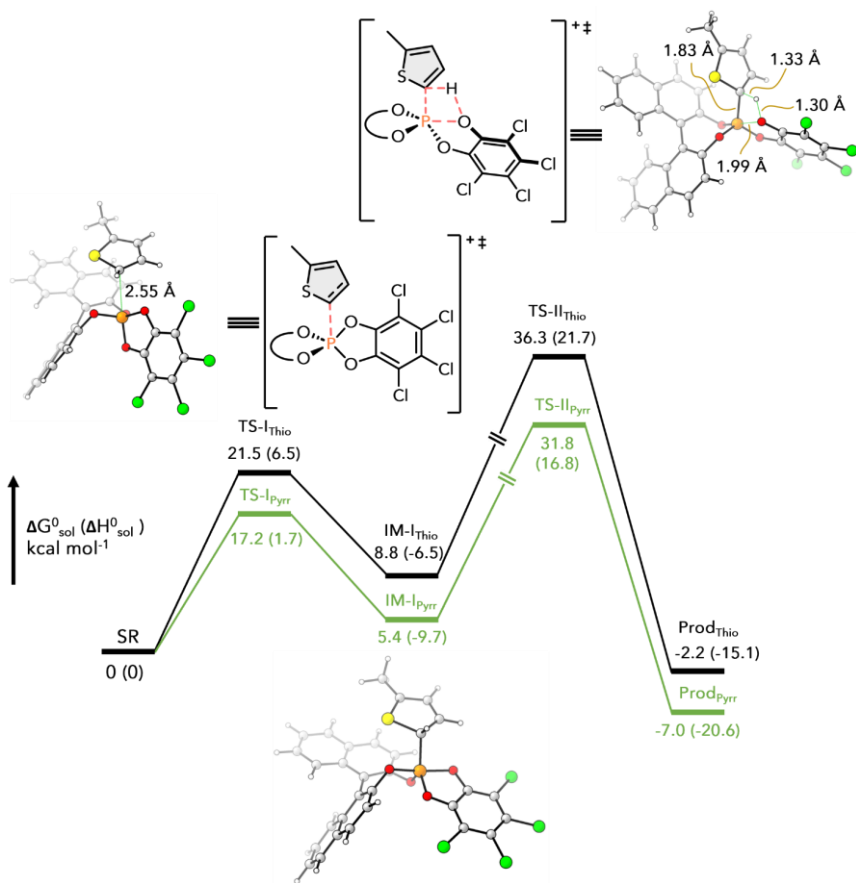
**Figure 3-14:** Computed free energy profile for the reaction of 3.3d with 2-methylthiophene (black) and 1-phenylpyrrole (green).

### 3.5.3 Reaction with Alkynes and Alkenes

Next, we explored the reactivity of catecholato-phosphonium ions toward unsaturated hydrocarbons by treatment of 3.3d with phenylacetylene. Immediate and intense coloration of the mixture occurred, and the phosphorus resonance of 3.3d was quantitatively replaced by two new doublets at 56.3 ($J_{PH}$ = 14.0 Hz) and 39.0 ppm ($J_{PH}$ = 7.5 Hz) in the $^{31}$P NMR spectrum. The combined multinuclear NMR

data were consistent with the regioisomeric products 3.13 and 3.14 of alkyne phosphaalkoxylation (fig. 3-15).
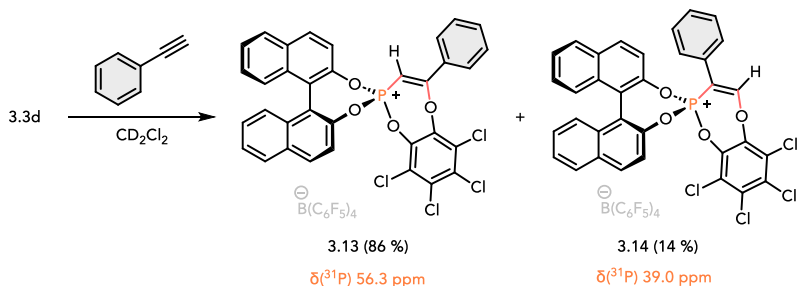


**Figure 3-15:** Reaction of phosphonium salt 3.3d with phenylacetylene.

The major product aligned with expectations for an electrophilic mechanism, due in part to better stabilization of the partial positive charge at the benzylic position after attack of the phosphorus at the terminal alkyne carbon.
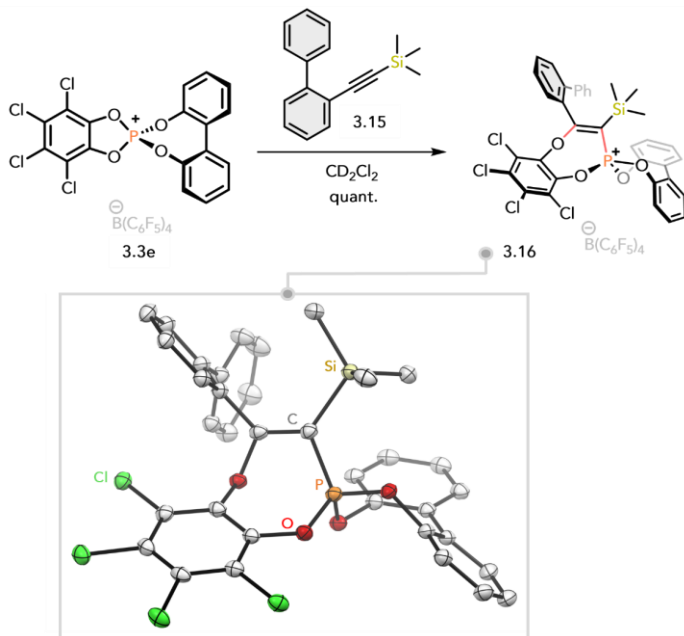


**Figure 3-16:** Reaction of 3.3e with an internal alkyne to give the addition product 3.16, as well as the solid-state structure thereof. The thermal ellipsoids are displayed at 30 % probability, hydrogen atoms and the counterion were omitted for clarity.

In similar fashion, the reaction of 3.3e with internal alkyne 3.15 proceeded cleanly to a single new product with spectral data in alignment with phosphaalkoxylation of the alkyne (fig. 3-16). The molecular structure of the product was corroborated by X-ray diffraction of suitable crystals that grew after cooling the reaction mixture to -40 °C. The regioselectivity of the alkyne addition followed the same logic as the previous one with the product 3.16 formed *via* the transition state with benzylic stabilization of the partial positive charge at carbon.

Parallel experiments monitoring the addition of norbornene to 3.3a or 3.3d proceeded within minutes under clean formation of new phosphorus-containing products in the $^{31}$P NMR, although an excess of substrate (6 equiv) was required to fully convert the starting phosphonium ions (fig. 3-17). In $^1$H-$^{31}$P HMBC experiments, the new phosphorus resonances showed correlations to protons in the aliphatic region, in line with phosphorus-ligand cooperative addition of the alkene.
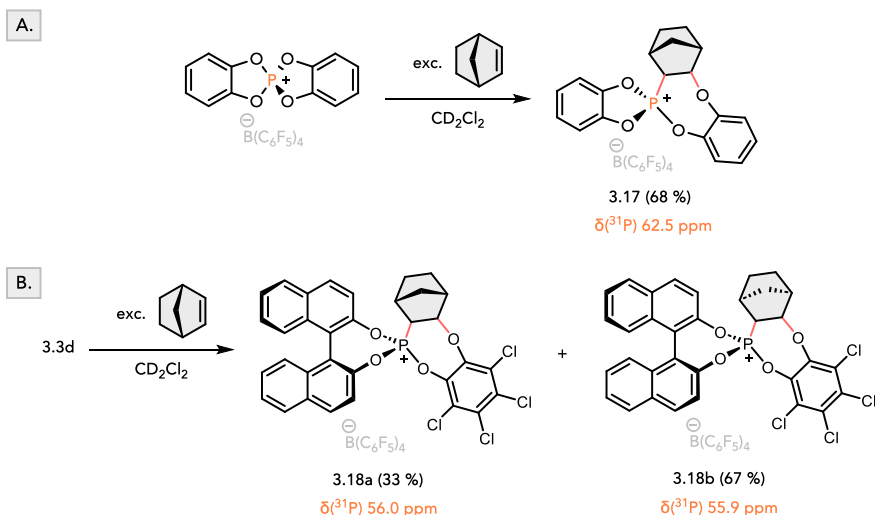


**Figure 3-17:** Reactions with norbornene by **A.** phosphonium salt 3.3a and **B.** 3.3d.

While for the reaction with 3.3a only a single product signal emerged in the $^{31}$P NMR, two closely situated singlets appeared with 3.3d at 56.0 and 55.9 ppm in approximately a 1:2 ratio. They were tentatively assigned to the two possible diastereomers arising from addition of norbornene faces to the chiral phosphonium ion with preferred formation of 3.18b over 3.18a due to less steric clashing with the

binaphthol backbone. The ability to discriminate the two faces of norbornene by 3.3d bodes well for potential future endeavors in enantioselective bond activation and catalysis.

## 3.6    Frustrated Lewis Pair Chemistry

Phosphorus compounds have primarily played the role of the Lewis base in frustrated Lewis pairs (FLPs), while their potential as Lewis acid components is much less explored.[94] Therefore, we sought to study the capacity of bis(catecholato)-phosphonium salts to play the role of Lewis acids for FLP-type chemistry. We initiated our investigation by trying to find a suitable, sterically encumbered Lewis bases capable of forming stable, frustrated Lewis pairs with bis(catecholato)-phosphonium ions 3.3a, 3.3b or 3.3d in solution. The experimental results we obtained by evaluating numerous candidate bases could be grouped broadly into three categories of reaction outcomes (fig. 3-18).

In the first case, unselective decomposition occurred in solution. Insufficient steric bulk of the Lewis base resulted in coordination to the Lewis acid (observed by NMR) and unselective follow-up reactions (e.g., *via* PLC, proposed for the piperidines and P($^t$Bu)$_3$) ensued. Other destructive pathways are also conceivable, for instance the reaction with trimesityl phosphine produced a deep purple colored solution, which suggested radical involvement perhaps through single-electron transfer to generate the unstable frustrated radical pair.[95] Sterically even less hindered Lewis bases afforded stable Lewis pairs, and the evaluated bidentate Lewis bases also coordinated *via* both donor sites. Only some of the 2,6-disubstituted pyridines were stable in the presence of the catecholato-phosphonium ions without coordination or decomposition, although broadened $^1$H and $^{31}$P NMR resonances in the presence of lutidine indicated a dynamic coordination equilibrium in solution. The frustrated Lewis pairs however were unreactive toward small molecules such as dihydrogen or carbon dioxide under the tested reaction condition. A possible explanation could be the tetrahedral coordination sphere at phosphorus in the relaxed state with relatively high lying LUMOs, as well as a barrier required to distort the Lewis acids towards the structure they assume upon Lewis base coordination (see the mechanism in fig. 3-14). The difficulties in dihydrogen activation with structurally related tetrahedral silanes were also previously reported in our group, although careful evaluation of reaction conditions and Lewis bases led to successful

dihydrogen activation in the end.[96] Another important consideration is that once the steric congestion becomes too much, the encounter complex may not be formed.
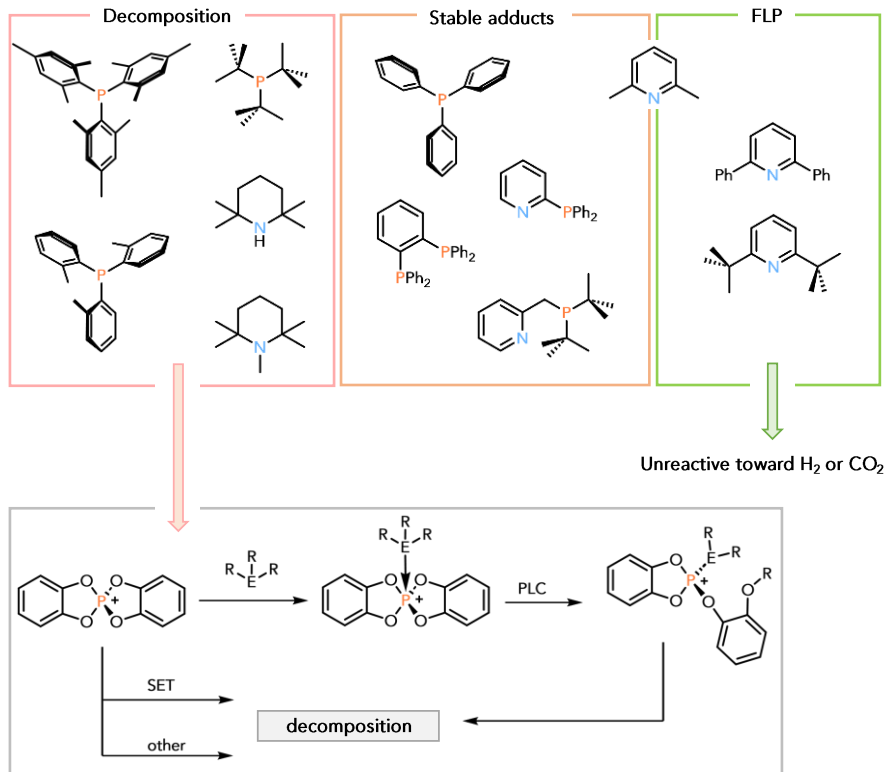


**Figure 3-18:** Summary of the frustrated Lewis pair chemistry attempted with the phosphonium salts 3.3a, 3.3b and 3.3c.

## 3.7   Conclusion

The first preparation and isolation of bis(catecholato)phosphonium salts, as well as chiral mono(catecholato)phosphonium salts were disclosed in this chapter. Computed anion affinities and experimental Gutmann-Beckett shifts assign exceptional Lewis acidities to the compounds without requiring perhalogenated substituents or multiple charges. Instead, structural constraint imparted by the rigid

catecholate ligand and resulting low preparation energies was identified by energy decomposition analysis as key contributor to the Lewis superacidity. These characteristics translated to high catalytic activity in several Lewis acid catalyzed reactions, such as the hydrosilylation of alkenes, hydrodeoxygenation of ketones, or carbonyl-olefin metathesis. The proximity of electrophilic phosphorus and nucleophilic oxygen led to new modes of reactivity for bond activation by phosphorus-ligand cooperativity. This way, the uncatalyzed, metal-free phosphorylation of heteroarenes by $C(sp^2)$-H activation was achieved and the mechanism scrutinized with computational methods. Selectivity complementary to the transition metals was granted this way, as demonstrated in the selective CH activation of 2-bromothiophene. Furthermore, cooperative addition of alkynes, alkenes, and silanes to the phosphonium ions was observed.

# Chapter 4

## Lewis Acidity and Phosphorus-Ligand-Cooperativity of Bis(amidophenolato)phosphonium Ions

## 4.1  Introduction

The previous chapter introduced structural constraint enforced by rigid catecholate-ligands as a way to generate highly Lewis acidic phosphonium salts active in catalysis and phosphorus-ligand cooperative activation of inert bonds. The exchange of catecholates by amidophenolates was envisioned to facilitate further control over the electronic and steric profile of the phosphonium ions to alter both the Lewis acidity and phosphorus-ligand cooperative reactivity (fig. 4-1A).[97]
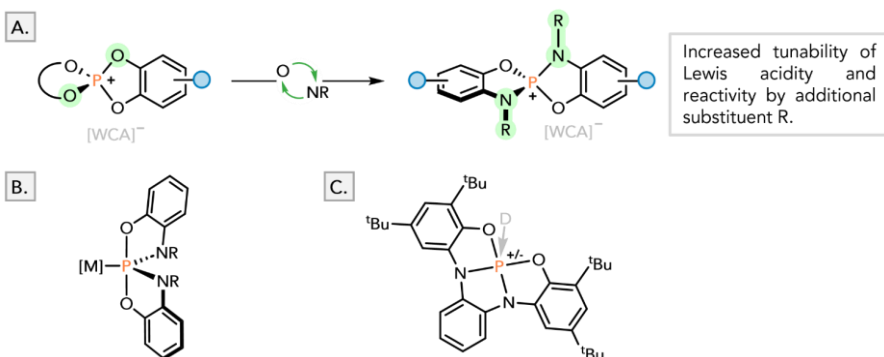


Figure 4-1: **A.** Strategical changes to phosphonium ions in this chapter. **B.** Structures of metallophosphoranes and **C.** structurally contrained phosphorus compounds based on amidophenolates.

Prior examples of phosphorus compounds ligated by amidophenolates were reported as substituents in organo-[47a, 98] and metallophosphoranes[99] or investigated for their potential as weakly coordinating anions.[100] A tethered bisamidophenolato scaffold was explored by Dobrovetsky and Alcarazo as ligand for structurally constrained phosphorus compounds with unique reactivity patterns.[101] Studies on the donor-free, tetracoordinate bis(amidophenolato)phosphonium ions however were without precedent prior to this work.

## 4.2   Synthesis

The aminophenols 4.1a and 4.1b were synthesized according to literature-known procedures in one or two steps starting from commercially available precursors at multi-gram scales.[100, 102] The synthetic procedure to access perfluorinated aminophenol 4.1c was recently developed in our group for the preparation of strong and soluble silicon-based Lewis acids.[103] The three-step procedure starts from nucleophilic substitution at hexafluorobenzene with $LiNH_2$, followed by conversion with propylene oxide and deprotection with *in situ* generated $AlI_3$. The installation of phosphorus at 4.1a – 4.1c proceeded cleanly *via* a condensation reaction with $PCl_5$, furnishing the chlorophosphoranes 4.2a – 4.2c in good to excellent yields after workup (fig. 4-2). In line with the lower E-H (E = O, N) acidities of 4.1a/b compared to 4.1c, harsher conditions were required to drive these two reactions to completion. Chloride abstraction from 4.2a and 4.2b with $Li[Al(OR^F)_4]$ ($R^F$ = $C(CF_3)_3$) finally gave the target bis(amidophenolato)phosphonium salts 4.3a and 4.3b in excellent yields, but no reaction of 4.2c occurred under the same conditions. For the successful dechlorination of 4.2c, $Et_3Si[B(C_6F_5)_4]$ had to be used in a weakly coordinating solvent such as chlorobenzene, as the reaction did not work in toluene or benzene. The fact that the reaction conditions employed to prepare the strongest isolable bis(catecholato)phosphonium ion 3.3c had failed to produce 4.3c already implied superior chloride ion affinity. All phosphonium salts could be prepared at multi-gram scales and the solids stored indefinitely without decomposition under an inert atmosphere. In contrast to 4.3a and 4.3b, 4.3c was only poorly soluble in dichloromethane but possessed good solubility in *o*-difluorobenzene. $^{31}P$ NMR analysis of the phosphonium ion series showed a downfield shift of resonances compliant with increased deshielding as the degree of fluorination in the ligand

backbone advanced.
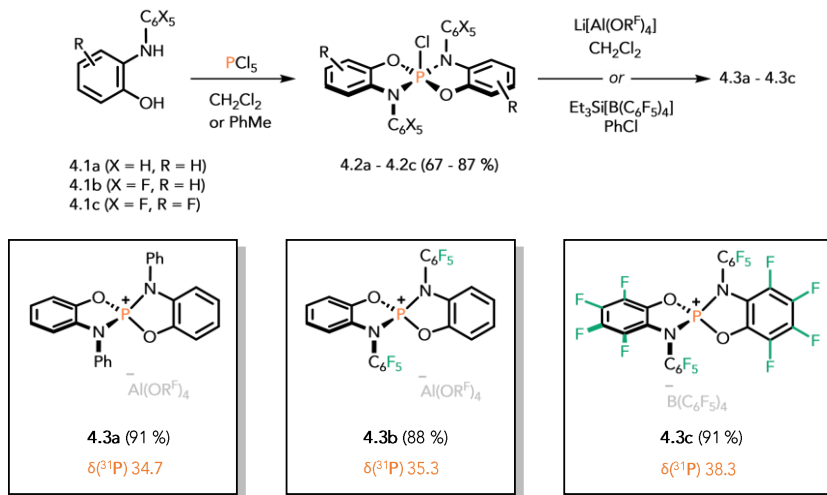


**Figure 4-2:** Synthesis of amidophenolato-phosphonium salts 4.3a – 4.3c. NMR chemical shifts (orange) are given in ppm. $R^F$ = $OC(CF_3)_3$.

Diffraction quality single crystals of 4.3a – 4.3c and 4.2c deposited from concentrated solutions in dichloromethane or toluene after vapor diffusion of pentane and cooling to -40 °C (fig. 4-3). The thermal ellipsoid plot of chlorophosphorane 4.2c depicts a distorted trigonal bipyramid created by the substituents around phosphorus, with a topology parameter of 0.72 (1 = ideal trigonal bipyramid, 0 = ideal square pyramid).[104] The phosphonium ions all adopted distorted, tetrahedral structures similar to the bis(catecholato)phosphonium ions and were otherwise devoid of any particularly notable structural features. No clear trends were discernable with increasing fluorination of the ligand periphery within the series 4.3 – 4.3c, aside from the more noticeable stacking of -$C_6F_5$ groups of 4.3b and 4.3c compared to the phenyl groups of 4.3a. The planes constructed by the aromatic carbon atoms are angled relative to each other at 5.4°, 16.3° and 24.6° for 4.3a, b and c, respectively. The favored coplanar orientation of the pentafluorophenyl groups is credited to the increasing dispersion interactions by the heavier fluorine atoms, as observed in similar systems.[105]
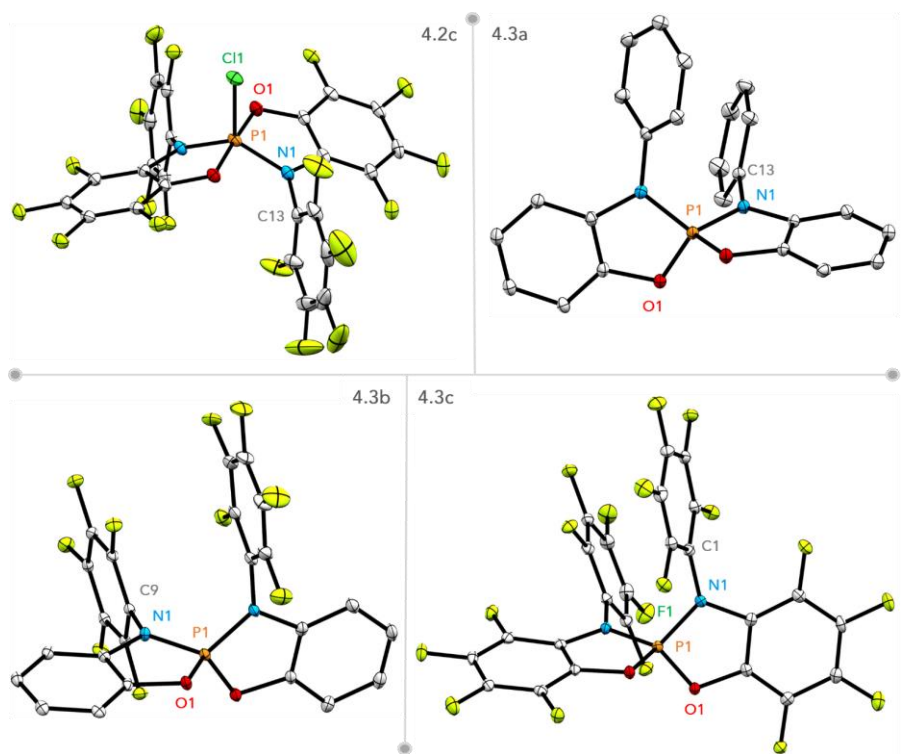
**Figure 4-3:** Solid-state structures of phosphonium ions 4.3a, 4.3b and 4.3c, as well as chlorophosphorane 4.2c. Ellipsoids are displayed at 30% probability, hydrogen atoms and counteranions were omitted for clarity. Selected bond lengths [Å] and angles [deg]: 3a: d(P1-N1) = 1.6266(13), d(P1-O1) = 1.5741(12), d(N1-C13) = 1.450(2), ∠O1-P1-N1 = 97.90(6); 3b: d(P1-N1) = 1.630(2), d(P1-O1) = 1.572(2), d(N1-C9) = 1.425(4), ∠O1-P1-N1 = 97.42(12); 3c: d(P1-N1) = 1.6304(17), d(P1-O1) = 1.5683(15), d(N1-C1) = 1.438(3), ∠O1-P1-N1 = 97.93(8).

## 4.3   Lewis Acidity Assessment

The effective Lewis acidity of the phosphonium ions was then gauged using the Gutmann-Beckett method.[14] Selective adduct formation was detected upon exposure of the phosphonium salts to triethylphosphine oxide in $CD_2Cl_2$ by emergence of two new sets of doublets in the $^{31}P(^1H)$ NMR spectra. The considerable downfield shifts relative to free $OPEt_3$ indicated extreme Lewis acidity and were comparable to those measured for the catecholato-phosphonium ions

(fig. 4-4). However, the shifts cover a greater range, which is consistent with more direct control of the Lewis acidity through the amidophenaloates. Noteworthily, the four fluorine atoms added to the amidophenolate ring impact the Lewis acidity more (7.8 ppm shift) than the five fluorine atoms attached to the *N*-phenyl ring (5.1 ppm shift). The same trend can be noted for effects of fluorination on the $^{31}$P NMR chemical shifts of compounds 4.3a – 4.3c (fig. 4-2).
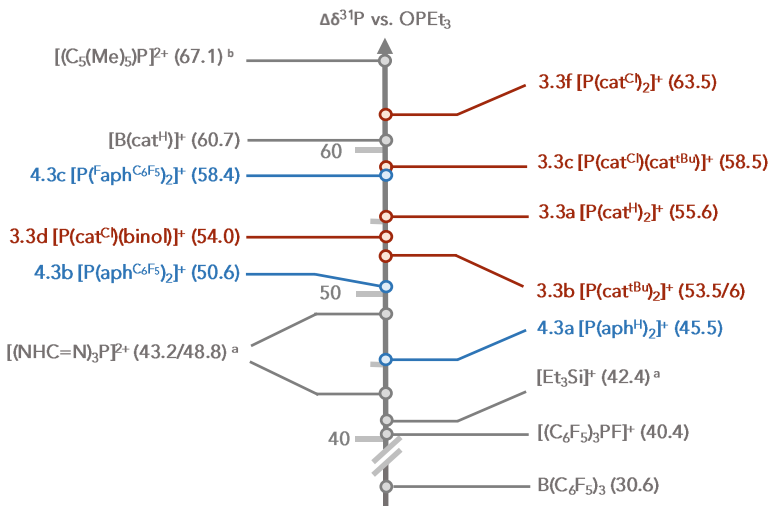


**Figure 4-4:** Scale of $^{31}$P NMR chemical shifts of OPEt$_3$ bound to various Lewis acids relative to free OPEt$_3$ in CD$_2$Cl$_2$. [a] Measured in C$_6$D$_6$, [b] Measured in oDFB.

The computed fluoride and hydride ion affinities both in the gas phase and with implicit solvation (CH$_2$Cl$_2$) qualitatively reproduced the trends set by the GB measurements and confirmed the extreme Lewis acidity of the bis(amidophenolato)phosphonium ions (table 4-1). The perfluorinated derivative 4.3c boasts the highest FIA and HIA of all computed, isolable phosphonium ions both in solution and in the gas phase. This does conflict with the lower GB shift compared to 3.3c and likely comes as the result of the increased steric bulk of 4.3c conferred by the amidophenolate substituents. The same reasoning applies to the observation of higher computed anion affinities of 4.3b compared to 3.3b, but lower experimental GB shifts.

**Table 4-1:** Computed fluoride and hydride ion affinities at the DLPNO-CCSD(T)/def2-TZVPP//ωB97X-D3(BJ)/def2-TZVPP (COSMO-RS) level of theory, solvent corrected values are in parentheses. Entries 1-3, 7-8 obtained from reference (see chapter 3.3).[106]

| Entry | Compound | FIA [kJmol$^{-1}$] | HIA [kJmol$^{-1}$] |
|:-----:|:--------:|:------------------:|:------------------:|
| 1 | [P(cat$^H$)$_2$]$^+$ | 776 (303) | 825 (486) |
| 2 | [P(cat$^{tBu}$)$_2$]$^+$ | 739 (292) | 787 (474) |
| 3 | [P(cat$^{tBu}$)(cat$^{Cl}$)]$^+$ | 792 (330) | 845 (517) |
| 4 | [P(aph$^{Ph}$)$_2$]$^+$ 4.3a | 687 (245) | 743 (430) |
| 5 | [P(aph$^{C6F5}$)$_2$]$^+$ 4.3b | 750 (296) | 808 (485) |
| 6 | [P($^F$aph$^{C6F5}$)$_2$]$^+$ 4.3c | 825 (352) | 890 (550) |
| 7 | [(C$_6$F$_5$)$_3$PF]$^+$ | 717 (248) | 799 (461) |
| 8 | B(C$_6$F$_5$)$_3$ | 445 (249) | 471 (401) |

## 4.4 Phosphorus-Ligand Cooperative Substrate Activation

### 4.4.1 Reaction with Silanes

Next, to evaluate how the structural differences of 4.3a – 4.3c relative to the catecholato-phosphoniums ions impact their phosphorus-ligand cooperative (PLC) reactivity, we started by monitoring their reactions with tertiary silanes. Treatment of 4.3a – 4.3c with triethylsilane in dichloromethane-$d_2$ gave no reaction for 4.3a, but immediate consumption of 4.3b and 4.3c was observed by $^{31}$P NMR. The phosphonium ion of 4.3b showed an unselective reaction to multiple phosphorus-containing products. By contrast, the reaction with 4.3c and triethylsilane proceeded cleanly to a single product represented by a doublet in the $^{31}$P NMR (fig. 4-5). The large coupling constant ($J_{PH}$ = 928.7 Hz) and the chemical shift at $\delta$($^{31}$P) = -49.6 ppm were consistent with a pentacoordinate P(V)-H species produced by hydride transfer from the silane to the phosphonium ion. Analysis of single crystals grown from the reaction mixture at -40 °C by SCXRD confirmed the hydride abstraction product 4.4. The thermodynamic feasibility of this reaction path was corroborated by computations, as the HIA of 4.3c in solution surpassed that of Et$_3$Si$^+$

by 25 kJ mol⁻¹. The triethylsilylium ion that is formed as byproduct was unstable in dichloromethane and decomposed into several different species, including the chloro- and fluorosilanes by halide abstraction from solvent molecules or the fluorinated anion. The outcomes of the reactions with silanes differed greatly from the ligand-assisted silane addition observed with the catecholato-phosphonium salts (see chapter 3.5.1).
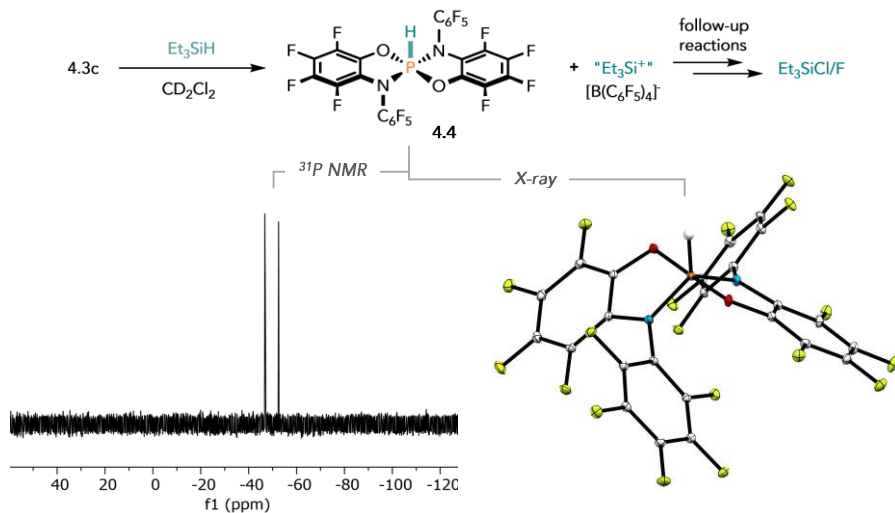


**Figure 4-5:** Reaction of 4.3c with triethylsilane, including an abridged ³¹P NMR spectrum and solid-state structure obtained from the reaction solution. Thermal ellipsoids are displayed at 30 % probability.

## 4.4.2    Reaction with Alkynes

To continue the comparison of amidophenolato- and catecholato- ligands on cooperative phosphonium ion reactivity, investigations were undertaken with alkynes as substrates. Upon treatment of 4.3c with diphenylacetylene in CD₂Cl₂, the ³¹P NMR resonance of 4.3c was rapidly and selectively replaced by a new singlet at 26.2 ppm (fig. 4-6). Related 1-phenylpropyne gave a similar reaction outcome with a singlet resonance appearing at 23.6 ppm in the ³¹P NMRA clearcut picture of the product structures was then provided by X-ray diffraction studies of the appropriate single crystals, which identified the product ofphenylacetylene addiction as

phosphine oxide 4.5 connected to an indolium fragment. The alkyne appeared to have inserted into the C-O bond of the amidophenolate moiety after connecting with the phosphorus atom, as well as one of the P-N bonds.



4.5 (R = Ph, >95 %, δ($^{31}$P) 26.2)

4.6 (R = Me, >95 %, δ($^{31}$P) 23.6)

4.7 (R = Me, >95 %, δ($^{31}$P) 17.1)
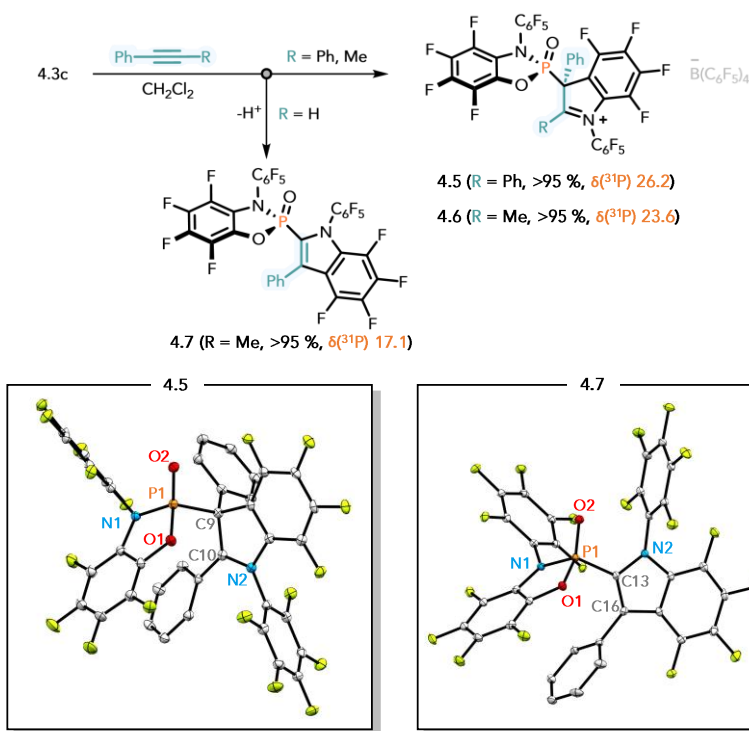
**Figure 4-6:** Reaction of 4.3c with different aromatic alkynes, as well as solid-state structures of products 4.5 and 4.7. The counterion for 4.5 and all hydrogen atoms were omitted for clarity, thermal ellipsoids are displayed at the 30 % probability level. Selected bond lengths [Å] of **4.5**: d(P1-O2) = 1.4452(15), d(P1-O1) = 1.6180(14), d(P1-N1) = 1.6899(17), d(C9-C10) = 1.521(3), d(C10-N2) = 1.327(2); and **4.7**: d(P1-O2) = 1.4601(19), d(P1-O1) = 1.6121(18), d(P1-N1) = 1.695(2), d(C13-C16) = 1.368(3), d(C13-N2) = 1.409(3).

By contrast, a parallel experiment monitoring the addition of a terminal alkyne in phenylacetylene gave a different outcome. Within minutes at room temperature, a new singlet at δ 17.1 ppm had replaced the signal of 4.3c in the 31P NMR spectrum, concomitant with disappearance of the alkyne proton signalfrom the proton NMR spectrum. Again, XRD analysis of single crystals obtained from the reaction mixture gave a clearer picture of the product connectivity.

It revealed a neutral phosphine oxide connected to an indole fragment (4.7), but with the connection to the carbon in 2-position of the indole (fig. 4-6). The divergent outcomes dependant on the alkyne provided an important clue towards figuring out the reaction mechanism (vide infra).Aliphatic alkynes such as 3-hexyne afforded a product 4.8 equivalent to 4.5 and 4.6 in the reaction with 4.3b (fig. 4-7A). Treatment with 4.3c, however, furnished a different species as major product in solution observed as a triplet ($J_{PH} = 27.9$ Hz) at $\delta(^{31}P) = 53.7$ ppm (fig. 4-7A). Integration of the appropriate $^1H$ NMR signals and $^{31}P$ HMBC correlations were consistent with a 1:1 adduct of 4.3c and 3-hexyne. The combined spectral data this time agreed with product 4.9 formed by cooperative addition of the alkyne along the P-O bond in similar fashion to the catecholato-phosphonium ions (see chapter 3.5.3).
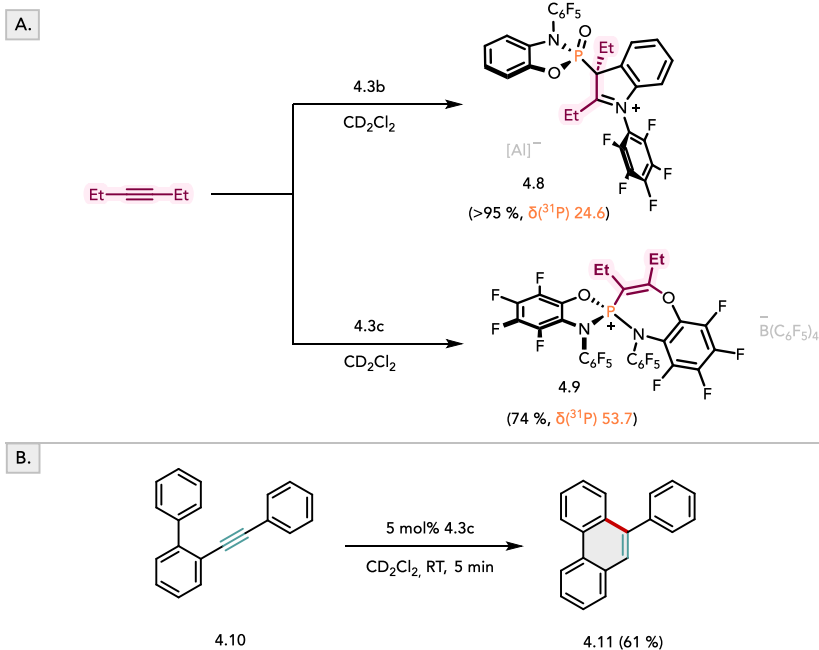


Figure 4-7: A. Reaction of 3-hexyne with 4.3b and 4.3c leading to two different products. B. Catalytic conversion of 2-(phenylethynyl)-1,1'-biphenyl to 9-phenylphenanthrene. Isolated yields are given.

The proposed product also had the best agreement with computed $^{31}$P NMR shifts. By placing a suitable nucleophilic group near the alkyne led to an intramolecular cyclization and turned the alkyne activation by 4.3c into a catalytic process. With 5 mol% of 4.3c, the alkyne substrate 4.10 was rapidly converted to 9-phenylphenanthrene within a few minutes at room temperature (fig. 4-7B).

#### 4.4.2.1  Mechanism

To shed light onto the mechanistic workings transforming the alkynes and bis(amidophenolato)phosphonium ions into the observed products, free energy profiles for the possible pathways were computed at the DSD-BLYP-D3(BJ)/def2-QZVPP+SMD(CH$_2$Cl$_2$)//r$^2$-SCAN-3c level of theory. [70b, 92] The reaction between 4.3b and 3-hexyne is initiated *via* electrophilic attack of the alkyne by 4.3b, forming a vinyl-phosphorus intermediate INT-I (fig. 4-8A). The vinyl cation can now interact with the four potential nucleophiles present in its vicinity, including the amidophenolate oxygen, nitrogen and the carbon atoms connected to them. Attack of the oxygen at phosphorus gives INT-IID, attack of the adjacent carbon yields INT-IIA, while attack at the amidophenolate-nitrogen or the adjacent carbon affords intermediates INT-IIB and INT-IIC, respectively (fig. 4-8A). The P-N cooperative addition product INT-IIB is thermodynamically the most stable but is also connected to INT-I *via* the highest transition state TS-IIB. Contrarily, no transition state could be located between INT-I and INT-IIA. The potential energy surface (PES) scans supported the notion that the conversion of INT-I to INT-IIA proceeds *via* a very low-lying or no transition state at all, making the nucleophilic attack of the aromatic carbon the most favorable pathway from INT-I. Compared to this, the lowest-lying transition states departing from INT-I along the reaction coordinate for the addition of either diphenylacetylene or 3-hexyne to perfluorinated 4.3c proceeded *via* nucleophilic attack of the oxygen to form the intermediates INT-IID (fig. 4-8B and C). The divergent reaction outcomes can be explained by the fact that for the reaction of 4.3c with diphenylacetylene the barrier leading back to INT-I is scalable at room temperature (13.4 kcal mol$^{-1}$), whereas the related intermediate INT-IID with 3-hexyne is predicted to be stable under ambient conditions with a calculated barrier of 27.1 kcal mol$^{-1}$ leading back to INT-I.
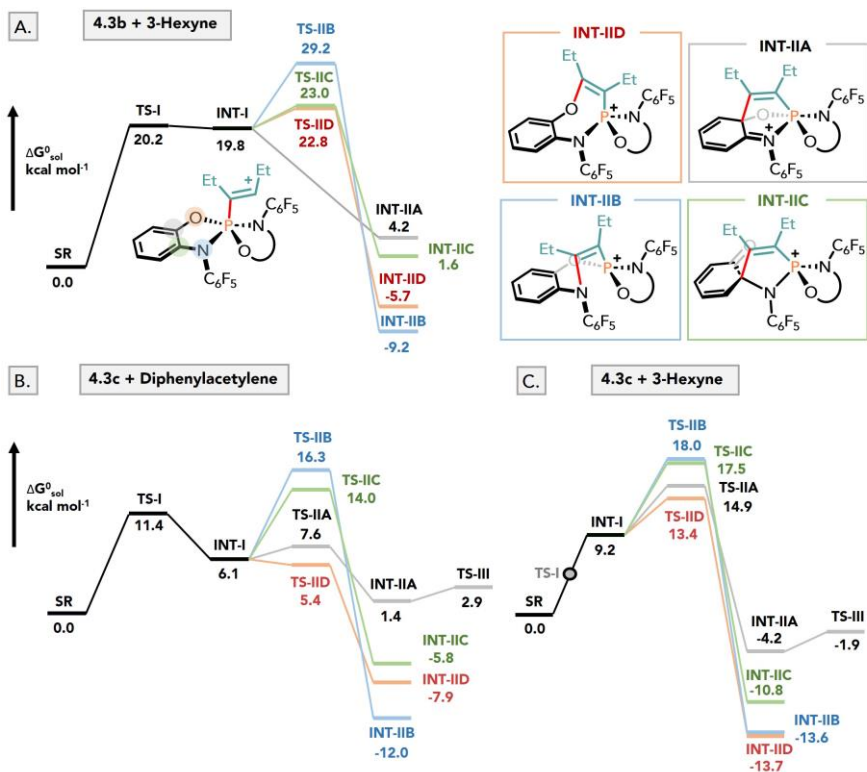
**Figure 4-8:** Abridged reaction coordinate diagrams compiled at the DSD-BLYP-D3(BJ)/def2-QZVPP+SMD(CH₂Cl₂)//r²-SCAN-3c level of theory for **A.** the reaction of 4.3b with 3-hexyne, **B.** 4.3c with diphenylacetylene and **C.** 4.3c with 3-hexyne.

For the reaction of 4.3c and diphenylacetylene, INT-I should then proceed through the second-lowest transition state TS-IIA leading to INT-IIA (fig. 4-8B). These results were consistent with the experimental observations that only the specific combination of 3-hexyne and 4.3c led to a different product.

In all scenarios, the intermediates of type INT-IIA easily undergo P-N bond scission to INT-III, followed by C-O bond cleavage furnishing INT-IV containing a phosphine oxide (fig. 4-9). The ring-closure of INT-IV *via* TS-V then leads to intermediate INT-V containing a stabilized carbocation. At this stage, if the substrate was a terminal alkyne such as phenylacetylene, fast deprotonation would yield the observed neutral product 4.7.

For the internal alkynes, a 1,2-phophorus shift generated a more stable iminium ion and the final product containing an indolium fragment, consistent with the experimental results.
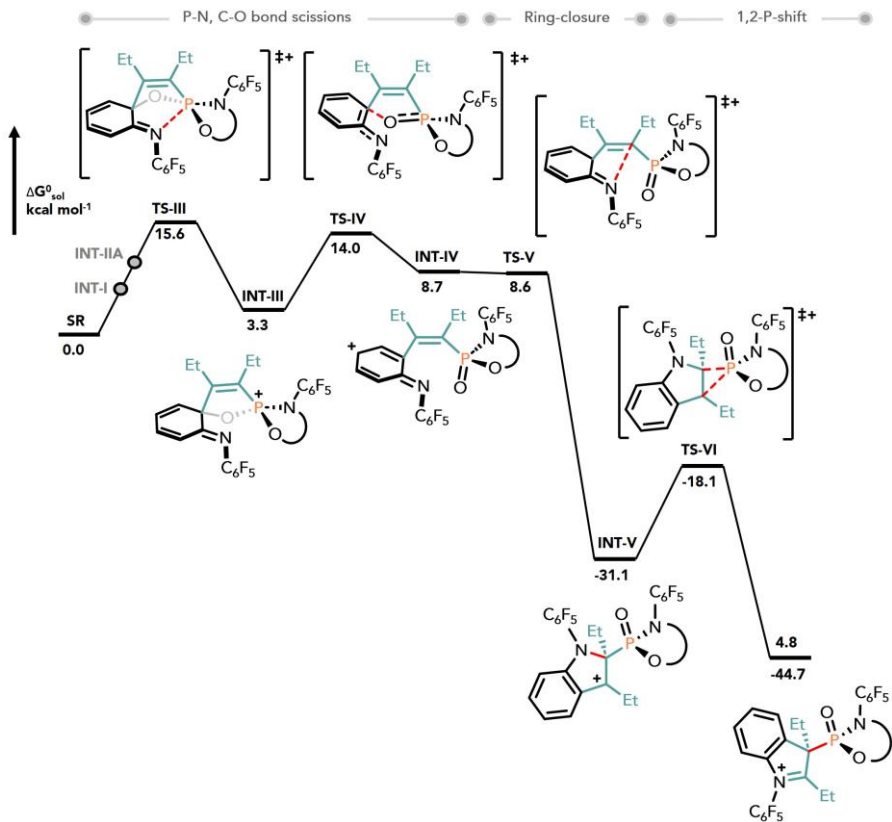


**Figure 4-9:** Rest of the reaction coordinate profile at the DSD-BLYP-D3(BJ)/def2-QZVPP+SMD(CH2Cl2)//r²-SCAN-3c level of theory for formation of 4.xx from 4.3b and 3-hexyne.

## 4.4.3    Reaction with Heteroarenes and Alkenes

The reactivity studies toward unsaturated hydrocarbons were extended by interrogation of exposure of compounds 4.3b and 4.3c to different heteroarenes and alkenes. After mixing 4.3c and thiophene, the starting materials were rapidly consumed as the phosphorylated thiophene 4.12 was cleanly formed (fig. 4-10). The

superior Lewis acidity of 4.3c compared to the other phosphonium ions supposedly generates an intermediate after cooperative C(sp$^2$)-H addition with high enough Brønsted acidity of the hydroxyl-group to protonate a second thiophene molecule. The characteristic resonances of protonated thiophene were observed in the proton NMR but decomposition occured within a day in solution. The connectivity of product 4.12 was unequivocally confirmed by SCXRD (fig. 4-10C). The phosphorane adopts a trigonal bipyramidal geometry close to ideal with a topology parameter of 0.90 (compard to 0.72 of the chlorophosphorane 4.2c).[104] Deactivated 2-bromothiophene was also quickly phosphorylated to give 4.13, albeit with lower selectivity.
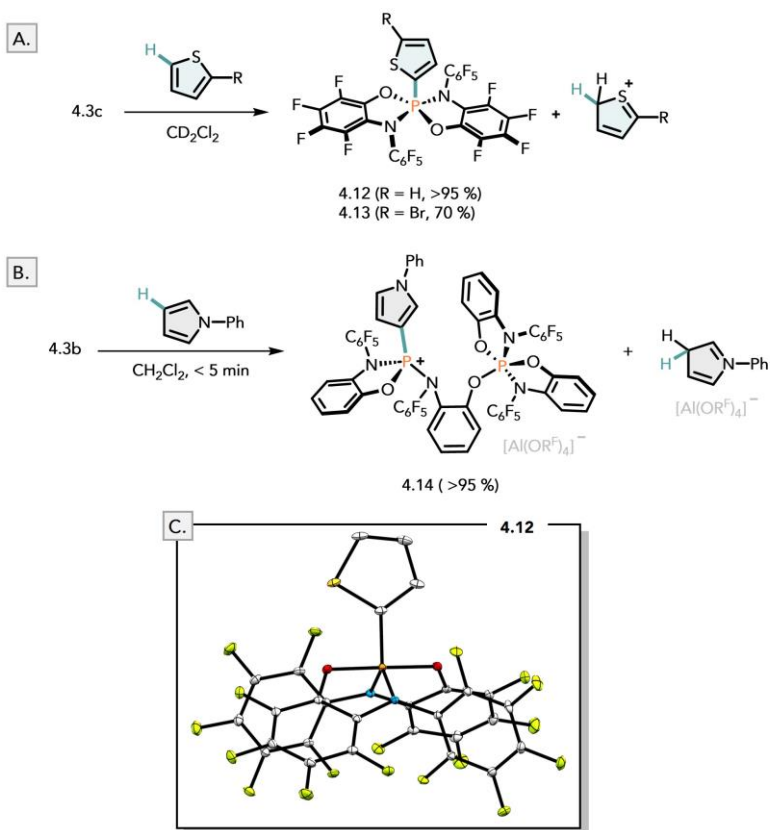


Figure 4-10: Reaction of A. 4.3c with thiophenes and B. 4.3b with 1-phenylpyrrole (conversion rates to the products were estimated from $^{31}$P NMR). C. Solid-state structure of 4.xx, thermal ellipsoids are displayed at 30 % probability.

By contrast, 4.3b undergoes reaction with 1-phenylpyrrole following the same C-H activation path as P(cat$^H$)$_2$$^+$ (3.3a), forming a product consisting with the pyrrole attached to a tetracoordinate phosphonium connected to a second, pentacoordinate bis(amidophenolato)phosphorane unit (fig. 4-10B). Apparently, the coordination of a second phosphonium ion to the C-H activation intermediate was faster than its deprotonation by another arene molecule.

An interesting reaction also unfolded upon addition of an excess of 2-norbornene to a solution of 4.3b in CD$_2$Cl$_2$ (fig. 4-11). Monitoring the reaction by $^{31}$P NMR revealed two major products at 72.8 and 20.1 ppm with $^{31}$P HMBC correlations to proton signals in the aliphatic region of the spectrum. After cooling the reaction solution and allowing vapor diffusion of pentane at -40 °C, single crystals suitable for X-ray diffraction had grown. The solid-state structure showed the cooperative addition product 4.15 that resulted from the intermediary formation of the non-classical norbornene cation after electrophilic attack of the alkene by 4.3b (fig. 4-10). Taking the multinuclear NMR data together with computed $^{31}$P NMR shifts into consideration, 4.15 was assigned to the major product at 20.1 ppm.



Figure 4-11: A. Reaction of 4.3b with norbornene, yields were estimated using $^{31}$P NMR. B. Abridged $^{31}$P($^1$H) NMR spectrum for the reaction. C. Solid-state structure of 4.15, ellipsoids are shown at the 30 % probability level, H atom and the counterion were omitted for clarity.

The other product at 72.8 ppm in the phosphorus NMR spectrum was tentatively assigned to product 4.16 of the alkene addition across the P-O bond. Rapid reactions were also observed with other alkenes, but low selectivities precluded exact identification of the products.

## 4.5    Conclusion

In summary, the first examples of bis(amidophenolato)phosphonium salts with different degrees of fluorination up to the perfluorinated derivate were prepared and fully characterized, including Gutmann-Beckett tests and computation of ion affinities to assess their Lewis acidities. The perfluorinated derivative presented the strongest isolated, monocationic phosphonium ion to date, surpassing the previously introduced catecholato-phosphonium ions. Depending on the degree of fluorination, differing modes of phosphorus-ligand cooperative reactivities toward silanes and unsaturated hydrocarbons were observed. The mechanism of the alkyne activation was deciphered by DFT calculations. The high activity in alkyne and alkene activation could offer new opportunities to design metal-free catalysts for π- and σ-catalysis.

# Chapter 5

## Structural Variability and E-H Bond Activation of (Catecholato) (N-pyridylamidophenolato) phosphonium Ions

### 5.1    Introduction

Chapter 3 of this work introduced the modular synthesis and first isolation of bis(catecholato)phosphonium salts as phosphorus-based Lewis superacids. The use of amidophenolate substituents in chapter 4 disclosed a way to not only further increase the Lewis acidity of the spirophosphonium ions upon perfluorination, but it also enabled more control over their electronic and steric profile. In this chapter, the preparation and reactivity investigation of mixed (catecholato)(*N*-pyridyl-amidophenolato)phosphonium salts is reported. The amidophenolate moiety enables the introduction of a pyridine donor in proximity to the electrophilic phosphorus center to create an intramolecular FLP, whose high Lewis acidity and reactivity is maintained through the catecholate moiety.

### 5.2    Synthesis

2-(pyridin-2-ylamino)phenol 5.1 was prepared according to a known literature procedure by a copper-catalyzed C-N cross-coupling of 2-aminophenol and 2-bromopyridine and was isolated in 81 % yield as a brown powder (fig. 5-1).

**Figure 5-1:** Synthesis of 2-(pyridin-2-ylamino)phenol.

The successive installation of both amidophenolate 5.1 and a catecholate substituent at phosphorus then capitalized on the stability and availability of the oxidized catechols (i.e. *o*-quinones) to prepare the trichlorophosphoranes 5.2 and 3.2 (see chapter 3.2) containing a single catecholate ligand by oxidative addition. Treatment of the respective *ortho*-quinones with PCl₃ gave the target products in excellent yields as a yellow oil and a pale green powder, respectively (fig. 5-2). In a condensation reaction of the aminophenol 5.1 and trichlorophosphorane 5.2 in the presence of triethylamine as base in toluene, the chlorophosphorane 5.3a was obtained in 67 % yield after workup. ³¹P NMR analysis of 5.3a indicated a mixture of two isomers in 3:1 ratio at chemical shifts of -24.7 and -25.4 ppm, differentiated only by the relative orientations of the *tert*-butyl and the pyridyl groups.



**Figure 5-2:** Synthesis of the chlorophosphorane 5.3a (major isomer is shown) containing 3,5-di-*tert*-butylcatecholate and the newly prepared ligand 5.1

The same synthesis of chlorophosphorane 5.4a proved to be significantly more cumbersome due to its similar solubility to the byproduct triethylammonium chloride in non-coordinating solvents. While optimization of the reaction conditions including the choice of solvent and base led to NMR yields as high as 80 %, separation of the analytically pure compound from the reaction byproducts was unsuccessful (fig. 5-3). Some of the tested reaction conditions are summarized in table 5-1. Noteworthily, the reaction outcome (as determined by ³¹P NMR) was highly sensitive to the order and timing with which the reaction components were added together. Using bases other than triethylamine was not productive, as for instance pyridine was not basic enough to prevent protonation of the pyridyl group of 5.3a by the condensation byproduct HCl.

**Figure 5-1: A.** Attempted synthesis of perchlorocatecholate-containing chlorophosphorane 5.4a and **B.** abridged $^{31}$P NMR spectrum of the reaction.

Other solvents such as toluene or benzene also afforded 5.4a as the major product in solution, but with lower selectivity.

**Table 5-1:** Tested reaction conditions for the synthesis of 5.4a by condensation of 5.1 and 3.2.

| Entry | Base (equiv) | Solvent | NMR Yield [%] | Comment |
|:---:|:---:|:---:|:---:|:---:|
| 1 | NEt$_3$ (1.1) | CD$_2$Cl$_2$ | 80 | Solution of 5.1 and NEt$_3$ added to 3.2 in CD$_2$Cl$_2$.* |
| 2 | NEt$_3$ (1.1) | PhMe-d$_8$ | 74 | |
| 3 | NEt$_3$ (1.1) | CD$_3$CN | - | Unselective reaction |
| 4 | NEt$_3$ (1.1) | C$_6$D$_6$ | - | 5.4a probably not very soluble in C$_6$D$_6$ |
| 5 | NEt$_3$ (2.2) | CD$_2$Cl$_2$ | 57 | |

79

| Entry | Base (equiv) | Solvent | NMR Yield [%] | Comment |
|---|---|---|---|---|
| 6 | Pyridine (2.0) | CD$_2$Cl$_2$ | - | Unselective reaction |
| 7 | Pyridine (2.0) | PhMe-d$_8$ | - | Unselective reaction |
| 8 | NEt$_3$ (1.1) | CH$_2$Cl$_2$ | 65 | Reaction at -42 °C, larger scale |
| 9 | KHMDS (2.0) | PhMe-d$_8$ | - | Unselective reaction |
| 10 | LDA (2.0) | PhMe-d$_8$ | - | Unselective reaction |

Consequently, other approaches to the synthesis of 5.4a were investigated that either circumvented the formation of inseparable triethylammonium chloride or would otherwise facilitate easier isolation of 5.4a. Installation of phosphorus first by condensation of PCl$_3$ and 5.1 in the presence of NEt$_3$ furnished σ$^3$-P compound 5.5, and analysis of X-ray diffraction quality single crystals corroborated the successful synthesis (fig. 5-4).



**Figure 5-4:** Preparative route to 5.4a *via* initial condensation of 5.1 and PCl$_3$, as well as the solid-state structures of the undesired byproduct and intermediate 5.5. Thermal ellipsoids are displayed at 30 % probability, disordered solvent molecules and hydrogen atoms were omitted for clarity.

However, the subsequent addition of tetrachloro-*ortho*-quinone to 5.5 only resulted in a complex, unidentifiable mixture of phosphorus-containing products. Despite this, single crystals suitable for SCXRD still grew after cooling the reaction mixture to -40 °C. The solid-state structure verified one of the products as the undesired compound 5.4a-$O_2C_6Cl_4$, resulting from twofold addition of the quinone to 5.5. It appeared as though chlorophosphorane 5.4a was not stable in the presence of the quinone and underwent cooperative addition to phosphorus and pyridine with concomitant transfer of the phosphorus-bound chloride to a quinone-carbon.

Next, we prepared the deprotonated ligand by treatment of 5.1 with *n*-buthyllithium to get the corresponding lithium salt. We surmised that this would circumvent the requirement for an exogenous base for the subsequent step and streamline the purification of 5.4a by avoiding the formation of the base hydrochloride byproduct (fig. 5-5). After addition of the deprotonated ligand to the trichlorophosphorane 3.2 at either room temperature or -40 °C, the desired product 5.4a was observed by $^{31}P$ NMR. Isolation of pristine 5.4a however was still not successful as the product was only produced with low selectivity. In similar fashion, the reactions of either protonated or deprotonated ligand 5.1 with $PCl_5$ were not expedient (fig. 5-5).



**Figure 5-5:** Unsuccessful preparative routes to the chlorophosphorane 5.4a.

In the absence of exogenous base, the hydrochloride [5.4a-H][Cl] was obtained selectively upon repeating the reaction of $Cat^{Cl}PCl_3$ (3.2) with 5.1. Several bases for the deprotonation to 5.4a were evaluated, with preference given to alkali salts that would furnish easily separable alkali chlorides as byproducts. The cleanest

deprotonation reaction was achieved with lithium pentamethylcyclopentadienide (LiCp*). Although the reaction looked very promising, final optimization of the purification process and complete characterization of pure 5.4a was still outstanding. Nevertheless, single crystals suitable for X-ray diffraction could be obtained by cooling a concentrated solution of the crude product in dichloromethane. The solid-state structure depicts a phosphorus center that adopts a coordination environment between a square-pyramid and a trigonal bipyramid with a topology parameter of 0.55 (1 = ideal trigonal bipyramid, 0 = ideal square pyramid).[104]



Figure 5-6: Two-step synthetic route to 5.4a and solid-state structure of 5.4a. Thermal ellipsoids are displayed at 30 % probability, hydrogen atoms were omitted for clarity. Selected bond distances [Å] and angles [deg] of 5.4a: d(P1-N1) = 1.6647(16), d(P1-O2) = 1.6490(14), d(P1-O3) = 1.7047(14), d(P1-O1) = 1.6577(14), ∠O1-P1-N1 = 90.87(7), ∠O2-P1-O3 = 90.40(7).

In the next step, the phosphonium ions were prepared by chloride abstraction with Li[Al(OR$^F$)$_4$] (R$^F$ = C(CF$_3$)$_3$). The reaction with 5.3a proceeded cleanly and afforded the phosphonium salt 5.3b in quantitative yield (fig. 5-7). As the starting material 5.4a had not been of analytical purity, 5.4b was only prepared *in situ* for preliminary, small-scale NMR studies of its reactivity. The spectral data for the two cations

differed significantly, as solutions of 5.3b displayed a sharp peak at 46.1 ppm in the $^{31}$P NMR spectrum, in the same region as previously prepared catecholato- or amidophenolato phosphonium ions (see chapters 3 and 4).



**Figure 5-7:** Synthesis of phosphonium salts 5.3b and 5.4b (not yet isolated), as well as the corresponding NMR data and abridged $^{31}$P NMR spectra.

The resonance was also in agreement with the computed phosphorus chemical shift at 54.9 ppm. On the other hand, the chloride abstraction from 5.4a resulted in a new, broad peak at 20.7 ppm in the $^{31}$P NMR spectra, at considerably higher field strengths than expected. The peak broadness also indicated dynamic behavior in solution. Further, the experimentally measured chemical shift did not agree with the computed value of either the 'open' or ring-'closed' structure. Taken together, these observations suggested the partial coordination of the pyridine to phosphorus and a dynamic equilibrium in solution. For both 5.3b and 5.4b, single crystals suitable for X-ray diffraction deposited after allowing vapor diffusion of

pentane into dichloromethane solutions at -40 °C for several days. The coordination of the pyridyl group (d(P-N) = 1.772(3) Å) leads to a pentacoordinate phosphorus center in 5.4b. The strain on the pyridylamidophenolato moiety results in significant folding along the P1-N1 axis of 5.4b, resulting in its adoption of a distorted, trigonal bipyramidal geometry with a bond angle ∠O4-P1-N2 = 122.43(9)° and a topology parameter of 0.71.[104]



**Figure 5-8:** Solid-state structures of 5.4b (left) and 5.3b (right). Thermal ellipsoids are displayed at 30 % probability, hydrogen atoms and the counterions (Al(OR$^F$)$_4^-$) were omitted for clarity. Selected bond distances [Å] and angles [deg] of 5.4b: d(P1-O2) = 1.6159(16), d(P1-O3) = 1.6486(17), d(P1-O4) = 1.5878(17), ∠N1-P1-N2 = 73.01(9), ∠O4-P1-N1 = 92.25(9), ∠O4-P1-N2 = 122.43(9) and 5.3b: d(P1-O2) = 1.559(3), d(P1-O3) = 1.566(2), d(P1-O4) = 1.563(3), ∠N1-P1-N2 = 73.01(9), ∠O4-P1-N1 = 92.25(9).

By contrast, the phosphorus center of 5.3b is tetracoordinate (d(P-N) = 2.621 Å), although the pyridine is oriented towards it. The higher coordination number of 5.4b (d(P-O) = 1.59 – 1.65 Å) affords phosphorus-oxygen bonds elongated compared to 5.3b (d(P-O) = 1.56 – 1.57 Å), but shortened relative to the neutral, pentacoordinate chlorophosphorane 5.4a (d(P-O) = 1.65 – 1.70 Å). Overall, the structural features support the observations made by NMR analysis in solution.

The ring-closure of 5.3b and 5.4b was then further investigated using DFT at the ωB97X-D3(BJ)/def2-TZVPP+SMD(CH$_2$Cl$_2$)//r$^2$-SCAN-3c level of theory.[70b, 92a, 92c, 107] The results were consistent with experimental observations, as the pyridine coordination was predicted to be endergonic for 5.3b and exergonic but close to thermoneutral for 5.4b (fig. 5-9).

**Figure 5-9:** Computed Gibbs free energies for the ring-closures of 5.3b and 5.4 at the ωB97X-D3(BJ)/def2-TZVPP+SMD(CH$_2$Cl$_2$)//r$^2$-SCAN-3c level of theory.


## 5.3  Reactivity Toward C(sp$^2$)-H Bonds

To initiate the investigation into the reactivity of the newly prepared phosphonium salts, a solution of 5.3b was exposed to 1-phenylpyrrole. NMR analysis after a few minutes of reaction time indicated full consumption of 5.3b and selective conversion to four new phosphorus-containing products. The $^{31}$P NMR resonances were measured between -27.7 and -34.6 ppm, consistent with formation of pentacoordinate phosphorus species (fig. 5-10). Taken together with the broad signals around 11 ppm in the proton NMR spectrum, the spectral data were indicative of the four possible isomeric products of pyrrole C-H bond cleavage. These include the products of C-H cleavage at the two- and three-position of the pyrrole and their respective diastereomers with different relative orientations of *tert*-butyl and pyridyl groups. The same reaction with 2-methylthiophene was a bit more sluggish, so the mixture was heated for five days at 60 °C until conversion to a single phosphorus-containing product was complete. The spectral data were coherent with addition product 5.7 of selective 2-methylthiophene phosphorylation at the 5-position. In line with its lower nucleophilicity, more forcing conditions were required to facilitate a reaction with toluene. Over the course of three days at 120 °C in toluene, conversion to 5.8 was indeed observed, albeit with lower selectivity. The connectivity was confirmed by SCXRD, although poor crystal quality prevented adequate refining to extract bond lengths and angles. No changes to the NMR

spectra occurred after treatment of 5.3b with triethylsilane or dihydrogen. At elevated temperatures, unselective decomposition was observed.



Figure 5-10: Reaction of 5.3b with different E-H substrates and the abridged $^{31}$P NMR spectrum of the reaction with 1-phenylpyrrole showing the four isomer resonances (bottom). Yields shown were estimated from the $^{1}$H and $^{31}$P NMR spectra.

The addition of phenylacetylene to 5.3b also produced an unselective reaction mixture of several phosphorus-containing products. Only one of them could be unequivocally identified as the phosphine oxide 5.10, where the alkyne had formally

inserted into the C-O and P-N bonds. The transformation likely followed a similar mechanism to the one proposed for the reactions of bis(amidophenolato)-phosphonium ions with alkynes (see chapter 4.4.2) and should be initiated by the ligand-assisted addition of the alkyne to give the intermediate 5.9 (fig. 5-11A).



Figure 5-11: A. Reaction of 5.3b with phenylacetylene and the solid-state structure of one of the products. Thermal ellipsoids are displayed at 30 % probability, hydrogen atoms and the counterion were omitted for clarity. B. C-H deprotonation of different thiophenes by 5.4b. Yields were not determined due to impurities in the starting material.

Preliminary experiments with 5.4b demonstrated enhanced reactivity toward heteroarenes relative to 5.3b, as both 2-methyl- and 2-bromothiophene were cleanly converted to the products 5.11 and 5.12 at room temperature (fig. 5-11B). Insights into the details of the E-H bond cleavages were delivered by computations at the ωB97X-D3(BJ)/def2-TZVPP+SMD(CH$_2$Cl$_2$)//r$^2$-SCAN-3c level of theory. [70b, 92a, 92c, 107] Despite the overall transformation being exergonic, the splitting of dihydrogen by 5.4b is impeded by a considerable barrier of 45.2 kcal mol$^{-1}$, owed to the rigidity of the pyridyl group and the resulting substantial deformation energy required to contort the relaxed structure to accommodate the dihydrogen molecule in the corresponding transition state (fig. 5-12). The unwillingness of the structure to be altered enough to add a two-atomic molecular unit is further underpinned by the fact that the addition of carbon dioxide is calculated to be endergonic.



**Figure 5-12:** Computed thermodynamic and kinetic data for small molecule activation by 5.4b at the ωB97X-D3(BJ)/def2-TZVPP+SMD(CH$_2$Cl$_2$)//r$^2$-SCAN-3c level of theory.

The situation changes for instance with the addition of benzene, where a Wheland intermediate with a pentacoordinate phosphorus precedes the deprotonation step and effectively lowers the amount of required structural deformation. Despite this, the barrier of 33.5 kcal mol$^{-1}$ is still considerable and elevated temperature should be required to facilitate a reaction even though the overall reaction is exergonic.

## 5.4 Gold Complex

With the pyridyl groups potentially serving as donor ligands to stabilize transition metal fragments within the vicinity of the electrophilic phosphorus center, preliminary investigations into the capacities of 5.3b and 5.4b as Z-type ligands were carried out. Treatment of 5.3b with one equivalent of dimethylsulfide (DMS) gold chloride in CD$_2$Cl$_2$ delivered two new phosphorus-containing products with broad



**Figure 5-13:** Reaction of 5.3c with DMS-AuCl and solid-state structure of one of the formed diastereomers. Thermal ellipsoids are displayed at 30 % probability, hydrogen atoms and the counterion (Al(OR$^F$)$_4$$^-$) were omitted for clarity. Selected bond distances [Å] and angles [deg] of 5.X: d(P1-O1) = 1.659(4), d(P1-O2) = 1.640(4), d(P1-O3) = 1.661(4), d(P1-N1) = 1.709(4), d(Au1-N2) = 2.049(5), d(Au1-S1) = 2.2426(17), ∠N2-Au1-S1 = 176.89(13).
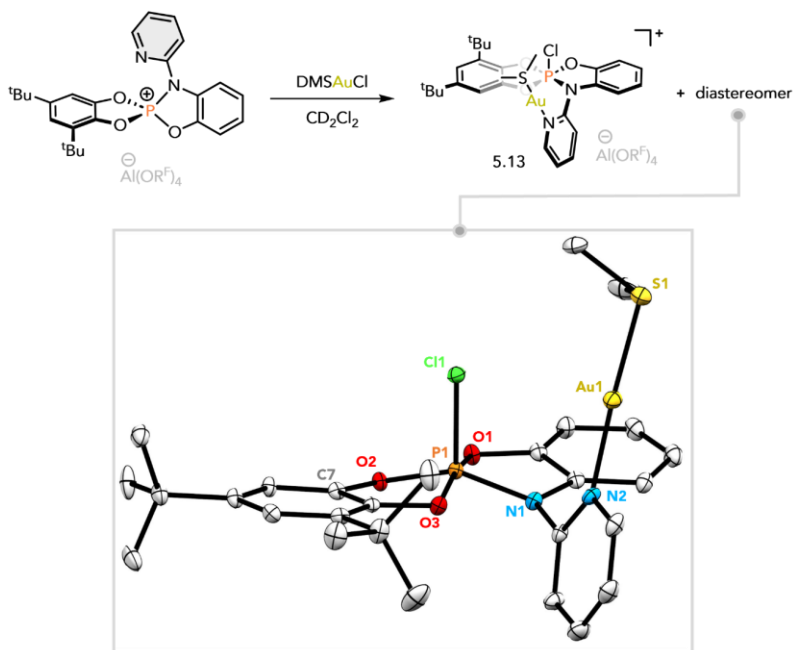
resonances in the ^{31}P NMR spectra at -24.8 and -25.4 ppm in the spectral region of pentacoordinate phosphorus (fig. 5-13). The chemical shifts closely resembled those measured for the diastereomers of chlorophosphoranes 5.3b. To corroborate the assignment, crystalline solids were grown from the reaction solution by vapor diffusion of pentane at -40 °C and analyzed by X-ray diffraction. The solid-state structure confirmed the chloride migration to phosphorus, while the pyridine coordinates to the DMS-gold fragment. The P-O and P-N bond lengths are comparable to those of 5.4b (see fig. 5-6), and the gold-pyridine bond length (d(Au1-N1) = 2.049(5) Å) was also within range of values measured for other gold-pyridine complexes.[108]

## 5.5    Conclusion

To summarize, synthetic procedures to phosphonium salts containing both a catecholate and a *N*-pyridylamidophenolato substituents were disclosed and the newly prepared compounds characterized. The propensity for cooperative or FLP-like bond activation between the electrophilic phosphorus and nucleophilic pyridyl group were tested with a range of different substrates. C(sp²)-H bonds of hetero(arenes) were selectively cleaved, but no reactions between the phosphonium ions and silanes, dihydrogen or carbon dioxide were observed under the tested reactions conditions. The experimental outcomes and substrate selectivities were elucidated by computational considerations of thermodynamics and kinetics.

# Chapter 6

## Reversible Oxidative Addition of Unactivated C-H Bonds to Structurally Constrained Phosphenium Ions

### 6.1    Introduction

Among the p-block elements, phosphorus sits at a privileged position to facilitate redox catalysis by cycling between the P(III)/P(V) redox couple without being overly biased for either the oxidative addition (OA) or reductive elimination (RE). Especially nontrigonal, non-VSEPR phosphorus(III) compounds have garnered substantial recent interest as a platform for main-group redox catalysis due enhanced biphilicity enforced by the structural constraint, as disclosed in chapter 1.4.[109] Still, previous examples of E-H bond activation *via* OA by pincer-ligated, structurally constrained P(III) compounds have been largely limited to polar bonds (E = O, N, S) with few examples of irreversible OA of less polarized C-H or H-H bonds.[23, 51, 64] In this chapter, we report on a new class of structurally constrained phosphenium ions based on a pyridymethyl-aminophenolate scaffold, leveraging a dative P-N bond and an improved Lewis acidity at phosphorus to facilitate increased reactivity towards unpolar E-H bonds.[110]

## 6.2 Synthesis

Starting from several commercially available 2-pyridinecarboxyaldehydes and 2-aminophenols, a series of pyridinylmethylaminophenol ligands were prepared by a facile two-step synthesis (fig. 6-1).



Y, X = H, H (70 %, a) = 6.1a
H, Br (71 %, a) = 6.2a
Cl, H (37 %, b) = 6.3a
Cl, Br (41 %, b) = 6.4a
H, Cl (51 %, a) = 6.5a
H, OMe (48 %, b) = 6.6a
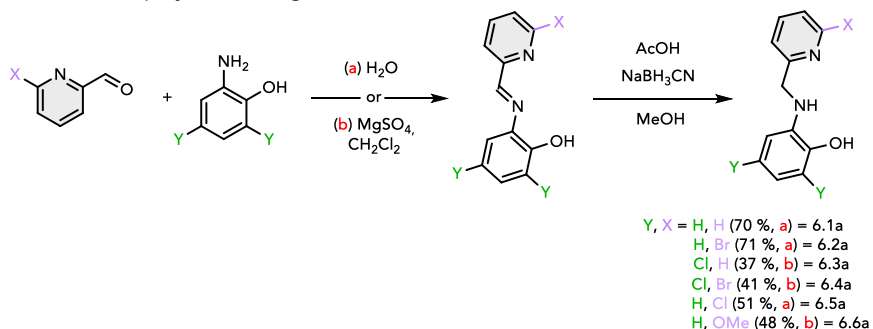
**Figure 6-1:** Synthesis of pyridinylmethylaminophenols.

Depending on the substitution pattern, the imine condensation step was either carried out in water or in dichloromethane in the presence of magnesium sulfate. The imines were then used directly without purification in the reduction with sodium cyanoborohydride, giving the desired ligands in decent to good yields over two steps at a multi-gram scale.



| X,Y = | | δ $^{31}$P (ppm) | | |
|---|---|---|---|---|
| H, H | 6.1b | 147.3 | 161.1 | 6.1c |
| Br, H | 6.2b | 162.1 | 182.8 | 6.2c |
| H, Cl | 6.3b | 133.7 | 161.2 | 6.3c |
| Br, Cl | 6.4b | 158.7 | 170.4 | 6.4c |
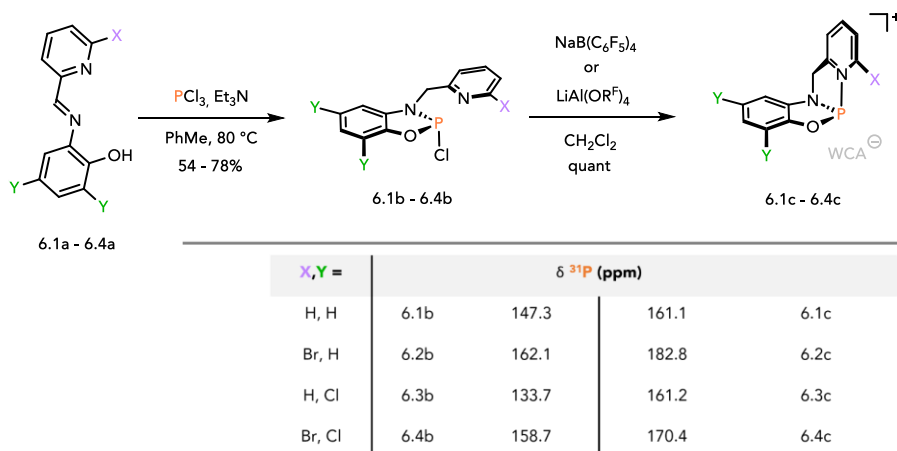
**Figure 6-2:** Synthesis of and chlorophosphites 6.1b – 6.4b and structurally constrained phosphenium salts 6.1c – 6.4c as well as their $^{31}$P NMR shifts.

Conveniently, aqueous workup followed by an ether wash furnished analytically pure compounds, obviating more laborious purification procedures. Phosphorus insertion to the chelates by treatment with PCl$_3$ and triethylamine in toluene proceeded selectively after heating to 80 °C to afford chlorophosphites 6.1b – 6.4b in good yields. Notably, the measured $^{31}$P NMR shifts differed considerably, ranging from 133.7 ppm for 6.1b to 162.1 ppm for 6.2b. The variance likely originates from changes in shielding at phosphorus due to different degrees of pyridine coordination to phosphorus in solution. The hypothesis was supported by solid-state structures derived from X-ray diffraction analysis of single crystals grown by cooling of concentrated solutions in toluene (fig. 6-3). The pyridine moieties are coplanar with the amidophenolates with varying degrees of coordination to phosphorus.
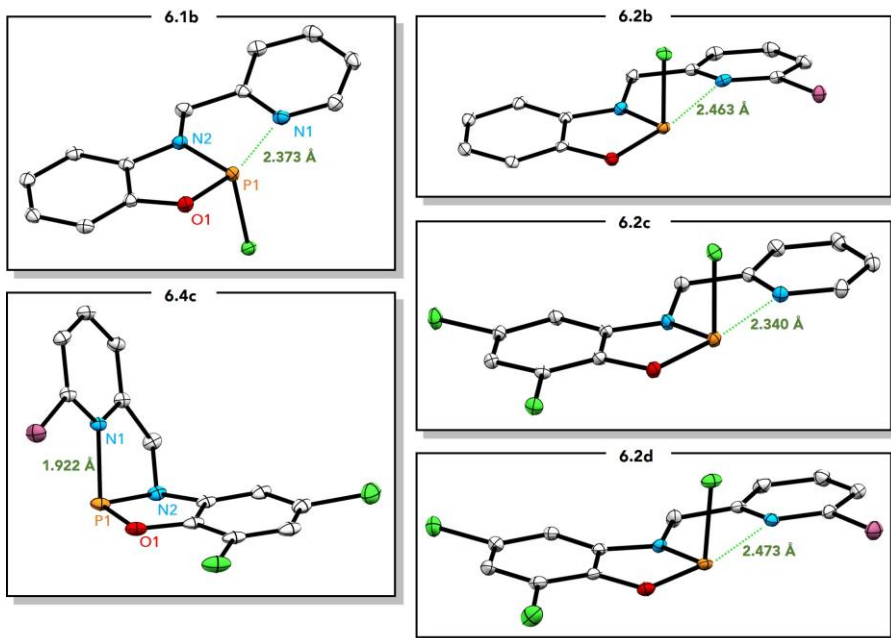


**Figure 6-3:** Solid-state structures of 6.1b – 6.4b (thermal ellipsoids at 30 % probability) and 6.4c (thermal ellipsoids at 15 % probability). The counteranion [Al(OR$^F$)$_4$]$^-$ (for 6.4c)and all carbon-based hydrogen atoms were omitted for clarity. Selected bond distances [Å] and angles [deg] of 6.1b: d(P1-N1) = 2.373, d(P1-N2) = 1.7032(16), d(P1-O1) = 1.6732(15), ∠O1-P1-N1 = 166.67, ∠O1-P1-N2 = 90.39(7), ∠N2-P1-N1 = 76.76, and 6.4c: d(P1-N1) = 1.922(2), d(P1-N2) = 1.702(3), d(P1-O1) = 1.620(2), ∠O1-P1-N1 = 108.05(9), ∠O1-P1-N2 = 94.38(11), ∠N2-P1-N1 = 85.86(10).

The trend of P1-N1 bonds lengths was mostly consistent with the $^{31}$P NMR shifts, as greater downfield shifted signals correlated to longer bonds. Treatment of the chlorophosphites with $NaB(C_6F_5)_4$ or $LiAl(OR^F)_4$ ($R^F$ = $C(CF_3)_3$) in dichloromethane then afforded the targeted phosphenium salts 6.1c – 6.4c in quantitative yields. The chloride abstractions were accompanied by disproportionate downfield shifts of phosphorus NMR signals by ~12 – 28 ppm dependent on the substitution pattern (fig. 6-2). Other potential chloride abstraction agents such as $LiPF_6$, $KSbF_6$, $AgSbF_6$ or $NaB_{12}Cl_{11}NMe_3$ were inefficacious as either no or unselective reactions were observed. Vapor diffusion of pentane into a concentrated solution of 6.4c in dichloromethane at -40 °C furnished a crystalline sample suitable for X-ray diffraction. The solid-state structure revealed a phosphenium ion that adopts a structure folded significantly along the P1-N1 axis with an ∠O1-P1-N1 angle of 108.05(9)°, leading to an overall $C_1$ symmetric solid-state structure. The asymmetry is reflected by the two dissimilar angles spanned by the heteroatoms around phosphorus, ∠O1-P1-N2 = 94.38(11)° and ∠N2-P1-N1 = 85.86(10)°. Both the P1-N2 (d = 1.792(3) Å) and P1-O1(d = 1.620(2) Å) bond lengths are unremarkable and similar to related structurally constrained P(III) compounds.[48-49, 49d] On the other hand, the P1-N1 bond (d = 1.922(2) Å) is elongated due to the dative nature, but significantly shorter than the corresponding bond in the neutral chlorophosphite 6.4b (d = 2.473 Å). It also exceeds the lengths of pyridine-phosphorus P-N bonds of the structurally constrained, pyrdine-based phosphenium cations by Dobrovetsky et al. (1.41 and 1.41, chapter 1.4).[49c, 49d]

## 6.3 Dynamic Solution Behavior

A high degree of dynamicism of the phosphenium ions in solution was inferred from the measured NMR spectra. The $^{31}$P NMR resonances all displayed varying degrees of signal broadening. Additionally, the diastereotopic methylene protons seated between the pyridine and amidophenolate moieties appeared as a lone doublet around 5 ppm for all cations despite being magnetically inequivalent. To potentially suppress the ongoing conformational process, the solutions were investigated by variable temperature (VT) NMR experiments (fig. 6-4). However, aside from minor signal shifts, no changes were observed even after lowering the temperature down to -80 °C. By contrast, the decoalescence of NMR signals for the diastereotopic methyl groups of the structurally related NNNP pincer compound 1.38 at -60 °C
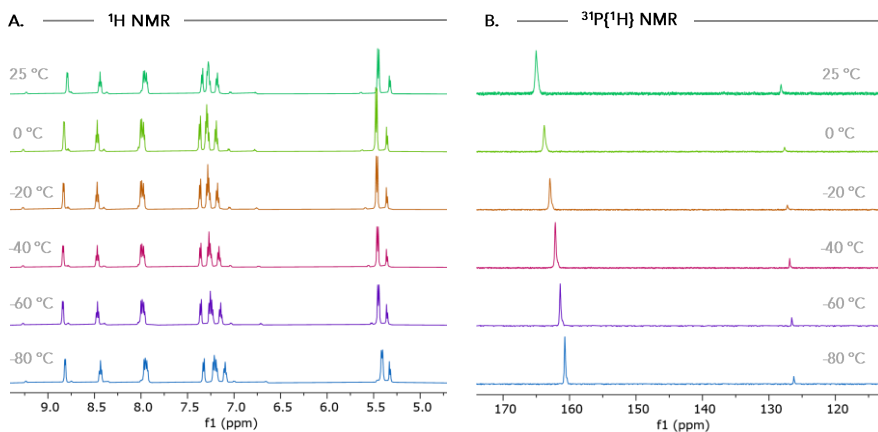
**Figure 6-4:** Stacked, abridged **A.** ${}^1$H and **B.** ${}^{31}$P NMR spectra of 6.1c in CD$_2$Cl$_2$ at different temperatures.

was observed by Radosevich and co-workers.[48] They experimentally determined a barrier of 10.7(5) kcal mol$^{-1}$ for the P-edge inversion process interconverting the two enantiomers. Consequently, the P-edge inversion of 6.1c was interrogated using DFT at the DSD-BLYP-D3(BJ)/def2-QZVPP+SMD(CH$_2$Cl$_2$)//r$^2$-SCAN-3c level of theory.[70b, 92a, 92c, 111] Consistent with the experimental, bent structure of 6.4c, DFT predicted the same geometry for the lowest energy conformers of phosphenium ions 6.1c – 6.4c. Following the PES along the reaction coordinate for P-edge inversion, T-shaped, C$_s$-symmetric intermediates IM-I were found only slightly higher in energy (4.1 kcal mol$^{-1}$ for 6.1c, even lower for 6.2c – 6.4c, see table 6-1). The low computed barrier (6.0 kcal mol$^{-1}$) connecting IM-I to the two bent conformers was consistent with the fast interconversion observed in solution. The other conceivable mechanism explaining the solution phase dynamism involving the pyridine dissociation from phosphorus was disregarded as unlikely. It followed a much steeper gradient on the PES and did not lead to a local minimum structure with a disconnected pyridine.

We surmised that the discovered planar, T-shaped intermediate IM-I might be the reactive species in solution and looked into its electronic structure. The assumption was underpinned by a comparison of the frontier orbitals between IM-I and the bent isomer (fig. 6-5C).
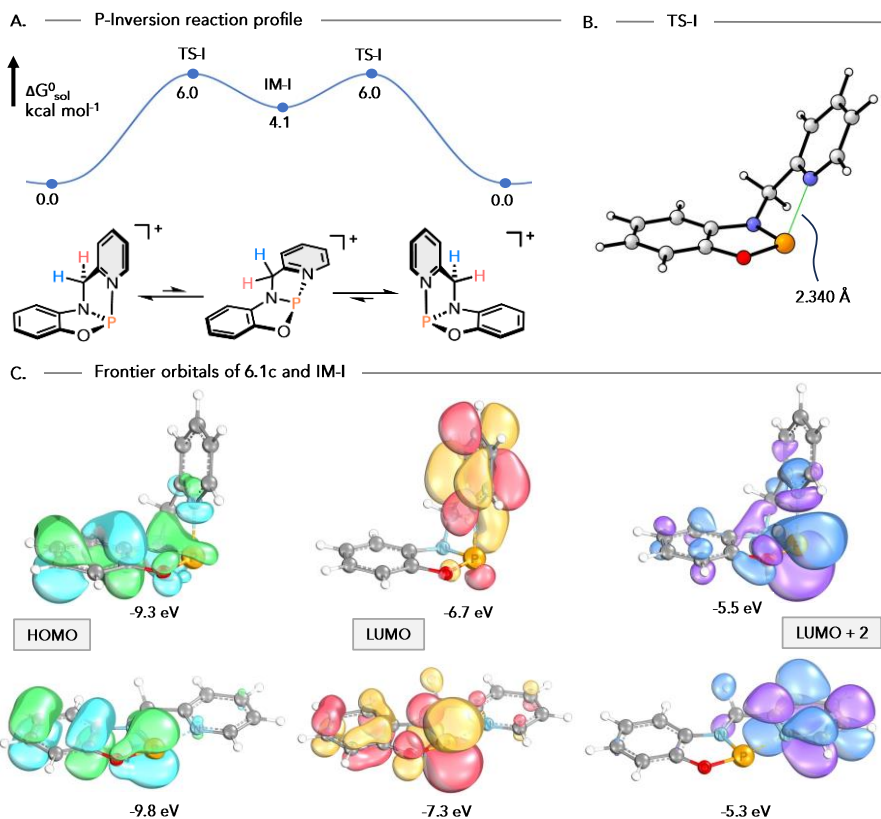
**Figure 6-5: A.** Computed free energy profile for the P-edge inversion of 6.1c at the DSD-BLYP-D3(BJ)/def2-QZVPP+SMD(CH₂Cl₂)//r²-SCAN-3c level of theory. **B.** Transition state TS-I for planarization of 6.1c. **C.** Frontier orbitals of the bent (top row) and planar (bottom row) isomers of 6.1c.

Neither HOMO, nor LUMO of the bent isomer reside at phosphorus and are located mostly on the ligand. Only the higher-lying LUMO+2 posseses significant contributions at phosphorus. The situation changes upon planarization, as suitable phosphorus-localized orbitals ascend/descend in energy to become the highest occupied and lowest unoccupied orbitals, respectively, separated by a small HOMO-LUMO gap (2.5 eV, fig. 6-5C). The relatively low energy penalty for planarization (i.e. 4.1 kcal mol⁻¹) should be easily compensated by Lewis base coordination, as observed in the solid-state structures of 6.1b – 6.4b (see fig. 6-3), which can be considered the formal chloride adducts of the planarized

intermediates IM-I.

## 6.4    Assessment of Lewis Acidity

The presence of a suitable low-lying acceptor orbital for the planar cations indicated pronounced Lewis acidity at phosphorus, which was investigated *via* the Gutmann-Beckett method. Treatment of the solvated phosphenium salts with triethylphosphine oxide proceeded cleanly under adduct formation, as established by spectroscopic data. Broad signals in the phosphorus spectra again hinted at solution dynamism and was strongly dependent of the phosphenium ion. For instance, the measured spectra with 6.2c showed the distinct P-P couplings of the adduct, while they were masked by the peak broadness in the spectrum of 6.4c (fig. 6-6A). The substantial downfield shifts of the coordinated OPEt$_3$ between 36.2 and 40.9 ppm verified high *effective* Lewis acidity on the Gutmann-Becket scale in the order 6.4c > 6.2c > 6.3c > 6.1c (fig. 6-6B).[14]
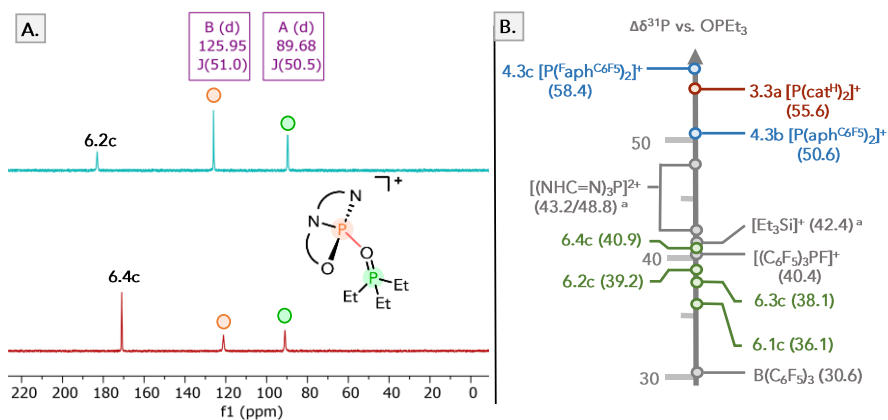


Figure 6-6: A. Stacked, abridged 31P(1H) NMR spectra of 6.2c (top) and 6.4c (bottom) with 0.5 equivalents of TEPO in CD$_2$Cl$_2$. B. Scale of $^{31}$P NMR chemical shifts of TEPO bound to various Lewis acids relative to free TEPO in CD$_2$Cl$_2$. [a] Measured in C$_6$D$_6$.

Surprisingly, the GB-shift of 6.4c even surpassed that of Stephan's perfluorinated fluorophosphonium cation (40.4 ppm).[28] All of the phosphenium ions are more Lewis acidic than BCF on the GB-scale, but fall behind both the bis(amidophenolato)- and bis(catecholato)phosphonium ions presented in chapters 3 and 4, as well as Dielmann's phosphorus dications.[31]

## 6.5    Oxidative Addition of E-H Bonds

To evaluate the potential of the newly prepared compounds 6.1c – 6.4c for activation of E-H bonds, we started by examining the reaction of 6.1c with a weakly basic amine such as diphenylamine that had no precedent for oxidative addition to phosphorus. Within minutes of mixing the two substances, rapid and quantitative conversion to the $\sigma^5$-P diphenylamido hydrido P(V) cation [6.1c]•[H][NPh$_2$] was detected by $^{31}$P NMR spectroscopy ($\delta$ -45.2 ppm, $^1J_{PH}$ = 858.3 Hz) (fig. 6-7). Intrigued by the high reactivity toward the amine, a solution of 6.1c in CD$_2$Cl$_2$ was next treated with 1-methylindole. Again, the combined multinuclear NMR data were consistent with a P(V)-H product ($\delta$ -44.0 ppm, $^1J_{PH}$ = 763.3 Hz) of oxidative addition, but in this case the C-H bond at the 3-position of the indole was cleaved. In similar fashion, the sp-hybridized C-H bond of phenylacetylene was oxidatively added to 6.1c to afford [6.1c]•[H][C$_2$Ph].
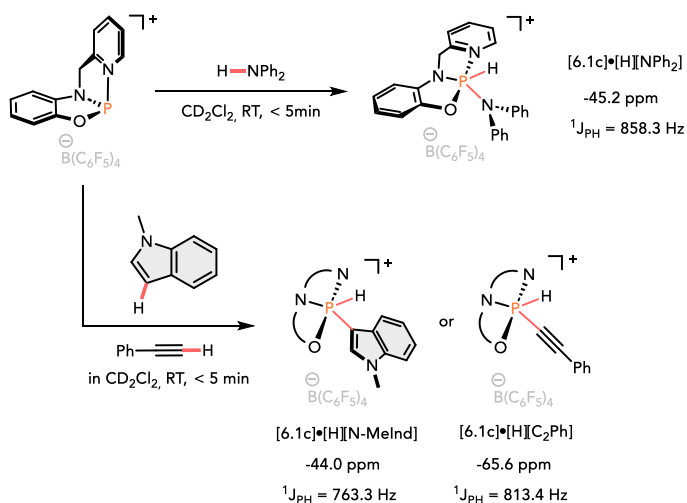


**Figure 6-7:** Reactions of 6.1c with diphenylamine, 1-methylindole and phenylacetylene, as well as $^{31}$P NMR chemical shifts and coupling constants of the products.

Other, more electron-poor substrates such as thiophene however could not be converted the same way even after heating to 80 °C, despite the previous reactions all running to completion within minutes at room temperature.

## 6.6  Reaction Mechanism

To elucidate the mechanism and identify the key factors that limited the scope, the reaction was studied at the DSD-BLYP-D3(BJ)/def2-QZVPP+SMD(CH$_2$Cl$_2$)//r$^2$-SCAN-3c level of theory.[70b, 92a, 92c, 111] Foregoing studies of E-H bond additions to structurally constrained phosphines had proposed bond cleavages by ligand-assisted pathways.[48, 49b] Prohibitive barriers (exceeding 50 kcal mol$^{-1}$) were computed for the alternative, single-site oxidative additions as seen in some transition-metal complexes. Depending on the specific phosphine, ring-chain σ$^3$-P/σ$^5$-P tautomerization ensued after cooperative E-H bond cleavage, which completed the overall oxidative addition process. In agreement with the precedent, concerted addition to 6.1c was ruled out with a computed barrier of 55 kcal mol$^{-1}$ for 1-methylindole as substrate.

Consequently, a ligand-assisted pathway was considered next, for which the mechanistic details are depicted in fig. 6-8. The sequence is initiated by isomerization of the folded, relaxed structure to the more reactive, T-shaped intermediate IM-I, as outlined previously (fig. 6-5A). As the substrate approaches IM-I, the pyridine moiety continually dissociates, and the now acidified proton is deprotonated *via* the seven-membered transition state TS-II. A conceptual similarity to the electrophilic concerted metalation deprotonation step seen in C-H activation by electropositive, late transition metals typically assisted by carboxylate ligands should be noted here (see chapter 1.5).[53-54] The intermediate IM-II then undergoes isomerization to IM-III with the pyridinium and phosphorus in the correct orientation to engage in the proton transfer. The ring-chain σ$^3$-P/σ$^5$-P tautomerization *via* TS-III completes the sequence and delivers the final product of oxidative addition. Due to better stabilization of the partial positive charge, the same reaction at the 2-position of 1-methylpyrrole has a lower barrier TS-II for the deprotonation. However, the subsequent proton transfer *via* TS-III ascends substantially in energy, disfavoring this pathway (table 6-1, entry 1).

Next, we investigated the impact of substituents and substrate combinations on the individual steps of the reaction (table 6-1). It was found that all substituents at all positions on the pyridine ring lower both TS-II and TS-III for all computed examples, which was true for both electron-withdrawing halides or an electron-donating methoxy group (for example by 4.9 and 3.4 kcal mol$^{-1}$ for bromo- and methoxy-substituents in pyridine-*ortho*-position, entries 2, 7, the only exception was
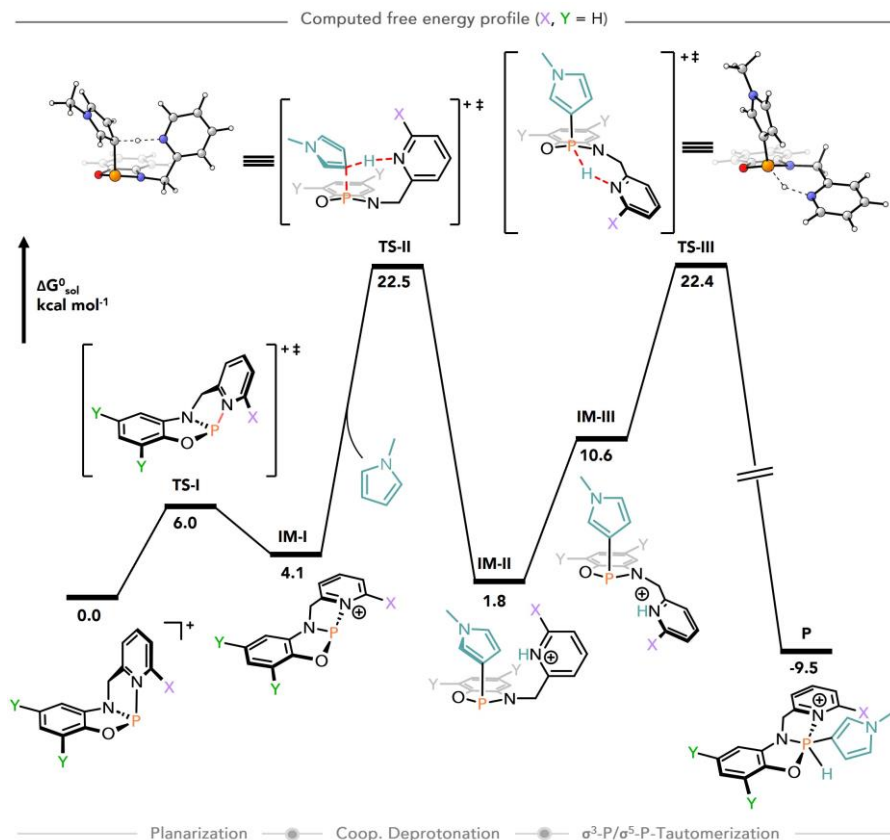
**Figure 6-8:** Computed free energy profile for the oxidative addition of 1-methylpyrrole to 6.1c at the DSD-BLYP(D3BJ)/def2-QZVPP-SMD(DCM)//r²-SCAN-3c level of theory.

The greatest effect on TS-II was felt after substituting the pyridine-*ortho*-position, as demonstrated with barriers computed for varying bromine-substitution patterns (see entries 2 – 5, table 6-1). Attaching functional groups to the amidophenolate ring instead of the pyridine has lower impacts on the reaction barriers, but the addition of two chlorine atoms makes the overall thermodynamics of the oxidative addition of 1-methylpyrrole more favorable (entry 9). The greatest product stabilization, however, was achieved with a methoxy group in the pyridine-*ortho*-position (entry 7).

**Table 6-1:** Calculated thermodynamics of C-H oxidative addition at the DSD-BLYP(D3BJ)/def2-QZVPP+SMD(CH₂Cl₂)//r²-SCAN-3c level of theory. *Values are given for reaction at the 3-position, values in brackets are for reaction at the 2-position.

| Entry | Compound | | | | | | 1-methylpyrrole* | | | | benzene | | | thiophene | | |
|---|---|---|---|---|---|---|---|---|---|---|---|---|---|---|---|---|
| | 1 | 2 | 3 | 4 | A | B | IM-I | P | TS-II | TS-III | P | TS-II | TS-III | P | TS-II | TS-III |
| 1 | H | H | H | H | H | H | 4.1 | -9.5 [-3.8] | 22.5 [20.9] | 22.4 [25.6] | -4.7 | 36.2 | 28.7 | -5.2 | 30.2 | 27.4 |
| 2 | Br | H | H | H | H | H | 1.1 | -8.8 | 17.6 | 20.2 | -3.9 | 34.1 | 25.9 | -3.9 | 24.6 | 24.6 |
| 3 | H | Br | H | H | H | H | 2.3 | -10.3 | 20.0 | | | | | | | |
| 4 | H | H | Br | H | H | H | 3.3 | -9.8 | 21.0 | | | | | | | |
| 5 | H | H | H | Br | H | H | 2.3 | -10.4 | 21.7 | | | | | | | |
| 6 | Cl | H | H | H | H | H | 1.1 | -9.1 | 18.0 | | | | | | | |
| 7 | OMe | H | H | H | H | H | | -14.2 | 19.1 | 16.9 | | | | | | |
| 8 | F | H | H | H | H | H | | -10.5 | 16.8 | | | | | | | |
| 9 | H | H | H | H | Cl | Cl | 5.0 | -11.6 | 20.4 | 21.3 | -6.3 | 34.9 | 26.3 | -6.2 | 28.8 | 26.9 |
| 10 | H | H | H | H | H | OMe | 3.8 | -9.2 | 22.9 | 23.2 | | | | | | |
| 11 | Br | H | H | H | Cl | Cl | 2.4 | -10.6 | 15.5 | 18.2 | -5.4 | 33.5 | 23.0 | -4.9 | 23.5 | 24.0 |
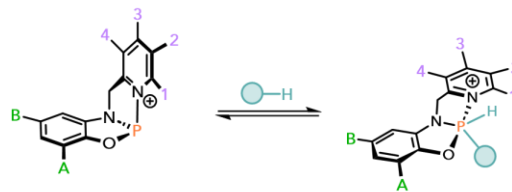
Overall, the substituents effects appeared to be stackable, as the total stabilization of products and transition states for multiply substituted phosphenium ions equaled the sum of stabilizations contributed by each individual substituent (compare entry 11 with 2 and 9). The combinatorial nature should enable precise tuning of both kinetics and thermodynamics of C-H bond activation. The equilibrium between bent and planar isomers IM-I was also greatly influenced by the substitution pattern and was tilted towards the planar IM-I for all but one of the investigated patterns (i.e. entry 10).

While TS-II and TS-III are predicted to be almost isoenergetic for the oxidative addition of 1-methylpyrrole to 6.1c, the relative barrier heights are shifted as the nucleophilicity of the arene substrate changes. As the nucleophilicity decreases for substrates such as thiophene or benzene, the deprotonation step TS-II becomes increasingly rate-determining as it is affected more prominently by the nature of the substrate. The high barrier for deprotonation of thiophene by 6.1c was consistent with the observed lack of reactivity. Importantly, the prepared salts 6.2c and 6.4c featured some of the lowest activation energies for oxidative addition of all investigated substrates. Of note here is that while TS-III of the methoxy-substituted cation (entry 7) is located the lowest in energy relative to the separated reactants, the deprotonated intermediate IM-II is stabilized by 3.0 kcal mol$^{-1}$ relative to the educts, resulting in an overall barrier of 19.9 kcal mol$^{-1}$ for the proton transfer to phosphorus.

## 6.7    Extended Scope of C-H Oxidative Addition

With an understanding of the factors driving the oxidative addition of C-H bonds, 6.2c and 6.4c were tested in the reaction with previously unreactive thiophene. In accordance with the computational results, oxidative addition occurred readily and cleanly at room temperature, and quantitative formation of the desired $\sigma^5$-P(V)-H cations [6.2c]•[H][C$_4$H$_3$S] and [6.4c]•[H][C$_4$H$_3$S] was achieved after 2 days and 5 hours, respectively (figure 6-9). For the reaction with 6.2c, X-ray quality crystals deposited after cooling the concentrated solution in dichloromethane. The resulting solid-state structure unequivocally identified the product of C(sp$^2$)-H oxidative addition of thiophene to 6.2c (figure 6-10). In the structure, the NNO chelating ligand coordinates meridionally at phosphorus, with the hydrido and thiophenyl groups occupying equatorial positions of the phosphorus-centered trigonal bipyramid.
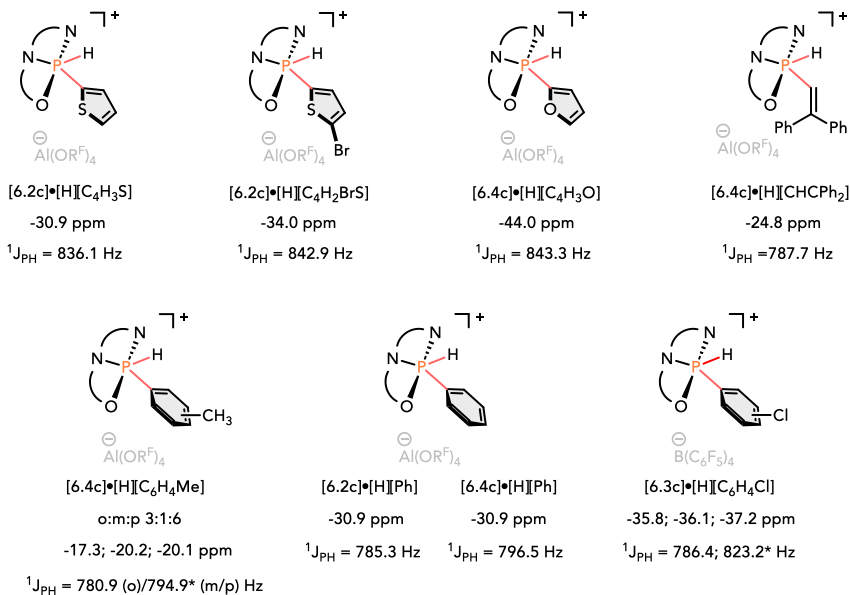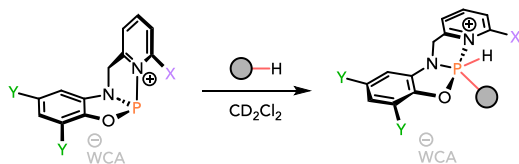
**Figure 6-9:** Extended scope for the oxidative addition of $C(sp^2)$-H bonds to 6.2 – 6.4c and $^{31}P$ NMR data. Yields were essentially quantitative in all cases.

The dichloro-substituted phosphenium ion of 6.3c only showed negligible conversion of thiophene at room temperature but could also be fully converted to the thiophenyl hydrido P(V) cation after heating to 60 °C for two hours. Other related heteroarenes such as 2-bromothiophene and furan were also oxidatively added to afford [6.2c]•[H][$C_4H_2BrS$] and [6.4c]•[H][$C_4H_3O$] in quantitative yields. Interestingly, the reaction with 2-bromothiophene only ran to completion with excess substrate, indicating a close to thermoneutral transformation and potential reversibility of the reaction. Going a step further to even less nucleophilic, unactivated benzene as substrate, 30 % conversion to the phenyl hydrido P(V) cation [6.4c]•[H][Ph] was observed after heating a solution of 6.4c in a 1:5 mixture of $CD_2Cl_2$ and benzene to 80 °C for a day. Complete conversion of 6.4c to the P(V)-H cation

was then achieved after heating for another day at 100 °C. The same reaction with 6.2c required two days at 110 °C to achieve quantitative oxidative addition. Vapor diffusion of pentane into the reaction solution led to single crystal deposition and a solid-state structure consistent with oxidative addition of benzene to 6.2c (fig. 6-10).
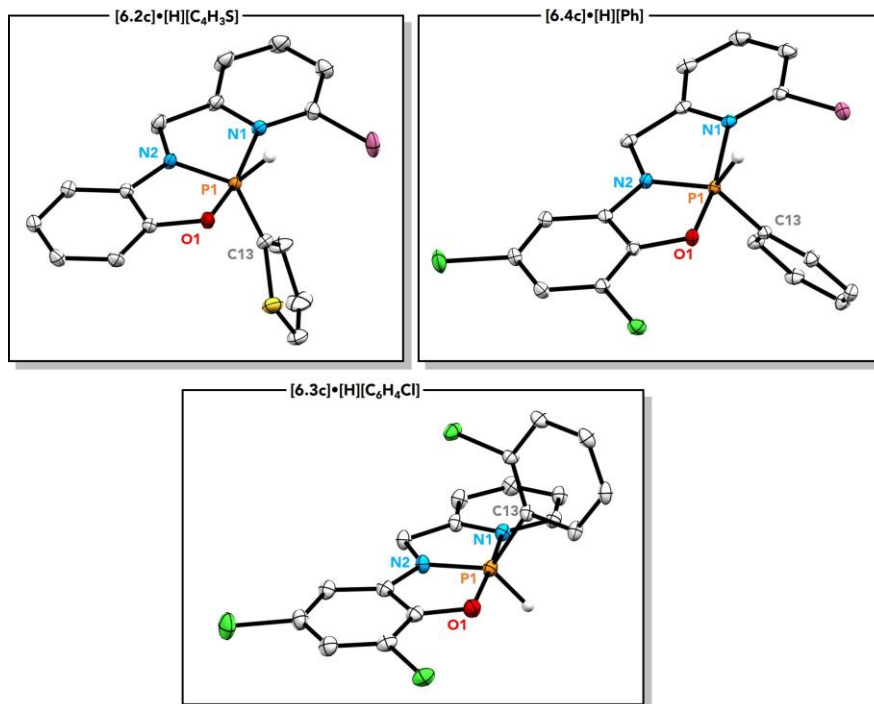


**Figure 6-10:** Solid-state structures of [6.2c]•[H][C₄H₃S] , [6.4c]•[H][Ph] , and [6.3c]•[H][C₆H₄Cl] at 30% probability. The counterion [B(C₆F₅)₄] and all carbon-based hydrogen atoms have been omitted for all structures for clarity. Selected bond distances [Å] and angles [deg] of **[6.2c]•[H][C₄H₃S]**: d(P1−N1) = 1.9760(14), d(P1−N2) = 1.6769(14), ∠O1−P1−N1 = 169.21(6), ∠O1−P1−N2 = 91.07(7), ∠N2−P1−N1 = 82.66(7); **[6.4c]•[H][Ph]**: d(P1−N1) = 1.9966(18), d(P1−N2) = 1.6735(17), ∠O1−P1−N1 = 170.90(7), ∠O1−P1−N2 = 91.22(8), ∠N2− P1−N1 = 82.34(8); **[6.3c]•[H][C₆H₄Cl]**: d(P1−N1) = 1.918(2), d(P1−N2) = 1.670(2), ∠O1−P1−N1 = 170.04(9), ∠O1−P1−N2 = 89.92(9), ∠N2−P1−N1 = 83.44(9).

Ligand and substrate are arranged analogously to [6.2c]•[H][C₄H₃S], and the phosphorus center adopts a trigonal bipyramidal geometry. The intermolecular, single-site oxidative addition of benzene presents an extremely challenging reaction, and the only existing precedents for main group compounds were

reported with highly nucleophilic aluminyl anions by Aldridge and Yamashita.[59, 61, 112] The scope was further extended to more activated arenes such as toluene and the reactions proceeded under milder conditions (one day at 70 °C). Integration of the appropriate $^1$H NMR resonances revealed a 3:1:6 mixture of *ortho*-, *meta*- and *para*-C-H activation, consistent with the proposed electrophilic C-H activation mechanism. Even the oxidative addition of deactivated chlorobenzene to 6.3c was achieved at 140 °C and a mixture of regioisomers was obtained. The product of *ortho*-C-H cleavage at chlorobenzene crystallized from the reaction mixture (fig. 6-10, ~10 % of the *para*-product was mixed into the crystal as disorder). Aside from arenes, the C-H bond of the alkene 1,1-diphenylethylene was also selectively severed by 6.4c at room temperature to afford [6.4c]•[H][CHCPh$_2$]. Other unactivated alkenes such as 1-hexene were also reactive but competing side reactions (i.e. isomerizations) resulting in low selectivities and precluded the unambiguous identification of the reaction products.

## 6.8 Reversibility of C-H Bond Activation

As described above, an excess of 2-bromothiophene was required to drive the reaction to completion, which had indicated a reaction close to thermoneutral and the potential reversibility of the oxidative addition. The fact that the OA products are not overly stabilized from a thermodynamic point of view (~4 – 6 kcal mol$^{-1}$) further underpinned that the reverse reaction, i.e. the reductive elimination should be feasible at elevated temperatures. To confirm the hypothesis, a solution of the isolated compound [6.2c]•[H][C$_4$H$_2$BrS] in CD$_2$Cl$_2$ was monitored by $^1$H and $^{31}$P NMR (fig. 6-11). The P(V)-H cation was stable at room temperature, but after heating to 60 °C continuous recovery of the starting materials 6.2c and bromothiophene was observed. The reaction proceeded until an equilibrium with the ratio of σ$^3$-P and σ$^5$-P compounds of 71:29 was reached after one day. The observations provided direct evidence for reductive elimination, making this the first example of reversible OA of C-H bonds at a main group element to the best of our knowledge. Next, we sought to generalize the reversibility of the C-H activations for substrate and phosphenium ions combinations further removed from thermoneutrality. To show this, we surmised that the phosphenium ions intermediately formed by reductive elimination could be intercepted by other substrates leading to thermodynamically

more stable products.
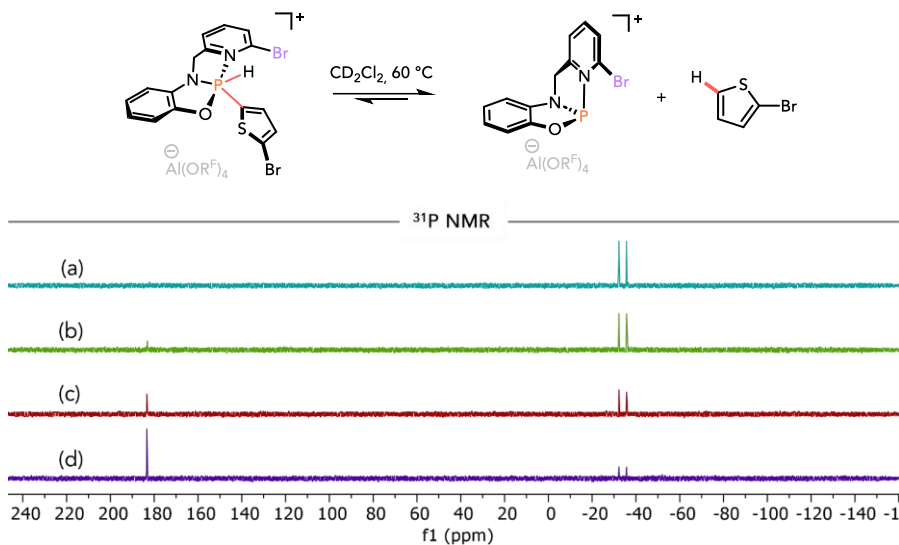
Treatment of 6.2c or 6.4c with 2-methylthiophene led to immediate and quantitative OA. To the $\sigma^5$-P products was then added 1-methylindole, and new ³¹P NMR signals emerged over the course of one day at room temperature, consistent with formation of the more stable indole addition products (fig. 6-12A). Complete arene exchange at the phosphenium ions was achieved after heating the reaction for two hours at 60 °C. By contrast, the analogous exchange at 6.1c occurred only after prolonged heating to 80 °C. By adjusting the reaction conditions, even the reductive elimination of benzene from [6.4c]•[H][Ph] was indirectly observed after heating the benzene adduct in toluene-d₈ at 130 °C. In this case, the aromatic C(sp²)-D bonds were cleaved, and a mixture of toluene-d₈ addition products was detected in the ³¹P NMR spectra along with the characteristic singlet of benzene in the proton NMR spectrum (fig. 6-12B). The proposed reductive elimination-oxidative addition sequence for the substrate exchange was supported by the absence of H/D scrambling product, disproving other conceivable proton transfer pathways.
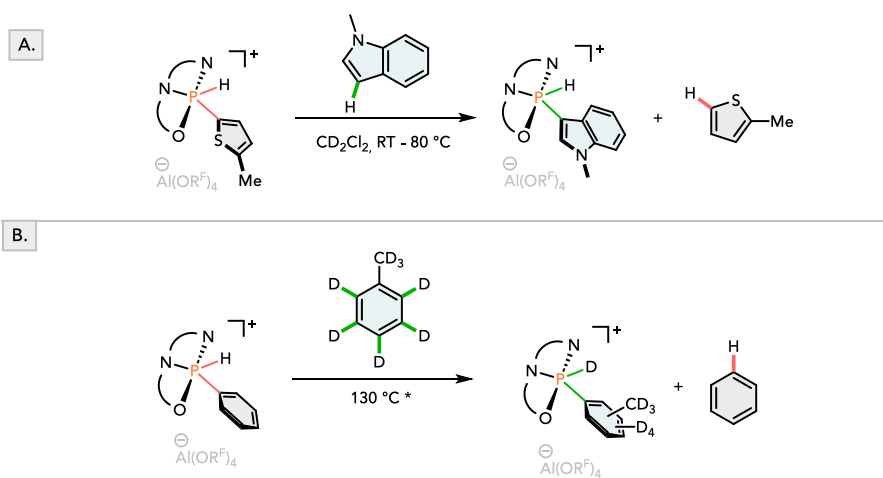
**Figure 6-12: A.** Exchange of 2-methylthiophene with 1-methylindole at 6.2c, 6.4c and 6.1c (the latter requiring 80 °C). **B.** Exchange of benzene with toluene-d8 at 6.4c. *A toluene-d8:CD2Cl2 5:1 mixture was used for better solubility.

Next, the solution of [6.4c]•[H][SC4H3-CH3] was treated with strong, non-basic donors such as *N*-methylpyrrolidone (NMP) to try and force the reductive elimination of 2-methylthiophene attached to 6.4c in a different way. Analysis of the solution disclosed a new doublet at $\delta$ -32.5 ppm ($^1J_{PH}$ = 608.4 Hz) in the $^{31}$P NMR spectrum that had quickly replaced the signal of the starting material (fig. 6-13B). Under consideration of the combined, multinuclear NMR data, it was assigned to product 6.5 (fig. 6-13A(i)), where the amide has displaced the pyridine from the coordination sphere of phosphorus. Over the course of a day of reaction time, follow-up reactions of 6.5 to other P(V)-H species were detected in solution (fig. 6-13B). To suppress the displacement reaction seen with NMP, the experiment was repeated using the bulkier amide *N*,*N*-diisopropylbenzamide (DIBA). However, only rapid deprotonation of [6.4c]•[H][SC4H3-CH3] to the corresponding phosphonite 6.6 was revealed by $^{31}$P NMR (fig. 6-13A,C).
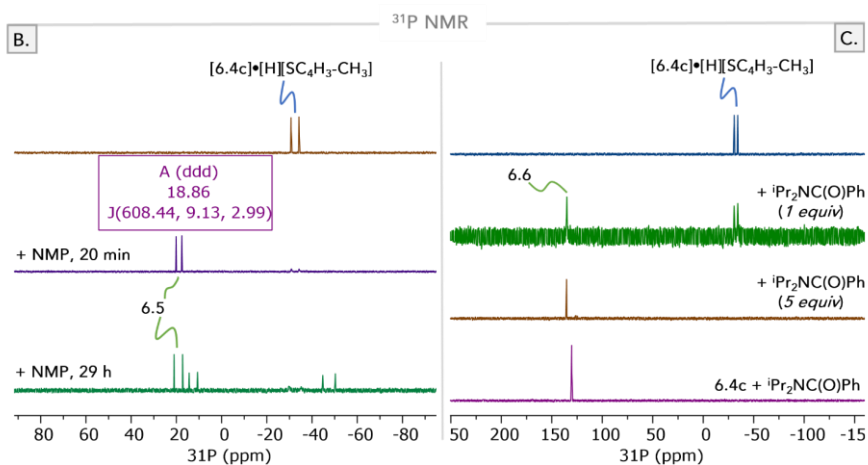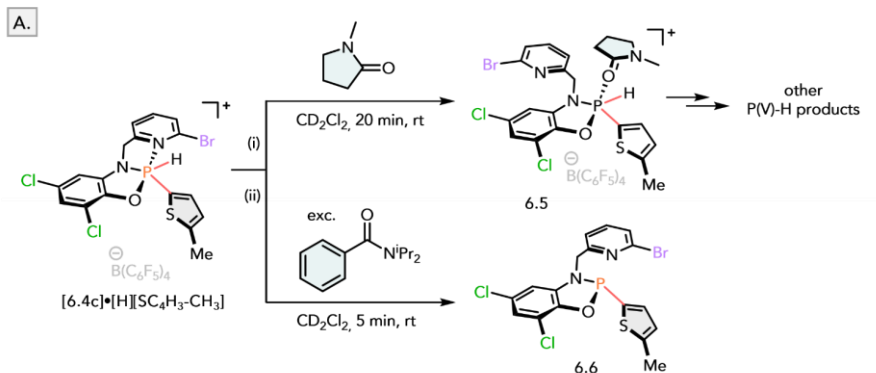
**Figure 6-13: A.** Reaction of [6.4c]•[H][SC₄H₃-CH₃] with different amides. Stacked, abridged NMR spectra of the reaction with **B.** NMP and **C.** DIBA (bottom NMR spectrum shows control with just 6.4c and DIBA).

## 6.9 Application to Arene Phosphorylation

Finally, we sought to demonstrate the feasibility of applying the unusual OA reactivity of the phosphenium ions prepared herein for the direct functionalization of arenes. Subjecting benzene to 6.4c under the optimized conditions, followed by hydrolysis of generated [6.4c]•[H][Ph] afforded phenylphosphinic acid in 91 % yield

over the course of twenty hours at room temperature, as well as the protonated ligand 6.4a as byproduct (fig. 6-14).
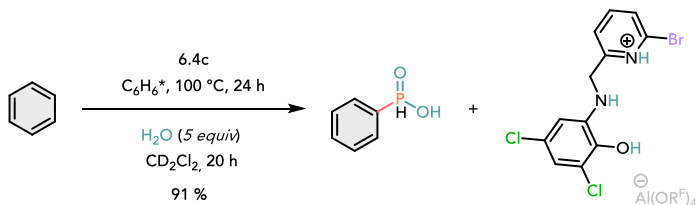


**Figure 6-14:** Protocol for the synthesis of phenylphosphinic acid from benzene and 6.4c. *For better solubility of the phosphenium salt, a 1:5 mixture of $CH_2Cl_2$ and benzene was used.

## 6.10 Reactivity Towards Silanes

Aside from C-H and N-H bonds, the pyridinylmethylamidophenolato-phosphenium ions were also reactive towards the Si-H bonds of tertiary silanes. Treating a solution of 6.1c with triethylsilane led to formation of two new products within a few hours, of which the major product was identified as the formal dihydrogen addition product 6.1c-$H_2$ (fig. 6-15A and B). Repeating the reactions with bulkier silanes such as $^iPr_3SiH$ or $Ph_3SiH$ initially produced mixtures of both 6.Xc-$H_2$ and a $\sigma^5$-P-H species identified as the product of oxidative addition. While further studies are required to decipher the mechanism that ends with the formation of 6.Xc-$H_2$, we propose that the oxidative addition of the silane presents an intermediate on the way there. Exposure of 6.1c or 6.2c to primary silanes such as $PhSiH_3$ or the borane 9-borabicyclo[3.3.1]nonane (9-BBN) led to the same reaction outcomes with the formal dihydrogen adduct as the end product (fig. 6-15A,C).

## 6.11 Conclusion

In conlusion, we have demonstrated the reversible oxidative addition of even unactivated $C(sp^2)$-H bonds at pyridylmethylamidophenolato-ligated phosphenium ions. A series of the phosphenium salts was prepared by a modular, facile synthetic procedure.The phosphenium ions adopt a bent structure, but undergo low-barrier isomerization to a more reactive, planar and T-shaped intermediate only ~4 kcal mol$^{-1}$ higher in energy.
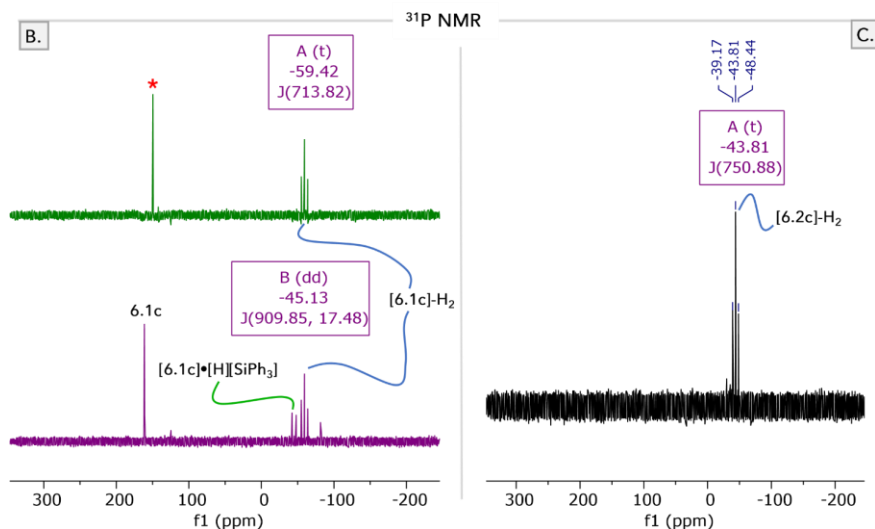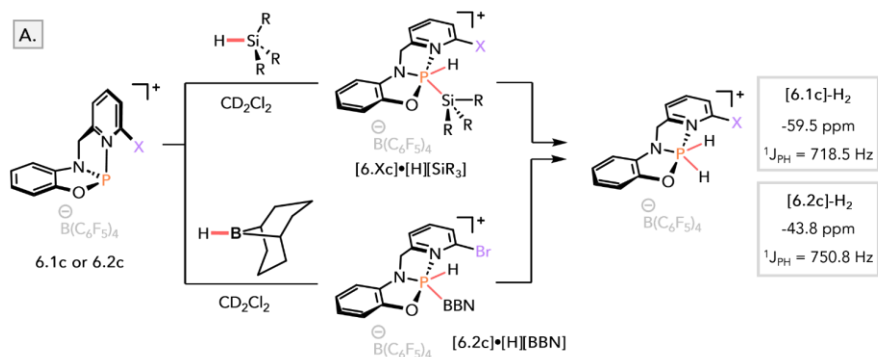
**Figure 6-15: A.** Reaction of 6.1c and 6.2c with different silanes (R = Ph, $^{i}$Pr, Et) and 9-BBN including $^{31}$P NMR data. **B.** Abridged $^{31}$P NMR spectra of the reaction of 6.1c with Et$_3$SiH (top) and Ph$_3$SiH (bottom). **C.** $^{31}$P NMR spectrum of the reaction of 6.2c with 9-BBN.

Theoretical insights by DFT calculations showed that the key to the C-H activation was a cooperative deprotonation step. Ensuing $\sigma^3$-P/$\sigma^5$-P ring-chain tautomerization led to overall oxidative addition of the substrate. Crucial to this reactivity was the high Lewis acidity at phosphorus, demonstrated experimentally with the Gutmann-Beckett method. Precise control over the reactivity could be exercised by modifications of the ligand periphery, and the transition states for C-H actication substantially lowered this way. Reversibility of the oxidative addition was shown

directly by reductive elimination at elevated temperature or exchange with other substrates. A stoichiometric application of the phosphenium ions to the direct synthesis of phenylphosphinic acid from benzene was shown, and catalytic arene functionalization might be possible in the future. The asymmetry of the phosphenium ions might also lead to future applications to stereo- or enantioselective bond activations.

112

# Summary

In this work, catecholate and amidophenolate substituents were employed to bestow p-block elements, namely germanium and phosphorus, with new modes of reactivity. The structural constraint enforced by the bidentate ligands not only created Lewis superacids, but also facilitated the activation of inert bonds by element-ligand cooperativity.

In the first part of this work perhalogenated bis(catecholato)germanes and their adducts were synthesized and characterized (fig. S1). Calculation of fluoride and hydride ion affinities categorized bis(perchlorocatecholato)germane as both a hard and soft Lewis superacid, which was confirmed experimentally using the acetonitrile adduct in abstraction experiments with $SbF_5$ and BCF. The water stability was rationalized by comparison of computed thermodynamics and structural features with the silicon counterparts. Gas phase acidity values also supported substantial Brønsted acidity of the water adduct. Preparation of the perfluorinated germane $Ge(cat^F)_2$ conferred improved solubility in water, as well as easier NMR characterization. A wide spectrum of applications for $Ge(cat^{Cl})_2$-$(CH_3CN)_2$ as versatile and robust Lewis acid catalyst was demonstrated, for instance in hydrodefluorination, hydrosilyation, transfer hydrogenations or carbonyl-olefin
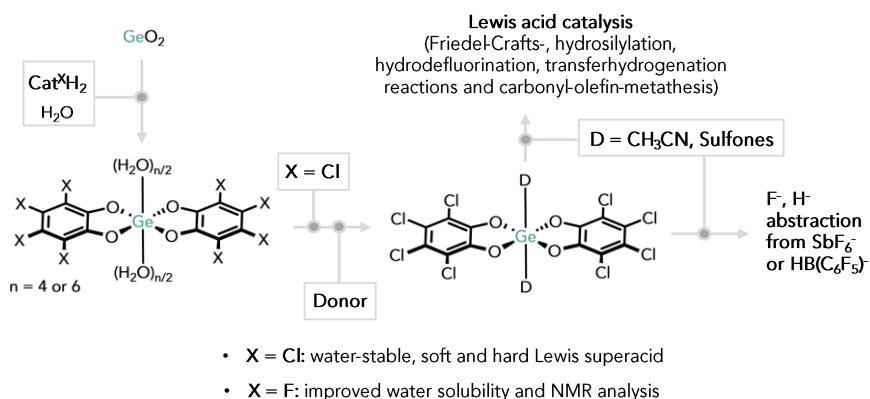
**Figure S1:** Schematic overview of the results from chapter 2.

metathesis reactions. Improvements to the catalytic efficacy could be made by synthesis of sulfone adducts, which delivered both enhanced chemical robustness and weaker coordination to the Lewis acid. The straightforward synthesis and handleability under benchtop conditions should yield many potential applications in organic synthesis and materials science.

The second part of this work disclosed the first synthesis and isolation of stable bis(catecholato)phosphonium salts, as well as chiral catecholato-phosphonium salts (fig. S2). Even without perhalogenated substituents or multiple charges, the phosphonium ions ranked among the strongest isolable Lewis acids according to computed anion affinities and experimental Gutmann-Beckett shifts. Energy decomposition analysis proposed a low preparation energy resulting from structural constraint imparted by the rigid catecholate ligands as key contributor to the Lewis superacidity. The phosphonium salts were potent Lewis acid catalysts for the hydrosilylation of alkenes, hydrodeoxygenation of ketones or ring-closing carbonyl-olefin metathesis to both five- and six-membered rings. New modes of phosphorus-ligand cooperative bond activations were facilitated by the juxtaposition of electrophilic phosphorus and nucleophilic oxygen sites. Depending on the deployed phosphonium salt, different activation modes in the ligand-assisted $C(sp^2)$-H activation were observed, which presented rare examples of uncatalyzed, electrophilic phosphorylations. Remarkably, non-acidic $C(sp^2)$-H bonds ($pk_A > 30$) were turned into highly acidic OH groups (estimated $pk_a < 3$). Quantum mechanical calculations disclosed a mechanism similar to electrophilic aromatic substitutions with intramolecular deprotonation of a Wheland-type intermediate. Selectivity complementary to transition metals was demonstrated in the selective CH activation of 2-bromothiophene. Unsaturated hydrocarbons such as alkynes and alkenes were also added by phosphorus-ligand cooperation. In the cleavage of Si-H bonds, umpolung of the hydride to an acidic proton and transfer of the silyl group to the catecholate oxygen was observed.

To obtain further control over the electronic and steric profile of the spirophosphonium ions, bis(amidophenolato)phosphonium salts with varying degrees of fluorination in the ligand periphery were synthesized (fig. S2).

Gutmann-Beckett tests and computed ion affinities attested to the greater range of achievable Lewis acidities. Importantly, the electron-withdrawing capabilities of the
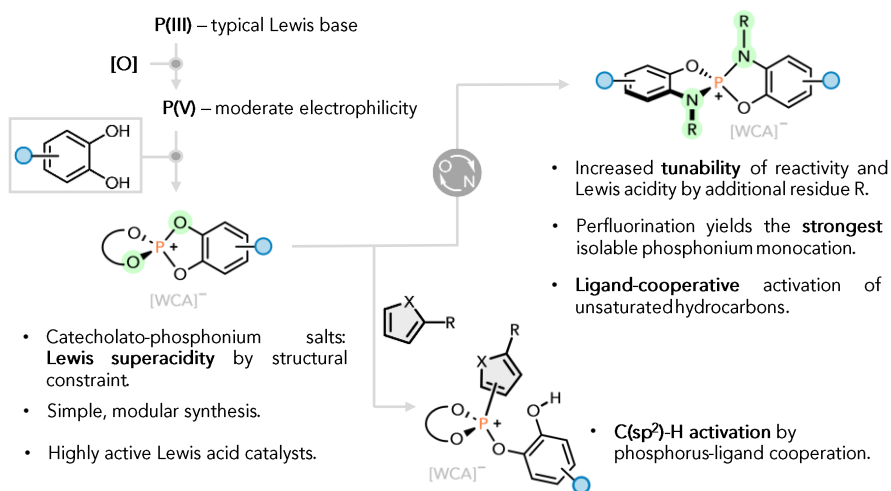
**Figure S2:** Schematic overview of the results from chapter 3 and 4.

perfluorinated amidophenolate led to isolation of the strongest, monocationic phosphonium ion to date, surpassing all isolated catecholato-phosphonium ions. The altered reactivity manifested in the different activations of Si-H and multiple carbon-carbon bonds. The mechanism for the alkyne addition leading to phosphine oxides connected to indol(ium) fragments was deciphered by DFT calculations and found to be initiated by cooperative alkyne addition to phosphorus and an amidophenolate carbon. By using a substrate with an intramolecular nucleophilic group, the alkyne activation could be turned into a catalytic process. Capitalizing on the high activity toward alkynes and alkenes, metal-free catalysts for π- and σ-catalysis could be developed in the future based on the presented scaffold.

Combining both catecholate and a *N*-pyridylamidophenolato substituents at phosphorus led to preparation of intramolecular frustrated Lewis pairs (fig. S3). The $C(sp^2)$-H bonds of even relatively unactivated arenes such as toluene could be cleaved between electrophilic phosphorus and nucleophilic pyridine *via* a FLP-type mechanism. Computational insights explained the lack of reaction towards other substrates such as silanes, dihydrogen, or carbon dioxide by the rigidity of the pyridyl linker resulting in a high deformation energy required to alter the structure enough to accommodate the weakly donating substrates. The last part of this work covered the synthesis and reactivity of structurally constrained phosphenium ions embedded in pyridylmethylamidophenolate ligands (fig. S4).
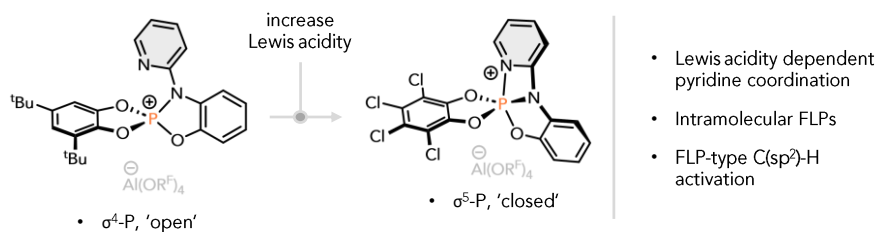
**Figure S3:** Schematic overview of the results from chapter 5.

The compounds were shown to activativate C-H bonds by oxidative addition. While the cations adopted a folded minimum structure, a more reactive, planar and T-shaped isomer (only ~4 kcal mol$^{-1}$ higher in energy) could be accessed by a low-barrier isomerization. This equilibrium, reaction kinetics and thermodynamics of the oxidative additions could be precisely tuned by variations in the ligand periphery. This way, even the C-H bonds of unactivated arenes such as benzene or chlorobenzene were selectively cleaved. DFT calculations predicted the C-H cleavage to occur by a cooperative deprotonation step, which was followed by $\sigma^3$-P/$\sigma^5$-P ring-chain tautemerization to complete the overall oxidative addition process. Direct observation of reductive elimination of 2-bromothiophene from the corresponding adduct at elevated temperatures corroborated the reversibility of the C-H oxidative addition, which was unprecedented for main-group compounds.
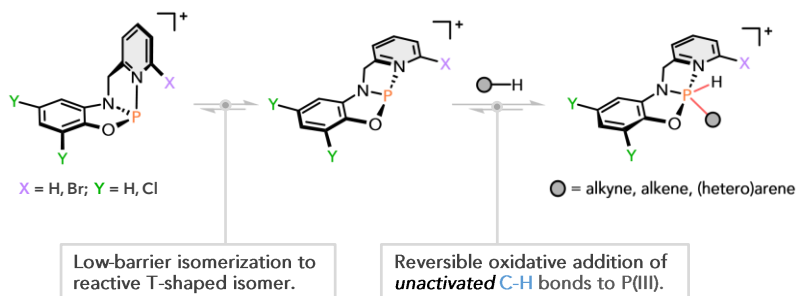


**Figure S3:** Schematic overview of the results from chapter 6.

The general nature of the reversibility was further evidenced by substrate exchange reactions. An application to the direct synthesis of phenylphosphinic acid from benzene was demonstrated with a protocol employing stoichiometric phosphenium

salt. Future endeavors may uncover applications to the catalytic functionalization of arenes, and the inherent asymmetry of phosphenium ions might also lend itself to stereo and enantioselective bond activations by appropriate modifications to the ligand framework.

# Chapter 7

# Experimental Section

## 7.1 General Information

### 7.1.1 Materials and Methods

Unless stated otherwise, all experiments were carried out under inert argon atmosphere using standard Schlenk techniques in flame-dried laboratory glassware or under a dry nitrogen atmosphere inside a glovebox (SylaTech (Y-05-G-7986), MBraun LABstar (MB-10-G) or MBraun LABmaster DP (MB-20-G)) to prevent oxidation or hydrolysis of air and moisture sensitive compounds. All solvents were rigorously dried by applying standard procedures, freshly degassed and stored over molecular sieve (3 Å resp. 4 Å) for at least two days prior to use. Argon used in the Schlenk-line was passed over a heated Cu-catalyst[113] and phosphorus pentoxide and molecular sieves (4 Å) to remove any traces of oxygen or moisture. All glassware, syringes, needles, and magnetic stirring bars were thoroughly dried.

Solvents and chemicals used in this work were acquired either from the chemical store of the chemical institutes at Heidelberg University or were purchased from commercial suppliers: Sigma Aldrich (Merck KGaA), abcr GmbH, Alfa Aesar and Acros Organics B.V.B.A. (Thermo Fisher Scientific), VWR, TCI Chemicals, Fluorochem, Oakwood Chemical, Strem, and BLD Pharm.

Dichloromethane, acetonitrile, hexane, diethyl ether and tetrahydrofuran were obtained from a solvent purification system (MB-SPS-800, MBraun). Deuterated solvents were purchased from Deutero GmbH, Eurisotop or Sigma Aldrich and

degassed by three or four freeze-pump-thaw cycles and stored over activated molecular sieves (3 or 4 Å) in for at least 24 h prior to use. Acetonitrile and DMSO were degassed by saturation with argon.

$Cat^{Cl}H_2$,[18a] $Cat^FH_2$,[114] $NaB(C_6F_5)_4$,[115] $LiAl(OC(CF_3)_3)_4$,[116] aminophenols 4.1a, 5.1[102], 4.1b[100] and 4.1c,[96] COM substrates 3.4,[74] 3.6a, 3.6b and 3.6c,[89b] [$^tBu_3PH$][$HB(C_6F_5)_3$],[117] 2-(Phenylethynyl)-1,1'-biphenyl[118] were prepared according to literature-known procedures.

Analytical data of the known compounds were in agreement with literature data for all the compounds.

## 7.1.2    Analytical Methods

Purity and identity of the prepared compounds were confirmed by high resolution multinuclear NMR spectroscopy, mass spectrometry, elemental analysis and where possible, X-ray diffraction analysis.

### Elemental Analysis
The determination of C-, H- and N-content [%] by elemental analysis was carried out by the staff of the microanalytical laboratory at Heidelberg University on an elemental analyzer (vario EL or vario MICRO cube, Elementar Analysensysteme GmbH).

### Mass Spectrometry
High resolution mass spectrometry (HR-MS) experiments were measured on a Bruker ApexQe FT-ICR instrument (ESI) or a JEOL AccuTOF GCx instrument (EI) by the Mass Spectrometry Facility at the Institute of Organic Chemistry at Heidelberg University.

### Nuclear Magnetic Resonance Spectroscopy
$^1H$, $^7Li$, $^{13}C$, $^{19}F$, $^{11}B$, $^{29}Si$ and $^{31}P$ NMR spectra were recorded at 295 K with a Bruker DRX200, Bruker Avance II 400, Bruker Avance Neo 500 or Bruker 2 Avance III 600 NMR spectrometer and referenced to the solvent in use.[119] Measurements were carried out by the NMR facility at the Institute of Inorganic Chemistry at Heidelberg University or by myself. $^{13}C$ NMR spectra were recorded $^1H$ decoupled. Chemical shifts are reported as dimensionless δ values in ppm, coupling constants J are given

in Hertz (Hz). Additionally, 2D NMR experiments were measured for the complete assignment of the signals.

## X-ray diffraction

Suitable crystals were taken directly from the mother liquor, immersed in a perfluorinated ether oil, and fixed on a cryo loop. The diffraction data was collected from a shock-cooled single crystal at 100 K (except if noted otherwise in the crystal structure data) on a Bruker D8 VENTURE dual wavelength Mo/Cu three-circle diffractometer with a microfocus sealed X-ray tube using mirror optics as monochromator and a Bruker PHOTON III detector. The diffractometer was equipped with an Oxford Cryostream 800 low temperature device and used Mo $K_\alpha$ radiation (λ = 0.71073 Å). Only the structure of [Et$_4$N]$_2$[2.1-Cl$_2$] was measured on an Agilent Technologies Supernova-E CCD diffractometer (Cu-Kα radiation, microfocus X-ray tubes, multilayer mirror optics). All data were integrated with SAINT and a multi-scan absorption correction using SADABS was applied.[120] The structures were solved by direct methods using SHELXT (for [Et$_4$N]$_2$[2.1-Cl$_2$], the structures was solved by ab initio dual space methods (SHELXD)) and refined by full-matrix least-squares methods against $F^2$ by SHELXL-2018/3 as implemented in ShelXle.[121] All non-hydrogen atoms were refined with anisotropic displacement parameters. The hydrogen atoms were refined isotropically on calculated positions using a riding model. Disorders were modelled with DSR whenever applicable.[122] Parts of the crystallographic data for the structures reported in this work have been deposited with the Cambridge Crystallographic Data Centre.[123] This data can be obtained free of charge from The Cambridge Crystallographic Data Centre via www.ccdc.cam.ac.uk/structures. Parts of this report and the CIF files were generated using FinalCif.[124]

Several datasets were collected from different batches of crystals of [Et$_4$N]$_2$[2.1-Cl$_2$]. Although the structures could be refined successfully to rather low R values, strong residual electron density features were still present in delta-F Fourier maps, notably a strong peak with the same x and y coordinates as the Ge atom ("Ge ghost peak"). In addition, the Flack asymmetry parameter did not refine to zero. Inspection of the total diffracted intensity pattern revealed diffuse features, regularly arranged among the sharp reflections used to solve and refine the structure. This pattern is characteristic of OD (oder-disorder) structures, possibly combined with allotwinning.[125] No attempt was made to model these effects. Upon scrutiny of the

available crystals under a polarisation microscope a tiny platelet was eventually selected of which data were collected at 250 K with copper radiation. In this dataset, diffuse diffraction features were hardly recognizable. Indeed, refinement against these data resulted in a model with residual electron density only a little above background noise and a satisfactory asymmetry index. Although even with this crystal some OD effects cannot be ruled out completely, we believe that the molecular structure of [Et$_4$N]$_2$[2.1-Cl$_2$] reported here is little if at all affected.

For data visualization, Mercury 2032.2.0 was used.[126] The thermal displacement ellipsoids are shown at the 30 % probability level unless noted otherwise.

## Infrared Spectroscopy

Infrared (IR) spectra of solids were collected by deposition on an ATR-FTIR spectrometer (Cary 630, Agilent) equipped with a diamond sampling module inside a glovebox under nitrogen atmosphere. The IR absorption bands are reported in wavenumbers $\tilde{\nu}$ [cm$^{-1}$] and the signal intensities assigened as s = strong, m = medium, w = weak and br = broad, relative to the strongest signal in the respective spectra.

## 7.1.3    Computational Methods

### General Information

All structure optimizations and single point energy calculations were computed with the Orca 4.1.1/4.1.2 (chapter 2), Orca 4.2.1 (chapter 3) or Orca 5.0.1/5.0.2/5.0.3 program package (chapters 4 – 6).[111a, 111b, 127] Computed molecular structures were visualized with CYLview.[128] Orbitals were plotted using IboView v20211019-RevA.[129]

For the Coulomb Integral, the RI approximation (RIJCOSX) was applied along with the corresponding auxiliary basis sets.[130] Thermochemistry data to obtain Gibbs free energies under standard conditions (298.15 K and 1 atm) were obtained using the rigid-rotor harmonic oscillator (RRHO) approximation and the Quasi-RRHO approach by Grimme for low frequencies as implemented in the default settings of Orca at the same level of theory as the structure optimizations.[131] Frequency calculations were carried out on all optimized structures to ensure the correct nature of the stationary points, with zero imaginary frequencies for ground states and one imaginary frequency corresponding to transition states. Additionally, intrinsic

reaction coordinate (IRC) calculations were conducted when necessary to ensure that transition states connected to the correct minimum structures. The conformational space of particularly flexible systems was searched with the conformer-rotamer ensemble sampling tool for the xtb program package and the lowest-energy conformer reoptimized as described.[132]

### 7.1.3.1 Fluoride and hydride ion affinities

Fluoride (FIA) and hydride (HIA) ion affinities in chapter 2 were computed based on structures optimized at the BP86-D3(BJ)/def2-SVP level of theory,[131] reoptimized at the PW6B95-D3(BJ)/def2-TZVPP level of theory,[70b, 92d, 133] and final single point energies refined at the DLPNO-CCSD(T)/aug-cc-pVQZ level of theory.[93a, 134] Using the scheme proposed by Krossing and co-workers, anion affinities were determined by an isodesmic reaction scheme using G3 anchor points (as described in chapter 1.2.1).[6b, 135] Solvation free enthalpies for all molecular structures were determined using COSMO-RS, as implemented in the ADF program package and based on solute-solvent interactions calculated at the BP86-D3/TZP level of theory.[136] Summation over solvation enthalpies for Lewis acid, fluoride anion, fluoride adduct and the respective DLPNO-CCSD(T) vacuum enthalpies gave the corresponding solvation corrected anion affinities.

The affinities disclosed in chapters 3 and 4 were derived from structures optimized with the hybrid functional ωB97X-D3BJ[107] and the basis set def2-TZVPP, with structures confirmed as energetic minima by frequency calculations at the revPBE-D3(BJ)[92d, 137]/ def2-TZVP level of theory. For the final anion affinities, single point energies were calculated at the DLPNO-CCSD(T)/def2-TZVPP level of theory using the tightpno scheme and anchor points from Greb and co-workers were used.[13]

The gas phase acidity was computed according to the scheme by Krossing at the BP86/def2-TZVP level of theory.[70c]

### 7.1.3.2 NMR shifts

NMR shifts were calculated at the PBE0/def2-TZVPP level of theory on the structures obtained using the $r^2$-SCAN-3c composite method.[138] The calculated $^{31}P$ NMR shifts were referenced against PPh$_3$ (measured at δ = -5.7 ppm in CD$_2$Cl$_2$) unless mentioned otherwise. $^{13}C$ NMR shifts were referenced against SiMe$_4$ (δ = 0.0 ppm).

### 7.1.3.3 Reaction free energy profiles

For the mechanistic calculations on the $C(sp^2)$-H deprotonation in chapter 3, structures were optimized using the PBEh-3c composite method,[93b] and single point energies were refined at the DLPNO-CCSD(T)/def2-TZVPP level of theory using normalpno settings. Solvation was accounted for by single point calculation using the combination of $\omega$B97X-D3BJ and def2-TZVPP with and without the SMD model and $CH_2Cl_2$ as solvent.[92c]

For free energy profiles described in chapters 4 and 6 (and the Si-H activation of chapter 3.5, fig. 3-11), structures were optimized with the $r^2$-SCAN-3c composite method[92a] and refined single point energies were obtained at the DSD-BLYP-D3(BJ)/def2-QZVPP[111c] level of theory with application of the SMD model to account for implicit solvation using $CH_2Cl_2$ as solvent.

Kinetic and thermodynamic data of chapter 5 was computed with structures optimized using $r^2$-SCAN-3c and single point energies refined at the $\omega$B97X-V/def2-TZVPP employing the SMD model and $CH_2Cl_2$ as solvent.[139]

## 7.2 Syntheses

### 7.2.1 General Procedure for the Gutmann-Beckett method

A J. Young type NMR tube was charged with a solution of the respective Lewis acid (1 equiv) and OPEt$_3$ (0.5 equiv, for 4.3c 1 equiv was used) in CD$_2$Cl$_2$ and the mixture probed using $^{31}$P($^1$H) NMR spectroscopy. Free triethlyphosphine oxide was measured at a chemical shift of δ($^{31}$P) 50.5 ppm in CD$_2$Cl$_2$.

### 7.2.2 2.1-(H$_2$O)$_6$
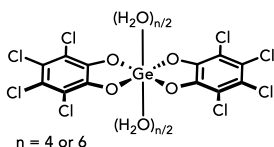
A suspension of GeO$_2$ (1.00 g, 9.61 mmol, 1 equiv) and perchlorocatechol (5.00 g, 20.2 mmol, 2.1 equiv) was heated in water (80 mL) to 60 °C and stirred for 4 h, resulting in complete dissolution of the starting materials. The solvent was removed *in vacuo* and the residue washed with dichloromethane and dried under high vacuum to give the product as a colorless solid (5.72 g, 8.99 mmol, 94 %). Elemental analysis suggests that about four water molecules are bound per formula unit. The product can be recrystallized from water (suitable for X-ray diffraction) to give colorless crystals. After crystallization, six molecules of water are bound per molecular unit, as supported by elemental and X-ray diffraction analysis.

**$^{13}$C NMR** (100 MHz, D$_2$O): δ 145.7, 119.3, 115.1.

**HRMS** (EI): [C$_{12}$Cl$_8$GeO$_4$]$^+$, calcd.: 561.6511, found: 561.6497.

**IR** (ATR): 3594, 3501 (br), 2917 (br), 1631, 1578, 1431, 1390, 1315, 1290, 1238, 999, 972, 810, 708, 666, 587, 508, 489 cm$^{-1}$.

**Anal.** Calcd. for C$_{12}$H$_{12}$Cl$_8$GeO$_{10}$: C, 21.43; H, 1.80; found C, 21.36; H, 1.75.

### 7.2.3    2.1-(CH₃CN)₂
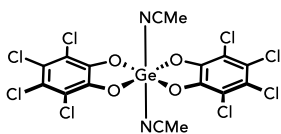


A suspension of 2.1-$(H_2O)_4$ (500 mg, 1.57 mmol, 1 equiv) in a mixture of acetonitrile (1 mL) and $CH_2Cl_2$ (10 mL) was stored over molecular sieves (3 Å) for three days. Undissolved colorless solid was filtered off and physically separated from the molecular sieve. The filtrate was concentrated *in vacuo* and $CH_2Cl_2$ (10 mL) added to promote further precipitation of a colorless solid, which was then filtered off. The solids were combined and dried *in vacuo* to furnish a colorless solid (482 mg, 746 μmol, 95 %). ¹H NMR spectroscopy in dry DMSO-$d_6$ and elemental analysis indicate the absence of water. Very slow displacement of acetonitrile by atmospheric water occurs under standard benchtop conditions.

**¹H NMR** (400 MHz, $CD_2Cl_2$): δ 1.97 (s, 6H).

**IR** (ATR): 3004, 2934, 2324, 2293, 1671, 1579, 1437, 1391, 1358, 1289, 1245, 1033, 996, 979, 948, 810, 709, 672, 593, 510 cm⁻¹.

**Anal.** Calcd. for $C_{16}H_6Cl_8GeN_2O_4$: C, 29.73; H, 0.94; N, 4.33 found C, 29.44; H, 1.01; N, 4.24.

## 7.2.4    2.1-(acetone)$_2$
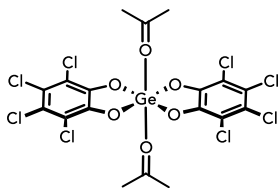
2.1-$(H_2O)_4$ (310 mg, 487 mmol, 1 equiv) was dissolved in acetone (15 mL) and stored over molsieve 3 Å for 24 h at 40°C. The molsieve was filtered off, the solution concentrated to half volume and pentane (25 mL) added, leading to the precipitation of a colorless solid. The precipitate was collected by filtration, washed with pentane (10 mL) and dried *in vacuo* to give the product as a colorless solid (301 mg, 442 mmol, 91 %). The purity was confirmed by $^1$H NMR spectroscopy in DMSO-d$_6$ or acetone-d$_6$.

**$^1$H NMR** (400 MHz, CD$_2$Cl$_2$): δ = 2.07 (s, 12H).
**$^{13}$C NMR** (100 MHz, acetone-d$_6$): δ = 210.0, 205.8, 148.9, 118.4, 115.1, 30.6.

**IR** (ATR): 1709, 1696, 1569, 1472, 1441, 1385, 1360, 1293, 1237, 1090, 993, 975, 915, 813, 800, 699 cm$^{-1}$.

### 7.2.5 [K@18-c-6][F-2.1] and [K@18-c-6][F-2.1-OH$_2$]
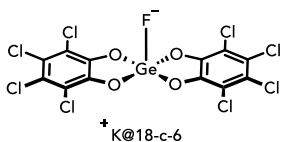


A suspension of 2.1-(CH$_3$CN)$_2$ (20.0 mg, 30.9 μmol, 1 equiv) in CD$_2$Cl$_2$ (0.5 mL) was treated with KF (1.80 mg, 30.9 μmol, 1 equiv) and 18-crown-6 (8.20 mg, 30.9 μmol, 1 eq.). After heating at 50 °C for 1.5 h a clear solution formed. The product was crystallized by gas phase diffusion of pentane into the solution at -40 °C (suitable for X-ray diffraction). After leaving the crystals under ambient conditions for several weeks, the water adduct [K@18-crown-6][F-Ge(cat$^{Cl}$)$_2$-OH$_2$] formed (crystals still suitable for X-ray diffraction).

**$^1$H NMR** (400 MHz, CD$_2$Cl$_2$): δ 3.55 (s, 12H).
**$^{19}$F NMR** (376 MHz, CD$_2$Cl$_2$): δ -141.8.
**$^{13}$C NMR** (100 MHz, CD$_2$Cl$_2$): δ 145.3, 121.2, 115.8, 70.5.

**HRMS** (ESI(-)): [C$_{12}$Cl$_8$FGeO$_4$]$^-$, calcd.: 580.6506, found: 580.6556.

## 7.2.6 [Ph$_4$P][2.1-Cl]
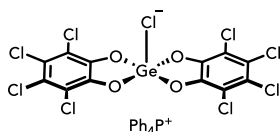
To a suspension of 2.1-(H$_2$O)$_4$ (100 mg, 157 µmol, 1 equiv) in 2 mL CH$_2$Cl$_2$ was added Ph$_4$PCl (58.9 mg, 157 µmol, 1equiv) which led to the immediate dissolution of most of the starting materials. Undissolved solid was filtered off and the product precipitated with pentane (10 mL), collected, and washed with pentane (3 x 4 mL) to give a colorless solid (120 mg, 128 µmol, 81 %).

**$^1$H NMR** (400 MHz, CD$_2$Cl$_2$): δ 7.89 – 7.86 (m, 1H), 7.74 – 7.69 (m, 2H), 7.61 – 7.56 (m, 2H).
**$^{31}$P NMR** (162 MHz, CD$_2$Cl$_2$): δ 23.3.
**$^{13}$C NMR** (100 MHz, CD$_2$Cl$_2$): δ 145.3, 136.1 (d, $J_{CP}$ = 3.03 Hz), 134.8 (d, $J_{CP}$ = 10.3 Hz), 131.0 (d, $J_{CP}$ = 12.9 Hz), 121.1, 118.3, 117.4, 115.8.

**HRMS** (ESI(-)): [C$_{12}$Cl$_9$GeO$_4$]$^-$, calcd.: 596.6211, found: 596.6210.
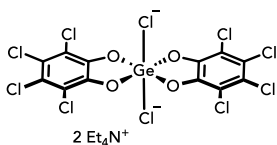
2.1-(H₂O)₄ (200 mg, 314 μmol, 1 equiv) was suspended in acetonitrile (3 mL) and Et₄NCl (104 mg, 629 μmol, 2 equiv) was added. After initial dissolution of the starting materials a colorless solid precipitated within a few minutes. The precipitate was filtered off and washed with pentane to give **5** as a colorless solid (155 mg, 173 μmol, 55 %). After recrystallization from acetonitrile, crystals suitable for X-ray diffraction analysis were obtained.

**¹H NMR** (400 MHz, DMSO-d₆): δ 3.20 (q, J = 7.3 Hz, 16H), 1.16 (tt, $^3J_{HH}$ = 7.2 Hz, $^1J_{HN}$ = 1.18 Hz, 24H).
**¹³C NMR** (100 MHz, DMSO-d₆): δ 146.7, 117.5, 113.8, 51.5 (t, $^1J_{CN}$ = 3.0 Hz), 7.1.

**IR** (ATR): 2987, 1563, 1482, 1462, 1442, 1395, 1384, 1369, 1333, 1290, 1244, 1173, 1074, 1053, 995, 973, 911, 812, 805, 786, 698, 626, 587, 563, 493, 471, 435, 420 cm⁻¹.

**Anal.** Calcd. for C₂₈H₃₈Cl₁₀GeN₂O₄: C, 37.63; H, 4.29; N, 3.13 found C, 37.50; H, 4.59; N, 3.06.

## 7.2.8    2.1 ('donor-free')
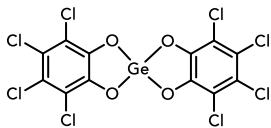
To a suspension of 2.1-(acetone)$_2$ (40.0 mg, 58.8 μmol, 1 equiv) in CD$_2$Cl$_2$ (0.7 mL) was added 9-BBN (15.8 mg, 129 μmol, 2.2 equiv) and the mixture was stirred for 20 h at rt resulting in a suspension of a colorless solid in a colorless solution. NMR spectroscopy revealed full conversion for the hydroboration of acetone (fig. S1). The colorless solid was separated from the solution by centrifugation and washed with pentane (3 x 2 mL) to give a colorless solid (25.0 mg, 75 %). The solid dissolves in DMSO-d$_6$ to give an analytically pure spectrum with traces of CH$_2$Cl$_2$ that could not be removed from the solid product even after prolonged exposure to high vacuum. This is also reflected in the elemental analysis.

**$^{13}$C NMR** (DMSO-d$_6$): δ 148.1, 116.6, 113.1.

**IR** (ATR): 1570, 1432, 1386, 1362, 1322, 1295, 1237, 1221, 1001, 972, 911, 818, 800, 732, 700 cm$^{-1}$

**Anal.** Calcd. for C$_{10}$Cl$_8$GeO$_4$: C, 25.54; calcd. for C$_{10}$Cl$_8$GeO$_4$ x CH$_2$Cl$_2$: C, 23.97; H 0.62 found C, 23.83; H, 0.56.

### 7.2.9 2.2-(H₂O)₆
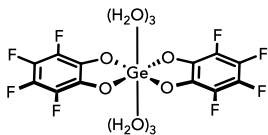
A suspension of perfluorocatechol (500 mg, 2.75 mmol, 2.10 equiv) and $GeO_2$ (137 mg, 1.31 mmol, 1 equiv) was stirred in water (50 ml) at 60 °C for 3 h, after which the starting materials had dissolved. The solvent was removed under reduced pressure. Washing the crude product with DCM (50 ml) and drying it *in vacuo* furnished the product as a colourless solid (620 mg, 2.39 mmol, 87 %).

**¹H NMR** (400 MHz, CDCl₃): δ 1.56 (s).
**¹³C NMR** (101 MHz, D₂O): δ 137.1 (br s), 134.9 (br s), 133.4 (br s).
**¹⁹F NMR** (376 MHz, CDCl₃): δ −164.9 (dd, $J_{FF}$ = 16.4, 10.6 Hz, 4F), −169.4 (dd, $J_{FF}$ = 16.7, 11.3 Hz, 4F).

**HR-MS** (EI): [$C_{12}F_8GeO_4$]⁺, calc. 433.8874, found 433.8871.

**Anal.** Calcd. for $C_{12}H_{12}F_8GeO_{10}$: C, 26.65; H, 2.24 found C, 26.64; H, 2.40.

## 7.2.10   2.1-(O$_2$SC$_2$H$_4$)$_2$
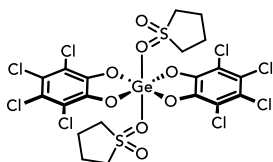


A deep red solution of GeI$_2$ (200 mg, 613 µmol, 1 equiv), *o*-chloranil (303 mg, 1.23 mmol, 2.01 equiv) and sulfolane (1.75 ml, 18.4 mmol, 30.0 equiv) in toluene (10 ml) was stirred for 17 h at 50 °C. The solution turned brown, and the precipitated off-white solid was collected by filtration and carefully washed with DCM, before the compound was dried *in vacuo*. The product was isolated as an off-white powder (326 mg, 405 µmol, 66 %).

**$^1$H NMR** (600 MHz, DMSO-d$_6$): δ 3.00 (m, 8H), 2.08 (m, 8H).
**$^{13}$C NMR** (151 MHz, DMSO-d$_6$): δ 51.0, 22.6.

**Anal.** Calcd. for C$_{20}$H$_{16}$Cl$_8$GeO$_8$S$_2$: C, 29.85; H, 2.00 found C, 29.18; H, 2.03.

## 7.2.11    2.1-(O$_2$SPh$_2$)$_2$
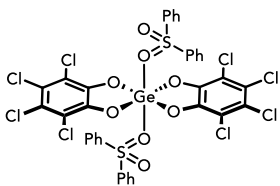
A dark green solution of GeI$_2$ (100 mg, 306 µmol, 1 equiv), *o*-chloranil (158 mg, 643 µmol, 2.10 equiv) and diphenyl sulfone (267 mg, 1.23 mmol, 4 equiv) in toluene (5 ml) was stirred for 22 h at 50 °C. After addition of equal volumes of pentane, the precipitated solid was collected by filtration and carefully washed with DCM and pentane. Drying the compound under reduced pressured afforded the product as a greenish powder (93.0 mg, 92.9 µmol, 30 %).

**$^1$H NMR** (400 MHz, CD$_2$Cl$_2$): δ 7.86 (d, *J* = 7.6 Hz, 8H), 7.61 (dd, *J* = 7.6 Hz, 4H), 7.51 (dd, *J* = 7.8 Hz, 8H), 0.90 (t, *J* = 8.0 Hz, 8H).

## 7.2.12    2.1-(O$_2$SBu$_2$)$_2$
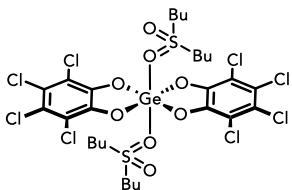
A deep brown solution of GeI$_2$ (100 mg, 306 µmol, 1 equiv), *o*-chloranil (158 mg, 643 µmol, 2.10 equiv) and dibutyl sulfone (218 mg, 1.23 mmol, 4 equiv) in toluene (5 mL) was stirred for 22 h at 50 °C. After addition of equal volumes of pentane, the precipitated off-white solid was collected by filtration and carefully washed with DCM and pentane until the solid was colorless. Drying the compound under reduced pressure afforded the product as a colorless powder (28.1 mg, 30.5 µmol, 10 %).

**$^1$H NMR** (400 MHz, CD$_2$Cl$_2$): δ 3.10 (pt, *J* = 8.0 Hz, 8H), 1.63 (pquint, *J* = 8.0 Hz, 8H), 1.38 (sext, *J* = 7.8 Hz, 8H), 0.90 (t, *J* = 7.4 Hz, 12H).

### 7.2.13 Cat$^{Cl}$PCl3 (3.2)
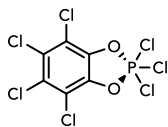
PCl$_3$ (1.96 mL, 22.4 mmol, 1.1 equiv) was added dropwise to a solution of $o$-chloranil (5.00 g, 20.3 mmol, 1 equiv) in CH$_2$Cl$_2$ (50 mL) at 0 °C and the mixture stirred overnight and thereby allowed to room temperature. All volatiles were then evaporated, the solid washed with CH$_2$Cl$_2$/pentane 1/20 (3 x 10 mL) and the product dried *in vacuo* to give a very pale green to colorless solid (7.52 g, 19.6 mmol, 97 %). The crude product was used without further purification in the following steps but may be recrystallized from pentane.

**¹³C NMR** (151 MHz, CD$_2$Cl$_2$): δ 139.6 (d, $J_{CP}$ = 2.6 Hz), 127.9, 115.9 (d, $J_{CP}$ = 20.3 Hz).
**³¹P NMR** (243 MHz, CD$_2$Cl$_2$): δ = -21.7 (s).

## 7.2.14    PCl(cat$^H$)$_2$ (3.1a)
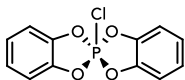
1,2-Dihydroxybenzene (10.0 g, 90.8 mmol, 1 equiv) was added to a suspension of PCl$_5$ (10.4 g, 50.0 mmol, 0.55 equiv) in CH$_2$Cl$_2$ (100 mL) at -45 °C in two portions. After stirring for 1 h at that temperature, the cooling bath was removed, and the mixture stirred for another 1 h. The solution was then concentrated to two thirds volume (accompanied by cooling) and the cold suspension filtrated to collect a colorless solid. The filtrate was then again concentrated to two thirds the original volume under reduced pressure and the precipitated solid again collected via filtration. The combined solids were washed twice with pentane (15 mL) and dried in vacuo to give a colorless, crystalline solid (8.95 g, 31.7 mmol, 70 %).

**$^1$H NMR** (400 MHz, CD$_2$Cl$_2$): δ 7.18 – 7.15 (m, 4H), 7.10 – 7.07 (m, 4H).
**$^{31}$P NMR** (162 MHz, CD$_2$Cl$_2$): δ -9.5 (s).
**$^{13}$C NMR** (101 MHz, CD$_2$Cl$_2$): δ 142.5 (d, $J_{CP}$ = 7.8 Hz), 123.6, 111.7 (d, $J_{CP}$ = 18.1 Hz).

**HRMS** (EI): [C$_{12}$H$_8$ClO$_4$P]$^+$, calcd.: 281.9843, found: 281.9838.

**Anal.** Calcd. for C$_{12}$H$_8$ClO$_4$P: C, 51.00; H, 2.85; found C, 50.58; H, 2.82.

## 7.2.15 PCl(cat^tBu)₂ (3.1b)
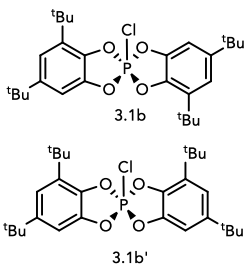


3,5-Di-tert-butylcatechol (1.75 g, 7.87 mmol, 1 equiv) dissolved in $CH_2Cl_2$ (4.4 mL) was added dropwise to a solution of $PCl_5$ (901 mg, 4.33 mmol, 0.55 equiv) in $CH_2Cl_2$ (8.8 mL) at -40 °C. The cooling bath was removed, and the mixture stirred for 1 h. Evaporation of all volatiles in vacuo and recrystallization from pentane gave the product as a crystalline, colorless solid (1.48 g, 2.92 mmol, 74 %).

**¹H NMR** (600 MHz, $CD_2Cl_2$): δ 7.12 (t, $J$ = 1.9 Hz, 1H, 3.1b), 7.07 (t, $J$ = 1.9 Hz, 1H, 1b'), 7.05 - 7. 04 (m, 2H, 3.1b/3.1b'), 1.44 (s, 9H, 3.1b'), 1.43 (s, 9H, 3.1b), 1.33 (s, 9H, 3.1b), 1.33 (s, 9H, 3.1b').

**³¹P NMR** (243 MHz, $CD_2Cl_2$): δ -10.8 (s, 3.1b), -11.1 (s, 3.1b').

**¹³C NMR** (101 MHz, $CD_2Cl_2$): δ 146.2, 142.5 (d, $J_{CP}$ = 6.0 Hz), 142.5 (d, $J_{CP}$ = 6.2 Hz), 138.2 (d, $J_{CP}$ = 5.1 Hz), 138.1 (d, $J_{CP}$ = 5.0 Hz), 134.6 (d, $J_{CP}$ = 14.2 Hz), 134.6 (d, $J_{CP}$ = 14.4 Hz), 117.3, 117.3, 106.9 (d, $J_{CP}$ = 17.6 Hz), 106.8 (d, $J_{CP}$ = 16.9 Hz), 35.4, 34.7, 31.8, 29.8, 29.7.

**HRMS** (EI(+)): [$C_{28}H_{40}ClO_4P$]⁺, calcd.: 506.2347, found: 506.2364.

**Anal.** Calcd. for $C_{28}H_{40}ClO_4P$: C, 66.33; H, 7.95; found C, 66.49; H, 8.32.

## 7.2.16   PCl(cat$^{Cl}$)(cat$^{tBu}$) (3.1c)
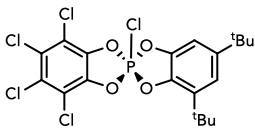


To the solid mixture of 3.2 (1.00 g, 2.48 mmol, 1 equiv) and 3,5-di-*tert*-butylcatechol (551 mg, 2.48 mmol, 1 equiv) was added dichloromethane (10 mL) and the mixture stirred at room temperature for 20 min. All volatiles were evaporated *in vacuo* and the crude product (pale brown solid) dissolved in pentane, cooled to -40 °C for two days and the formed solid collected by filtration and washed with cold pentane (-40 °C, 2 x 1 mL). The filtrate was then concentrated *in vacuo* and again cooled to -40 °C for two days, the resulting solid collected by filtration and again washed with cold pentane. The product was isolated as a colorless, crystalline solid (701 mg, 1.32 mmol, 53 %).

**$^1$H NMR** (600 MHz, CD$_2$Cl$_2$): δ 7.13 (t, $J_{HH}$ = 1.9 Hz, 1H), 7.09 (t, $J_{HH}$ = 1.6 Hz ,1H), 1.43 (s, 9H), 1.32 (s, 9H).
**$^{31}$P NMR** (243 MHz, CD$_2$Cl$_2$): δ -9.1 (s).
**$^{13}$C NMR** (101 MHz, CD$_2$Cl$_2$): δ 147.1, 142.2 (d, $J_{CP}$ = 7.9 Hz), 139.4 (dd, $J_{CP}$ = 13.9 Hz, $J_{CH}$ = 10.5 Hz), 137.8 (d, $J_{CP}$ = 6.9 Hz), 135.1 (d, $J_{CP}$ = 14.2 Hz), 127.1 (d, $J_{CP}$ = 9.6 Hz), 118.1, 116.2 (dd, $J_{CP}$ = 19.8 Hz, $J_{CH}$ = 12.4 Hz), 107.1 (d, $J_{CP}$ = 18.1 Hz), 35.4, 34.8, 31.7, 29.7.

**HRMS** (EI(+)): [C$_{20}$H$_{20}$Cl$_5$O$_4$P]$^+$, calcd.: 529.9542, found: 529.9540.
**Anal.** Calcd. for C$_{20}$H$_{20}$Cl$_5$O$_4$P: C, 45.10; H, 3.79; found C, 45.49; H, 3.92.

### 7.2.17 R(+) or S(-)-PCl(cat^Cl)(binol) (3.1d)
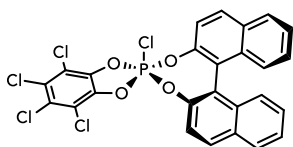
To a solution of 3.2 (2.00 g, 5.22 mmol, 1.1 equiv) in CH$_2$Cl$_2$ (15 mL) was added R(+)/S(-)-binol (1.36 g, 4.74 mmol, 1 equiv) and the resulting solution stirred for 20 min at room temperature. Initial dissolution of the starting materials was followed by precipitation of a colorless solid. The suspension was cooled to -40 °C for 1 h, the solid collected by filtration and washed with pentane. The product was isolated as a colorless, voluminous powder after drying *in vacuo* (2.28 g, 3.82 mmol, 81 %).

**¹H NMR** (600 MHz, CD$_2$Cl$_2$): δ 8.11 (d, *J* = 8.8 Hz, 1H), 8.09 (d, *J* = 8.9 Hz, 1H), 8.00 (t, *J* = 8.8 Hz, 2H), 7.80 (d, *J* = 8.9 Hz, 1H), 7.73 (d, *J* = 8.9 Hz, 1H), 7.54 – 7.45 (m, 4H), 7.32 (dt, *J* = 7.4; 1.4 Hz; 2H).

**³¹P NMR** (243 MHz, CD$_2$Cl$_2$): δ -13.0 (s).

**¹³C NMR** (150 MHz, CD$_2$Cl$_2$): δ 150.9 (d, *J*$_{CP}$ = 17.0 Hz), 148.8 (d, *J*$_{CP}$ = 15.8 Hz), 139.7 (d, *J*$_{CP}$ = 5.2 Hz), 132.4 (*d*, J$_{CP}$ = 2.1 Hz), 132.2 (d, *J*$_{CP}$ = 1.4 Hz), 132.1 (d, *J*$_{CP}$ = 2.3 Hz), 131.8 (d, *J*$_{CP}$ = 2.3 Hz), 131.3 (d, *J*$_{CP}$ = 1.1 Hz), 130.9 (d, *J*$_{CP}$ = 1.8 Hz), 128.9 (d, *J*$_{CP}$ = 1.3 Hz), 128.8 (d, *J*$_{CP}$ = 1.6 Hz), 127.7 (d, *J*$_{CP}$ = 0.9 Hz), 127.4 (d, *J*$_{CP}$ = 1.2 Hz), 127.1 (d, *J*$_{CP}$ = 1.0 Hz), 126.9 (d, *J*$_{CP}$ = 1.3 Hz), 126.5 (d, *J*$_{CP}$ = 1.4 Hz), 126.1, 126.1 (d, *J*$_{CP}$ = 1.7 Hz), 123.4 (d, *J*$_{CP}$ = 2.7 Hz), 122.1 (d, *J*$_{CP}$ = 4.7 Hz), 121.3 (d, *J*$_{CP}$ = 4.8 Hz), 115.2 (d, *J*$_{CP}$ = 19.0 Hz).

**HRMS** (EI(+)): [C$_{26}$H$_{12}$Cl$_5$O$_4$P]$^+$, calcd.: 593.8916, found: 593.9033.

**Anal.** Calcd. for C$_{26}$H$_{12}$Cl$_5$O$_4$P: C, 52.34; H, 2.03; found C, 52.63; H, 2.89.

### 7.2.18  PCl(cat$^{Cl}$)(biphenol) (3.1e)
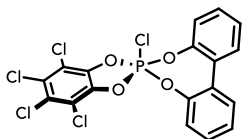


To a solution of 3.2 (1.50 g, 3.91 mmol, 1.1 equiv) in CH$_2$Cl$_2$ (20 mL) was added 2,2'-biphenol (663 mg, 3.56 mmol, 1 equiv) and the resulting solution stirred for 10 min at room temperature. Initial dissolution of the starting materials was followed by precipitation of a colorless solid. The suspension was cooled to -40 °C for 2 h, the solid collected by filtration and washed with pentane. The product was isolated as a white powder after drying *in vacuo* (1.33 g, 2.68 mmol, 75 %).

**$^1$H NMR** (600 MHz, CD$_2$Cl$_2$) δ 7.64 (dd, *J* = 7.5, 1.3 Hz, 2H), 7.55 – 7.48 (m, 4H), 7.45 – 7.39 (m, 2H).
**$^{31}$P NMR** (243 MHz, CD$_2$Cl$_2$) δ -15.5.
**$^{13}$C NMR** (151 MHz, CD$_2$Cl$_2$) δ 139.7 (d, *J* = 5.4 Hz), 130.2, 130.1, 129.4, 128.9 (d, *J* = 2.2 Hz), 126.8, 126.1, 123.4, 115.2 (d, *J* = 19.0 Hz).

### 7.2.19 [P(cat^H)₂][B(C₆F₅)₄] (3.3a)
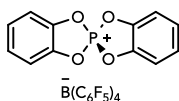
To the solid mixture of NaBArF$_{20}$ (875 mg, 1.25 mmol, 1.1 equiv) and **3.1a** (320 mg, 1.13 mmol, 1 equiv) was added CH$_2$Cl$_2$ (15 mL), the resulting suspension stirred for 5 h at room temperature and the solid removed by filtration. Removal of all volatiles *in vacuo* from the filtrate and recrystallization by layering a solution in CH$_2$Cl$_2$ with pentane and allowing for diffusion at -40 °C overnight furnished a colorless, crystalline solid (880 mg, 0.95 mmol, 84 %).

**¹H NMR** (400 MHz, CD$_2$Cl$_2$): δ 7.64 – 7.57 (m, 8H).

**³¹P NMR** (162 MHz, CD$_2$Cl$_2$): δ 46.8 (s).

**¹³C NMR** (101 MHz, CD$_2$Cl$_2$): δ 149.8 – 149.6 (m, BArF$_{20}$), 147.4 – 147.1 (m, BArF$_{20}$), 143.3 (d, $J_{CP}$ = 5.3 Hz), 140.0 – 139.6 (m, BArF$_{20}$), 138.0 – 137.3 (m, BArF$_{20}$), 135.6 – 135.3 (m, BArF$_{20}$), 129.4 (s), 115.2 (d, $J_{CP}$ = 14.8 Hz).

**¹¹B NMR** (128 MHz, CD$_2$Cl$_2$): δ -16.7.

**¹⁹F NMR** (376 MHz, CD$_2$Cl$_2$): δ -133.2 (s, 8F, *o*-C-F), -163.6 (t, $^3J_{FF}$ = 20.4 Hz, 4F, *p*-C-F), -167.5 (t, $^3J_{FF}$ = 17.6 Hz, 8F, *m*-C-F).

**HRMS** (ESI(+)): [C$_{12}$H$_8$O$_4$P]$^+$, calcd.: 247.0155, found: 247.0147.

**Anal.** Calcd. for C$_{36}$H$_8$BF$_{20}$O$_4$P: C, 46.68; H, 0.87; found C, 46.46; H, 1.11.

### 7.2.20 [P(cat^H)₂][Al(OC(CF₃)₃)₄] (3.3a')
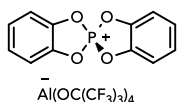


To the solid mixture of LiAl(OC(CF₃)₃)₄ (2.41 g, 2.48 mmol, 1 equiv) and 3.1a (700 mg, 2.48 mmol, 1 equiv) was added CH₂Cl₂ (40 mL), the resulting suspension stirred for 20 min at room temperature and the solid removed by filtration. Removal of all volatiles *in vacuo* from the filtrate and washing the solid with pentane yielded a colorless powder (2.92 g, 2.40 mmol, 97 %).

**¹H NMR** (600 MHz, CD₂Cl₂): δ 7.66 – 7.60 (m, 8H).
**³¹P NMR** (243 MHz, CD₂Cl₂): δ 46.8 (s).
**¹³C NMR** (151 MHz, CD₂Cl₂): δ 142.8 (d, $J_{CP}$ = 5.3 Hz), 129.1, 121.2 (q, $J_{CF}$ = 292.5 Hz, OC(*C*F₃)₄), 114.8 (d, $J_{CP}$ = 14.8 Hz).
**¹⁹F NMR** (376 MHz, CD₂Cl₂): δ -75.8 (s, 36F).

**Anal.** Calcd. for C₂₈H₈AlF₃₆O₈P: C, 27.70; H, 0.66; found C, 27.69; H, 1.08.

### 7.2.21 [P(cat^tBu)_2][B(C_6F_5)_4] (3.3b)
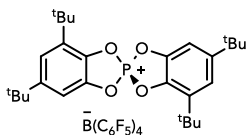


To a suspension of NaBArF_{20} (1.16 g, 1.66 mmol, 1.05 equiv) in $CH_2Cl_2$ (10 mL) was added a solution of 3.1b (800 mg, 1.58 mmol, 1 equiv) in $CH_2Cl_2$ (5 mL). The resulting suspension was stirred for 3 h at room temperature and the solid removed by filtration. Removal of all volatiles *in vacuo* from the filtrate furnished a colorless solid (1.78 g, 1.55 mmol, 98 %).

**$^1$H NMR** (600 MHz, $CD_2Cl_2$): δ = 7.48 (s, 2H), 7.43 (t, $J$ = 2.0 Hz, 2H), 1.44 (s, 18H), 1.36 (s, 18H).

**$^{31}$P NMR** (243 MHz, $CD_2Cl_2$): δ = 45.4 (s).

**$^{13}$C NMR** (151 MHz, $CD_2Cl_2$): δ = 153.3, 149.5 – 149.2 (m, BArF_{20}), 147.6 – 147.9 (m, BArF_{20}), 143.7 (d, $J_{CP}$ = 4.6 Hz), 139.9 (d, $J_{CP}$ = 4.7 Hz), 139.3 - 139.6 (m, BArF_{20}), 138.4 (d, $J_{CP}$ = 11.7 Hz), 137.7-137.9 (m, BArF_{20}), 137.4 – 137.6 (m, BArF_{20}), 135.7 - 136.0 (m, BArF_{20}), 123.4, 109.9 (d, $J_{CP}$ = 14.5 Hz), 36.3 (s, $C$(CH)_3), 35.5 (s, $C$(CH)_3), 31.2 (s, C($C$H_3)_3), 29.7 (s, C($C$H_3)_3).

**$^{11}$B NMR** (128 MHz, $CD_2Cl_2$): δ = -16.7.

**$^{19}$F NMR** (376 MHz, $CD_2Cl_2$): δ = -133.2 (s, 8F, *o*-C-F), -163.6 (t, $^3J_{FF}$ = 20.4 Hz, 4F, *p*-C-F), -167.5 (t, $^3J_{FF}$ = 17.6 Hz, 8F, *m*-C-F).

**HRMS** (ESI(+)): $[C_{28}H_{40}O_4P]^+$, calcd.: 471.2659, found: 471.2636.

**Anal.** Calcd. for $C_{52}H_{40}BF_{20}O_4P$ x 0.1 $CH_2Cl_2$: C, 53.99; H, 3.50; found C, 53.73; H, 3.55 ($CH_2Cl_2$ content estimated from $^1$H NMR measurements and could not be removed even after prolong drying under reduced pressure).

## 7.2.22 [P(cat^tBu)(cat^Cl)][B(C₆F₅)₄] (3.3c)
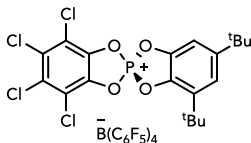
To a solution of [Ph₃C][B(C₆F₅)₄] (364 mg, 394 µmol, 1.05 equiv) in benzene (5 mL) was added a solution of Et₃SiH (75.0 µL, 469 µmol, 1.2 equiv) in benzene (2 mL), and the solution was stirred vigorously for 10 min to give a two-phase system with a colorless solution over a pale yellow oil. The solution was decanted, and the oil washed twice with benzene (3 mL). 4 mL of benzene was then added to the oil along with a solution of 3.1c (200 mg, 376 µmol, 1 equiv) in benzene (3 mL) and the solution stirred for 15 min, after which a voluminous, colorless solid precipitated spontaneously. Pentane (8 mL) and five drops of $CH_2Cl_2$ were added to the slurry and the mixture stirred for another three minutes. The solid was collected by filtration, washed with benzene (3 mL) and pentane (3 x 6 mL), then dried *in vacuo* to give a colorless powder (394 mg, 335 µmol, 89 %). Even after extended drying times under reduced pressure, the product still contained benzene. The solid can be stored at room temperature for several months without any signs of decomposition.

**¹H NMR** (600 MHz, $CD_2Cl_2$): δ = 7.54 (s, 1H), 7.47 (t, $^3J_{HH}$ = 2.0 Hz, 1H), 1.44 (s, 9H), 1.36 (s, 9H).
**³¹P NMR** (243 MHz, $CD_2Cl_2$): δ = 46.4 (s).
**¹³C NMR** (151 MHz, $CD_2Cl_2$): δ = 154.2 (s), 149.4 – 149.2 (m, BArF₂₀), 147.8 – 147.6 (m, BArF₂₀), 148.9 (d, $J_{CP}$ = 4.6 Hz), 140.1 (d, $J_{CP}$ = 4.7 Hz), 139.1 (d, $J_{CP}$ = 8.1 Hz), 148.9 (d, $J_{CP}$ = 4.6 Hz), 139.5 – 139.3 (m, BArF₂₀), 138.8 (d, $J_{CP}$ = 11.4 Hz), 137.9 – 137.3 (m, BArF₂₀), 136.0 – 135.7 (m, BArF₂₀), 134.5 (s), 124.3 (s), 119.8 (d, $J_{CP}$ = 16.0 Hz), 110.1 (d, $J_{CP}$ = 14.7 Hz), 36.5 (s), 35.6 (s), 31.1 (s), 29.7 (s).
**¹¹B NMR** (128 MHz, $CD_2Cl_2$): δ = -16.7.
**¹⁹F NMR** (376 MHz, $CD_2Cl_2$): δ = -133.2 (s, 8F, *o*-C-F), -163.6 (t, $^3J_{FF}$ = 20.4 Hz, 4F, *p*-C-F), -167.5 (t, $^3J_{FF}$ = 17.6 Hz, 8F, *m*-C-F).

**Anal.** Calcd. for $C_{52}H_{40}BF_{20}O_4P$ x $C_6H_6$ : C, 47.88; H, 2.09; found C, 48.10; H, 2.65 ($C_6H_6$ content estimated from ¹H NMR measurements).

### 7.2.23   [R(+) or S(-)-P(cat^Cl)(binol)][B(C₆F₅)₄] (3.3d)
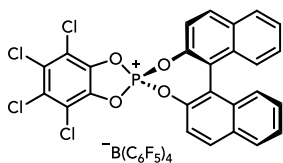


To the solid mixture of NaBArF₂₀ (1.36 g, 1.94 mmol, 1.05 equiv) and 3.1d (1.10 g, 1.84 mmol, 1 equiv) was added CH₂Cl₂ (15 mL), the resulting suspension stirred for 3 h at room temperature and subsequently the solid removed by filtration. Removal of all volatiles *in vacuo* from the filtrate, washing of the resulting solid with pentane and drying *in vacuo* furnished the product as an off-white powder (2.22 g, 1.79 mmol, 97 %).

**¹H NMR** (600 MHz, CD₂Cl₂): δ 8.38 (d, $^3J_{HH}$ = 9.1 Hz, 4H), 8.17 (d, $^3J_{HH}$ = 8.3 Hz, 4H), 7.76 (t, $^3J_{HH}$ = 7.4 Hz, 4H), 7.73 (d, $^3J_{HH}$ = 9.2 Hz, 4H), 7.54 – 7.51 (m, 4H) ,7.39 (d, $^3J_{HH}$ = 8.6 Hz, 4H).

**³¹P NMR** (243 MHz, CD₂Cl₂): δ 27.5 (s).

**¹³C NMR** (151 MHz, CD₂Cl₂): δ 149.4 – 149.2 (m, BArF₂₀), 147.8 – 147.6 (m, BArF₂₀), 145.4 (d, $J_{CP}$ = 11.0 Hz), 139.6 (d, $J_{CP}$ = 7.8 Hz), 139.5 – 139.3 (m, BArF₂₀), 137.9 – 137.3 (m, BArF₂₀), 136.0 – 135.7 (m, BArF₂₀), 135.2, 133.8 (d, $J_{CP}$ = 15.1 Hz), 132.2, 129.6 (d, $J_{CP}$ = 3.2 Hz), 129.1, 127.5, 119.8 (d, $J_{CP}$ = 15.0 Hz), 119.3 (d, $J_{CP}$ = 1.7 Hz), 117.1 (d, $J_{CP}$ = 4.4 Hz).

**¹¹B NMR** (128 MHz, CD₂Cl₂): δ -16.7.

**¹⁹F NMR** (376 MHz, CD₂Cl₂): δ -133.2 (s, 8F, *o*-C-F), -163.6 (t, $^3J_{FF}$ = 20.4 Hz, 4F, *p*-C-F), -167.5 (t, $^3J_{FF}$ = 17.6 Hz, 8F, *m*-C-F).

**HRMS** ESI(+), product could not be detected.

**Anal.** Calcd. for C₅₀H₁₂BF₂₀O₄P: C, 48.42; H, 0.98; found C, 48.13; H, 1.27.

### 7.2.24 [R(+) or S(-)-P(cat^Cl)(binol)][Al(OC(CF₃)₃)₄] (3.3d')
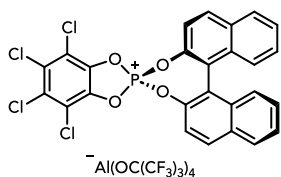


To the solid mixture of LiAl(OC(CF₃)₃)₄ (490 mg, 503 μmol, 1 equiv) and 3.1d (300 mg, 503 μmol, 1 equiv) was added CH₂Cl₂ (15 mL), the resulting suspension stirred for 20 min at room temperature and the solid removed by filtration. Removal of all volatiles *in vacuo* from the filtrate and washing the solid with pentane yielded a colorless powder (721 mg, 472 μmol, 94 %).

**¹H NMR** (600 MHz, CD₂Cl₂): δ = 8.40 (d, $^3J_{HH}$ = 9.1 Hz, 2H), 8.18 (d, $^3J_{HH}$ = 8.3 Hz, 2H), 7.77 (d, $^3J_{HH}$ = 7.5 Hz, 2H), 7.75 (d, $^3J_{HH}$ = 8.9 Hz, 2H), 7.54 (t, $^3J_{HH}$ = 4.1 Hz, 2H), 7.40 (d, $^3J_{HH}$ = 8.6 Hz, 2H).
**³¹P NMR** (243 MHz, CD₂Cl₂): δ = 27.5 (s).
**¹³C NMR** (151 MHz, CD₂Cl₂): δ = 145.2 (d, $J_{CP}$ = 11.0 Hz), 139.6 (d, $J_{CP}$ = 7.9 Hz), 135.3, 133.9 (d, $J_{CP}$ = 24.5 Hz), 132.2, 129.6 (d, $J_{CP}$ = 8.5 Hz), 129.2, 127.5, 121.2 (q, $J_{CF}$ = 292.5 Hz, OC(***C***F₃)₄), 119.8 (d, $J_{CP}$ = 14.9 Hz), 119.3 (d, $J_{CP}$ = 1.8 Hz), 117.1 (d, $J_{CP}$ = 4.4 Hz).
**¹⁹F NMR** (376 MHz, CD₂Cl₂): δ = -75.8 (s, 36F).

**Anal.** Calcd. for C₄₂H₁₂AlCl₄F₃₆O₈P: C, 33.01; H, 0.79; found C, 32.92; H, 0.98.

## 7.2.25 [P(cat$^{Cl}$)(biphenol)][B(C$_6$F$_5$)$_4$] (3.3e)
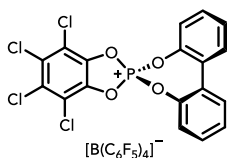


To the solid mixture of NaBArF$_{20}$ (1.93 g, 2.75 mmol, 1.05 equiv) and 3.1e (1.30 g, 2.62 mmol, 1 equiv) was added CH$_2$Cl$_2$ (20 mL), the resulting suspension stirred for 20 min at room temperature and subsequently the solid was removed by filtration. Removal of all volatiles *in vacuo* from the filtrate, washing of the resulting solid with pentane and drying *in vacuo* furnished the product as an off-white powder (2.94 g, 2.58 mmol, 98 %).

**$^1$H NMR** (600 MHz, CD$_2$Cl$_2$) δ 7.88 – 7.82 (m, 1H), 7.81 – 7.73 (m, 2H), 7.61 – 7.54 (m, 1H).

**$^{13}$C NMR** (151 MHz, CD$_2$Cl$_2$) δ 149.4 – 149.2 (m, BArF$_{20}$), 147.8 – 147.6 (m, BArF$_{20}$), 146.6 (d, $J$ = 10.5 Hz), 139.6 (d, $J$ = 7.9 Hz), 139.5 – 139.3 (m, BArF$_{20}$), 137.9 – 137.3 (m, BArF$_{20}$), 136.0 – 135.7 (m, BArF$_{20}$), 133.8, 133.4, 132.7 (d, $J$ = 1.3 Hz), 131.6 (d, $J$ = 1.7 Hz), 124.8 (d, $J$ = 1.1 Hz), 120.8 (d, $J$ = 6.3 Hz), 119.7 (d, $J$ = 15.0 Hz).

**$^{31}$P NMR** (243 MHz, CD$_2$Cl$_2$) δ 25.3.

**$^{11}$B NMR** (128 MHz, CD$_2$Cl$_2$): δ -16.7.

**$^{19}$F NMR** (376 MHz, CD$_2$Cl$_2$): δ -133.2 (s, 8F, *o*-C-F), -163.6 (t, $^3J_{FF}$ = 20.4 Hz, 4F, *p*-C-F), -167.5 (t, $^3J_{FF}$ = 17.6 Hz, 8F, *m*-C-F).

## 7.2.26    S(-)-(C₅H₆S)P(cat^Cl)(binol) (3.8b)
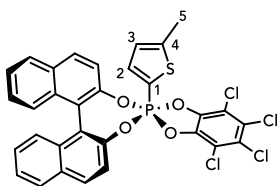


To a solution of S(-)-3.3d (300 mg, 242 µmol, 1 equiv) in CH₂Cl₂ (5 mL) was added 2-methylthiophene (25.8 µL, 266 µmol, 1.1 equiv) and the solution stirred for 10 min. Pyridine (19.5 µmol, 242 µmol, 1 equiv) was added and the mixture stirred another 10 min before the solvent was removed under reduced pressure and the solid suspended in a 1:5 mixture of CH₂Cl₂ and pentane (10 mL). The solid was removed by filtration and the filtrate concentrated *in vacuo* to give the product as a colorless solid (147 mg, 223 µmol, 92 %).

**¹H NMR** (600 MHz, CD₂Cl₂): δ 8.09 (d, *J* = 8.9 Hz, 1H), 8.00 (d, *J* = 8.2 Hz, 1H), 7.93 (d, *J* = 8.1 Hz, 1H), 7.89 (d, *J* = 8.8 Hz, 1H), 7.84 (dd, *J* = 7.4; 3.9 Hz, 1H, H2), 7.83 (d, *J* = 9.1 Hz, 1H), 7.52 – 7.46 (m, 4H), 7.40 (d, *J* = 8.8 Hz, 1H), 7.32 (t, *J* = 7.7 Hz, 2H), 6.86 ( dd, *J* = 6.8; 4.0 Hz, 1H, H3), 2.45 (s, 3H, H5).
**³¹P NMR** (243 MHz, CD₂Cl₂): δ -23.3 (t, $J_{PH}$ = 7.0 Hz).
**¹³C NMR** (151 MHz, CD₂Cl₂): δ 156.2 (d, $J_{CP}$ = 7.1 Hz, C4), 150.2 (d, $J_{CP}$ = 11.8 Hz), 149.2 (d, $J_{CP}$ = 13.8 Hz), 145.4 (d, $J_{CP}$ = 12.1 Hz, C2), 132.2 (t, $J_{CP}$ = 1.8 Hz), 132.0 (d, $J_{CP}$ = 1.8 Hz), 131.4 (d, $J_{CP}$ = 1.5 Hz), 130.5 (d, $J_{CP}$ = 1.1 Hz), 130.3 (d, $J_{CP}$ = 1.3 Hz), 128.7 (d, $J_{CP}$ = 3.0 Hz), 128.7, 128.2 (d, $J_{CP}$ = 21.2 Hz, C3), 127.7, 127.2, 126.7, 126.5, 126.0, 125.5, 125.2 (d, $J_{CP}$ = 261.2 Hz, C1) 124.3 (d, $J_{CP}$ = 1.6 Hz), 122.8 (d, $J_{CP}$ = 2.7 Hz), 122.5 (d, $J_{CP}$ = 2.9 Hz), 121.9 (d, $J_{CP}$ = 4.4 Hz), 15.8 (d, $J_{CP}$ = 2.3 Hz, C5).

**HRMS** (EI(+)): [C₃₁H₁₇Cl₄O₄PS]⁺, calcd.: 655.9334, found: 655.9323.

**Anal.** Calcd. for C₃₁H₁₇Cl₄O₄PS: C, 56.56; H, 2.60; found C, 56.51; H, 3.12.

### 7.2.27 S(-)-(C$_6$H$_5$-C$_4$H$_3$N)P(cat$^{Cl}$)(binol) (3.9b)
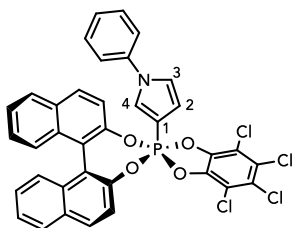


1-Phenylpyrrole (34.6 mg, 242 µmol, 1 equiv) and S(-)-3.3d (300 mg, 242 µmol, 1 equiv) were dissolved in CH$_2$Cl$_2$ (5 mL), the solution stirred for 10 min, before 2,6-diphenylpyridine (56.0 mg, 242 µmol, 1 equiv) was added to the solution and the mixture stirred again for 10 min. The solvent was then removed under reduced pressure. The solid was suspended in benzene (8 mL), the undissolved solid removed by filtration and the filtrate concentrated *in vacuo*. The solid was then washed with diethyl ether (2 x 3 mL) and dried *in vacuo*, furnishing the product as a colorless powder (153 mg, 218 µmol, 90 %).

**$^1$H NMR** (600 MHz, CD$_2$Cl$_2$): δ 8.08 (d, *J* = 8.9 Hz, 1H), 7.99 (d, *J* = 8.2 Hz, 1H), 7.90 (d, *J* = 9.1 Hz, 1H), 7.88 (d, *J* = 10.0 Hz, 1H), 7.85 (d, *J* = 8.8 Hz, 1H), 7.76 (d, *J* = 1.9 Hz, 1H, H3), 7.50 (d, *J* = 9.5 Hz, 1H), 7.49 (d, *J* = 9.8 Hz, 1H), 7.47 – 7.42 (m, 3H), 7.40 – 7.39 (m, 2H), 7.34 – 7.33 (m, 2H), 7.31 – 7.28 (m, 3H), 7.06 (dt, *J* = 7.2, 2.7 Hz, 1H, H2), 6.76 (q, *J* = 2.4 Hz, 1H, H4).
**$^{31}$P NMR** (243 MHz, CD$_2$Cl$_2$): δ -18.2 (d, *J*$_{PH}$ = 6.8 Hz).
**$^{13}$C NMR** (151 MHz, CD$_2$Cl$_2$): δ 150.5 (d, *J*$_{CP}$ = 11.6 Hz).
149.5 (d, J$_{CP}$ = 13.5 Hz), 139.8 (d, *J*$_{CP}$ = 1.9 Hz), 133.5 (d, *J*$_{CP}$ = 26.9 Hz, C4), 132.4 (t, *J*$_{CP}$ = 2.0 Hz), 132.0 (d, *J*$_{CP}$ = 1.8 Hz), 131.3 (d, *J*$_{CP}$ = 1.6 Hz), 130.3 (d, *J*$_{CP}$ = 1.3 Hz), 130.1 (d, *J*$_{CP}$ = 1.5 Hz), 130.1, 128.7 (dd, *J*$_{CP}$ = 3.0, 1.0 Hz), 127.7, 127.2, 126.5 (d, *J*$_{CP}$ = 20.2 Hz), 125.8 (d, *J*$_{CP}$ = 1.1 Hz), 125.3, 124.7 (d, *J*$_{CP}$ = 1.8 Hz), 123.0 (d, *J*$_{CP}$ = 2.7 Hz), 122.3 (d, *J*$_{CP}$ = 2.8 Hz), 122.2 (d, *J*$_{CP}$ = 4.4 Hz), 122.0 (d, *J*$_{CP}$ = 17.6 Hz, C2), 121.5, 119.1 (d, *J*$_{CP}$ = 13.0 Hz, C3), 111.4 (d, *J*$_{CP}$ = 264.7 Hz, C1).

**HRMS** (EI(+)): [C$_{36}$H$_{20}$Cl$_4$NO$_4$P]$^+$, calcd.: 700.9879, found: 700.9886.

**Anal.** Calcd. for C$_{36}$H$_{20}$Cl$_4$NO$_4$P: C, 61.48; H, 2.87; N, 1.99; found C, 60.83; H, 3.15; N, 1.93.

## 7.2.28    S(-)-3.8a
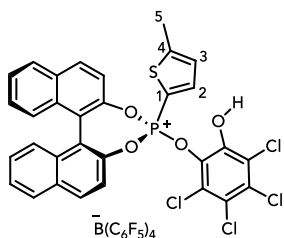
To a solution of S(-)-3.3d (200 mg, 161 μmol, 1 equiv) in CH₂Cl₂ (10 mL) was added 2-methylthiophene (17.2 μL, 177 μmol, 1.1 equiv) and the mixture stirred at room temperature for 20 h. The solvent was then removed under reduced pressure and the remaining solid washed with pentane, furnishing the product as an orange solid (205 mg, 153 μmol, 95 %).

**¹H NMR** (600 MHz, CD₂Cl₂): δ 8.24 (d, $J$ = 9.0 Hz, 1H), 8.11 (t, $J$ = 8.3 Hz, 2H), 8.03 (d, $J$ = 8.2 Hz, 1H), 8.00 (dd, $J$ = 8.5, 4.0 Hz, 1H, H2), 7.76 (d, $J$ = 9.0 Hz, 1H), 7.65 (q, $J$ = 7.7 Hz, 2H), 7.44 (m, 2H), 7.37 (t, $J$ = 9.8 Hz, 2H), 7.33 (d, $J$ = 8.6 Hz, 1H), 7.11 (ddd, $J$ = 5.2, 4.1, 1.1 Hz, 1H, H3), 6.36 (s, 1H, OH), 2.63 (s, 3H, H5).

**³¹P NMR** (243 MHz, CD₂Cl₂): δ 35.2 (dd, $J_{PH}$ = 8.40, 5.52 Hz).

**¹³C NMR** (151 MHz, CD₂Cl₂): δ 163.5 (d, $J_{CP}$ = 9.9 Hz, C4), 149.4 – 149.2 (m, BArF₂₀), 147.8 – 147.6 (m, BArF₂₀),  147.0 (d, $J_{CP}$ = 14.1 Hz, C2), 145.2 (d, $J_{CP}$ = 11.2 Hz), 144.3 (d, $J_{CP}$ = 8.8 Hz), 143.2 (d, $J_{CP}$ = 2.9 Hz), 139.5 – 139.3 (m, BArF₂₀), 137.9 – 137.3 (m, BArF₂₀), 136.0 – 135.7 (m, BArF₂₀), 133.9, 133.39, 133.3, 133.1, 132.5, 130.7 (d, $J_{CP}$ = 20.8 Hz, C3), 129.3 (d, $J_{CP}$ = 2.6 Hz), 128.7 (d, $J_{CP}$ = 14.8 Hz), 128.1 (d, $J_{CP}$ = 20.7 Hz), 127.5 (d, $J_{CP}$ = 11.5 Hz), 126.2 (d, $J_{CP}$ = 35.2 Hz), 121.3 (d, $J_{CP}$ = 2.2 Hz), 121.1, 120.7 (d, $J_{CP}$ = 2.3 Hz), 119.0 (d, $J_{CP}$ = 3.4 Hz), 118.5 (d, $J_{CP}$ = 3.9 Hz), 103.4 (d, $J_{CP}$ = 235.4 Hz, C1), 16.3 (d, $J_{CP}$ = 2.2 Hz, C5).

**HRMS** ESI(+), product could not be detected.

**IR** (ATR): 3504, 1642, 1511, 1459, 1395, 1374, 1275, 1212, 1185, 1084, 1045, 974, 920, 865, 812, 756, 683, 661 cm⁻¹.

**Anal.** Calcd. for C₅₅H₁₈BCl₄O₄F₂₀PS: C, 48.28; H, 1.39; found C, 49.06; H, 1.86.

### 7.2.29    Catalysis

### 7.2.29.1    Friedel-Crafts-Dimerization of 1,1-diphenylethylene

To a solution of 1,1-DPE (53.0 µL, 300 µmol, 1 equiv) in $CD_2Cl_2$ (0.6 mL) was added 3.3a (1.89 mg, 1.5 µmol, 0.005 equiv), the mixture stirred for 1 min and then investigated by ^{1}H NMR. After completion of the reaction was confirmed, the solution was filtered through a short silica plug, eluted with pentane and the solvent removed *in vacuo* to give 1-methyl-1,3,3-triphenyl-2,3-dihydro-1H-indene as a colorless oil (52.0 mg, 146 µmol, 96 %).

**1-methyl-1,3,3-triphenyl-2,3-dihydro-1H-indene:**

**^{1}H NMR** (600 MHz, $CDCl_3$): δ 7.40 – 7.12 (m, 20H), 3.50 (d, $J$ = 13.6 Hz, 1H), 3.20 (d, $J$ = 13.6 Hz, 1H), 1.64 (s, 3H).
**^{13}C NMR** (151 MHz, $CDCl_3$): δ 150.7, 149.5, 149.0, 148.6, 147.6, 128.9, 128.8, 128.1, 128.0, 127.7, 127.6, 127.5, 127.0, 126.9, 126.1, 125.8, 125.7, 125.2, 61.5, 61.1, 51.3, 29.0.

### 7.2.29.2    Hydrosilylation of 2-Norbornene

To a solution of norbornene (0.1 mmol, 1 equiv) and triethylsilane (0.1 mmol, 1 equiv) in $CD_2Cl_2$ (0.6 mL) was added the catalyst (0.01 eq. 3.3a/b/d) inside a glovebox, the solution stirred for 1 min and then probed by ^{1}H NMR to determine the reaction progress. Full conversion was achieved for both 3.3b and 3.3d after <5 min, while with 3.3a, only minor amounts of the product were seen. An isolated yield (on a 0.3 mmol scale) was determined for the reaction with 3.3b by filtering the solution through a short silica plug, eluting with $CH_2Cl_2$ and removal of all volatiles *in vacuo* to give the product as a colorless oil (61.1 mg, 290 µmol, 97 %).

**(Bicyclo[2.2.1]heptan-2-yl)triethylsilane:**

**$^1$H NMR** (600 MHz, CDCl$_3$): δ 2.22 (s, 1H), 2.17 (s, 1H), 1.55 – 1.49 (m, 2H), 1.45 – 1.41 (m, 1H), 1.39 – 1.35 (m, 1H), 1.21 – 1.16 (m, 3H), 1.13 – 1.11 (m, 1H), 0.94 (t, $J$ = 8.0 Hz, 9H), 0.66 - 0.63 (m, 1H), 0.51 (qd, $J$ =  7.9, 1.3 Hz, 6H).
**$^{13}$C NMR** (151 MHz, CDCl$_3$): δ 38.3, 38.0, 36.9, 34.6, 33.0. 29.0, 26.3, 7.9, 2.9.

### 7.2.29.3    Hydrodeoxygenation of Acetophenone

To a solution of acetophenone (0.20 mmol, 1 equiv) and triethylsilane (0.42 mmol, 2.1 equiv) in CD$_2$Cl$_2$ (0.6 mL) was added 3.3a (2.52 mg, 2 µmol, 0.01 equiv) and the mixture probed by NMR. Full conversion was achieved within the time it took to measure the NMR (~5 minutes). The yield was determined by integration against an internal standard (mesitylene).

**Ethylbenzene:**

**$^1$H NMR** (600 MHz, CD$_2$Cl$_2$): δ 7.31 – 7.18 (m, 5H), 2.68 (q, $J$ = 7.6 Hz, 2H), 1.27 (t, $J$ = 7.6 Hz, 3H).
**$^{13}$C NMR** (151 MHz, CD$_2$Cl$_2$): δ 144.9, 128.8, 128.3, 126.0, 29.4, 16.0.

### 7.2.29.4    Carbonyl-Olefin Metathesis

To a solution of the substrate (13.7 mg, 0.05 mmol, 1 equiv) in CD$_2$Cl$_2$ (0.6 mL) was added 3.3a (0.63 mg, 0.50 µmol, 0.01 equiv or 1.89 mg, 1.50 µmol, 0.03 equiv) and the mixture probed by NMR after 10 min, after which full conversion of the starting material was achieved. To determine an isolated yield with substrate 3.4, the reaction was repeated on a 0.15 mmol scale. The solution after 10 min was filtered through a short silica plug, eluted with additional CH$_2$Cl$_2$ and all volatiles were removed under reduced pressure to give the product as a yellow oil (31.7 mg, 147 µmol, 98 %). Yields of six-membered rings were determined by integration against an internal standard (mesitylene, acenaphthene or methylcarbamate) after

stirring for 24 h, filtration through a short silica plug, removal of solvent and addition of CDCl$_3$ (0.6 mL).

**Ethyl 2-phenylcyclopent-2-ene-1-carboxylate:**

**¹H NMR** (CDCl$_3$): δ 7.44 – 7.43 (m, 2H), 7.31 – 7.29 (m, 2H), 7.23 – 7.21 (m, 1H), 6.34 (m, 1H), 4.11 - 4.07 (m, 2H), 3.98 – 3.96 (m, 1H), 2.74 – 2.69 (m, 1H), 2.57 – 2.53 (m, 1H), 2.39 – 2.33 (m, 1H), 2.25 (ddt, $J$ = 13.1, 8.7, 4.3 Hz; 1H), 1.15 (t, $J$ = 7.0 Hz, 3H). **¹³C NMR** (151 MHz, CDCl$_3$): δ 175.4, 141.2, 135.5, 130.2, 128.4, 127.3, 125.9, 60.6, 51.4, 32.6, 29.4, 14.2.

## 7.2.30    PCl(aph^Ph)₂ (4.2a)
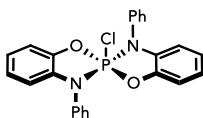
2-(Phenylamino)phenol (2.00 g, 10.8 mmol, 2.1 equiv) and PCl₅ (1.07 g, 5.14 mmol, 1 equiv) were dissolved in toluene (20 mL). The solution was heated at 100 °C for 24 h, after which the solvent was removed under reduced pressure. The crude product was recrystallized from a dichloromethane/*n*-hexane mixture at -40 °C to give the product as a brown solid (1.48 g, 3.42 mmol, 67 %).

**¹H NMR** (600 MHz, CD₂Cl₂) δ 7.54 (s, 2H), 7.49 – 7.42 (m, 1H), 7.18 (s, 1H), 6.82 – 6.73 (m, 2H), 6.50 (ddd, $J$ = 7.1, 2.1, 1.2 Hz, 1H), 6.26 (ddd, $J$ = 6.6, 2.3, 1.3 Hz, 1H).
**¹³C NMR** (151 MHz, CD₂Cl₂) δ 144.1, 140.7 (d, $J$ = 1.4 Hz), 134.6 (d, $J$ = 30.3 Hz), 130.0, 129.3 (d, $J$ = 3.5 Hz), 128.2 (d, $J$ = 1.9 Hz), 121.6 (d, $J$ = 1.6 Hz), 121.4, 111.4 (d, $J$ = 13.4 Hz), 109.7 (d, $J$ = 10.7 Hz).
**³¹P NMR** (243 MHz, CD₂Cl₂) δ -40.5.

**HRMS** (EI): [C₂₄ClH₁₈N₂O₂P]⁺, calcd.: 432.0789, found: 432.0779.

**Anal.** Calcd. for C₂₄H₁₈ClN₂O₂P: C, 66.60; H, 4.19; N, 6.47; found C, 66.28; H, 4.36; N, 6.70.

**IR (ATR-FTIR)** ṽ [cm⁻¹] 1594 (m), 1490 (s), 1477 (s), 1356 (m), 1307(m), 1278 (m), 1240 (s), 1198 (s), 1103 (m), 1024 (m), 963 (s).

### 7.2.31 PCl(aph$^{C6F5}$)$_2$ (4.2b)
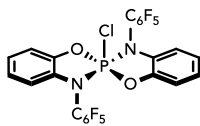
2-(pentafluorophenylamino)phenol (1.20 g, 4.36 mmol, 2.2 equiv) and PCl$_5$ (413 mg, 1.98 mmol, 1 equiv) were dissolved in toluene (15 mL). The solution was heated at 100 °C for 24 h, after which the solvent was removed under reduced pressure. The crude product was recrystallized from *n*-hexane at -40 °C to give the product as a brown solid (1.03 g, 1.69 mmol, 85 %).

**¹H NMR** (600 MHz, CD$_2$Cl$_2$) δ 7.00 – 6.89 (m, 2H), 6.76 (dt, J = 7.7, 1.3 Hz, 1H), 6.41 (dd, J = 7.6, 1.5 Hz, 1H).

**¹³C NMR** (151 MHz, CD$_2$Cl$_2$) δ 143.8 (d, J = 1.2 Hz), 130.8 (d, J = 29.5 Hz), 123.4 (d, J = 1.5 Hz), 122.5 (d, J = 0.8 Hz), 110.9 (d, J = 10.5 Hz), 110.5 (d, J = 12.8 Hz). -C$_6$F$_5$ carbon signals were not assigned due to low intensities due to coupling with fluorine atoms.

**³¹P NMR** (243 MHz, CD$_2$Cl$_2$) δ -41.0.

**¹⁹F NMR** (376 MHz, CD$_2$Cl$_2$) δ -143.9 (d, *J* = 21.8 Hz), -146.1 – -148.0 (m), -153.7 (td, *J* = 21.3, 3.5 Hz), -161.6 – -161.8 (m), -161.8 – -162.0 (m).

**HRMS** (EI): [C$_{24}$ClH$_8$F$_{10}$N$_2$O$_2$P]$^+$, calcd.: 611.9847, found: 611.9849.

**Anal.** Calcd. for C$_{24}$H$_8$ClF$_{10}$N$_2$O$_2$P: C, 47.04; H, 1.32; N, 4.57; found C, 47.41; H, 1.63; N, 4.67.

**IR (ATR-FTIR)** $\tilde{v}$ [cm$^{-1}$] 1520 (s), 1486 (w), 1467 (m), 1348 (m), 1297 (s), 1274 (s), 1239 (s), 1208 (s), 1184 (s), 1095 (s), 1087 (s), 1052 (m), 1019 (m), 1001 (s), 969 (s).

## 7.2.32    PCl(ᶠaph^C6F5)₂ 4.2c
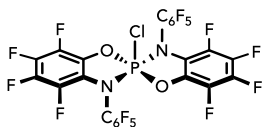


Nonafluoro-2-phenylaminophenol (1.85 g, 5.33 mmol, 2.1 equiv) and PCl₅ (529 mg , 2.54 mmol, 1 equiv) were dissolved in 25 mL of dichloromethane and the resulting solution stirred for 24 h at room temperature. The solvent was removed under reduced pressure and the crude product dissolved in a pentane/dichloromethane mixture and crystallized by storing the solution at -40 °C for three days (crystals obtained this way were suitable for X-ray diffraction). The solid was collected by filtration and dried *in vacuo* to give the product as a crystalline, white solid. The solvent of the filtrate was removed under reduced pressure and the residue again recrystallized from pentane to give a second batch of product (1.44 g, 1.81 mmol, 71 %).  Approx. 9 % of products contain one less fluorine atom, as indicated from $^{31}$P NMR and the mass spectrum. The hydrodefluorination likely occurs during the ligand synthesis and this byproduct could not be removed.

$^{19}$**F NMR** (376 MHz, CD₂Cl₂): δ = -144.2 (d, J = 21.9 Hz, 2F), -147.5 (d, J = 18.2 Hz), 2F), -151.1 (t, J = 21.3 Hz, 2F), -161.1 (t, J = 21.6 Hz, 2F), -161.5 (m, 2F), -163.2 (m, 2F), -163.4 (m, 2F), -163.6 (t, J = 20.6 Hz, 2F), -165.0 (t, J = 41.4 Hz; 2F);
$^{31}$**P NMR** (162 MHz, CD₂Cl₂): δ = -36.2 (s);
$^{13}$**C NMR** were not assigned due to low intensities due to coupling with fluorine atoms.

**HRMS** (EI): [C₂₄ClF₁₈N₂O₂P]⁺, calcd.: 755.9093, found: 755.9069.

**Anal.** Calcd. for C₂₄ClF₁₈N₂O₂P: C, 38.10; N, 3.70; found C, 38.56; N, 3.87.

**IR (ATR-FTIR)** ṽ [cm⁻¹] 1656 (w), 1511 (s), 1497 (s), 1463 (s), 1426 (m), 1262 (m), 1221 (m), 1164 (m), 1062 (s), 1027 (s), 988 (s).

### 7.2.33 [P(aph^Ph)₂][Al(OC(CF₃)₃)₄] (4.3a)
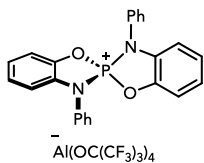


To the solid mixture of 4.2a (700 mg, 1.62 mmol, 1 equiv) and Li[Al(OC(CF₃)₃)₄] (1.58 g, 1.62 mmol, 1 equiv) was added CH₂Cl₂ (15 mL), the suspension stirred for 5 min and the solid removed by filtration. The solvent was then removed under reduced pressure, the solid washed with pentane and dried *in vacuo* to give the product as a brown solid (2.01 g, 1.48 mmol, 91 %).

**¹H NMR** (600 MHz, CD₂Cl₂) δ 7.66 – 7.61 (m, 1H), 7.60 – 7.56 (m, 2H), 7.55 – 7.51 (m, 1H), 7.40 – 7.31 (m, 3H), 7.20 (dt, *J* = 8.6, 1.3 Hz, 3H), 6.89 (dt, *J* = 8.4, 1.7 Hz, 1H).

**¹³C NMR** (151 MHz, CD₂Cl₂) δ 142.0 (d, *J* = 3.3 Hz), 132.5 (d, *J* = 23.6 Hz), 132.0 (dd, *J* = 2.6, 1.5 Hz), 128.9 (d, *J* = 2.7 Hz), 127.7, 127.1 (d, *J* = 4.3 Hz), 126.2 (d, *J* = 1.8 Hz), 121.6 (q, *J* = 293.0 Hz), 114.2 (d, *J* = 11.7 Hz), 113.2 (d, *J* = 11.8 Hz).

**¹⁹F NMR** (376 MHz, CD₂Cl₂) δ -75.8 (s, 36F).

**³¹P NMR** (243 MHz, CD₂Cl₂) δ 34.7.

**HRMS** (ESI): [C₂₄H₁₈N₂O₂P]⁺, calcd.: 397.1101, found: 397.1111.

**Anal.** Calcd. for C₄₀H₁₈AlF₃₆N₂O₆P: C, 35.21; H, 1.33; N, 2.05; found C, 35.17; H, 1.73; N, 2.21.

**IR (ATR-FTIR)** ṽ [cm⁻¹] 1595 (w), 1497 (m), 1474 (s), 1350 (m), 1295 (s), 1274 (s), 1240 (s), 1210 (s), 1196 (s), 1160 (s), 1100 (s), 969 (s), 949 (s).

## 7.2.34 [P(aph$^{C6F5}$)$_2$][Al(OC(CF$_3$)$_3$)$_4$] (4.3b)
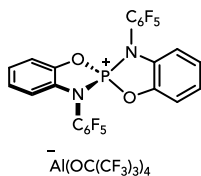
To the solid mixture of 4.2b (552 mg, 901 µmol, 1 equiv) and Li[Al(OC(CF$_3$)$_3$)$_4$] (921 mg, 946 µmol, 1.05 equiv) was added CH$_2$Cl$_2$ (10 mL), the suspension stirred for two hours and the solid removed by filtration. The solvent was then removed under reduced pressure, the solid washed with pentane and dried *in vacuo* to give the product as an off-white solid (1.22 g, 790 µmol, 88 %).

**¹H NMR** (400 MHz, CD$_2$Cl$_2$) δ 7.63 (d, *J* = 7.9 Hz, 1H), 7.49 (dtd, *J* = 9.0, 7.9, 6.6 Hz, 2H), 6.84 (d, *J* = 7.6 Hz, 1H).

**¹³C NMR** (151 MHz, CD$_2$Cl$_2$) δ 142.2 (d, *J* = 1.7 Hz), 130.3 (d, *J* = 23.8 Hz), 128.8, 128.1 (d, *J* = 1.8 Hz), 121.6 (q, *J* = 292.7 Hz), 115.1 (d, *J* = 11.5 Hz), 112.7 (d, *J* = 11.1 Hz). -C$_6$F$_5$ carbon signals were not assigned due to low intensities due to coupling with fluorine atoms.

**¹⁹F NMR** (376 MHz, CD$_2$Cl$_2$) δ -141.6 – -142.0 (m, 1F), -142.5 (tq, *J* = 21.4, 4.4 Hz, 1F), -143.4 (d, *J* = 17.3 Hz, 1F), -154.9 (td, *J* = 21.8, 5.4 Hz, 1F), -156.2 (td, *J* = 21.4, 6.9 Hz, 1F).

**³¹P NMR** (162 MHz, CD$_2$Cl$_2$) δ 35.3.

**HRMS;** high reactivity and instability under non-inert conditions precluded detection by mass spectrometry.

**Anal.** Calcd. for C$_{40}$H$_8$AlF$_{46}$N$_2$O$_6$P: C, 31.11; H, 0.52; N, 1.81; found C, 31.18; H, 0.94; N, 1.90.

**IR (ATR-FTIR):** ṽ [cm$^{-1}$] 1520 (s), 1488 (m), 1467 (m), 1350 (m), 1298 (s), 1276 (s), 1238 (s), 1210 (s), 1185 (s), 1161 (s), 1095 (s), 1088 (s), 1051 (m), 1017 (m), 1001 (s), 967 (s).

## 7.2.35  [P(aph$^{C6F5}$)$_2$][B(C$_6$F$_5$)$_4$] (4.3c)
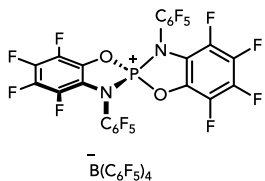


To a solution of [Ph$_3$C][BArF$_{20}$] (225 mg, 244 µmol, 0.97 equiv) in chlorobenzene (5 mL) was added triethylsilane (41.0 µL, 257 µmol, 1.02 equiv) and the solution was stirred for 2 min until it turned almost colorless, before a solution of 4.2c (200 mg, 252 µmol, 1 equiv) in chlorobenzene (3 mL) was added to give a yellow solution, which was stirred for 5 min. The solvent was then removed under reduced pressure and the resulting yellow solid that has now become sparsely soluble in dichloromethane was washed with dichloromethane (3 mL) and pentane (2 x 5 mL). After drying *in vacuo*, the product is obtained as a very pale yellow solid (330 mg, 229 µmol, 91 %). As seen with 4.2c, the product also contains approx. 9 % of mono-hydrodefluorinated product.

**$^{19}$F NMR** (376 MHz, CD2Cl2): δ = -131.4 (s, 8F), -136.9 (tq, J = 21.1, 4.6 Hz, 2F), -139.7 (d, J = 19.3 Hz, 2F), -141.8 (s, 2F), -147.9 (td, J = 20.8, 3.1 Hz, 2F), -151.4 (td, J = 21.9, 5.2 Hz, 2F), -152.6 (td, J = 21.4, 7.1 Hz, 2F), -156.3 (dd, J = 21.2, 10.7 Hz, 2F), -162.0 (t, J = 20.3 Hz, 4F), -166.0 (t, J = 19.2 Hz, 8F).
**$^{31}$P NMR** (162 MHz, CD$_2$Cl$_2$): δ = 38.3 (s).
**$^{13}$C NMR** were not assigned due to solubility issues/ low intensities due to coupling with fluorine atoms.

**HRMS**; high reactivity and instability under non-inert conditions precluded detection by mass spectrometry. The calculated mass for [C$_{24}$ClF$_{18}$N$_2$O$_2$P]$^+$, calcd.: 720.9405 was however detected in the EI(+) measurements of compound 2c at 720.99381.

**Anal.** Calcd. for C$_{48}$BF$_{38}$N$_2$O$_2$P: C, 41.17; N, 2.00; found C, 41.33; N, 2.25.

**IR (ATR-FTIR)** $\tilde{v}$ [cm$^{-1}$] 1644 (m), 1547 (s), 1507 (s), 1457 (s), 1441 (s), 1373 (m), 1279 (m), 1224 (m), 1159 (m), 1125 (s), 1092 (s), 1051 (s), 1002 (s), 974 (s).

## 7.2.36　General procedure for the reaction of 4.3c with alkynes

To a suspension of 4.3c (20.0 mg, 14.3 μmol, 1 equiv) in CD$_2$Cl$_2$ in a J. Young type NMR tube was added the respective alkyne (17.1 μmol, 1.2 equiv), the mixture was stirred, leading to immediate dissolution of residual undissolved 3c and the resulting solution was investigated by NMR. Single crystals suitable for X-ray diffraction of 4.5 were obtained by slow evaporation of the reaction solution in dichloromethane, crystals of 4.7 by vapor diffusion of pentane into the reaction solution at -40 °C.

For further purification of 4.5, the reaction mixture was dried under reduced pressure and washed with *n*-pentane. The greenish powder was taken up in CH$_2$Cl$_2$ (0.2 mL) and the solution layered with *n*-hexane (0.4 mL). The mixture was stored for 2 d at –40 °C, after which a dark viscous oil formed. The supernatant was separated, and the viscous oil washed with *n*-pentane, upon which the compound solidified. The greenish powder was dried *in vacuo* (15.1 mg, 9.58 μmol, 67%).

For the separation of 4.7 from residual components, the reaction mixture was concentrated in *vacuo* and extracted with *n*-pentane. The extracts were freed from solvent and the resulting off-white solid (9.4 mg) dissolved in CH$_2$Cl$_2$ (0.2 mL). The solution was stored at –40 °C for 2 d, and the formed colorless precipitate separated from the supernatant, and dried *in vacuo* to give the product as an off-white solid (8.1 mg, 9.87 μmol, 69%).

## Analytic data of 4.5:



**¹H NMR** (600 MHz, CD$_2$Cl$_2$) δ 7.83 (t, *J* = 7.6 Hz, 1H), 7.79 (t, *J* = 7.6 Hz, 1H), 7.62 (t, *J* = 8.1 Hz, 1H), 7.44 (s, 2H), 7.39 – 7.33 (m, 2H), 7.27 (d, *J* = 8.1 Hz, 2H).

**³¹P NMR** (243 MHz, CD$_2$Cl$_2$) δ 26.2.

**¹⁹F NMR** (376 MHz, CD$_2$Cl$_2$) δ -129.5 (s, 1F), -133.2 (s, 12F), -137.6 – -138.0 (m, 1F), -139.1 – -139.4 (m, 1F), -140.8 (s, 1F), -141.0 (td, *J* = 20.2, 7.1 Hz, 1F), -141.7 – -142.7 (m, 2F), -142.6 (s, 1F), -145.0 – -147.1 (m, 1F), -149.2, -152.3 (qd, *J* = 21.9, 6.4 Hz, 2F), -156.8 (q, *J* = 16.1 Hz, 1F), -157.1 (td, *J* = 21.9, 6.3 Hz, 1F), -157.3 – -157.6 (m, 2F), -158.3 – -158.6 (m, 1F), -158.9 (td, *J* = 21.9, 6.1 Hz, 1F), -163.8 (t, J = 20.3 Hz, 6F), -167.7 (t, J = 19.5 Hz, 12F).

**¹¹B NMR** (193 MHz, CD$_2$Cl$_2$) δ -16.7.
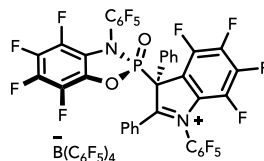
**Analytic data of 4.6:**

**¹H NMR** (600 MHz, CD₂Cl₂) δ 7.74 (t, $J$ = 7.5 Hz, 1H), 7.62 (t, $J$ = 8.0 Hz, 2H), 7.49 (d, $J$ = 8.1 Hz, 2H), 2.95 (s, 3H).

**³¹P NMR** (243 MHz, CD₂Cl₂) δ 23.6.

**¹⁹F NMR** (376 MHz, CD₂Cl₂) δ -133.3 (s, 12F), -136.8 (tt, $J$ = 21.5, 6.4 Hz, 1F), -140.0 (dt, $J$ = 21.5, 7.4 Hz, 1F), -140.3 – -140.8 (m, 2F), -141.8 (ddt, $J$ = 19.2, 12.6, 6.5 Hz, 1F), -144.2, -145.6 (td, $J$ = 21.4, 3.8 Hz, 1F), -148.1 (dd, $J$ = 24.0, 9.7 Hz, 2F), -152.3 (td, $J$ = 21.8, 6.6 Hz, 1F), -152.5 (td, $J$ = 21.6, 6.3 Hz, 1F), -155.8 (dt, $J$ = 19.9, 9.5 Hz, 1F), -156.2 – -156.8 (m, 2F), -157.3 (t, $J$ = 20.7 Hz, 1F), -158.6 – -159.1 (m, 2F), -163.7 (t, $J$ = 20.3 Hz, 6F), -167.7 (t, J = 19.5 Hz, 12F).

**¹¹B NMR** (193 MHz, CD₂Cl₂) δ -16.7.
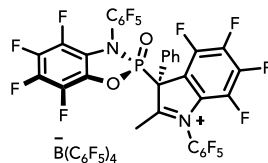
**Analytic data of 4.7:**

**¹H NMR** (400 MHz, CD₂Cl₂) δ 7.49 (d, $J$ = 8.1 Hz, 1H), 7.43 – 7.35 (m, 1H), 7.31 (d, $J$ = 7.8 Hz, 1H), 7.26 (tt, $J$ = 7.5, 1.3 Hz, 1H), 7.14 – 7.05 (m, 1H).

**³¹P NMR** (243 MHz, CD₂Cl₂) δ 17.0.

**¹⁹F NMR** (376 MHz, CD₂Cl₂) δ -142.9 (dt, $J$ = 22.4, 7.0 Hz, 1F), -144.5 (ddt, $J$ = 21.1, 13.5, 6.6 Hz, 1F), -145.4 (dtd, $J$ = 22.4, 6.3, 2.5 Hz, 1F), -147.5 (t, $J$ = 18.3 Hz, 1F), -148.8 (td, $J$ = 14.6, 7.1 Hz, 1F), -150.7 (tt, $J$ = 12.5, 9.4 Hz, 2F), -155.4 (t, $J$ = 19.1 Hz, 1F), -159.6 (dd, $J$ = 20.8, 10.2 Hz, 1F), -160.0 (td, $J$ = 21.7, 6.3 Hz, 1F), -161.1 (td, $J$ = 22.4, 7.1 Hz, 1F), -161.8 (td, $J$ = 21.9, 6.2 Hz, 1F), -162.5 (td, $J$ = 22.0, 6.3 Hz, 1F), -163.2 (t, $J$ = 20.7 Hz, 1F), -163.4 (t, $J$ = 18.5 Hz, 1F), -164.1 (t, $J$ = 19.0 Hz, 1F), -164.4 (ddd, $J$ = 20.7, 10.3, 3.1 Hz, 1F), -165.3 (td, $J$ = 20.7, 3.2 Hz, 1F).
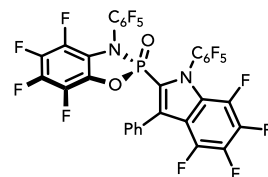
## 7.2.37    4.8
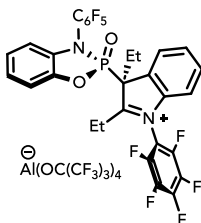


To a solution of 4.3b (150 mg, 97.1 μmol, 1 equiv) in CH$_2$Cl$_2$ (5 mL) was added 3-hexyne (22.1 μL, 194 μmol, 2 equiv) and the solution turned orange-brownish after stirring for 5 min. The solvent was then removed under reduced pressure and the solid washed with pentane and dried *in vacuo* to give the product as a yellow solid (137 mg, 84.2 μmol, 87 %).

**$^1$H NMR** (400 MHz, CD$_2$Cl$_2$) δ 7.80 – 7.68 (m, 3H), 7.33 (dd, *J* = 8.2, 1.2 Hz, 1H), 7.25 (d, *J* = 8.1 Hz, 1H), 7.22 (tt, *J* = 8.0, 1.1 Hz, 1H), 7.14 (td, *J* = 7.9, 1.2 Hz, 1H), 6.43 (dd, *J* = 7.9, 1.3 Hz, 1H), 3.34 – 3.20 (m, 3H), 3.13 (dp, *J* = 14.4, 7.2 Hz, 1H), 1.15 (t, *J* = 7.6 Hz, 3H), 0.68 (t, *J* = 7.4 Hz, 3H).

**$^{13}$C NMR** (151 MHz, CD$_2$Cl$_2$) δ 202.0 (d, *J* = 4.0 Hz), 144.9 (d, *J* = 1.3 Hz), 143.3 (d, *J* = 5.6 Hz), 134.1 (d, *J* = 15.6 Hz), 133.1 (d, *J* = 2.1 Hz), 132.9 (d, *J* = 1.5 Hz), 131.1 (d, *J* = 4.9 Hz), 126.3, 126.2 (d, *J* = 3.0 Hz), 125.5, 121.6 (q, *J* = 292.7 Hz), 115.2, 113.6 (d, *J* = 9.0 Hz), 112.0 (d, *J* = 8.6 Hz), 72.5 (d, *J* = 112.1 Hz), 28.7 (d, *J* = 5.9 Hz), 24.6, 11.2. Signals for -C$_6$F$_5$ residues were not assigned due to very low intensity.

**$^{19}$F NMR** (376 MHz, CD$_2$Cl$_2$) δ -75.8, -138.7 (d, *J* = 22.5 Hz), -139.1 – -140.0 (m), -141.1 – -142.1 (m), -143.0, -145.9 (t, *J* = 22.2 Hz), -147.8 (t, *J* = 21.2 Hz), -152.8 (tt, *J* = 21.7, 7.2 Hz), -157.2 (td, *J* = 22.0, 6.7 Hz), -158.6 – -160.0 (m).

**$^{31}$P NMR** (162 MHz, CD$_2$Cl$_2$) δ 24.4.

**HRMS** (ESI): [C$_{30}$H$_{18}$F$_{10}$N$_2$O$_2$P]$^+$, calcd.: 659.0941, found: 659.0933.

**Anal.** Calcd. for C$_{46}$H$_{18}$AlF$_{46}$N$_2$O$_6$P: C, 33.87; H, 1.12; N, 1.72; found C, 34.01; H, 1.68; N, 1.86.

## 7.2.38 4.12
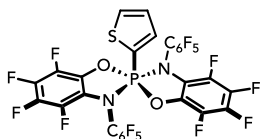
To a suspension of 4.3c (20.0 mg, 14.3 μmol, 1 equiv) in CD$_2$Cl$_2$ in a J. Young type NMR tube was added thiophene (2.28 μL, 17.1 μmol, 2 equiv), the mixture was stirred, leading to immediate dissolution of all solids. After removal of the solvent under reduced pressure, the crude reaction mixture was extracted with *n*-pentane. The combined extracts were concentrated to approx. 0.2 mL and stored at –40 °C, furnishing a colorless crystalline solid after 2 d. The supernatant was taken off and the residue dried *in vacuo* to give the product as a colorless solid (9.7 mg, 12.0 μmol, 84%).

**¹H NMR** (600 MHz, CD$_2$Cl$_2$) δ 7.96 (ddd, *J* = 8.4, 5.0, 1.2 Hz, 1H), 7.79 (ddd, *J* = 8.4, 4.0, 1.2 Hz, 1H), 7.30 (ddd, *J* = 5.9, 5.0, 3.9 Hz, 1H).
**¹³C NMR** (151 MHz, CD$_2$Cl$_2$) δ 141.2 (d, *J* = 14.9 Hz), 139.2 (d, *J* = 8.7 Hz), 130.0 (d, *J* = 24.2 Hz). Only ¹³C signals of bound thiophene are listed.
**³¹P NMR** (243 MHz, CD$_2$Cl$_2$) δ -48.5.
**¹⁹F NMR** (376 MHz, CD$_2$Cl$_2$) δ -144.9 (d, *J* = 22.4 Hz, 2F), -147.3 (d, *J* = 11.2 Hz, 2F), -152.6 (t, *J* = 21.3 Hz, 2F), -162.0 (t, *J* = 21.9 Hz, 2F), -162.2 (s, 2F), -164.2 (dd, *J* = 21.0, 8.5 Hz, 2F), -165.6 (d, *J* = 19.3 Hz, 4F), -166.6 – -167.0 (m, 2F).

### 7.2.39    Catalytic Synthesis of 9-Phenylphenanthrene

**NMR scale**: Inside a J. Young type NMR tube, 4.3c (27.5 mg, 19.7 µmol, 0.05 equiv) was added to a solution of 2-(phenylethynyl)-1,1'-biphenyl (100 mg, 393 µmol, 1 equiv) in $CD_2Cl_2$ (0.6 mL). The solution was probed by NMR after 10 min reaction time indicating full conversion of the starting material and formation of 9-phenylphenanthrene. A yield of 64 % was determined using hexamethylbenzene as an internal standard.

**Preparative scale**: Inside a glovebox, 4.3c (27.5 mg, 19.7 µmol, 0.05 equiv) was added to a stirred solution of 2-(phenylethynyl)-1,1'-biphenyl (100 mg, 393 µmol, 1 equiv) in $CH_2Cl_2$ (3 mL). The solution turned dark green and was stirred for five minutes before the solvent was removed under reduced pressure and the residue purified by flash column chromatography ($SiO_2$, PE) to give the product 9- phenylphenanthrene as a colorless, crystalline solid (61.3 mg, 241 µmol, 61 %).

**9-Phenylphenanthrene:**

**^{1}H NMR** (600 MHz, CDCl3) δ 8.77 (dd, $J$ = 32.2, 8.3 Hz, 2H), 7.92 (ddd, $J$ = 14.2, 8.0, 1.3 Hz, 2H), 7.72 – 7.65 (m, 3H), 7.65 – 7.60 (m, 1H), 7.59 – 7.51 (m, 4H), 7.49 – 7.43 (m, 1H).
**^{13}C NMR** (151 MHz, CDCl3) δ 140.9, 138.9, 131.7, 131.3, 130.7, 130.2, 130.1, 128.8, 128.4, 127.7, 127.5, 127.1, 127.0, 126.7, 126.6, 126.6, 123.0, 122.7.

### 7.2.40 P(aph^Pyr)(cat^tBu)Cl (5.3a)
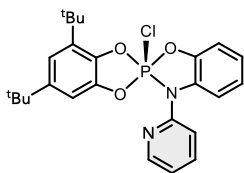
To a solution of Cat^tBuPCl₃ 5.2 (470 mg, 1.26 mmol, 1 equiv) in $CH_2Cl_2$ (7 mL) was added a solution of 5.1 (235 mg, 1.26 mmol, 1 equiv) in $CH_2Cl_2$ (7 mL). The solution was stirred for 10 min before the solvent was removed under reduced pressure and the solid extracted with a 10:1 mixture of pentane and dichloromethane. (2 x 11 mL). The suspension was filtered, and the filtrate concentrated under reduced pressure. The crude product was purified by recrystallization from a pentane and dichloromethane mixture. After storage for one day at -40 °C, a colorless solid precipitated, which was collected by filtration (hydrochloride byproduct). The filtrate was again concentrated under reduced pressure to give the product as a colorless solid (401 mg, 849 μmol, 67 %).

**¹H NMR** (600 MHz, CD₂Cl₂) δ 8.71 (d, $J$ = 5.2 Hz, 1H), 8.28 (t, $J$ = 7.7 Hz, 1H), 7.76 – 7.61 (m, 2H), 7.17 – 7.10 (m, 2H), 7.06 (tt, $J$ = 7.9, 1.2 Hz, 1H), 7.00 – 6.89 (m, 2H), 6.26 (dt, $J$ = 7.8, 1.4 Hz, 1H), 1.30 (s, 9H), 0.87 (s, 9H). Only the signals for the major isomer are listed.

**³¹P NMR** (243 MHz, CD₂Cl₂) δ -24.6 (major isomer), -25.4 (minor isomer).

**¹³C NMR** (151 MHz, CD₂Cl₂) δ 150.6 (d, $J$ = 3.6 Hz), 146.9, 145.5 (d, $J$ = 1.1 Hz), 144.1, 143.0 (d, $J$ = 1.5 Hz), 141.8 (d, $J$ = 7.6 Hz), 139.0 (d, $J$ = 3.9 Hz), 134.1 (d, $J$ = 11.3 Hz), 132.4 (d, $J$ = 29.6 Hz), 126.2 (d, $J$ = 3.3 Hz), 125.5, 123.3 (d, $J$ = 1.9 Hz), 122.2, 117.9, 111.2 (d, $J$ = 13.3 Hz), 110.8 (d, $J$ = 13.5 Hz), 107.3 (d, $J$ = 18.7 Hz), 35.2, 34.0, 31.6, 29.3. Only the signals for the major isomer are listed.

## 7.2.41 [P(aph$^{Pyr}$)(cat$^{tBu}$)][B(C$_6$F$_5$)$_4$] (5.3b)
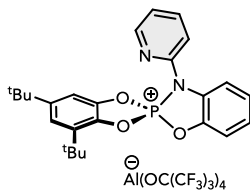


To a solution of 5.3a (250 mg, 531 µmol, 1 equiv) in CH$_2$Cl$_2$ (10 mL) was added LiAl(OC(CF$_3$)$_3$)$_4$ (543 mg, 557 µmol, 1.05 equiv) and the suspension stirred for five minutes before the solid was removed by filtration and the filtrate concentrated under reduced pressure. The solid was dissolved in CH$_2$Cl$_2$ (1.5 mL) and layered with pentane (~5 mL). A green oil formed at the bottom of the vial after cooling to -40 °C for one day. The colorless supernatant was and the oil dried under reduced pressure, furnishing a pale-green solid. The solid was washed with pentane and dried under reduced pressure to give a pale-green powder (561 mg, 400 µmol, 75 %).

**$^1$H NMR** (600 MHz, CD$_2$Cl$_2$) δ 8.11 (tt, $J$ = 8.0, 1.9 Hz, 1H), 7.77 (dd, $J$ = 8.2, 1.6 Hz, 1H), 7.70 – 7.65 (m, 2H), 7.61 (ddt, $J$ = 8.9, 6.7, 1.3 Hz, 2H), 7.52 (tt, $J$ = 8.0, 1.2 Hz, 1H), 7.47 – 7.44 (m, 1H), 7.36 (t, $J$ = 2.0 Hz, 1H), 7.33 (dd, $J$ = 7.6, 5.0 Hz, 1H), 1.39 (s, 9H), 1.38 (s, 9H).
**$^{31}$P NMR** (243 MHz, CD$_2$Cl$_2$) δ 46.1.
**$^{13}$C NMR** (151 MHz, CD$_2$Cl$_2$) δ 152.0, 148.1, 148.0 (d, $J$ = 3.8 Hz), 144.1 (d, $J$ = 4.9 Hz), 142.5 (d, $J$ = 1.5 Hz), 141.5 (d, $J$ = 6.8 Hz), 140.0 (d, $J$ = 4.7 Hz), 137.8 (d, $J$ = 11.8 Hz), 127.9 (d, $J$ = 1.0 Hz), 127.1 (d, $J$ = 1.8 Hz), 126.5 (d, $J$ = 21.1 Hz), 123.6, 122.0, 121.6 (q, $J$ = 293.0 Hz), 115.0 (d, $J$ = 13.6 Hz), 113.8 (d, $J$ = 14.5 Hz), 111.0 (d, $J$ = 11.8 Hz), 109.4 (d, $J$ = 14.7 Hz), 36.1, 35.2, 31.4, 29.5.

### 7.2.42 P(aph<sup>Pyr</sup>)Cl (5.5)
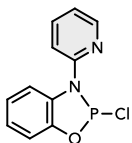
To a solution of 5.1 (200 mg, 1.07 mmol, 1 equiv) in $CH_2Cl_2$ (5 mL) was added $PCl_3$ (98.6 µL, 1.13 mmol, 1.05 equiv) and triethylamine (449 µL, 3.22 mmol, 3 equiv) and the mixture stirred for 10 min. The solvent was removed under reduced pressure and the solid extracted with diethyl ether (10 mL). After drying the ether extract under reduced pressure, the solid was recrystallized from diethyl ether to give the product as a colorless solid (102 mg, 399 µmol, 38 %).

**$^1$H NMR** (600 MHz, $CD_2Cl_2$) δ 8.45 (ddd, $J$ = 4.9, 1.9, 0.9 Hz, 1H), 7.84 (ddd, $J$ = 8.2, 7.3, 1.9 Hz, 1H), 7.63 (dd, $J$ = 8.0, 1.3 Hz, 1H), 7.44 (dd, $J$ = 8.3, 1.0 Hz, 1H), 7.30 (dd, $J$ = 8.0, 1.3 Hz, 1H), 7.22 (td, $J$ = 7.8, 1.3 Hz, 1H), 7.17 – 7.11 (m, 2H).
**$^{31}$P NMR** (243 MHz, $CD_2Cl_2$) δ 154.2.
**$^{13}$C NMR** (151 MHz, $CD_2Cl_2$) δ 151.9 (d, $J$ = 10.6 Hz), 151.9 (d, $J$ = 9.8 Hz), 149.1 (d, $J$ = 1.8 Hz), 139.4 (d, $J$ = 1.7 Hz), 129.1 (d, $J$ = 3.9 Hz), 124.1, 123.3, 119.8 (d, $J$ = 1.2 Hz), 115.0 (d, $J$ = 0.7 Hz), 113.5 (d, $J$ = 1.0 Hz), 111.8 (d, $J$ = 3.1 Hz).

## 7.2.43   2-((Pyridin-2-ylmethyl)amino)phenol (6.1a)
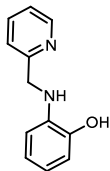
2-Pyridinecarboxaldehyde (3.82 mL, 40.0 mmol, 1 equiv) dissolved in $H_2O$ (10 mL) was added dropwise to a suspension of o-aminophenol (4.38 g, 40.0 mmol, 1 equiv) in $H_2O$ (300 mL) with stirring at room temperature. After 1 h, a yellow solid had precipitated from solution, which was collected by filtration, washed with water, and dried under reduced pressure to give the imine product as a yellow powder (7.37 g, 37.2 mmol, 93 %). The crude product was used without further purification in the next step. To a solution of (2-((pyridin-2-ylmethylene)amino)phenol (4.00 g, 20.2 mmol, 1 equiv) in methanol (50 mL) was added a few (~20) drops of glacial acetic acid and a solution of sodium cyanoborohydride (2.54 g, 40.4 mmol, 2 equiv) in MeOH (20 mL) at 0 °C. The solution was stirred overnight, thereby warming to room temperature. The solvent was removed *in vacuo* and the resulting red solid partitioned between 250 mL DCM and 100 mL brine, and the pH of the aqueous layer adjusted to ~7 with 1M $HCl_{(aq)}$. After separation of the aqueous layer, the organic phase was washed with 50 % brine (100 mL) and brine (100 mL), dried over $MgSO_4$, and concentrated under reduced pressure to give a pale orange-brownish solid. It was washed twice with both $Et_2O$ (2 x 20 mL) and pentane (2 x 50 mL) and then dried under reduced pressure to give the product as a faded, soft pink colored powder (3.02 g, 15.0 mmol, 75 %).

**¹H NMR** (400 MHz, $CD_3CN$) δ 8.57 (dd, *J* = 4.9, 0.8 Hz, 1H), 7.72 (td, *J* = 7.7, 1.8 Hz, 1H), 7.37 (d, *J* = 7.8 Hz, 1H), 7.29 – 7.21 (m, 1H), 6.76 (dd, *J* = 8.1, 1.5 Hz, 1H), 6.72 (td, *J* = 7.6, 1.4 Hz, 1H), 6.57 – 6.45 (m, 2H), 4.46 (s, 2H).
**¹³C NMR** (126 MHz, $CD_3CN$) δ 160.3, 149.9, 144.9, 138.1, 137.6, 123.0, 122.3, 121.5, 117.6, 114.7, 111.9, 49.5.

Spectroscopic data are in agreement with the literature.[140]

### 7.2.44  2-(((6-Bromopyridin-2-yl)methyl)amino)phenol (6.2a)
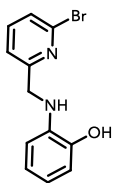


6-Bromo-2-pyridinecarboxaldehyde (6.00 g, 32.3 mmol, 1 equiv) was added portionwise to a suspension of 2-aminophenol (3.52 g, 32.3 mmol, 1 equiv) in $H_2O$ (200 mL) with stirring at room temperature. A voluminous yellow solid appeared, and the suspension was stirred another hour at room temperature. The solid was collected by filtration, washed with water, and dried under reduced pressure. The crude imine was used without further purification and suspended in methanol (150 mL). Glacial acetic acid (1 mL) was added, followed by a solution of sodium cyanoborohydride (4.05 g, 64.5 mmol, 2 equiv) in methanol (100 mL) at 0 °C.  The suspension was stirred overnight, followed by cooling to -20 °C for two hours. The precipitated solid was collected by filtration, washed with water (3 x 50 mL), diethyl ether (3 x 20 mL) and dried under reduced pressure to give the product as a white solid (6.32 g, 22.6 mmol, 70 %).

**$^1$H NMR** (600 MHz, CD$_3$CN) δ 7.61 (t, $J$ = 7.7 Hz, 1H), 7.44 (dd, $J$ = 7.9, 0.8 Hz, 1H), 7.36 (dd, $J$ = 7.6, 0.8 Hz, 1H), 6.96 (s, 1H), 6.76 (dd, $J$ = 7.7, 1.4 Hz, 1H), 6.70 (td, $J$ = 7.7, 1.4 Hz, 1H), 6.54 (td, $J$ = 7.6, 1.5 Hz, 1H), 6.47 (dd, $J$ = 7.9, 1.5 Hz, 1H), 5.13 (s, 1H), 4.45 (s, 2H).
**$^{13}$C NMR** (151 MHz, CD$_3$CN) δ 162.7, 144.7, 141.9, 140.5, 137.6, 127.1, 121.6, 121.3, 114.7, 111.7, 49.1.

**HRMS** (EI): [C$_{12}$H$_{11}$BrN$_2$O]$^+$, calcd.: 278.0049, found: 278.0035.

**Anal.** Calcd. for C$_{12}$H$_{11}$BrN$_2$O: C, 51.63; H, 3.97; N, 10.04; found C, 51.62; H, 4.17; N, 10.25.

### 7.2.45   2,4-Dichloro-6-((pyridin-2-ylmethyl)amino)phenol (6.3a)
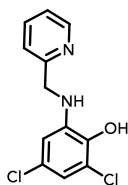
2-Pyridinecarboxaldehyde (2.71 mL, 28.5 mmol, 1 equiv) was added to a solution of 2-amino-4,6-dichlorophenol (5.08 g, 28.5 mmol, 1 equiv) in dichloromethane (100 mL), the solution stirred for twenty minutes at room temperature, after which MgSO$_4$ (7 g) was added, and the suspension stirred another ten minutes. The solid was removed by filtration, the filtrate concentrated *in vacuo*, the solid redissolved in MeOH (200 mL), cooled to 0 °C and acetic acid (1 mL) and sodium cyanoborohydride (3.59 g, 57.1 mmol, 2 equiv) were added. The resulting brown solution was stirred overnight, after which a solid had precipitated. The suspension was cooled to -20 °C for two hours, the solid collected by filtration and washed with cold methanol (2 x 10 mL) and diethyl ether (3 x 20 mL). The resulting solid was redissolved in dichloromethane (300 mL), undissolved solid removed by filtration and the filtrate concentrated under reduced pressure to give the product as a brown, microcrystalline solid (2.81 g, 10.4 mmol, 37 %).

**$^1$H NMR** (600 MHz, CD$_3$CN) δ 8.59 (ddd, *J* = 4.9, 1.8, 0.9 Hz, 1H), 7.75 (td, *J* = 7.7, 1.8 Hz, 1H), 7.36 (dt, *J* = 7.8, 0.9 Hz, 1H), 7.28 (ddd, *J* = 7.5, 4.9, 1.1 Hz, 1H), 7.12 (s, 1H), 6.68 (d, *J* = 2.4 Hz, 1H), 6.49 (d, *J* = 2.4 Hz, 1H), 5.72 (s, 1H), 4.46 (s, 2H).
**$^{13}$C NMR** (151 MHz, CD$_3$CN) δ 158.8, 149.9, 140.5, 139.4, 137.7, 126.4, 123.2, 122.4, 120.6, 116.1, 110.0, 48.9.

**HRMS** (EI): [C$_{12}$H$_{10}$Cl$_2$N$_2$O]$^+$, calcd.: 268.0165, found: 268.0140.

**Anal.** Calcd. for C$_{12}$H$_{11}$ClN$_2$O: C, 53.56; H, 3.75; N, 10.41; found C, 53.39; H, 3.73; N, 10.60.

### 7.2.46  2-(((6-bromopyridin-2-yl)methyl)amino)-4,6-dichlorophenol (6.4a)
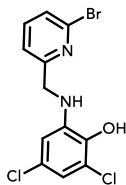


6-Bromo-2-pyridinecarboxaldehyde (1.90 g, 10.2 mmol, 1 equiv) was added to a suspension of 4,6-dichloro-2-aminophenol (1.82 g, 10.2 mmol, 1 equiv) in dichloromethane (100 mL), the suspension stirred for ten minutes at room temperature, after which MgSO$_4$ (5 g) was added, and the suspension stirred another hour. The solid was removed by filtration, the filtrate concentrated *in vacuo* (orange-brown oil), redissolved in MeOH (200 mL), cooled to 0 °C and acetic acid (0.5 mL) and sodium cyanoborohydride (1.28 g, 20.4 mmol, 2 equiv) were added. The orange solution was stirred overnight. The solvent was removed under reduced pressure, the resulting orange solid suspended in dichloromethane (200 mL) and 100 mL brine and the aqueous phase pH adjusted to ~7. The phases were separated, and the organic phase washed with 50 % brine (100 mL) and brine (100 mL), dried over MgSO$_4$ and concentrated under reduced pressure. The crude product was washed with diethyl ether (3 x 5 mL) and dried *in vacuo* to give the product as light-brown powder (1.47 g, 4.22 mmol, 41 %).

**¹H NMR** (600 MHz, CD$_3$CN) δ 7.64 (t, *J* = 7.7 Hz, 1H), 7.47 (d, *J* = 7.9 Hz, 1H), 7.35 (d, *J* = 7.6 Hz, 1H), 6.91 (s, 1H), 6.69 (d, *J* = 2.4 Hz, 1H), 6.43 (d, *J* = 2.4 Hz, 1H), 5.55 (s, 1H), 4.46 (d, *J* = 5.7 Hz, 2H).
**¹³C NMR** (151 MHz, CD$_3$CN) δ 161.3, 142.0, 140.7, 140.1, 139.2, 127.4, 126.4, 121.4, 120.6, 116.3, 109.7, 48.6.

**HRMS** (EI): [C$_{12}$H$_{10}$Cl$_2$N$_2$O]$^+$, calcd.: 345.9270, found: 345.9262.

**Anal.** Calcd. for C$_{12}$H$_8$Cl$_2$BrN$_2$O: C, 41.41; H, 2.61; N, 8.05; found C, 41.11; H, 2.72; N, 7.87.

## 7.2.47  P(aph$^{CH2Pyr}$)Cl (6.1b)
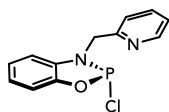
To a suspension of 2-((pyridin-2-ylmethyl)amino)phenol (2.00 g, 9.99 mmol, 1 equiv) in toluene (75 mL) was added PCl$_3$ (961 µL, 11.0 mmol, 1.1 equiv), the mixture stirred for three minutes, after which triethylamine (3.06 mL, 22.0 mmol, 2.2 equiv) was added. The suspension was heated to 80 °C for four hours, cooled to room temperature and the solid removed by filtration. The filtrate was concentrated under reduced pressure to ~70 % volume and cooled to -40 °C overnight. The precipitate was collected by filtration, washed with acetonitrile (3 x 5 mL), diethyl ether (3 x 5 mL), pentane (3 x 10 mL) and dried under reduced pressure to give the product as an off-white solid (2.06 g, 7.77 mmol, 78 %). Single crystals suitable for X-ray diffraction were grown by cooling a concentrated solution in toluene.

**$^1$H NMR** (600 MHz, CD$_2$Cl$_2$) δ 8.65 (d, J = 5.0 Hz, 1H), 7.81 (td, J = 7.7, 1.7 Hz, 1H), 7.45 (d, J = 7.9 Hz, 1H), 7.37 (dd, J = 7.5, 5.0 Hz, 1H), 7.20 (dd, J = 7.9, 1.2 Hz, 1H), 7.12 (td, J = 7.6, 1.2 Hz, 1H), 7.04 (tt, J = 7.7, 1.1 Hz, 1H), 6.97 (dd, J = 7.7, 1.3 Hz, 1H), 5.00 (d, J = 12.6 Hz, 2H).
**$^{31}$P NMR** (243 MHz, CD$_2$Cl$_2$) δ 147.3.
**$^{13}$C NMR** (151 MHz, CD$_2$Cl$_2$) δ 153.2 (d, J = 1.8 Hz), 149.2 (d, J = 7.9 Hz), 146.8 (d, J = 3.0 Hz), 138.1, 134.4 (d, J = 8.5 Hz), 123.7, 123.5 (d, J = 1.3 Hz), 122.0, 121.8, 113.5 (d, J = 1.6 Hz), 111.5 (d, J = 3.4 Hz), 50.5 (d, J = 3.2 Hz).

**HRMS** (EI): [C$_{12}$H$_{10}$N$_2$OPCl]$^+$, calcd.: 264.0214, found: 264.0194.

**Anal.** Calcd. for C$_{12}$H$_{10}$ClN$_2$OP: C, 54.46; H, 3.81; N, 10.59; found C, 53.95; H, 3.85; N, 10.60.

### 7.2.48 P(aph<sup>CH2Pyr-Br</sup>)Cl (6.2b)
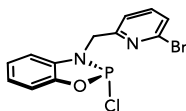
To a suspension of 2-(((6-Bromopyridin-2-yl)methyl)amino)phenol (2.00 g, 7.16 mmol, 1 equiv) in toluene (50 mL) was added $PCl_3$ (689 µL, 7.88 mmol, 1.1 equiv), the mixture stirred for three minutes, after which triethylamine (2.20 mL, 15.8 mmol, 2.2 equiv) was added. The suspension was heated to 80 °C for four hours, cooled to room temperature and the solid removed by filtration. The filtrate was concentrated under reduced pressure to ~70 % volume and cooled to -40 °C overnight. The precipitate was collected by filtration, washed with acetonitrile (3 x 3 mL), diethyl ether (3 x 5 mL), pentane (3 x 10 mL) and dried under reduced pressure to give the product as a white solid (1.33 g, 3.86 mmol, 54 %). Single crystals suitable for X-ray diffraction were grown by cooling a concentrated solution in toluene.

**¹H NMR** (400 MHz, CD₂Cl₂) δ 7.58 (t, $J$ = 7.7 Hz, 1H), 7.48 (dd, $J$ = 7.9, 0.8 Hz, 1H), 7.37 (dd, $J$ = 7.5, 0.8 Hz, 1H), 7.26 (dd, $J$ = 7.8, 1.4 Hz, 1H), 7.12 (td, $J$ = 7.7, 1.3 Hz, 1H), 7.09 – 6.98 (m, 1H), 6.89 (dd, $J$ = 7.6, 1.5 Hz, 1H), 4.93 (d, $J$ = 11.7 Hz, 2H).
**³¹P NMR** (162 MHz, CD₂Cl₂) δ 160.6.
**¹³C NMR** (151 MHz, CD₂Cl₂) δ 156.6 (d, $J$ = 3.9 Hz), 149.4 (d, $J$ = 9.8 Hz), 141.5, 140.0, 133.7 (d, $J$ = 5.9 Hz), 127.9, 124.2, 122.3, 121.1 (d, $J$ = 1.2 Hz), 114.1, 111.8 (d, $J$ = 2.6 Hz), 48.8 (d, $J$ = 9.4 Hz).

**HRMS** (EI): [C₁₂H₉N₂OPBrCl]⁺, calcd.: 341.9319, found: 341.9311.

**Anal.** Calcd. for C₁₂H₁₀ClN₂OPBr: C, 41.95; H, 2.64; N, 8.15; found C, 42.39; H, 2.81; N, 8.28.

### 7.2.49    P(<sup>Cl2</sup>aph<sup>CH2Pyr</sup>)Cl (6.3b)
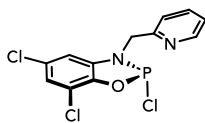
To a suspension of 2,4-dichloro-6-((pyridin-2-ylmethyl)amino)phenol (500 mg, 1.86 mmol, 1 equiv) in toluene (50 mL) was added PCl$_3$ (179 μL, 2.04 mmol, 1.1 equiv), the mixture stirred for three minutes, after which triethylamine (580 μL, 4.09 mmol, 2.2 equiv) was added. The suspension was heated to 80 °C for four hours, cooled to room temperature and the solid collected by filtration. The solid was washed with dichloromethane (3 x 5 mL), pentane (2 x 5 mL) and dried under reduced pressure to give the product as an off-white solid (352 mg, 179 mmol, 57 %). Single crystals suitable for X-ray diffraction were grown by cooling a concentrated solution in toluene.

**¹H NMR** (600 MHz, CD$_2$Cl$_2$) δ 8.66 (dd, J = 5.1, 2.5 Hz, 1H), 7.94 (td, J = 7.7, 1.6 Hz, 1H), 7.52 (d, J = 7.8 Hz, 1H), 7.49 (dd, J = 7.5, 5.2 Hz, 1H), 7.04 (dd, J = 2.1, 1.1 Hz, 1H), 6.86 (d, J = 2.0 Hz, 1H), 5.02 (d, J = 12.8 Hz, 2H).
**³¹P NMR** (243 MHz, CD$_2$Cl$_2$) δ 133.7 (s, br).
**¹³C NMR** (151 MHz, CD$_2$Cl$_2$) δ 150.7 (d, J = 5.6 Hz), 144.6 (d, J = 7.7 Hz), 144.3 (d, J = 4.1 Hz), 139.6, 136.9 (d, J = 10.3 Hz), 127.9, 124.5 (d, J = 1.8 Hz), 121.8, 121.7, 118.6, 110.3 (d, J = 3.8 Hz), 51.1.

**HRMS** (EI): [C$_{12}$H$_8$N$_2$OPCl$_3$]$^+$, calcd.: 331.9434, found: 331.9433.

**Anal.** Calcd. for C$_{12}$H$_{10}$Cl$_3$N$_2$OP: C, 43.21; H, 2.42; N, 8.40; found C, 42.57; H, 2.67; N, 8.35.

## 7.2.50 P(<sup>Cl2</sup>aph<sup>CH2Pyr-Br</sup>)Cl (6.4b)
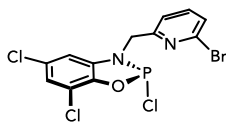


To a suspension of 2-(((6-bromopyridin-2-yl)methyl)amino)-4,6-dichlorophenol (1.35 g, 3.88 mmol, 1 equiv) in toluene (50 mL) was added $PCl_3$ (373 μL, 4.27 mmol, 1.1 equiv), the mixture stirred for three minutes, after which triethylamine (1.19 mL, 8.53 mmol, 2.2 equiv) was added. The suspension was heated to 80 °C for four hours, cooled to room temperature and the solid removed by filtration. The filtrate was concentrated under reduced pressure to ~70 % volume and cooled to -40 °C overnight. The precipitate was collected by filtration, washed with acetonitrile (3 x 3 mL), diethyl ether (3 x 5 mL), pentane (3 x 10 mL) and dried under reduced pressure to give the product as a white solid (901 mg, 2.18 mmol, 56 %). Single crystals suitable for X-ray diffraction were grown by cooling a concentrated solution in diethyl ether.

**¹H NMR** (600 MHz, $CD_2Cl_2$) δ 7.66 (t, *J* = 7.7 Hz, 1H), 7.53 (dd, *J* = 7.9, 0.8 Hz, 1H), 7.37 (dt, *J* = 7.7, 0.8 Hz, 1H), 7.07 (dd, *J* = 2.0, 0.9 Hz, 1H), 6.84 (d, *J* = 2.0 Hz, 1H), 4.91 (qd, *J* = 16.2, 11.7 Hz, 2H).
**³¹P NMR** (162 MHz, $C_6D_6$) δ 158.6 (t, *J* = 11.9 Hz).
**¹³C NMR** (151 MHz, $CD_2Cl_2$) δ 154.5, 144.5, 140.6 (d, *J* = 2.1 Hz), 140.4, 136.7 (d, *J* = 8.0 Hz), 129.2 (d, *J* = 1.8 Hz), 128.4, 122.1, 120.9 (d, *J* = 1.4 Hz), 119.4, 110.6 (d, *J* = 2.5 Hz), 50.1 (d, *J* = 1.1 Hz).

**Anal.** Calcd. for $C_{12}H_7BrCl_3N_2OP$: C, 34.95; H, 1.71; N, 6.79; found C, 35.00; H, 1.86; N, 6.96.

## 7.2.51 [P(aph$^{CH2Pyr}$)][B(C$_6$F$_5$)$_4$] (6.1c)
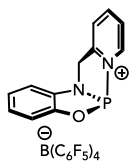
To the solid mixture of 6.1b (500 mg, 1.89 mmol, 1 equiv) and NaB(C$_6$F$_5$)$_4$ (1.37 g, 1.95 mmol, 1.03 equiv) was added dichloromethane (15 mL) and the suspension stirred for five minutes before the solid was removed by filtration. The filtrate was concentrated under reduced pressure to give the product as an off-white solid (1.64 g, 1.81 mmol, 96 %). Dissolving the product in CD$_2$Cl$_2$, $^{31}$P NMR shows minor amounts of an unidentified impurity at 124.6 ppm (~10 %), which can however be converted to the product by heating at 80 °C overnight. Also, a single product is observed after addition of a substrate, indicating the impurity to be some isomer.

**$^1$H NMR** (600 MHz, CD$_2$Cl$_2$) δ 8.79 (dq, $J$ = 5.8, 1.1 Hz, 1H), 8.44 (td, $J$ = 7.8, 1.4 Hz, 1H), 8.02 – 7.90 (m, 2H), 7.38 – 7.32 (m, 1H), 7.32 – 7.23 (m, 2H), 7.18 (td, $J$ = 7.8, 1.4 Hz, 1H), 5.45 (d, $J$ = 8.9 Hz, 2H).
**$^{31}$P NMR** (162 MHz, CD$_2$Cl$_2$) δ 161.2.
**$^{13}$C NMR** (151 MHz, CD$_2$Cl$_2$) δ 150.6 (d, $J$ = 13.9 Hz), 149.4 – 149.2 (m, BArF$_{20}$), 148.3 (d, $J$ = 1.7 Hz), 147.9 (d, $J$ = 10.0 Hz), 147.8 – 147.6 (m, BArF$_{20}$), 141.8 (d, $J$ = 6.3 Hz), 139.6 – 139.4 (m, BArF$_{20}$), 137.9 – 137.7 (m, BArF$_{20}$), 137.7 - 137.3 (m, BArF$_{20}$), 137.1 (d, $J$ = 4.0 Hz), 136.0 – 135.7 (m, BArF$_{20}$), 135.3 (d, $J$ = 4.6 Hz), 128.4 (d, $J$ = 3.2 Hz), 126.3, 124.7 (d, $J$ = 1.5 Hz), 116.1 (d, $J$ = 5.0 Hz), 114.8 (d, $J$ = 1.6 Hz), 56.9 (d, $J$ = 8.3 Hz).
**$^{11}$B NMR** (128 MHz, CD$_2$Cl$_2$) δ -16.7.
**$^{19}$F NMR** (376 MHz, CD$_2$Cl$_2$) δ -132.9 – -133.1 (m), -163.3 (t, $J$ = 20.3 Hz), -167.3 (t, $J$ = 17.6 Hz).

**HRMS** (ESI): [C$_{12}$H$_{10}$N$_2$OP]$^+$, calcd.: 229.0525, found: 229.0529.

**Anal.** Calcd. for C$_{36}$H$_{12}$BF$_{20}$N$_2$OP: C, 47.61; H, 1.11; N, 3.08; found C, 48.09; H, 1.64; N, 3.16.

## 7.2.52 [P(aph<sup>CH2Pyr-Br</sup>)][B(C₆F₅)₄] (6.2c)
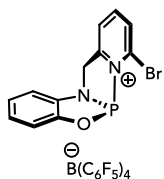


To the solid mixture of 6.2b (800 mg, 2.33 mmol, 1 equiv) and NaB(C₆F₅)₄ (1.68 g, 2.40 mmol, 1.03 equiv) was added dichloromethane (20 mL) and the suspension stirred for five minutes before the solid was removed by filtration. The filtrate was concentrated under reduced pressure and washed with pentane to give the product as an off-white solid (2.24 g, 2.27 mmol, 98 %).

**¹H NMR** (600 MHz, CD2Cl2) δ 8.17 (t, J = 7.8 Hz, 1H), 7.93 (d, J = 7.9 Hz, 1H), 7.83 (d, J = 7.7 Hz, 1H), 7.54 (d, J = 8.2 Hz, 1H), 7.50 – 7.43 (m, 2H), 7.43 – 7.37 (m, 1H), 5.66 (d, J = 8.6 Hz, 2H).

**³¹P NMR** (243 MHz, CD₂Cl₂) δ 182.6.

**¹³C NMR** (151 MHz, CD₂Cl₂) δ 151.6 (d, $J$ = 9.3 Hz), 149.6 (d, $J$ = 8.5 Hz), 149.4 – 149.2 (m, BArF₂₀), 147.8 – 147.6 (m, BArF₂₀), 147.3, 139.6 – 139.4 (m, BArF₂₀), 137.9 – 137.7 (m, BArF₂₀), 137.7 - 137.3 (m, BArF₂₀), 137.1 (d, $J$ = 4.0 Hz), 136.0 – 135.7 (m, BArF₂₀), 134.7 (d, $J$ = 4.7 Hz), 132.0 (d, $J$ = 2.7 Hz), 127.7, 122.3, 115.3, 115.2 (d, $J$ = 4.7 Hz), 56.9 (d, $J$ = 10.0 Hz).

**¹¹B NMR** (128 MHz, CD₂Cl₂) δ -16.7.

**¹⁹F NMR** (376 MHz, CD₂Cl₂) δ -132.9 – -133.1 (m), -163.3 (t, $J$ = 20.3 Hz), -167.3 (t, $J$ = 17.6 Hz).

**HRMS** (ESI): [C₁₂H₉N₂OBrP]⁺, calcd.: 306.9630, found: 306.9630.

**Anal.** Calcd. for C₃₆H₁₁BF₂₀N₂OPBr: C, 43.80; H, 0.92; N, 2.84; found C, 44.29; H, 1.35; N, 3.05.

## 7.2.53  [P(aph^CH2Pyr-Br)][Al(OC(CF$_3$)$_3$)$_4$] (6.2c)

To the solid mixture of 6.2b (263 mg, 766 µmol, 1 equiv) and LiAl(OC(CF$_3$)$_3$)$_4$ (761 mg, 781 µmol, 1.02 equiv)  was added dichloromethane (10 mL) and the suspension stirred for five minutes before the solid was removed by filtration. The filtrate was concentrated under reduced pressure and washed with pentane to give the product as a white solid (965 mg, 757 µmol, 99 %).

**¹H NMR** (600 MHz, CD$_2$Cl$_2$) δ 8.18 (t, $J$ = 7.8 Hz, 1H), 7.94 (d, $J$ = 7.9 Hz, 1H), 7.85 (d, $J$ = 7.7 Hz, 1H), 7.56 (d, $J$ = 8.2 Hz, 1H), 7.49 (d, $J$ = 4.1 Hz, 2H), 7.43 (ddd, $J$ = 8.5, 5.1, 3.8 Hz, 1H), 5.66 (d, $J$ = 8.7 Hz, 2H).
**³¹P NMR** (162 MHz, CD$_2$Cl$_2$) δ 182.2.
**¹³C NMR** (151 MHz, CD$_2$Cl$_2$) δ 151.7 (d, $J$ = 8.8 Hz), 149.7 (d, $J$ = 8.5 Hz), 147.1, 137.4, 134.7 (d, $J$ = 4.7 Hz), 132.0 (d, $J$ = 2.5 Hz), 127.7 (d, $J$ = 7.5 Hz), 122.2, 121.7 (q, $J$ = 292.7 Hz), 115.3, 115.1 (d, $J$ = 4.7 Hz), 56.6 (d, $J$ = 9.4 Hz).
**¹⁹F NMR** (376 MHz, CD$_2$Cl$_2$) δ -75.7.

**Anal.** Calcd. for C$_{28}$H$_9$AlF$_{36}$N$_2$O$_5$PBr: C, 26.37; H, 0.71; N, 2.20; found C, 26.21; H, 1.57; N, 2.55.

## 7.2.54 [P(<sup>Cl2</sup>aph<sup>CH2Pyr</sup>)][B(C₆F₅)₄] (6.3c)
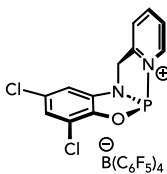
To the solid mixture of 6.3b (300 mg, 899 µmol, 1 equiv) and NaB(C₆F₅)₄ (650 mg, 926 µmol, 1.03 equiv) was added dichloromethane (20 mL) and the suspension stirred for five minutes before the solid was removed by filtration. The filtrate was concentrated under reduced pressure to give the product as an off-white solid (863 mg, 883 µmol, 98 %).

**¹H NMR** (600 MHz, CD₂Cl₂) δ 8.89 (d, $J$ = 5.7 Hz, 1H), 8.52 (td, $J$ = 7.8, 1.3 Hz, 1H), 8.06 – 8.00 (m, 2H), 7.25 (d, $J$ = 2.0 Hz, 1H), 7.23 (d, $J$ = 2.0 Hz, 1H), 5.41 (d, $J$ = 8.5 Hz, 2H).
**³¹P NMR** (162 MHz, CD₂Cl₂) δ 161.2.
**¹³C NMR** (151 MHz, CD₂Cl₂) δ 150.1 (d, $J$ = 13.5 Hz), 149.4 – 149.2 (m, BArF₂₀), 149.1 (d, $J$ = 1.6 Hz), 147.8 – 147.6 (m, BArF₂₀), 143.5 (d, $J$ = 10.7 Hz), 142.1 (d, $J$ = 7.1 Hz), 139.5 – 139.3 (m, BArF₂₀), 138.0, 137.9 – 137.7 (m, BArF₂₀), 137.7 - 137.3 (m, BArF₂₀), 136.0 – 135.7 (m, BArF₂₀), 132.8, 128.8 (d, $J$ = 2.9 Hz), 126.7, 125.0 (d, $J$ = 1.5 Hz), 121.1 (d, $J$ = 2.9 Hz), 115.3 (d, $J$ = 5.0 Hz), 57.2 (d, $J$ = 8.3 Hz).
**¹¹B NMR** (128 MHz, CD₂Cl₂) δ -16.7.
**¹⁹F NMR** (376 MHz, CD₂Cl₂) δ -132.9 – -133.1 (m), -163.3 (t, $J$ = 20.3 Hz), -167.3 (t, $J$ = 17.6 Hz).

**HRMS** (ESI): [C₁₂H₈N₂OCl₂P]⁺, calcd.: 296.9751, found: 296.9746.

**Anal.** Calcd. for C₃₆H₁₀BF₂₀N₂OPCl₂: C, 44.25; H, 0.83; N, 2.87; found C, 44.94; H, 1.41; N, 3.00.

## 7.2.55 [P($^{Cl2}$aph$^{CH2Pyr-Br}$)][B(C$_6$F$_5$)$_4$] (6.4c)
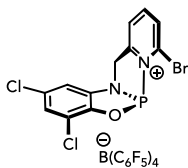


To the solid mixture of 6.4b (600 mg, 1.45 mmol, 1 equiv) and NaB(C$_6$F$_5$)$_4$ (1.05 g, 1.50 mmol, 1.03 equiv) was added dichloromethane (20 mL) and the suspension stirred for five minutes before the solid was removed by filtration. The filtrate was concentrated under reduced pressure and washed with pentane to give the product as a pale-yellow solid (1.48 g, 1.40 mmol, 96 %).

**$^1$H NMR** (600 MHz, CD$_2$Cl$_2$) δ 8.29 (t, $J$ = 7.8 Hz, 1H), 8.03 (d, $J$ = 7.9 Hz, 1H), 7.90 (d, $J$ = 7.8 Hz, 1H), 7.30 (d, $J$ = 2.0 Hz, 1H), 7.25 (d, $J$ = 2.0 Hz, 1H), 5.47 (d, $J$ = 8.5 Hz, 2H).
**$^{31}$P NMR** (162 MHz, CD$_2$Cl$_2$) δ 170.3.
**$^{13}$C NMR** (151 MHz, CD$_2$Cl$_2$) δ 152.2 (d, $J$ = 14.3 Hz), 149.4 – 149.2 (m, BArF$_{20}$), 147.8 – 147.6 (m, BArF$_{20}$), 143.8 (d, $J$ = 11.0 Hz), 139.5 – 139.3 (m, BArF$_{20}$), 137.9 – 137.7 (m, BArF$_{20}$), 137.7 - 137.3 (m, BArF$_{20}$),  137.4 (d, $J$ = 4.7 Hz), 137.0 (d, $J$ = 8.2 Hz), 136.0 – 135.7 (m, BArF$_{20}$), 133.0, 132.9 (d, $J$ = 3.9 Hz), 126.9, 123.0 (d, $J$ = 1.6 Hz), 121.3, 114.6, 57.0.
**$^{11}$B NMR** (128 MHz, CD$_2$Cl$_2$) δ -16.7.
**$^{19}$F NMR** (376 MHz, CD$_2$Cl$_2$) δ -132.9 – -133.1 (m), -163.3 (t, $J$ = 20.3 Hz), -167.3 (t, $J$ = 17.6 Hz).

**Anal.** Calcd. for C$_{36}$H$_9$BF$_{20}$N$_2$OPBrCl$_2$: C, 40.95; H, 0.67; N, 2.65; found C, 40.81; H, 0.94; N, 2.64.

### 7.2.56 [P($^{Cl2}$aph$^{CH2Pyr-Br}$)][Al(OC(CF$_3$)$_3$)$_4$] (6.4c)
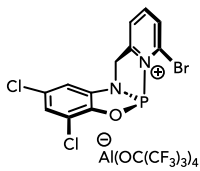


To the solid mixture of 6.4b (248 mg, 601 µmol, 1 equiv) and LiAl(OC(CF$_3$)$_3$)$_4$ (603 mg, 619 µmol, 1.03 equiv) was added dichloromethane (10 mL) and the suspension stirred for five minutes before the solid was removed by filtration. The filtrate was concentrated under reduced pressure and washed with pentane to give the product as a white solid (797 mg, 593 µmol, 99 %).

**¹H NMR** (600 MHz, CD$_2$Cl$_2$) δ 8.32 (t, $J$ = 7.8 Hz, 1H), 8.06 (dd, $J$ = 8.0, 0.8 Hz, 1H), 7.94 (d, $J$ = 7.7 Hz, 1H), 7.33 (d, $J$ = 2.0 Hz, 1H), 7.30 (d, $J$ = 2.0 Hz, 1H), 5.51 (d, $J$ = 8.5 Hz, 2H).
**³¹P NMR** (162 MHz, CD$_2$Cl$_2$) δ 170.8.
**¹³C NMR** (151 MHz, CD$_2$Cl$_2$) δ 152.0 (d, $J$ = 14.8 Hz), 149.4, 143.8 (d, $J$ = 11.3 Hz), 137.4 (d, $J$ = 4.8 Hz), 137.2 (d, $J$ = 8.5 Hz), 133.3, 133.0 (d, $J$ = 4.0 Hz), 127.1, 122.9, 121.7 (q, $J$ = 293.1 Hz), 121.4, 114.7 (d, $J$ = 4.7 Hz), 57.3 (d, $J$ = 9.1 Hz).
**¹⁹F NMR** (376 MHz, CD$_2$Cl$_2$) δ -75.7.

**Anal.** Calcd. for C$_{28}$H$_7$AlF$_{36}$N$_2$O$_5$PBrCl$_2$: C, 25.02; H, 0.52; N, 2.08; found C, 24.56; H, 1.07; N, 2.18.

## 7.2.57 Preparation of oxidative addition products

**General Procedure:**

The phosphenium salts 6.1c – 6.4c (40.0 μmol, 1 equiv) were dissolved in either CD$_2$Cl$_2$ (0.6 mL), the respective arene (i.e. chlorobenzene) or a 5:1 mixture of arene (0.5 mL, i.e. for toluene or benzene) and CD$_2$Cl$_2$ (0.1 mL). If required, to the solution in CD$_2$Cl$_2$ was then added one or two equivalents of the substrate. After NMR analysis indicated completion of the reaction, the solvent was removed under reduced pressure and the residue suspended in 7 mL pentane and stirred for one hour. The solid was collected by filtration, washed further with pentane (4 x 7 mL) and dried *in vacuo* furnishing the products in essentially quantitative yields.

### 7.2.57.1 [6.1c]•[H][NPh$_2$]
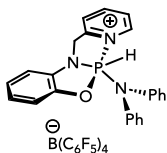


One equivalent of diphenylamine was used, the reaction was complete within five minutes at room temperature and the product is an off-white solid.

**$^1$H NMR** (600 MHz, CD$_2$Cl$_2$) δ 9.40 (dd, *J* = 857.9, 2.8 Hz, 1H), 8.21 (tt, *J* = 7.6, 1.2 Hz, 1H), 7.79 (t, *J* = 6.7 Hz, 1H), 7.67 (d, *J* = 8.0 Hz, 1H), 7.30 – 7.23 (m, 4H), 7.23 – 7.14 (m, 3H), 7.15 – 7.05 (m, 2H), 6.98 – 6.91 (m, 4H), 6.85 (dd, *J* = 7.8, 1.3 Hz, 1H), 4.89 (t, *J* = 16.9 Hz, 1H), 4.78 (dt, *J* = 17.1, 3.2 Hz, 1H).
**$^{31}$P NMR** (243 MHz, CD$_2$Cl$_2$) δ -45.2 (dd, *J* = 858.4, 16.7 Hz).
**$^{13}$C NMR** (151 MHz, CD$_2$Cl$_2$) δ 149.4 – 149.2 (m, BArF$_{20}$), 148.6 (d, *J* = 7.9 Hz), 147.8 – 147.6 (m, BArF$_{20}$), 145.5 (d, *J* = 3.8 Hz), 145.4, 142.2 (d, *J* = 6.1 Hz), 139.5 – 139.3 (m, BArF$_{20}$),  138.5 (d, *J* = 7.3 Hz), 137.9 – 137.7 (m, BArF$_{20}$), 137.7 - 137.3 (m, BArF$_{20}$), 136.0 – 135.7 (m, BArF$_{20}$), 130.6, 128.5 (d, *J* = 22.7 Hz), 128.0 (d, *J* = 1.6 Hz), 127.4 (d, *J* = 3.9 Hz), 127.2 (d, *J* = 2.0 Hz), 124.6, 123.7, 123.4, 112.2 (d, *J* = 6.3 Hz), 111.2 (d, *J* = 13.2 Hz), 44.2 (d, *J* = 2.5 Hz).
**$^{11}$B NMR** (128 MHz, CD$_2$Cl$_2$) δ -16.7.
**$^{19}$F NMR** (376 MHz, CD$_2$Cl$_2$) δ -132.9 – -133.1 (m), -163.3 (t, *J* = 20.3 Hz), -167.3 (t, *J* = 17.6 Hz).

**HRMS** (ESI): [C$_{24}$H$_{21}$N$_3$OP]$^+$, calcd.: 398.1417, found: 398.1417.

## 7.2.57.2  [6.1c]•[H][*N*-MeInd]



One equivalent of 1-methylindole was used, the reaction was complete within five minutes at room temperature and the product is an off-white solid.

**¹H NMR** (600 MHz, CD₂Cl₂) δ 9.44 (dd, *J* = 761.7, 3.4 Hz, 1H), 8.58 – 8.29 (m, 2H), 8.10 (d, *J* = 8.0 Hz, 1H), 7.86 (t, *J* = 6.7 Hz, 1H), 7.43 (dd, *J* = 8.4, 2.8 Hz, 1H), 7.34 – 7.29 (m, 2H), 7.09 (dd, *J* = 8.2, 7.2 Hz, 1H), 7.06 – 6.97 (m, 3H), 6.94 (d, *J* = 6.8 Hz, 1H), 6.66 (d, *J* = 8.3 Hz, 1H), 5.20 – 5.03 (m, 2H), 3.80 (s, 3H).

**³¹P NMR** (162 MHz, CD₂Cl₂) δ -44.0 (d, *J* = 761.9 Hz).

**¹³C NMR** (151 MHz, CD₂Cl₂) δ 149.4 (d, *J* = 6.9 Hz), 149.4 – 149.2 (m, BArF₂₀), 147.8 – 147.6 (m, BArF₂₀), 146.7 (d, *J* = 3.6 Hz), 145.5, 140.0 (d, *J* = 28.6 Hz), 139.7 (d, *J* = 6.8 Hz), 139.5 – 139.3 (m, BArF₂₀),  138.3 (d, *J* = 15.5 Hz), 137.9 – 137.7 (m, BArF₂₀), 137.7 - 137.3 (m, BArF₂₀), 136.0 – 135.7 (m, BArF₂₀), 129.4 (d, *J* = 23.4 Hz), 128.0 (d, *J* = 14.3 Hz), 127.5, 124.3 (d, *J* = 10.2 Hz), 123.6, 123.2, 122.7, 119.2, 111.6 (d, *J* = 5.6 Hz), 111.5 (d, *J* = 1.5 Hz), 110.9 (d, *J* = 13.3 Hz), 99.8 (d, *J* = 186.8 Hz), 44.8 (d, *J* = 2.5 Hz), 34.2.

**¹¹B NMR** (128 MHz, CD₂Cl₂) δ -16.7.

**¹⁹F NMR** (376 MHz, CD₂Cl₂) δ -132.9 – -133.1 (m), -163.3 (t, *J* = 20.3 Hz), -167.3 (t, *J* = 17.6 Hz).

**Anal.** Calcd. for C₄₅H₁₉BF₂₀N₃OP: C, 52.00; H, 1.84; N, 4.04; found C, 51.37; H, 2.26; N, 4.18.

## 7.2.57.2  [6.1c]•[H][*N*-MeInd]



One equivalent of 1-methylindole was used, the reaction was complete within five minutes at room temperature and the product is an off-white solid.

**$^1$H NMR** (600 MHz, CD$_2$Cl$_2$) δ 9.44 (dd, *J* = 761.7, 3.4 Hz, 1H), 8.58 – 8.29 (m, 2H), 8.10 (d, *J* = 8.0 Hz, 1H), 7.86 (t, *J* = 6.7 Hz, 1H), 7.43 (dd, *J* = 8.4, 2.8 Hz, 1H), 7.34 – 7.29 (m, 2H), 7.09 (dd, *J* = 8.2, 7.2 Hz, 1H), 7.06 – 6.97 (m, 3H), 6.94 (d, *J* = 6.8 Hz, 1H), 6.66 (d, *J* = 8.3 Hz, 1H), 5.20 – 5.03 (m, 2H), 3.80 (s, 3H).

**$^{31}$P NMR** (162 MHz, CD$_2$Cl$_2$) δ -44.0 (d, *J* = 761.9 Hz).

**$^{13}$C NMR** (151 MHz, CD$_2$Cl$_2$) δ 149.4 (d, *J* = 6.9 Hz), 149.4 – 149.2 (m, BArF$_{20}$), 147.8 – 147.6 (m, BArF$_{20}$), 146.7 (d, *J* = 3.6 Hz), 145.5, 140.0 (d, *J* = 28.6 Hz), 139.7 (d, *J* = 6.8 Hz), 139.5 – 139.3 (m, BArF$_{20}$),  138.3 (d, *J* = 15.5 Hz), 137.9 – 137.7 (m, BArF$_{20}$), 137.7 - 137.3 (m, BArF$_{20}$), 136.0 – 135.7 (m, BArF$_{20}$), 129.4 (d, *J* = 23.4 Hz), 128.0 (d, *J* = 14.3 Hz), 127.5, 124.3 (d, *J* = 10.2 Hz), 123.6, 123.2, 122.7, 119.2, 111.6 (d, *J* = 5.6 Hz), 111.5 (d, *J* = 1.5 Hz), 110.9 (d, *J* = 13.3 Hz), 99.8 (d, *J* = 186.8 Hz), 44.8 (d, *J* = 2.5 Hz), 34.2.

**$^{11}$B NMR** (128 MHz, CD$_2$Cl$_2$) δ -16.7.

**$^{19}$F NMR** (376 MHz, CD$_2$Cl$_2$) δ -132.9 – -133.1 (m), -163.3 (t, *J* = 20.3 Hz), -167.3 (t, *J* = 17.6 Hz).

**Anal.** Calcd. for C$_{45}$H$_{19}$BF$_{20}$N$_3$OP: C, 52.00; H, 1.84; N, 4.04; found C, 51.37; H, 2.26; N, 4.18.

### 7.2.57.3 [6.1c]•[H][C₂Ph]
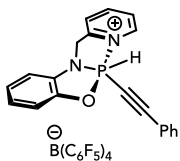
One equivalent of phenylacetylene was used, the reaction was complete within five minutes at room temperature, the product is an off-white solid. Small amounts (~9 %) of an inseparable isomeric impurity are present, which based on the multinuclear NMR date is tentatively assigned to the cooperative addition product of the alkyne along the P-N(pyridine) bond.

**¹H NMR** (600 MHz, CD₂Cl₂) δ 9.11 (ddd, $J$ = 817.3, 3.6, 1.3 Hz, 1H), 8.92 (ddt, $J$ = 6.2, 5.1, 1.1 Hz, 1H), 8.49 (tt, $J$ = 7.7, 1.2 Hz, 1H), 8.05 (ddd, $J$ = 7.3, 5.9, 1.1 Hz, 1H), 7.99 (dt, $J$ = 8.0, 1.0 Hz, 1H), 7.53 (td, $J$ = 7.4, 1.3 Hz, 1H), 7.52 – 7.45 (m, 2H), 7.42 – 7.36 (m, 2H), 7.16 – 7.10 (m, 3H), 7.03 (ddd, $J$ = 5.3, 3.0, 1.2 Hz, 1H), 5.08 (ddd, $J$ = 16.7, 5.6, 3.6 Hz, 1H), 5.00 (dd, $J$ = 16.7, 13.9 Hz, 1H).

**³¹P NMR** (162 MHz, CD₂Cl₂) δ -62.9 – -68.5 (m).

**¹³C NMR** (151 MHz, CD₂Cl₂) δ 148.0 (d, $J$ = 8.4 Hz), 146.3 (d, $J$ = 3.0 Hz), 145.7, 138.5 (d, $J$ = 7.8 Hz), 137.9 – 137.7 (m, BArF₂₀), 137.7 - 137.3 (m, BArF₂₀), 133.3 (d, $J$ = 2.3 Hz), 132.9, 129.3, 127.9 (d, $J$ = 25.8 Hz), 127.9 (d, $J$ = 1.7 Hz), 124.4, 124.3, 123.4, 117.8 (d, $J$ = 5.5 Hz), 112.0 (d, $J$ = 7.1 Hz), 111.5 (d, $J$ = 14.5 Hz), 107.2 (d, $J$ = 53.5 Hz), 78.6 (d, $J$ = 276.7 Hz), 44.4 (d, $J$ = 3.3 Hz).

**¹¹B NMR** (128 MHz, CD₂Cl₂) δ -16.7.

**¹⁹F NMR** (376 MHz, CD₂Cl₂) δ -132.9 – -133.1 (m), -163.3 (t, $J$ = 20.3 Hz), -167.3 (t, $J$ = 17.6 Hz).

**Anal.** Calcd. for C₄₄H₁₆BF₂₀N₂OP: C, 52.31; H, 1.60; N, 2.77; found C, 52.02; H, 1.80; N, 2.85.

**HRMS** (ESI): [C₂₀H₁₆N₂OP]⁺, calcd.: 331.0995, found: 331.0947.

## 7.2.57.4 [6.2c]•[H][C$_4$H$_3$S]
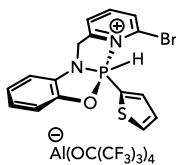
Two equivalents of thiophene were used, the reaction was complete within two days at room temperature, the product is a white solid. The analogous reaction with 6.4c (Al(OC(CF$_3$)$_3$)$_4$⁻) and thiophene was complete within five hours at room temperature, while the reaction with 6.3crequired heating to 60 °C for two hours to achieve complete conversion. The products of the latter two reactions were not isolated. No reaction of 6.1c and thiophene was observed after one day at 80 °C.

**¹H NMR** (600 MHz, CD$_2$Cl$_2$) δ 10.93 – 8.94 (m, 1H), 8.32 (t, $J$ = 7.9 Hz, 1H), 8.07 (d, $J$ = 8.0 Hz, 1H), 7.98 (dd, $J$ = 7.8, 1.1 Hz, 1H), 7.94 (ddd, $J$ = 6.3, 4.9, 1.2 Hz, 1H), 7.45 (ddd, $J$ = 8.7, 3.9, 1.2 Hz, 1H), 7.26 (dt, $J$ = 4.9, 3.8 Hz, 1H), 7.20 – 7.16 (m, 1H), 7.14 – 7.08 (m, 2H), 6.99 – 6.92 (m, 1H), 5.15 – 5.03 (m, 2H).
**³¹P NMR** (162 MHz, CD$_2$Cl$_2$) δ -30.6 (d, $J$ = 836.6 Hz).
**¹³C NMR** (151 MHz, CD$_2$Cl$_2$) δ 151.9 (d, $J$ = 7.0 Hz), 146.4, 146.0 (d, $J$ = 3.6 Hz), 141.4 (d, $J$ = 14.5 Hz), 139.1 (d, $J$ = 6.9 Hz), 136.3 (d, $J$ = 4.1 Hz), 133.6 (d, $J$ = 1.8 Hz), 130.7 (d, $J$ = 19.6 Hz), 129.0 (d, $J$ = 21.6 Hz), 126.5 (d, $J$ = 170.6 Hz), 124.5, 123.9, 123.3 (d, $J$ = 1.3 Hz), 121.7 (q, $J$ = 293.1 Hz), 112.4 (d, $J$ = 5.7 Hz), 111.4 (d, $J$ = 13.3 Hz).
**¹⁹F NMR** (376 MHz, CD$_2$Cl$_2$) δ -75.7.

**Anal.** Calcd. for C$_{32}$H$_{13}$AlBrF$_{36}$N$_2$O$_5$PS: C, 28.28; H, 0.96; N, 2.06; found C, 28.10; H, 1.66; N, 2.67.

### 7.2.57.5  [6.2c]•[H][C₄H₂SBr]
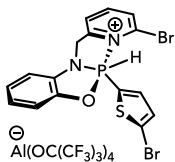


Thirty equivalents of 2-bromothiophene were used, the reaction was complete within one day at 60 °C, the product is a white solid. The product appears to be stable in solution at room temperature but converts back to the starting materials after heating.

**¹H NMR** (600 MHz, CD₂Cl₂) δ 11.08 – 8.75 (m, 1H), 8.35 (t, *J* = 7.9 Hz, 1H), 8.16 – 8.07 (m, 1H), 7.99 (dd, *J* = 7.8, 1.0 Hz, 1H), 7.23 (t, *J* = 4.1 Hz, 1H), 7.20 – 7.17 (m, 1H), 7.13 (ddt, *J* = 6.3, 4.3, 1.5 Hz, 2H), 7.10 (dd, *J* = 9.8, 4.2 Hz, 1H), 7.01 – 6.95 (m, 1H), 5.19 – 5.00 (m, 2H).

**³¹P NMR** (243 MHz, CD₂Cl₂) δ -34.0 (d, *J* = 840.1 Hz).

**¹³C NMR** (151 MHz, CD₂Cl₂) δ 152.0 (d, *J* = 7.2 Hz), 146.7, 145.8 (d, *J* = 3.7 Hz), 141.5 (d, *J* = 12.3 Hz), 136.2 (d, *J* = 4.4 Hz), 133.9 (d, *J* = 16.7 Hz), 133.8 (d, *J* = 1.8 Hz), 128.8 (d, *J* = 21.6 Hz), 127.9 (d, *J* = 169.4 Hz), 127.5 (d, *J* = 7.9 Hz), 124.7, 124.1, 123.5 (d, *J* = 1.2 Hz), 121.7 (q, *J* = 292.6 Hz), 112.5 (d, *J* = 5.6 Hz), 111.6 (d, *J* = 13.5 Hz), 45.6.

**¹⁹F NMR** (376 MHz, CD₂Cl₂) δ -75.7.

**HRMS** (ESI): [C₁₆H₁₂Br₂N₂OPS]⁺, calcd.: 468.8769, found: 468.8770.

**Anal.** Calcd. for C₃₂H₁₂AlBr₂F₃₆N₂O₅PS: C, 26.72; H, 0.84; N, 1.95; found C, 27.10; H, 1.34; N, 2.35.

### 7.2.57.6 [6.4c]•[H][C₄H₃O]
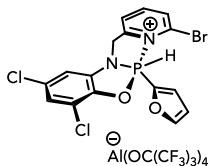
Two equivalents of furane were used, the reaction was complete within one day at room temperature, the product is a white solid. No washing required, excess furane could be removed by drying under reduced pressure.

**¹H NMR** (600 MHz, CD₂Cl₂) δ 10.88 – 8.81 (m, 1H), 8.35 (t, $J$ = 7.9 Hz, 1H), 8.12 (dt, $J$ = 8.0, 0.9 Hz, 1H), 7.97 (dd, $J$ = 7.9, 1.0 Hz, 1H), 7.74 (dd, $J$ = 3.7, 1.2 Hz, 1H), 7.66 (ddd, $J$ = 4.1, 1.7, 0.8 Hz, 1H), 7.17 (d, $J$ = 2.0 Hz, 1H), 6.88 (dd, $J$ = 2.0, 1.1 Hz, 1H), 6.73 (td, $J$ = 3.5, 1.7 Hz, 1H), 5.09 – 4.99 (m, 2H).

**³¹P NMR** (162 MHz, CD₂Cl₂) δ -44.0 (d, $J$ = 843.6 Hz).

**¹³C NMR** (151 MHz, CD₂Cl₂) δ 152.4 (d, $J$ = 10.9 Hz), 151.1 (d, $J$ = 8.0 Hz), 146.8, 141.6 (d, $J$ = 2.6 Hz), 137.2 (d, $J$ = 212.6 Hz), 136.2 (d, $J$ = 5.2 Hz), 133.6 (d, $J$ = 29.1 Hz), 133.5 (d, $J$ = 1.6 Hz), 130.7 (d, $J$ = 21.8 Hz), 128.9, 124.5, 123.3, 121.6 (q, $J$ = 292.4 Hz), 118.4 (d, $J$ = 5.8 Hz), 114.7 (d, $J$ = 12.5 Hz), 110.7 (d, $J$ = 13.4 Hz), 45.7.

**¹⁹F NMR** (376 MHz, CD₂Cl₂) δ -75.7.

**HRMS** (ESI): [$C_{16}H_{11}BrCl_2N_2O_2P$]⁺, calcd.: 442.9113, found: 442.9148.

## 7.2.57.7    [6.2c]•[H][Ph]
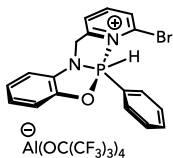


The reaction was conducted in a 5:1 benzene:CD$_2$Cl$_2$ solvent mixture, the reaction was complete within two days at 110 °C, the product is a white solid.

**$^1$H NMR** (600 MHz, CD$_2$Cl$_2$) δ 9.65 (dd, *J* = 784.6, 3.4 Hz, 1H), 8.22 (t, *J* = 7.9 Hz, 1H), 7.95 (dd, *J* = 7.8, 1.0 Hz, 1H), 7.91 (dd, *J* = 7.9, 1.0 Hz, 1H), 7.70 – 7.64 (m, 1H), 7.57 – 7.45 (m, 4H), 7.12 (tt, *J* = 7.5, 1.5 Hz, 1H), 7.08 (td, *J* = 7.7, 1.5 Hz, 1H), 7.04 (ddd, *J* = 7.4, 6.0, 1.5 Hz, 2H), 5.35 (ddd, *J* = 18.3, 6.0, 4.1 Hz, 1H), 5.15 (dd, *J* = 17.0, 10.4 Hz, 1H).

**$^{31}$P NMR** (162 MHz, CD$_2$Cl$_2$) δ -18.7 (d, *J* = 785.3 Hz).

**$^{13}$C NMR** (151 MHz, CD$_2$Cl$_2$) δ 151.0 (d, J = 5.9 Hz), 146.2 (d, J = 3.9 Hz), 145.8, 135.6 (d, J = 3.5 Hz), 134.7 (d, J = 3.7 Hz), 133.8 (d, J = 1.7 Hz), 130.8 (d, J = 13.8 Hz), 130.1 (d, J = 17.2 Hz), 129.9 (d, J = 151.5 Hz), 129.2 (d, J = 21.9 Hz), 124.5, 123.6, 122.8, 121.7 (q, J = 293.7 Hz), 112.3 (d, J = 5.4 Hz), 111.4 (d, J = 12.9 Hz), 46.3.

**$^{19}$F NMR** (376 MHz, CD$_2$Cl$_2$) δ -75.7.

**Anal.** Calcd. for C$_{34}$H$_{15}$AlF$_{36}$N$_2$O$_5$PBr: C, 30.18; H, 1.12; N, 2.07; found C, 29.63; H, 1.54; N, 2.25.

## 7.2.57.8 [6.4c]•[H][Ph]
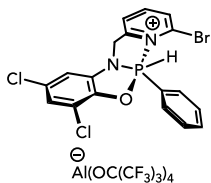


The reaction was conducted in a 5:1 benzene:CD$_2$Cl$_2$ mixture, the reaction was complete within one day at 100 °C, the product is a white solid.

**$^1$H NMR** (600 MHz, CD$_2$Cl$_2$) δ 9.70 (dd, $J$ = 795.5, 3.4 Hz, 1H), 8.28 (t, $J$ = 7.9 Hz, 1H), 7.98 (dd, $J$ = 11.8, 7.9 Hz, 1H), 7.84 – 7.66 (m, 1H), 7.56 (td, $J$ = 7.9, 5.6 Hz, 2H), 7.49 (ddd, $J$ = 17.3, 8.4, 1.4 Hz, 2H), 7.12 (d, $J$ = 2.0 Hz, 1H), 6.95 (dd, $J$ = 2.0, 1.0 Hz, 1H), 5.43 – 5.23 (m, 1H), 5.12 (dd, $J$ = 16.9, 10.4 Hz, 1H).

**$^{31}$P NMR** (162 MHz, CD$_2$Cl$_2$) δ -20.9 (d, $J$ = 796.5 Hz).

**$^{13}$C NMR** (151 MHz, CD$_2$Cl$_2$) δ 150.5 (d, $J$ = 6.0 Hz), 146.5, 141.7 (d, $J$ = 3.3 Hz), 135.6 (d, $J$ = 4.5 Hz), 135.2 (d, $J$ = 3.7 Hz), 134.3 (d, $J$ = 1.6 Hz), 131.1 (d, $J$ = 13.8 Hz), 130.9 (d, $J$ = 21.8 Hz), 130.4 (d, $J$ = 17.3 Hz), 128.9 (d, $J$ = 151.3 Hz), 128.5, 124.7, 123.1 (d, $J$ = 1.2 Hz), 121.7 (q, $J$ = 291.5 Hz), 118.3 (d, $J$ = 5.8 Hz), 110.7 (d, $J$ = 13.0 Hz), 46.3.

**$^{19}$F NMR** (376 MHz, CD$_2$Cl$_2$) δ -75.7.

**HRMS** (ESI): [C$_{18}$H$_{13}$BrCl$_2$N$_2$OP]$^+$, calcd.: 452.9320, found: 452.9358.

## 7.2.57.9 [6.4c]•[H][CHCPh₂]
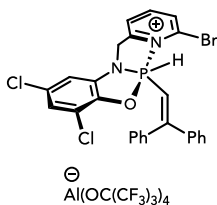
Two equivalents of 1,1-diphenylethylene were used, the reaction was complete within one day at room temperature, the product is a white solid.

**¹H NMR** (400 MHz, CD₂Cl₂) δ 9.29 (dd, *J* = 787.2, 3.3 Hz, 1H), 8.06 (t, *J* = 7.8 Hz, 1H), 7.99 (d, *J* = 7.8 Hz, 1H), 7.50 – 7.31 (m, 5H), 7.27 – 7.14 (m, 5H), 7.06 (s, 1H), 6.69 (d, *J* = 2.1 Hz, 1H), 6.60 (d, *J* = 7.5 Hz, 2H), 4.47 (dd, *J* = 16.7, 12.1 Hz, 1H), 3.66 (d, *J* = 16.7 Hz, 1H).

**³¹P NMR** (162 MHz, CD₂Cl₂) δ -24.9 (ddd, *J* = 787.4, 43.8, 12.1 Hz).

**¹³C NMR** (151 MHz, CD₂Cl₂) δ 160.7, 150.7 (d, *J* = 6.4 Hz), 145.5, 141.7 (d, *J* = 2.8 Hz), 138.9 (d, *J* = 23.6 Hz), 137.2 (d, *J* = 10.2 Hz), 134.1 (d, *J* = 4.0 Hz), 133.6 (d, *J* = 1.4 Hz), 131.9, 130.6 (d, *J* = 22.0 Hz), 130.5, 129.6, 129.4, 128.6 (d, *J* = 8.9 Hz), 128.5, 128.4, 128.1 (d, *J* = 1.8 Hz), 124.7, 122.3, 121.6 (q, *J* = 292.7 Hz), 118.3 (d, *J* = 5.5 Hz), 114.6 (d, *J* = 150.9 Hz), 110.6 (d, *J* = 13.1 Hz), 45.4.

**¹⁹F NMR** (376 MHz, CD₂Cl₂) δ -75.7.

**HRMS** (ESI): [C₂₆H₁₉N₂OBrCl₂P]⁺, calcd.: 554.9790, found: 554.9793.

## 7.2.57.10 [6.4c]•[H][Tol]
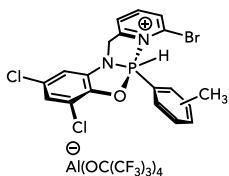
The reaction was conducted in a 5:1 toluene:CD$_2$Cl$_2$ mixture, the reaction was complete within one day at 70 °C, the product is a white solid.

**$^1$H NMR** (600 MHz, CD$_2$Cl$_2$) *major product* (*para*-addition): δ 9.66 (dd, *J* = 794.5, 3.3 Hz, 1H), 8.27 (t, *J* = 7.9 Hz, 1H), 7.97 (td, *J* = 7.4, 6.9, 0.9 Hz, 2H), 7.38 – 7.28 (m, 4H), 7.11 (d, *J* = 2.0 Hz, 1H), 6.93 (dd, *J* = 2.1, 1.0 Hz, 1H), 5.31 – 5.25 (m, 1H), 5.16 – 4.98 (m, 1H), 2.41 (d, *J* = 1.2 Hz, 3H). *minor product* (*ortho*-addition): δ 9.68 (dd, J = 779.5, 3.4 Hz, 1H), 8.23 (t, J = 7.9 Hz, 1H), 7.95 – 7.90 (m, 1H), 7.55 (tt, J = 7.6, 1.7 Hz, 1H), 7.47 (t, J = 8.6 Hz, 1H), 7.18 (td, J = 7.8, 3.5 Hz, 1H), 6.98 (dd, *J* = 2.1, 1.0 Hz, 1H), 6.68 (dd, *J* = 18.5, 7.9 Hz, 1H), 5.38 (ddd, *J* = 16.9, 6.1, 3.4 Hz, 1H), 5.19 – 5.11 (m, 1H), 2.93 (s, 3H). The product signals of the third isomer could not be reliably assigned due to low intensity and an overlap of signals.
**$^{31}$P NMR** (243 MHz, CD$_2$Cl$_2$) δ -17.2 (d, *J* = 780.6 Hz, minor product (*ortho*-addition)), -20.0 (d, *J* = 794.9 Hz, minor product (*meta*-addition)), -20.2 (d, *J* = 794.9 Hz, major product (*para*-addition)). The last two coupling constants could not be determined reliably due to signal overlap.
**$^{13}$C NMR** (151 MHz, CD$_2$Cl$_2$) *major product* (*para*-addition): δ 150.6 (d, *J* = 6.1 Hz), 147.0 (d, *J* = 3.7 Hz), 146.3, 141.7 (d, *J* = 3.2 Hz), 135.7 (d, *J* = 4.3 Hz), 134.6 (d, *J* = 3.3 Hz), 134.2 (d, *J* = 1.6 Hz), 133.1 (d, *J* = 16.0 Hz), 131.2 (d, *J* = 3.4 Hz), 131.1 (d, *J* = 6.9 Hz), 127.3 (d, *J* = 15.7 Hz), 125.2 (d, *J* = 153.9 Hz), 124.5, 123.1, 121.7 (q, *J* = 293.2 Hz), 110.6 (d, *J* = 12.9 Hz), 46.3, 21.8 (d, *J* = 1.8 Hz). The minor product signals could not be reliably assigned due to low intensity and an overlap of signals.

**HRMS** (ESI): [C$_{19}$H$_{15}$BrCl$_2$N$_2$OP]$^+$, calcd.: 466.9477, found: 466.9479.

## 7.2.57.11 [6.3c]•[H][C₆H₄Cl]
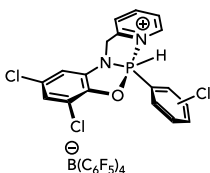


Reaction was done in chlorobenzene, the reaction was complete within one day at 140 °C, the product is an off-white solid.

**¹H NMR** (600 MHz, CD₃CN) δ 9.57 (d, $J$ = 797.1 Hz, 1H), 8.46 (t, $J$ = 7.8 Hz, 1H), 8.34 (s, 1H), 8.08 (d, $J$ = 8.1 Hz, 1H), 7.83 (t, $J$ = 6.8 Hz, 1H), 7.70 – 7.61 (m, 1H), 7.60 – 7.51 (m, 2H), 7.18 (s, 1H), 7.14 (d, $J$ = 2.1 Hz, 0H), 5.30 (dd, $J$ = 18.5, 8.7 Hz, 1H), 5.11 (dd, $J$ = 17.0, 9.3 Hz, 1H). Only the peaks for the major product are listed.

**³¹P NMR** (243 MHz, CD₃CN) δ -35.8 (d, $J$ = 786.4 Hz), -36.1 (d, $J$ = 823.2 Hz*), -37.3 (d, $J$ = 823.2 Hz*, main product). *Coupling constant could not be determined reliably due to signal overlap.

**¹³C NMR** (151 MHz, CD₃CN) Peaks could not be assigned reliably due to broadening, low intensity and/or signal overlap.

**¹¹B NMR** (128 MHz, CD₂Cl₂) δ -16.7.

**¹⁹F NMR** (565 MHz, CD₃CN) δ -133.8 (dt, $J$ = 16.5, 8.2 Hz), -163.9 (t, $J$ = 19.7 Hz), -168.3 (t, $J$ = 18.6 Hz).

**Anal.** Calcd. for $C_{42}H_{13}BCl_3F_{20}N_2OP$: C, 46.29; H, 1.20; N, 2.57; found C, 46.09; H, 1.83; N, 2.99.

### 7.2.58    Hydrolysis of [6.4c]•[H][Ph] to phenylphosphinic acid

To a solution of [6.4c]•[H][Ph] (40.0 mg, 29.6 µmol, 1 equiv) was added water (2.66 µL, 148 µmol, 5 equiv) and the reaction progress followed by NMR. After 8 h at room temperature, the hydrolysis to give protonated ligand and phenylphosphinic acid (91 % NMR yield) was complete.

# References

[1]     (a) R. M. Bullock, *Catalysis without precious metals*, John Wiley & Sons, **2011**; (b) B. List, Chemical Reviews, **2007**, pp. 5413-5415.

[2]     (a) P. P. Power, *Nature* **2010**, *463*, 171-177; (b) C. Weetman, S. Inoue, *ChemCatChem* **2018**, *10*, 4213-4228; (c) R. L. Melen, *Science* **2019**, *363*, 479-484.

[3]     R. Mason, *Nature* **1968**, *217*, 543-545.

[4]     (a) T. Chu, G. I. Nikonov, *Chem. Rev.* **2018**, *118*, 3608-3680; (b) A. Maiti, R. Yadav, L. Greb, in *Inorganic Chemistry in Germany*, **2023**, pp. 261-299.

[5]     (a) D. W. Stephan, *J. Am. Chem. Soc.* **2015**, *137*, 10018-10032; (b) D. W. Stephan, G. Erker, *Angew. Chem. Int. Ed.* **2009**, *49*, 46-76.

[6]     (a) L. Greb, *Chem. Eur. J.* **2018**, *24*, 17881-17896; (b) L. O. Müller, D. Himmel, J. Stauffer, G. Steinfeld, J. Slattery, G. Santiso-Quiñones, V. Brecht, I. Krossing, *Angew. Chem. Int. Ed.* **2008**, *47*, 7659-7663.

[7]     A. Corma, H. García, *Chem. Rev.* **2003**, *103*, 4307-4366.

[8]     G. N. Lewis, *Valence and the structure of atoms and molecules, Vol. 43*, The Chemical Catalog Co., Inc., New York, **1923**.

[9]     R. G. Pearson, *J. Am. Chem. Soc.* **1963**, *85*, 3533-3539.

[10]    R. Drago, *Coord. Chem. Rev.* **1980**, *33*, 251-277.

[11]    P. Muller, *Pure Appl. Chem.* **1994**, *66*, 1077-1184.

[12]    M. O'Keeffe, *J. Am. Chem. Soc.* **1986**, *108*, 4341-4343.

[13]    (a) P. Erdmann, J. Leitner, J. Schwarz, L. Greb, *ChemPhysChem* **2020**, *21*, 987-994; (b) P. Erdmann, L. Greb, *ChemPhysChem* **2021**, *22*, 935-943.

[14]    (a) U. Mayer, V. Gutmann, W. Gerger, *Monatsh. Chem.* **1975**, *106*, 1235-1257; (b) M. A. Beckett, G. C. Strickland, J. R. Holland, K. Sukumar Varma, *Polymer* **1996**, *37*, 4629-4631; (c) P. Erdmann, L. Greb, *Angew. Chem. Int. Ed.* **2022**, *61*, e202114550.

[15]    J. N. Bentley, S. A. Elgadi, J. R. Gaffen, P. Demay-Drouhard, T. Baumgartner, C. B. Caputo, *Organometallics* **2020**, *39*, 3645-3655.

[16]    (a) A. R. Jupp, T. C. Johnstone, D. W. Stephan, *Dalton Trans.* **2018**, *47*, 7029-7035; (b) H. F. T. Klare, L. Albers, L. Süsse, S. Keess, T. Müller, M. Oestreich, *Chem. Rev.* **2021**, *121*, 5889-5985.

[17]    J. B. Lambert, S. Zhang, C. L. Stern, J. C. Huffman, *Science* **1993**, *260*, 1917-1918.

[18]    (a) R. Maskey, M. Schädler, C. Legler, L. Greb, *Angew. Chem. Int. Ed.* **2018**, *57*, 1717-1720; (b) D. Hartmann, M. Schadler, L. Greb, *Chem. Sci.* **2019**, *10*, 7379-7388; (c) T. Thorwart, D. Roth, L. Greb, *Chem. Eur. J.* **2021**.

[19]    (a) D. Hartmann, L. Greb, *Angew. Chem. Int. Ed.* **2020**, *59*, 22510-22513; (b) D. Hartmann, T. Thorwart, R. Müller, J. Thusek, J. Schwabedissen, A.

Mix, J.-H. Lamm, B. Neumann, N. W. Mitzel, L. Greb, *J. Am. Chem. Soc.* **2021**, *143*, 18784-18793.

[20]   (a) B. Pan, F. P. Gabbaï, *J. Am. Chem. Soc.* **2014**, *136*, 9564-9567; (b) J. Zhou, L. L. Liu, L. L. Cao, D. W. Stephan, *Chem* **2018**, *4*, 2699-2708; (c) J. Zhou, L. L. Liu, L. L. Cao, D. W. Stephan, *Angew. Chem. Int. Ed.* **2019**, *58*, 5407-5412.

[21]   (a) A. Maercker, in *Organic Reactions*, **2011**, pp. 270-490; (b) J. M. Bayne, D. W. Stephan, *Chem. Soc. Rev.* **2016**, *45*, 765-774.

[22]   K. Dimroth, P. Hoffmann, *Angew. Chem. Int. Ed.* **1964**, *3*, 384-384.

[23]   A. H. Cowley, R. A. Kemp, C. A. Stewart, *J. Am. Chem. Soc.* **1982**, *104*, 3239-3240.

[24]   (a) D. Gudat, A. Haghverdi, H. Hupfer, M. Nieger, *Chem. Eur. J.* **2000**, *6*, 3414-3425; (b) B. E. Maryanoff, R. O. Hutchins, *J. Org. Chem.* **1972**, *37*, 3475-3480; (c) S. Fleming, M. K. Lupton, K. Jekot, *Inorg. Chem.* **1972**, *11*, 2534-2540; (d) C. A. Caputo, J. T. Price, M. C. Jennings, R. McDonald, N. D. Jones, *Dalton Trans.* **2008**.

[25]   (a) N. Burford, P. J. Ragogna, *J. Chem. Soc., Dalton Trans.* **2002**, 4307-4315; (b) A. L. Brazeau, C. A. Caputo, C. D. Martin, N. D. Jones, P. J. Ragogna, *Dalton Trans.* **2010**, *39*.

[26]   E. L. Muetterties, W. Mahler, R. Schmutzler, *Inorg. Chem.* **1963**, *2*, 613-618.

[27]   M. Terada, M. Kouchi, *Tetrahedron* **2006**, *62*, 401-409.

[28]   C. B. Caputo, L. J. Hounjet, R. Dobrovetsky, D. W. Stephan, *Science* **2013**, *341*, 1374-1377.

[29]   (a) C. B. Caputo, D. Winkelhaus, R. Dobrovetsky, L. J. Hounjet, D. W. Stephan, *Dalton Trans.* **2015**, *44*, 12256-12264; (b) J. M. Bayne, M. H. Holthausen, D. W. Stephan, *Dalton Trans.* **2016**, *45*, 5949-5957; (c) M. H. Holthausen, M. Mehta, D. W. Stephan, *Angew. Chem. Int. Ed.* **2014**, *53*, 6538-6541; (d) M. H. Holthausen, J. M. Bayne, I. Mallov, R. Dobrovetsky, D. W. Stephan, *J. Am. Chem. Soc.* **2015**, *137*, 7298-7301.

[30]   (a) M. Pérez, L. J. Hounjet, C. B. Caputo, R. Dobrovetsky, D. W. Stephan, *J. Am. Chem. Soc.* **2013**, *135*, 18308-18310; (b) M. Pérez, Z.-W. Qu, C. B. Caputo, V. Podgorny, L. J. Hounjet, A. Hansen, R. Dobrovetsky, S. Grimme, D. W. Stephan, *Chem. Eur. J.* **2015**, *21*, 6491-6500.

[31]   P. Mehlmann, T. Witteler, L. F. B. Wilm, F. Dielmann, *Nat. Chem.* **2019**, *11*, 1139-1143.

[32]   (a) C. Gunanathan, D. Milstein, *Acc. Chem. Res.* **2011**, *44*, 588-602; (b) J. R. Khusnutdinova, D. Milstein, *Angew. Chem. Int. Ed.* **2015**, *54*, 12236-12273.

[33]   (a) C. Gunanathan, Y. Ben-David, D. Milstein, *Science* **2007**, *317*, 790-792; (b) C. Gunanathan, D. Milstein, *Science* **2013**, *341*.

[34]   (a) Y. Soltani, F.-G. Fontaine, in *Frustrated Lewis Pairs*, **2021**, pp. 113-166; (b) M.-A. Légaré, M.-A. Courtemanche, É. Rochette, F.-G. Fontaine, *Science* **2015**, *349*, 513-516.

[35]    L. Greb, F. Ebner, Y. Ginzburg, L. M. Sigmund, *Eur. J. Inorg. Chem.* **2020**, *2020*, 3030-3047.

[36]    (a) I. L. Fedushkin, M. V. Moskalev, E. V. Baranov, G. A. Abakumov, *J. Organomet. Chem* **2013**, *747*, 235-240; (b) M. V. Moskalev, A. N. Lukoyanov, E. V. Baranov, I. L. Fedushkin, *Dalton Trans.* **2016**, *45*, 15872-15878.

[37]    S. Yao, C. van Wüllen, M. Driess, *Chem. Commun.* **2008**.

[38]    A. Jana, I. Objartel, H. W. Roesky, D. Stalke, *Inorg. Chem.* **2008**, *48*, 798-800.

[39]    L. J. Hounjet, C. B. Caputo, D. W. Stephan, *Angew. Chem. Int. Ed.* **2012**, *51*, 4714-4717.

[40]    G. A. Abakumov, A. I. Poddel'sky, E. V. Grunova, V. K. Cherkasov, G. K. Fukin, Y. A. Kurskii, L. G. Abakumova, *Angew. Chem. Int. Ed.* **2005**, *44*, 2767-2771.

[41]    J. Abbenseth, J. M. Goicoechea, *Chem. Sci.* **2020**, *11*, 9728-9740.

[42]    K. Lee, A. V. Blake, A. Tanushi, S. M. McCarthy, D. Kim, S. M. Loria, C. M. Donahue, K. D. Spielvogel, J. M. Keith, S. R. Daly, A. T. Radosevich, *Angew. Chem. Int. Ed.* **2019**, *58*, 6993-6998.

[43]    S. A. Culley, A. J. Arduengo, *J. Am. Chem. Soc.* **1984**, *106*, 1164-1165.

[44]    G. Zeng, S. Maeda, T. Taketsugu, S. Sakaki, *ACS Catal.* **2016**, *6*, 4859-4870.

[45]    N. L. Dunn, M. Ha, A. T. Radosevich, *J. Am. Chem. Soc.* **2012**, *134*, 11330-11333.

[46]    M. A. Pudovik, V. V. Ovchinnikov, R. A. Cherkasov, A. N. Pudovik, *Russ. Chem. Rev* **1983**, *52*, 361-376.

[47]    (a) C. Malavaud, J. Barrans, *Tetrahedron Lett.* **1975**, *16*, 3077-3080; (b) M. T. Boisdon, C. Malavaud, B. Tangour, J. Barrans, *Phosphorus, Sulfur Relat. Elem.* **1980**, *8*, 305-313; (c) B. Tangour, C. Malavalid, M. T. Boisdon, J. Barrans, *Phosphorus, Sulfur Relat. Elem.* **1988**, *40*, 33-39.

[48]    W. Zhao, S. M. McCarthy, T. Y. Lai, H. P. Yennawar, A. T. Radosevich, *J. Am. Chem. Soc.* **2014**, *136*, 17634-17644.

[49]    (a) T. P. Robinson, D. M. De Rosa, S. Aldridge, J. M. Goicoechea, *Angew. Chem. Int. Ed.* **2015**, *54*, 13758-13763; (b) J. Abbenseth, O. P. E. Townrow, J. M. Goicoechea, *Angew. Chem. Int. Ed.* **2021**, *60*, 23625-23629; (c) S. Volodarsky, R. Dobrovetsky, *Chem. Commun.* **2018**, *54*, 6931-6934; (d) S. Volodarsky, D. Bawari, R. Dobrovetsky, *Angew. Chem. Int. Ed.* **2022**, *61*.

[50]    S. M. McCarthy, Y.-C. Lin, D. Devarajan, J. W. Chang, H. P. Yennawar, R. M. Rioux, D. H. Ess, A. T. Radosevich, *J. Am. Chem. Soc.* **2014**, *136*, 4640-4650.

[51]    D. Bawari, K. Jaiswal, D. Toami, R. Dobrovetsky, **2023**.

[52]    (a) T. Dalton, T. Faber, F. Glorius, *ACS Cent. Sci.* **2021**, *7*, 245-261; (b) J. Wencel-Delord, F. Glorius, *Nat. Chem.* **2013**, *5*, 369-375; (c) P. Gandeepan, T. Müller, D. Zell, G. Cera, S. Warratz, L. Ackermann, *Chem. Rev.* **2018**, *119*, 2192-2452.

[53]    K. M. Altus, J. A. Love, *Commun. Chem.* **2021**, *4*.

[54]    L. Ackermann, *Chem. Rev.* **2011**, *111*, 1315-1345.

[55]     D. L. Davies, S. A. Macgregor, C. L. McMullin, *Chem. Rev.* **2017**, *117*, 8649-8709.

[56]     (a) S. A. Iqbal, J. Pahl, K. Yuan, M. J. Ingleson, *Chem. Soc. Rev.* **2020**, *49*, 4564-4591; (b) M. J. Ingleson, *ACS Catal.* **2023**, *13*, 7691-7697.

[57]     K. Chernichenko, M. Lindqvist, B. Kotai, M. Nieger, K. Sorochkina, I. Papai, T. Repo, *J. Am. Chem. Soc.* **2016**, *138*, 4860-4868.

[58]     (a) C. Cui, H. W. Roesky, H.-G. Schmidt, M. Noltemeyer, H. Hao, F. Cimpoesu, *Angew. Chem. Int. Ed.* **2000**, *39*, 4274-4276; (b) T. Chu, I. Korobkov, G. I. Nikonov, *J. Am. Chem. Soc.* **2014**, *136*, 9195-9202.

[59]     J. Hicks, P. Vasko, J. M. Goicoechea, S. Aldridge, *Nature* **2018**, *557*, 92-95.

[60]     J. Hicks, P. Vasko, J. M. Goicoechea, S. Aldridge, *J. Am. Chem. Soc.* **2019**, *141*, 11000-11003.

[61]     S. Kurumada, S. Takamori, M. Yamashita, *Nat. Chem.* **2019**, *12*, 36-39.

[62]     J. Hicks, P. Vasko, A. Heilmann, J. M. Goicoechea, S. Aldridge, *Angew. Chem. Int. Ed.* **2020**, *59*, 20376-20380.

[63]     Z. R. Turner, *Chem. Eur. J.* **2016**, *22*, 11461-11468.

[64]     N. Đorđević, R. Ganguly, M. Petković, D. Vidović, *Inorg. Chem.* **2017**, *56*, 14671-14681.

[65]     P. Bevillard, *Bull. Soc. Chim. Fr.* **1954**, *21*, 296-303.

[66]     (a) G. I. Kurnevich, V. B. Vishnevskii, *J. Appl. Spectrosc.* **1970**, *13*, 1201-1204; (b) A. C. Sau, R. R. Holmes, *Inorg. Chem.* **1981**, *20*, 4129-4135.

[67]     (a) M. Glavinovic, M. Krause, L. Yang, J. A. McLeod, L. Liu, K. M. Baines, T. Friscic, J. P. Lumb, *Sci. Adv.* **2017**, *3*, e1700149; (b) F. A. Torralvo, C. Fernández-Pereira, *Miner. Eng.* **2011**, *24*, 35-41.

[68]     D. Roth, Master Thesis thesis, Heidelberg University (Institute of Inorganic Chemistry), **2019**.

[69]     F. Cheng, M. F. Davis, A. L. Hector, W. Levason, G. Reid, M. Webster, W. Zhang, *Eur. J. Inorg. Chem.* **2007**, *2007*, 2488-2495.

[70]     (a) A. D. Becke, *Phys. Rev. A* **1988**, *38*, 3098-3100; (b) F. Weigend, R. Ahlrichs, *Phys. Chem. Chem. Phys.* **2005**, *7*, 3297-3305; (c) A. Kraft, J. Beck, G. Steinfeld, H. Scherer, D. Himmel, I. Krossing, *Organometallics* **2012**, *31*, 7485-7491.

[71]     (a) A. L. Liberman-Martin, R. G. Bergman, T. D. Tilley, *J. Am. Chem. Soc.* **2015**, *137*, 5328-5331; (b) L. Süsse, J. H. W. LaFortune, D. W. Stephan, M. Oestreich, *Organometallics* **2019**, *38*, 712-721.

[72]     D. W. Wang, D. S. Wang, Q. A. Chen, Y. G. Zhou, *Chem. Eur. J.* **2010**, *16*, 1133-1136.

[73]     M. Mehta, J. M. Goicoechea, *Angew. Chem. Int. Ed.* **2020**, *132*, 2737-2741.

[74]     J. R. Ludwig, P. M. Zimmerman, J. B. Gianino, C. S. Schindler, *Nature* **2016**, *533*, 374-379.

[75]     J. A. K. Howard, V. J. Hoy, D. O'Hagan, G. T. Smith, *Tetrahedron* **1996**, *52*, 12613-12622.

[76]     D. H. McDaniel, H. C. Brown, *J. Org. Chem.* **1958**, *23*, 420-427.

[77]     R. Maskey, H. Wadepohl, L. Greb, *Angew. Chem. Int. Ed.* **2019**, *58*, 3616-3619.

[78]    D. Roth, H. Wadepohl, L. Greb, *Angew. Chem. Int. Ed.* **2020**, *59*, 20930-20934.

[79]    (a) C. Y. Wong, D. K. Kennepohl, R. G. Cavell, *Chem. Rev.* **1996**, *96*, 1917-1952; (b) F. H. Osman, F. A. El-Samahy, *Chem. Rev.* **2002**, *102*, 629-678.

[80]    (a) J. Lacour, me, C. Ginglinger, C. Grivet, G. Bernardinelli, *Angew. Chem. Int. Ed.* **2003**, *36*, 608-610; (b) J. Lacour, *C. R. Chimie* **2010**, *13*, 985-997; (c) P. W. Siu, D. P. Gates, *Organometallics* **2009**, *28*, 4491-4499; (d) P. W. Siu, K. Hazin, D. P. Gates, *Chem. Eur. J.* **2013**, *19*, 9005-9014; (e) I. M. Riddlestone, A. Kraft, J. Schaefer, I. Krossing, *Angew. Chem. Int. Ed.* **2018**, *57*, 13982-14024.

[81]    (a) J. Gloede, H. Gross, *Journal für Praktische Chemie* **1978**, *320*, 140-142; (b) K. B. Dillon, R. N. Reeve, T. C. Waddington, *J. Chem. Soc., Dalton Trans.* **1978**.

[82]    R. Kluger, S. D. Taylor, *J. Am. Chem. Soc.* **1990**, *112*, 6669-6671.

[83]    L. Yang, D. R. Powell, R. P. Houser, *Dalton Trans.* **2007**, 955-964.

[84]    H. Großekappenberg, M. Reißmann, M. Schmidtmann, T. Müller, *Organometallics* **2015**, *34*, 4952-4958.

[85]    M. v. Hopffgarten, G. Frenking, *Wiley Interdiscip. Rev. Comput. Mol. Sci.* **2011**, *2*, 43-62.

[86]    (a) S. E. Denmark, B. D. Griedel, D. M. Coe, M. E. Schnute, *J. Am. Chem. Soc.* **1994**, *116*, 7026-7043; (b) S. E. Denmark, R. T. Jacobs, G. Dai-Ho, S. Wilson, *Organometallics* **1990**, *9*, 3015-3019; (c) J. W. A. Kinnaird, P. Y. Ng, K. Kubota, X. Wang, J. L. Leighton, *J. Am. Chem. Soc.* **2002**, *124*, 7920-7921.

[87]    (a) S. G. Nelson, B.-K. Kim, T. J. Peelen, *J. Am. Chem. Soc.* **2000**, *122*, 9318-9319; (b) S. G. Nelson, C. Zhu, X. Shen, *J. Am. Chem. Soc.* **2003**, *126*, 14-15.

[88]    J. H. LaFortune, T. C. Johnstone, M. Pérez, D. Winkelhaus, V. Podgorny, D. W. Stephan, *Dalton Trans.* **2016**, *45*, 18156-18162.

[89]    (a) H. Albright, P. S. Riehl, C. C. McAtee, J. P. Reid, J. R. Ludwig, L. A. Karp, P. M. Zimmerman, M. S. Sigman, C. S. Schindler, *J. Am. Chem. Soc.* **2019**, *141*, 1690-1700; (b) A. J. Davis, R. B. Watson, D. J. Nasrallah, J. L. Gomez-Lopez, C. S. Schindler, *Nat. Catal.* **2020**, *3*, 787-796.

[90]    (a) L. Catti, K. Tiefenbacher, *Angew. Chem. Int. Ed.* **2018**, *57*, 14589-14592; (b) R. Wang, Y. Chen, M. Shu, W. Zhao, M. Tao, C. Du, X. Fu, A. Li, Z. Lin, *Chem. Eur. J* **2020**, *26*, 1941-1946.

[91]    Y.-C. Lin, E. Hatzakis, S. M. McCarthy, K. D. Reichl, T.-Y. Lai, H. P. Yennawar, A. T. Radosevich, *J. Am. Chem. Soc.* **2017**, *139*, 6008-6016.

[92]    (a) S. Grimme, A. Hansen, S. Ehlert, J.-M. Mewes, *J. Chem. Phys.* **2021**, *154*; (b) S. Kozuch, D. Gruzman, J. M. Martin, *J. Phys. Chem. C* **2010**, *114*, 20801-20808; (c) A. V. Marenich, C. J. Cramer, D. G. Truhlar, *J. Phys. Chem. B* **2009**, *113*, 6378-6396; (d) S. Grimme, J. Antony, S. Ehrlich, H. Krieg, *J. Chem. Phys.* **2010**, *132*, 154104.

[93]    (a) C. Riplinger, F. Neese, *J. Chem. Phys.* **2013**, *138*, 034106; (b) S. Grimme, J. G. Brandenburg, C. Bannwarth, A. Hansen, *J. Chem. Phys.* **2015**, *143*, 054107.

[94]    T. vom Stein, M. Peréz, R. Dobrovetsky, D. Winkelhaus, C. B. Caputo, D. W. Stephan, *Angew. Chem. Int. Ed.* **2015**, *54*, 10178-10182.

[95]    M. Ju, Z. Lu, L. F. T. Novaes, J. I. Martinez Alvarado, S. Lin, *J. Am. Chem. Soc.* **2023**, *145*, 19478-19489.

[96]    T. Thorwart, D. Hartmann, L. Greb, *Chem. Eur. J.* **2022**, *accepted article*.

[97]    D. Roth, T. Thorwart, C. Douglas, L. Greb, *Chem. Eur. J.* **2022**, *29*.

[98]    (a) H. R. Allcock, R. L. Kugel, *Chem. Commun.* **1968**; (b) T. Koizumi, Y. Watanabe, Y. Yoshida, E. Yoshii, *Tetrahedron Lett.* **1974**, *15*, 1075-1078; (c) C. D. Reddy, S. S. Reddy, M. S. R. Naidu, *Synthesis* **1980**, *1980*, 1004-1005; (d) J. Hernández-Díaz, R. Contreras, B. Wrackmeyer, *Heteroat. Chem* **2000**, *11*, 11-15; (e) S. A. Terent'eva, I. L. Nikolaeva, A. R. Burilov, D. I. Kharitonov, E. V. Popova, M. A. Pudovik, I. A. Litvinov, A. T. Gubaidullin, A. I. Konovalov, *Russ. J. Gen. Chem.* **2001**, *71*, 389-395; (f) H. R. Allcock, R. L. Kugel, *J. Am. Chem. Soc.* **1969**, *91*, 5452-5456; (g) H. R. Allcock, R. L. Kugel, G. Y. Moore, *Inorg. Chem.* **1975**, *14*, 2831-2837; (h) D. Krasowska, J. Chrzanowski, P. Kiełbasiński, J. Drabowicz, *Molecules* **2016**, *21*; (i) N. J. O'Brien, Y. Koda, H. Maeda, N. Kano, *Polyhedron* **2020**, *192*.

[99]    (a) K. Kubo, H. Nakazawa, K. Kawamura, T. Mizuta, K. Miyoshi, *J. Am. Chem. Soc.* **1998**, *120*, 6715-6721; (b) H. Nakazawa, K. Kawamura, K. Kubo, K. Miyoshi, *Organometallics* **1999**, *18*, 2961-2969; (c) H. Nakazawa, K. Kubo, K. Miyoshi, *Bull. Soc. Chim. Jpn.* **2001**, *74*, 2255-2267; (d) B. J. Jelier, C. D. Montgomery, F. G. L. Parlane, *Inorg. Chim. Acta.* **2014**, *413*, 121-127.

[100]   C. Zhan, Z. Han, B. O. Patrick, D. P. Gates, *Dalton Trans.* **2018**, *47*, 12118-12129.

[101]   (a) S. Volodarsky, I. Malahov, D. Bawari, M. Diab, N. Malik, B. Tumanskii, R. Dobrovetsky, *Chem. Sci.* **2022**; (b) M. Alcarazo, S. B. H. Karnbrock, C. Golz, R. A. Mata, *Angew. Chem. Int. Ed.* **2022**.

[102]   D. Maiti, S. L. Buchwald, *J. Am. Chem. Soc.* **2009**, *131*, 17423-17429.

[103]   T. Thorwart, D. Hartmann, L. Greb, *Chem. Eur. J.* **2022**, *28*.

[104]   E. P. A. Couzijn, J. C. Slootweg, A. W. Ehlers, K. Lammertsma, *J. Am. Chem. Soc.* **2010**, *132*, 18127-18140.

[105]   M. Linnemannstons, J. Schwabedissen, B. Neumann, H. G. Stammler, R. J. F. Berger, N. W. Mitzel, *Chem. Eur. J.* **2020**, *26*, 2169-2173.

[106]   D. Roth, J. Stirn, D. W. Stephan, L. Greb, *J. Am. Chem. Soc.* **2021**, *143*, 15845-15851.

[107]   A. Najibi, L. Goerigk, *J. Chem. Theory Comput.* **2018**, *14*, 5725-5738.

[108]   (a) S. Orbisaglia, B. Jacques, P. Braunstein, D. Hueber, P. Pale, A. Blanc, P. de Frémont, *Organometallics* **2013**, *32*, 4153-4164; (b) A. C. Reiersølmoen, D. Csókás, S. Øien-Ødegaard, A. Vanderkooy, A. K. Gupta, A.-C. C. Carlsson, A. Orthaber, A. Fiksdahl, I. Pápai, M. Erdélyi, *J. Am. Chem. Soc.* **2020**, *142*, 6439-6446.

[109] J. M. Lipshultz, G. Li, A. T. Radosevich, *J. Am. Chem. Soc.* **2021**, *143*, 1699-1721.

[110] D. Roth, A. T. Radosevich, L. Greb, *J. Am. Chem. Soc.* **2023**, *145*, 24184-24190.

[111] (a) F. Neese, *Wiley Interdiscip. Rev. Comput. Mol. Sci.* **2012**, *2*, 73-78; (b) F. Neese, *Wiley Interdiscip. Rev. Comput. Mol. Sci.* **2022**, *12*; (c) S. Kozuch, D. Gruzman, J. M. L. Martin, *J. Phys. Chem. C* **2010**, *114*, 20801-20808.

[112] S. Grams, J. Eyselein, J. Langer, C. Färber, S. Harder, *Angew. Chem. Int. Ed.* **2020**, *59*, 15982-15986.

[113] M. Schütze, *Angew. Chem.* **1958**, *70*, 697-699.

[114] S. Ramanathan, D. Sang, V. Kumar, D. M. Lemal, in *Efficient Preparations of Fluorine Compounds*, **2012**, pp. 252-255.

[115] L. Omann, M. Oestreich, *Organometallics* **2016**, *36*, 767-776.

[116] I. Krossing, *Chem. Eur. J.* **2001**, *7*, 490-502.

[117] G. C. Welch, D. W. Stephan, *J. Am. Chem. Soc.* **2007**, *129*, 1880-1881.

[118] T. Wurm, J. Bucher, S. B. Duckworth, M. Rudolph, F. Rominger, A. S. K. Hashmi, *Angew. Chem. Int. Ed.* **2017**, *56*, 3364-3368.

[119] G. R. Fulmer, A. J. M. Miller, N. H. Sherden, H. E. Gottlieb, A. Nudelman, B. M. Stoltz, J. E. Bercaw, K. I. Goldberg, *Organometallics* **2010**, *29*, 2176-2179.

[120] (a) S. Bruker, V8.40B, Bruker AXS Inc., Madison, Wisconsin, USA; (b) L. Krause, R. Herbst-Irmer, G. M. Sheldrick, D. Stalke, *J. Appl. Crystallogr.* **2015**, *48*, 3-10.

[121] (a) G. M. Sheldrick, *Acta Cryst. C.* **2015**, *71*, 3-8; (b) G. M. Sheldrick, *Acta Cryst. A.* **2015**, *71*, 3-8; (c) T. R. Schneider, G. M. Sheldrick, *Acta Cryst. D.* **2002**, *58*, 1772-1779; (d) C. B. Hübschle, G. M. Sheldrick, B. Dittrich, *J. Appl. Crystallogr.* **2011**, *44*, 1281-1284.

[122] D. Kratzert, J. J. Holstein, I. Krossing, *J. Appl. Crystallogr.* **2015**, *48*, 933-938.

[123] C. R. Groom, I. J. Bruno, M. P. Lightfoot, S. C. Ward, *Acta Cryst. B.* **2016**, *72*, 171-179.

[124] D. Kratzert, *FinalCif*, *V85*, https://www.xs3.uni-freiburg.de/research/finalcif.

[125] (a) M. Nespolo, G. Ferraris, *Eur. J. Mineral.* **2001**, *13*, 1035-1045; (b) C. Larvor, B. Stöger, M. Weil, *Z. Kristallogr. – Cryst. Mater.* **2018**, *233*, 849-859.

[126] (a) I. J. Bruno, J. C. Cole, P. R. Edgington, M. Kessler, C. F. Macrae, P. McCabe, J. Pearson, R. Taylor, *Acta Cryst. B* **2002**, *58*, 389-397; (b) C. F. Macrae, P. R. Edgington, P. McCabe, E. Pidcock, G. P. Shields, R. Taylor, M. Towler, J. Streek, *J. Appl. Crystallogr.* **2006**, *39*, 453-457; (c) C. F. Macrae, I. Sovago, S. J. Cottrell, P. T. Galek, P. McCabe, E. Pidcock, M. Platings, G. P. Shields, J. S. Stevens, M. Towler, *J. Appl. Crystallogr.* **2020**, *53*, 226-235.

[127] F. Neese, *Wiley Interdiscip. Rev. Comput. Mol. Sci.* **2017**, *8*, 73-78.

[128] C. Y. Legault, *CYLview20* **2020**, *Université de Sherbrooke*.

[129]    G. Knizia, *J. Chem. Theory Comput.* **2013**, *9*, 4834-4843.
[130]    (a) F. Neese, F. Wennmohs, A. Hansen, U. Becker, *Chem. Phys.* **2009**, *356*, 98-109; (b) K. Eichkorn, O. Treutler, H. Oehm, M. Häser, R. Ahlrichs, *Chem. Phys.* **1995**, *242*, 652-660; (c) K. Eichkorn, F. Weigend, O. Treutler, R. Ahlrichs, *Theor. Chem. Acc.* **1997**, *97*, 119-124.
[131]    S. Grimme, *Chem. Eur. J.* **2012**, *18*, 9955-9964.
[132]    (a) P. Pracht, F. Bohle, S. Grimme, *Phys. Chem. Chem. Phys* **2020**, *22*, 7169-7192; (b) C. Bannwarth, E. Caldeweyher, S. Ehlert, A. Hansen, P. Pracht, J. Seibert, S. Spicher, S. Grimme, *Wiley Interdiscip. Rev. Comput. Mol. Sci.* **2020**, *11*.
[133]    (a) Y. Zhao, D. G. Truhlar, *J. Phys. Chem. A* **2005**, *109*, 5656-5667; (b) S. Grimme, S. Ehrlich, L. Goerigk, *J. Comput. Chem.* **2011**, *32*, 1456-1465; (c) A. D. Becke, E. R. Johnson, *J. Chem. Phys.* **2005**, *123*, 154101; (d) A. D. Becke, E. R. Johnson, *J. Chem. Phys.* **2005**, *122*, 154104.
[134]    (a) F. Neese, A. Hansen, D. G. Liakos, *J. Chem. Phys.* **2009**, *131*, 064103; (b) C. Riplinger, B. Sandhoefer, A. Hansen, F. Neese, *J. Chem. Phys.* **2013**, *139*, 134101.
[135]    H. Böhrer, N. Trapp, D. Himmel, M. Schleep, I. Krossing, *Dalton Trans.* **2015**, *44*, 7489-7499.
[136]    (a) A. Klamt, *J. Phys. Chem.* **1995**, *99*, 2224-2235; (b) F. Eckert, A. Klamt, *AIChE J.* **2002**, *48*, 369-385; (c) A. Klamt, B. Mennucci, J. Tomasi, V. Barone, C. Curutchet, M. Orozco, F. J. Luque, *Acc. Chem. Res.* **2009**, *42*, 489-492; (d) G. t. Te Velde, F. M. Bickelhaupt, E. J. Baerends, C. Fonseca Guerra, S. J. van Gisbergen, J. G. Snijders, T. Ziegler, *J. Comput. Chem.* **2001**, *22*, 931-967; (e) E. Van Lenthe, E. J. Baerends, *J. Comput. Chem.* **2003**, *24*, 1142-1156.
[137]    Y. Zhang, W. Yang, *Phys. Rev. Lett.* **1998**, *80*, 890.
[138]    C. Adamo, V. Barone, *J. Chem. Phys.* **1999**, *110*, 6158-6170.
[139]    N. Mardirossian, M. Head-Gordon, *Phys. Chem. Chem. Phys.* **2014**, *16*.
[140]    C. G. Pitt, Y. Bao, J. Thompson, M. C. Wani, H. Rosenkrantz, J. Metterville, *J. Med. Chem.* **2002**, *29*, 1231-1237.

# Appendix

## List of Abbreviations

| | | | |
|---|---|---|---|
| 9-BBN | 9-borabicylo(3.3.1)nonane | DMAP | dimethylaminopyridine |
| 18-c-6 | 18-crown-6 | DMS | dimethylsulfide |
| a.u. | atomic unit | DMSO | dimethyl sulfoxide |
| anhyd. | anhydrous | dtb | di-*tert*-butyl |
| aph | amidophenolate | *dtbpy* | 2,6-di-tbutylpyridine |
| ATR | attenuated total reflection | *e.g.* | for example |
| BArF$_{20}$ | tetrakis(pentafluorophenyl)borate | EA | electron affinity |
| BArF$_{24}$ | tetrakis(3,5-bis(trifluoromethyl)phenyl)borate | EDA | energy decomposition analysis |
| | | EI | electron ionization |
| BCF | Tris(pentafluorophenyl)borane | ELC | element-ligand cooperativity |
| br | broad | EPR | electron paramagnetic resonance |
| calc. | calculated | | |
| cat | catecholate | equiv | equivalent |
| conc. | concentrated | ESI | electrospray ionization |
| Cp | cyclopentadiene | Et | ethyl |
| Cp* | decamethylcyclopentadiene | *et al.* | and others |
| d/D | doublet/donor | exp. | experimental |
| DCM | dichloromethane | FIA | fluoride ion affinity |
| DEPT | distortionless enhancement by polarization transfer | GA | gas phase acidity |
| | | GEI | global electrophilicity index |
| DFT | density functional theory | HIA | hydride ion affinity |
| DIBA | diisopropylbenzamide | HOMO | highest occupied molecular orbital |

| | | | |
|---|---|---|---|
| HR | high resolution | NHC | *N*-heterocyclic carbene |
| HSQC | heteronuclear single quantum coherence | NHP | *N*-heterocyclic phosphenium |
| INVGATE | inverse-gated | NMP | N-methylpyrrolidone |
| i | *iso* | NMR | Nuclear magnetic resonance |
| i.e. | that is | Pyr | pyridine |
| IM | intermediate | $^n$Pr | *n*-propyl |
| iPr | *iso*-propyl | *o*- | *ortho*- |
| IR | infrared | OA | oxidative addition |
| IRC | intrinsic reaction coordinate | *o*-dfb | *o*-difluorobenzene |
| ISC | intersystem crossing | ORTEP | Oak Ridge thermal ellipsoid plot |
| KHMDS | potassium bis(trimethylsilyl)-amide | OTf | trifluoromethanesulfonate |
| L | ligand | ox. | oxidation |
| LA | Lewis Acid | *p*- | *para*- |
| LDA | Lithium diisopropylamide | Ph | phenyl |
| LiHMDS | lithium bis(trimethylsilyl)-amide | PLC | phosphorus-ligand cooperativity |
| LUMO | lowest unoccupied molecular orbital | q | quaternary |
| LSA | Lewis superacid | RE | reductive elimination |
| LSB | Lewis superbase | red | reduction |
| *m*/m/M | *meta*-, multiplet or medium /metal | $R^F$ | -C(CF$_3$)$_3$ |
| MLC | metal-ligand cooperativity | s | strong or singlet |
| | | SCXRD | single crystal X-ray diffraction |
| MS | mass spectrometry | SET | single electron transfer |
| *n* | normal | sext | sextet |
| $^n$Bu | *n*-butyl | sept | septet |
| neg. | negative | sh | shoulder |

| | |
|---|---|
| SMD | Universal solvation model based on solute electron density |
| *solv* | solvated |
| SR | separated reactants |
| t/T | *tert* or triplet/triplet |
| $^{t}$Bu | *tert*-butyl |
| THF | tetrahydrofuran |
| tip | tri-*iso*-propyl |
| TMB | 1,2,3,4-tetramethylbenzene |
| TMEDA | Tetramethylethylene-diamine |
| triphos | 1,1,1-tris(diphenyl-phosphinomethyl)-ethane |
| TS | transition state |
| UV | ultraviolet |
| *vs.* | *versus* |
| VSEPR | valence-shell electron repulsion |
| VT | variable temperature |
| w | weak |
| *WCA* | weakly coordinating anion |
| XANES | X-ray absorption near-edge spectroscopy |

# List of Symbols

| | |
|---|---|
| $\angle$ | angle [°] |
| ‡ | transition state |
| E | energy |
| G | Gibbs free energy in [kcal mol$^{-1}$] or [kJ mol$^{-1}$] |
| H | Reaction enthalpy in [kcal mol$^{-1}$] or [kJ mol$^{-1}$] |
| $I$ | nuclear spin or intensity |
| $ln$ | logarithmus naturalis |
| $m/z$ | mass-to-charge ratio |
| $^{n}J_{AB}$ | NMR coupling constant [Hz] |
| $pK_a$ | negative common logarithm of the acid dissociation constant |
| ppm | parts per million |
| $d$ | distance [Å] |
| $R$ | universal gas constant |
| $S$ | electron spin |
| $T$ | temperature [°C] or [K] |
| $\tilde{v}$ | wavenumber [cm$^{-1}$] |
| $\delta$ | chemical shift [ppm] |
| Δ | difference |
| $\lambda$ | wavelength [nm] |
| $\mu_B$ | Bohr magneton |
| $\sigma_P$ | (para) Hammett parameter |

# Computational Data Tables

**Table A1:** Computational data for chapter 5 (r²-SCAN-3c level of theory).

| Compound | E[H] | H [kJ mol⁻¹] | G [kJ mol⁻¹] | ΔH [kJ mol⁻¹] | ΔG [kJ mol⁻¹] |
|---|---|---|---|---|---|
| $H_2$ | -1.169382 | -3034.7 | -3073.5 | | |
| $CO_2$ | -188.570062 | -495050.7 | -495114.3 | | |
| $C_6H_6$ | -232.183143 | -609320.2 | -609401.8 | | |
| 5.3b (open) | -1645.595442 | -4319166.8 | -4319384.2 | 0.0 | 0.0 |
| 5.3b (closed) | -1645.589301 | -4319150.5 | -4319364.7 | 16.2 | 19.5 |
| 5.4b (open) | -3169.466860 | -8320794.6 | -8320986.6 | 0.0 | 0.0 |
| 5.4b (closed) | -3169.465662 | -8320791.3 | -8320980.3 | 3.3 | 6.3 |
| 5.4b-$H_2$ | -3170.678660 | -8323915.2 | -8324109.6 | -89.3 | -55.9 |
| 5.4b-$CO_2$ | -3358.03785 | -8815841.5 | -8816042.3 | 0.5 | 52.3 |
| 5.4b-$C_6H_6$ | -3401.699702 | -8930234.7 | -8930453.8 | -120.0 | -65.4 |
| 5.4b-$H_2$ (TS) | -3170.595795 | -8323722.1 | -8323911.9 | 103.9 | 141.8 |
| 5.4b-$C_6H_6$ (TS) | -3401.641990 | -8930097.5 | -8930312.0 | 14.0 | 70.1 |

**Table A2:** Computational data for chapter 5 (ωB97X-D3(BJ)/def2-TZVPP+SMD(CH₂Cl₂) single point energies).

| Compound | E[H] | ΔH [kJ mol⁻¹] | ΔG [kJ mol⁻¹] |
|---|---|---|---|
| $H_2$ | -1.172536 | | |
| $CO_2$ | -188.603746 | | |
| $C_6H_6$ | -232.272027 | | |
| 5.3b (open) | -1646.097939 | 0.0 | 0.0 |
| 5.3b (closed) | -1646.094255 | 9.8 | 13.0 |
| 5.4b (open) | -3169.695822 | 0.0 | 0.0 |
| 5.4b (closed) | -3169.698914 | -8.0 | -4.9 |
| 5.4b-$H_2$ | -3170.91284 | -83.4 | -50.0 |
| 5.4b-$CO_2$ | -3358.31091 | -15.5 | 36.2 |
| 5.4b-$C_6H_6$ | -3402.00884 | -97.1 | -42.5 |
| 5.4b-$H_2$ (TS) | -3170.81423 | 151.1 | 189.0 |
| 5.4b-$C_6H_6$ (TS) | -3401.93743 | 84.1 | 140.2 |

# NMR Spectroscopy
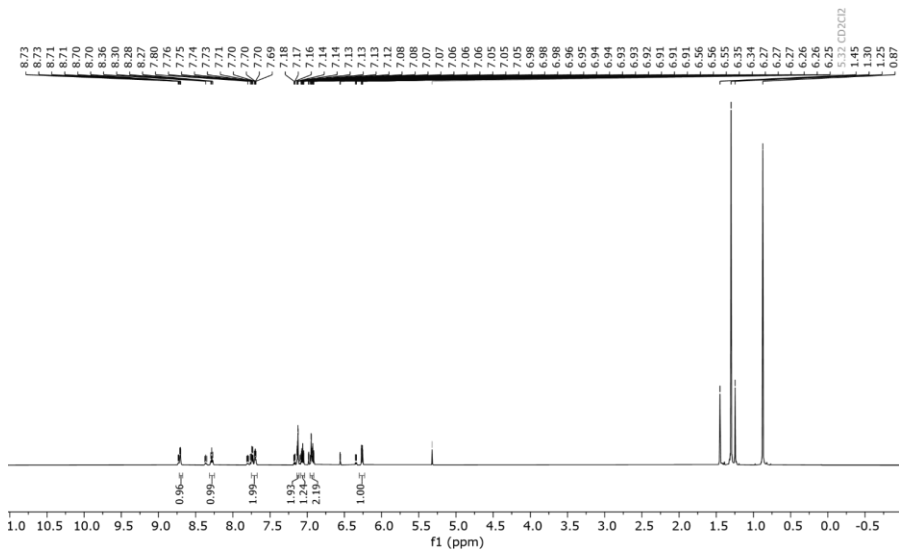


**Figure A 1:** $^{1}$H NMR (600 MHz, CD$_2$Cl$_2$) of 5.3a.
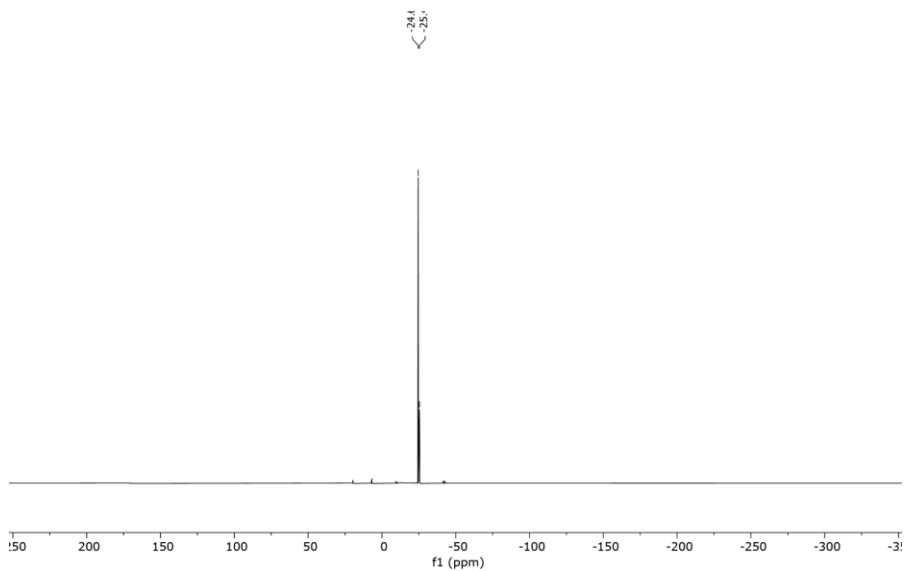


**Figure A 2:** $^{31}$P NMR (243 MHz, CD$_2$Cl$_2$) of 5.3a.
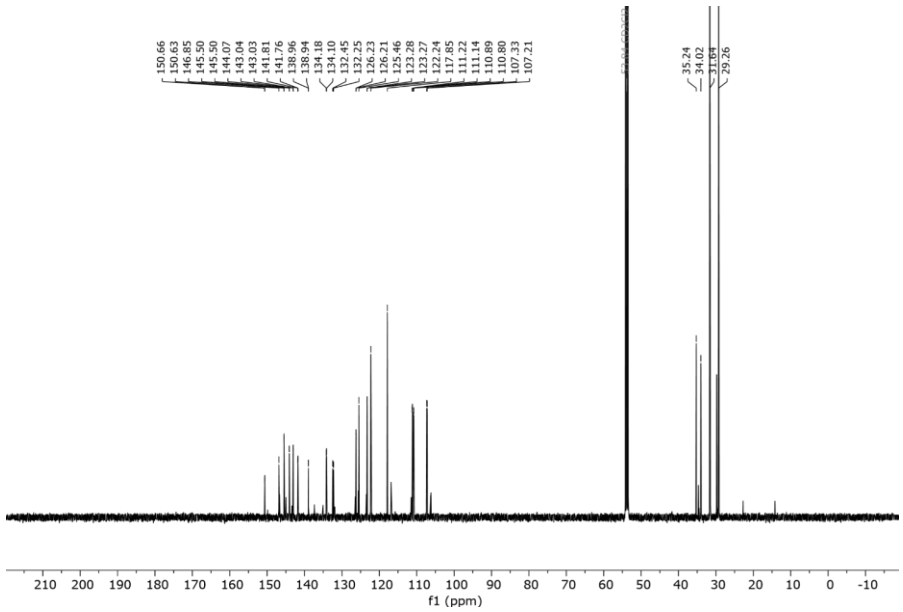
**Figure A 3:** $^{13}C$ NMR (151 MHz, $CD_2Cl_2$) of 5.3a.
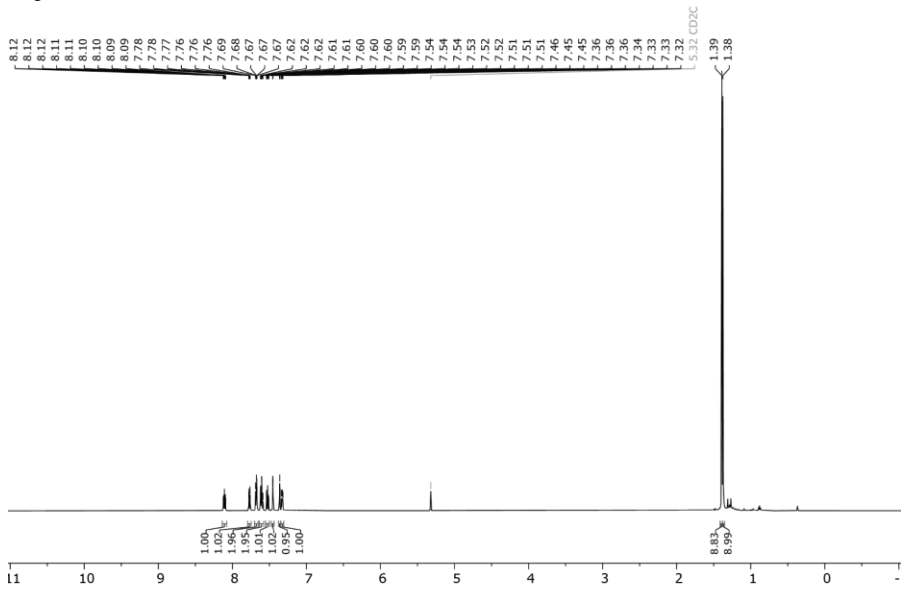


**Figure A 4:** $^1H$ NMR (600 MHz, $CD_2Cl_2$) of 5.4a.
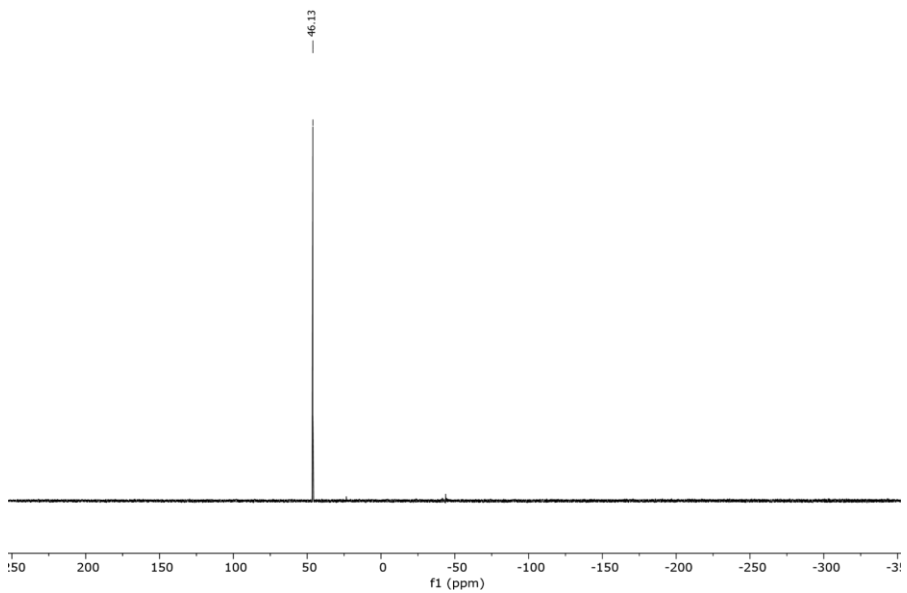
**Figure A 5:** $^{31}$P NMR (243 MHz, CD$_2$Cl$_2$) of 5.4a.
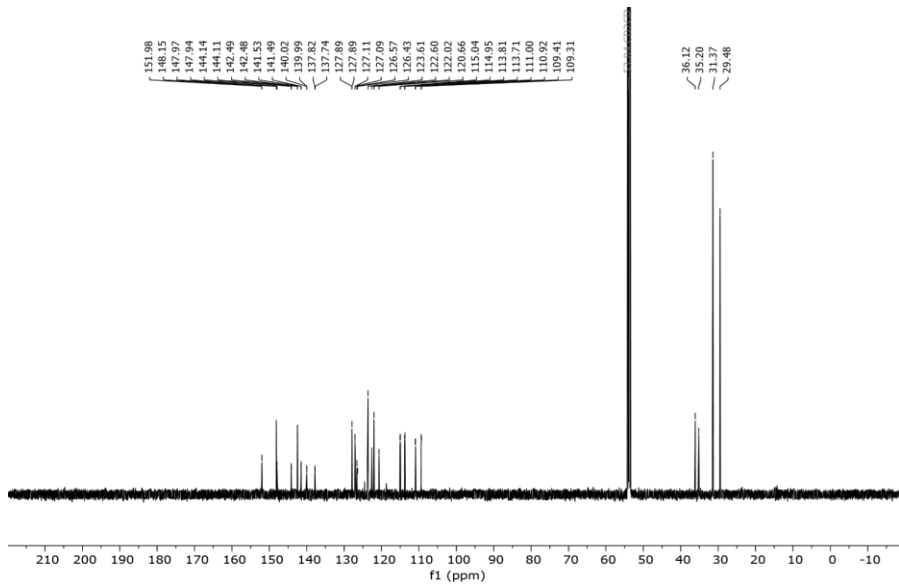


**Figure A 6:** $^{13}$C NMR (151 MHz, CD$_2$Cl$_2$) of 5.4a.
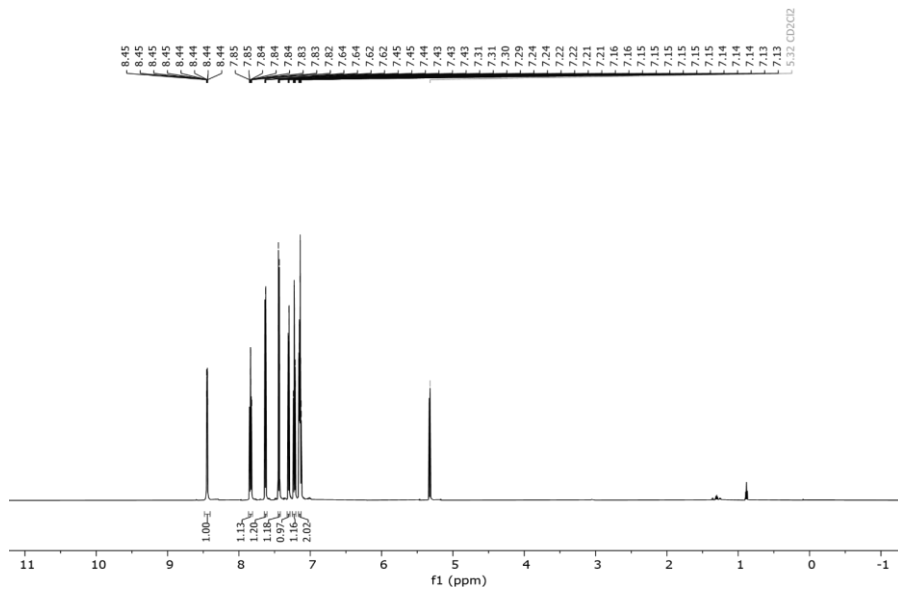
**Figure A 8:** $^1$H NMR (600 MHz, CD$_2$Cl$_2$) of 5.5.
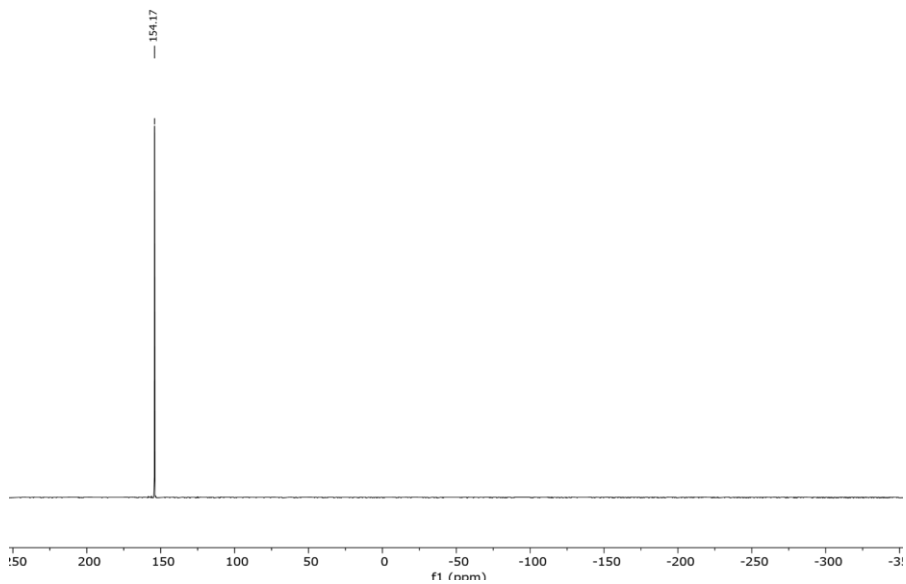


**Figure A 7:** $^{31}$P NMR (243 MHz, CD$_2$Cl$_2$) of 5.5.
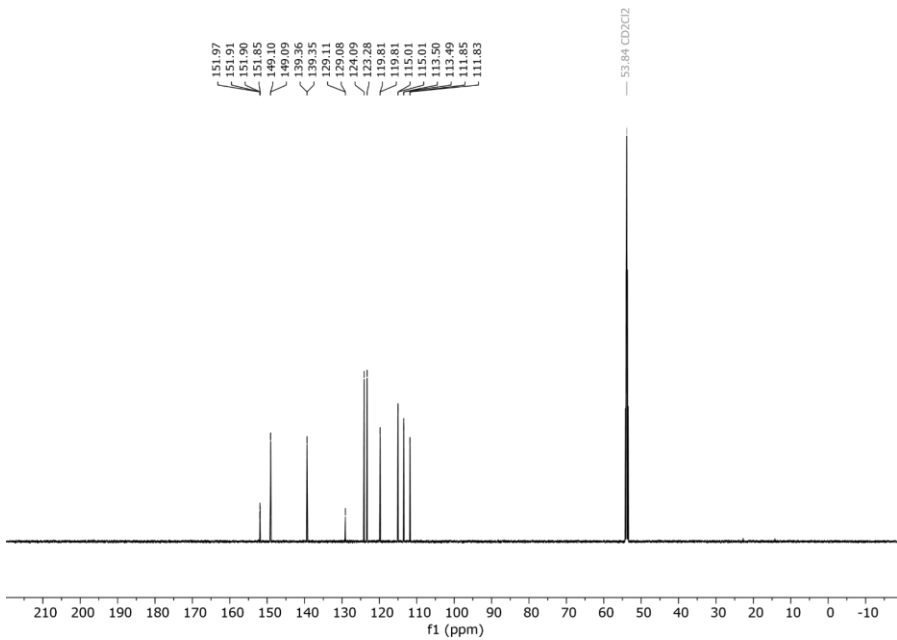
**Figure A 9:** $^{13}C$ NMR (151 MHz, CD$_2$Cl$_2$) of 5.5.

X

# Crystallographic Data

| Compound | [Et₄N]₂[2.1-Cl₂] | 2.1-(O₂SPh₂)₂ |
|---|---|---|
| Identification code | gr_dr2c | mo_drna70c_0m |
| CCDC number | 2015938 | n/a |
| Empirical formula | C28 H40 Cl10 Ge N2 O4 | $C_{36}H_{20}Cl_8GeO_8S_2$ |
| Formula weight | 895.71 | 1000.83 |
| Temperature [K] | 250 | 100.0 |
| Crystal system | orthorhombic | triclinic |
| Space group | $Pca2_1$ | $P\overline{1}$ |
| $a$ [Å] | 14.79859(8) | 9.7165(12) |
| $b$ [Å] | 10.67273(9) | 9.9403(12) |
| $c$ [Å] | 23.43687(11) | 10.0974(12) |
| α [°] | 90 | 69.791(5) |
| β [°] | 90 | 87.830(5) |
| γ [°] | 90 | 88.784(6) |
| Volume [Å³] | 3701.65(4) | 914.53(19) |
| $Z$ | 4 | 1 |
| $\rho_{calc}$ [g·cm³] | 1.607 | 1.817 |
| $\mu$ [mm⁻¹] | 8.072 | 1.591 |
| $F$(000) | 1824 | 500.0 |
| Crystal size [mm³] | 0.12 × 0.05 × 0.02 | 0.083 × 0.063 × 0.054 |
| Radiation | Cu-$K_\alpha$ (λ = 1.54184 Å) | Mo-$K_\alpha$ (λ = 0.71073 Å) |
| 2θ range [°] | 3.8 to 71.0 | 4.3 to 55.028 |
| Index ranges | −18 ≤ h ≤ 18, −12 ≤ k ≤ 12, −28 ≤ l ≤ 28 | -12 ≤ h ≤ 12, -12 ≤ k ≤ 12, -13 ≤ l ≤ 13 |
| Reflections collected | 131980 | 14383 |
| Independent reflections | 7030, $R_{int}$ = 0.0508 | 4061, $R_{int}$ = 0.0717 |
| Compl. to θ = 25.242° | 100.0 % | 100.0 % |
| Data/Restraints/Parameters | 7030/1/414 | 4061/0/250 |
| Goodness-of-fit on $F^2$ | 1.069 | 1.048 |
| Final $R$ indexes [$I{\geq}2\sigma(I)$] | $R_1$ = 0.0382, w$R_2$ = 0.0931 | $R_1$ = 0.0501, w$R_2$ = 0.1080 |
| Final $R$ indexes [all data] | $R_1$ = 0.0429, w$R_2$ = 0.0958 | $R_1$ = 0.0809, w$R_2$ = 0.1210 |
| Largest peak/hole [e·Å⁻³] | 1.571/−0.402 | 0.76/−0.99 |

| Compound | [K@18-c-6][2.1-F] | [K@18-c-6][H₂O-2.1-F] |
|---|---|---|
| Identification code | dr158a | rm451 |
| CCDC number | 2015936 | 2015937 |
| Empirical formula | $C_{24}H_{24}Cl_8FGeKO_{10}$ | $C_{24}H_{26}Cl_8FGeKO_{11}$ |
| Formula weight | 886.72 | 904.74 |
| Temperature [K] | 100.0 | 100.0 |
| Crystal system | monoclinic | monoclinic |
| Space group | $Pc$ | $Pc$ |
| $a$ [Å] | 9.7184(7) | 9.7518(10) |
| $b$ [Å] | 15.9776(12) | 15.8621(15) |
| $c$ [Å] | 10.9063(8) | 10.8766(11) |
| α [°] | 90 | 90 |
| β [°] | 106.512(3) | 104.845(4) |
| γ [°] | 90 | 90 |
| Volume [Å³] | 1623.7(2) | 1626.3(3) |
| $Z$ | 2 | 2 |
| $\rho_{calc}$ [g·cm³] | 1.814 | 1.848 |
| $\mu$ [mm⁻¹] | 1.789 | 1.790 |
| $F$(000) | 888 | 908 |
| Crystal size [mm³] | 0.399 x 0.317 x 0.156 | 0.1 x 0.1 x 0.1 |
| Radiation | Mo-$K_\alpha$ (λ = 0.71073 Å) | Mo-$K_\alpha$ (λ = 0.71073 Å) |
| 2θ range [°] | 2.186 to 30.070 | 2.161 to 30.543°. |
| Index ranges | -13<=h<=13, -22<=k<=22, -15<=l<=14 | -13<=h<=13, -22<=k<=22, -15<=l<=15 |
| Reflections collected | 37081 | 61517 |
| Independent reflections | 8998, R(int) = 0.0672 | 9917, R(int) = 0.0462 |
| Compl. to θ = 25.242° | 100.0 % | 99.9 % |
| Data/Restraints/Parameters | 8998 / 2 / 407 | 9917 / 2 / 419 |
| Goodness-of-fit on $F^2$ | 1.033 | 1.077 |
| Final $R$ indexes [$I{\geq}2\sigma(I)$] | $R_1$ = 0.0453, w$R_2$ = 0.0975 | $R_1$ = 0.0357, w$R_2$ = 0.0701 |
| Final $R$ indexes [all data] | $R_1$ = 0.0734, w$R_2$ = 0.1118 | $R_1$ = 0.0533, w$R_2$ = 0.0779 |
| Largest peak/hole [e·Å⁻³] | 0.876/ -0.951 | 1.060/ -0.825 |
| Flack parameter | 0.312(12) | 0.285(9) |

| Compound | 3.3a | 3.3e |
|---|---|---|
| Identification code | mo_dr368_0m | mo_dr477f_0m_a |
| CCDC number | 2099891 | n/a |
| Empirical formula | $C_{36}H_8BF_{20}O_4P$ | $C_{68}H_{16}Al_2Cl_8F_{72}O_{16}P_2$ |
| Formula weight | 1353.64 | 2856.31 |
| Temperature [K] | 100(2) | 100(2) |
| Crystal system | triclinic | triclinic |
| Space group | $P\overline{1}$ | $P\overline{1}$ |
| $a$ [Å] | 8.5919(5) | 10.951(6) |
| $b$ [Å] | 12.4187(7) | 12.916(7) |
| $c$ [Å] | 18.6688(12) | 34.610(19) |
| $\alpha$ [°] | 93.997(2) | 89.378(18) |
| $\beta$ [°] | 93.040(2) | 89.88(2) |
| $\gamma$ [°] | 91.973(2) | 72.722(16) |
| Volume [Å³] | 1982.9(2) | 4674(4) |
| $Z$ | 2 | 2 |
| $\rho_{calc}$ [g·cm³] | 1.551 | 2.030 |
| $\mu$ [mm⁻¹] | 0.201 | 0.502 |
| $F(000)$ | 912.0 | 2784 |
| Crystal size [mm³] | 0.124 × 0.089 × 0.077 | 0.32×0.24×0.22 |
| Radiation | Mo-$K_\alpha$ ($\lambda$ = 0.71073 Å) | Mo-$K_\alpha$ ($\lambda$ = 0.71073 Å) |
| 2θ range [°] | 4.382 to 59.144 | 3.90 to 54.36 (0.78 Å) |
| Index ranges | -11 ≤ h ≤ 11, -17 ≤ k ≤ 17, -25 ≤ l ≤ 25 | −14 ≤ h ≤ 14, −16 ≤ k ≤ 16, −44 ≤ l ≤ 44 |
| Reflections collected | 106343 | 194237 |
| Independent reflections | 11039, $R_{int}$ = 0.0975, $R_{sigma}$ = 0.0492 | 20687, $R_{int}$ = 0.0796, $R_{sigma}$ = 0.0402 |
| Compl. to θ = 25.242° | 100.0 % | 99.9 % |
| Data/Restraints/Parameters | 11039/0/559 | 20687/12856/2114 |
| Goodness-of-fit on $F^2$ | 1.069 | 1.185 |
| Final $R$ indexes [$I \geq 2\sigma(I)$] | $R_1$ = 0.0428, w$R_2$ = 0.1050 | $R_1$ = 0.0900, w$R_2$ = 0.1940 |
| Final $R$ indexes [all data] | $R_1$ = 0.0718, w$R_2$ = 0.1158 | $R_1$ = 0.0965, w$R_2$ = 0.1973 |
| Largest peak/hole [e·Å⁻³] | 0.28/-0.41 | 1.10/-0.67 |
| Flack parameter | n/a | n/a |

| Compound | HP(cat$^{Cl}$)$_2$ | [3.7b-PdCl$_2$]$_2$ |
|---|---|---|
| Identification code | mo_drna73_0m | Mo_dr598a_3_0m_1 |
| CCDC number | 2099890 | 2206700 |
| Empirical formula | C$_{12}$HCl$_8$O$_4$P | C$_{36}$H$_{46}$Cl$_4$O$_8$P$_2$Pd$_2$Si$_2$ |
| Formula weight | 523.70 | 1079.45 |
| Temperature [K] | 293(2) | 104(2) |
| Crystal system | triclinic | monoclinic |
| Space group | $P\bar{1}$ | $P2_1/n$ |
| $a$ [Å] | 7.737(5) | 9.8140(7) |
| $b$ [Å] | 8.566(7) | 19.9800(13) |
| $c$ [Å] | 14.54(2) | 12.1868(7) |
| α [°] | 73.27(6) | 90 |
| β [°] | 81.78(4) | 111.601(2) |
| γ [°] | 64.59(2) | 90 |
| Volume [Å$^3$] | 833.4(15) | 2221.8(3) |
| $Z$ | 2 | 2 |
| $\rho_{calc}$ [g·cm$^3$] | 2.087 | 1.614 |
| $\mu$ [mm$^{-1}$] | 1.465 | 1.222 |
| $F$(000) | 512 | 1088 |
| Crystal size [mm$^3$] | 0.211×0.112×0.057 | 0.289×0.117×0.103 |
| Radiation | Mo-$K_\alpha$ (λ = 0.71073 Å) | Mo-$K_\alpha$ (λ = 0.71073 Å) |
| 2θ range [°] | 5.44 to 55.03 (0.77 Å) | 4.08 to 61.24 (0.70 Å) |
| Index ranges | -9 ≤ h ≤ 10, -11 ≤ k ≤ 11, -18 ≤ l ≤ 18 | -14 ≤ h ≤ 14, -28 ≤ k ≤ 28, -17 ≤ l ≤ 17 |
| Reflections collected | 18624 | 110367 |
| Independent reflections | 3798, $R_{int}$ = 0.0762, $R_{sigma}$ = 0.0547 | 6814, $R_{int}$ = 0.0649, $R_{sigma}$ = 0.0233 |
| Compl. to θ = 25.242° | 100.0 % | 100.0 % |
| Data/Restraints/Parameters | 3798/0/229 | 6814/376/385 |
| Goodness-of-fit on $F^2$ | 1.019 | 1.064 |
| Final $R$ indexes [$I$≥2σ($I$)] | $R_1$ = 0.0400, w$R_2$ = 0.0830 | $R_1$ = 0.0335, w$R_2$ = 0.0769 |
| Final $R$ indexes [all data] | $R_1$ = 0.0643, w$R_2$ = 0.0925 | $R_1$ = 0.0416, w$R_2$ = 0.0824 |
| Largest peak/hole [e·Å$^{-3}$] | 0.66/-0.46 | 1.18/-0.59 |

| Compound | 3.9b | 3.12 |
| --- | --- | --- |
| Identification code | mo_dr497c_0m_a | mo_dr489f_0m_a |
| CCDC number | 2099892 | 2099893 |
| Empirical formula | $C_9H_5ClN_{0.25}OP_{0.25}$ | $C_{202}H_{100}Al_4Cl_4F_{144}N_4O_{48}P_8$ |
| Formula weight | 175.82 | 6584.33 |
| Temperature [K] | 100(2) | 293(2) |
| Crystal system | monoclinic | triclinic |
| Space group | $P2_1$ (4) | $P\bar{1}$ |
| $a$ [Å] | 10.632(3) | 15.906(9) |
| $b$ [Å] | 9.771(2) | 23.618(17) |
| $c$ [Å] | 15.487(5) | 35.75(2) |
| $\alpha$ [°] | 90 | 104.89(3) |
| $\beta$ [°] | 106.361(11) | 95.911(12) |
| $\gamma$ [°] | 90 | 109.016(14) |
| Volume [Å$^3$] | 1543.7(7) | 12013(13) |
| $Z$ | 8 | 2 |
| $\rho_{calc}$ [g·cm$^3$] | 1.513 | 1.820 |
| $\mu$ [mm$^{-1}$] | 0.479 | 0.305 |
| $F$(000) | 716 | 6520 |
| Crystal size [mm$^3$] | 0.494×0.070×0.055 | 0.377×0.218×0.187 |
| Radiation | Mo-$K_\alpha$ ($\lambda$ = 0.71073 Å) | Mo-$K_\alpha$ ($\lambda$ = 0.71073 Å) |
| 2Θ range [°] | 3.99 to 54.16 (0.78 Å) | 3.85 to 52.92 (0.80 Å) |
| Index ranges | -13 ≤ h ≤ 13, -12 ≤ k ≤ 12, -19 ≤ l ≤ 19 | -26 ≤ h ≤ 26, -16 ≤ k ≤ 16, -31 ≤ l ≤ 31 |
| Reflections collected | 52037 | 277081 |
| Independent reflections | 6790, $R_{int}$ = 0.0985, $R_{sigma}$ = 0.0416 | 13898, $R_{int}$ = 0.0657, $R_{sigma}$ = 0.0218 |
| Compl. to Θ = 25.242° | 100.0 % | 99.9 % |
| Data/Restraints/Parameters | 6790/1/415 | 13898/0/982 |
| Goodness-of-fit on $F^2$ | 0.992 | 1.010 |
| Final $R$ indexes [$I \geq 2\sigma(I)$] | $R_1$ = 0.0291, w$R_2$ = 0.0704 | $R_1$ = 0.0377, w$R_2$ = 0.0945 |
| Final $R$ indexes [all data] | $R_1$ = 0.0361, w$R_2$ = 0.0723 | $R_1$ = 0.0493, w$R_2$ = 0.1022 |
| Largest peak/hole [e·Å$^{-3}$] | 0.33/-0.29 | 0.44/-0.48 |
| Flack X parameter | 0.033(16) | n/a |

| Compound | 3.16 | 3.3a-PPh₃ |
|---|---|---|
| Identification code | mo_dr648a_0ma | mo_dr574c_om_sq |
| CCDC number | n/a | n/a |
| Empirical formula | $C_{85.50}H_{27}B_2Cl_9F_{40}N_0NaO_4PSi$ | $C_{3.83}H_{1.92}Al_{0.08}F_{2.96}O_{0.71}P_{0.17}$ |
| Formula weight | 2300.79 | 122.92 |
| Temperature [K] | 100(2) | 100(2) |
| Crystal system | monoclinic | triclinic |
| Space group | $C2/c$ | $P1$ |
| $a$ [Å] | 15.1056(13) | 15.1356(13) |
| $b$ [Å] | 40.252(3) | 15.4663(12) |
| $c$ [Å] | 28.762(2) | 15.8762(13) |
| α [°] | 90 | 61.645(3) |
| β [°] | 90.675(3) | 61.615(3) |
| γ [°] | 90 | 63.414(3) |
| Volume [Å³] | 17487(3) | 2756.8(4) |
| $Z$ | 8 | 24 |
| $\rho_{calc}$ [g·cm³] | 1.748 | 1.777 |
| $\mu$ [mm⁻¹] | 0.464 | 0.268 |
| $F$(000) | 9080 | 1459 |
| Crystal size [mm³] | 0.265×0.100×0.081 | 0.567×0.455×0.434 |
| Radiation | Mo-$K_\alpha$ (λ = 0.71073 Å) | Mo-$K_\alpha$ (λ = 0.71073 Å) |
| 2θ range [°] | 4.02 to 51.37 (0.82 Å) | 5.07 to 59.15 (0.72 Å) |
| Index ranges | −18 ≤ h ≤ 18, −49 ≤ k ≤ 49, −35 ≤ l ≤ 35 | −21 ≤ h ≤ 21, −21 ≤ k ≤ 21, −22 ≤ l ≤ 22 |
| Reflections collected | 164501 | 121821 |
| Independent reflections | 16603, $R_{int}$ = 0.0576, $R_{sigma}$ = 0.0323 | 30134. $R_{int}$ = 0.0645, $R_{sigma}$ = 0.0515 |
| Compl. to θ = 25.242° | 100.0 % | 99.8 % |
| Data/Restraints/Parameters | 16603/130/1353 | 30134/3/1675 |
| Goodness-of-fit on $F^2$ | 1.024 | 1.047 |
| Final $R$ indexes [$I \geq 2\sigma(I)$] | $R_1$ = 0.0570, w$R_2$ = 0.1497 | $R_1$ = 0.0449, w$R_2$ = 0.1175 |
| Final $R$ indexes [all data] | $R_1$ = 0.0846, w$R_2$ = 0.1708 | $R_1$ = 0.0592, w$R_2$ = 0.1280 |
| Largest peak/hole [e·Å⁻³] | 1.32/-0.64 | 0.94/-0.67 |
| Flack X parameter | n/a | 0.41(7) |

| Compound | 4.2c | 4.3a |
|---|---|---|
| Identification code | mo_dr515_0m | mo_drcd16_0m |
| CCDC number | 2206701 | 2206707 |
| Empirical formula | $C_{24}ClF_{18}N_2O_2P$ | $C_{40}H_{18}AlF_{36}N_2O_6P$ |
| Formula weight | 756.68 | 1364.51 |
| Temperature [K] | 100(2) | 100(2) |
| Crystal system | monoclinic | monoclinic |
| Space group | $P2_1/c$ | $P2_1/c$ |
| $a$ [Å] | 17.9471(18) | 11.634(4) |
| $b$ [Å] | 6.4105(7) | 20.645(4) |
| $c$ [Å] | 21.698(2) | 20.732(4) |
| $\alpha$ [°] | 90 | 90 |
| $\beta$ [°] | 96.796(4) | 101.364(10) |
| $\gamma$ [°] | 90 | 90 |
| Volume [Å$^3$] | 2478.8(4) | 4882(2) |
| $Z$ | 4 | 4 |
| $\rho_{calc}$ [g·cm$^3$] | 2.028 | 1.857 |
| $\mu$ [mm$^{-1}$] | 0.387 | 0.262 |
| $F$(000) | 1472 | 2688 |
| Crystal size [mm$^3$] | 0.292×0.129×0.039 | 0.325×0.265×0.243 |
| Radiation | Mo-$K_\alpha$ ($\lambda$ = 0.71073 Å) | Mo-$K_\alpha$ ($\lambda$ = 0.71073 Å) |
| 2Θ range [°] | 4.18 to 52.74 (0.80 Å) | 3.95 to 68.50 (0.63 Å) |
| Index ranges | -22 ≤ h ≤ 22, -8 ≤ k ≤ 8, -27 ≤ l ≤ 27 | -18 ≤ h ≤ 18, -32 ≤ k ≤ 31, -32 ≤ l ≤ 31 |
| Reflections collected | 64048 | 294176 |
| Independent reflections | 5045, $R_{int}$ = 0.0571, $R_{sigma}$ = 0.0266 | 20106, $R_{int}$ = 0.1126, $R_{sigma}$ = 0.0495 |
| Compl. to Θ = 25.242° | 100.0 % | 100.0 % |
| Data/Restraints/Parameters | 5045/0/433 | 20106/2850/775 |
| Goodness-of-fit on $F^2$ | 1.185 | 1.113 |
| Final $R$ indexes [$I \geq 2\sigma(I)$] | $R_1$ = 0.0530, w$R_2$ = 0.1119 | $R_1$ = 0.0537, w$R_2$ = 0.1266 |
| Final $R$ indexes [all data] | $R_1$ = 0.0606, w$R_2$ = 0.1148 | $R_1$ = 0.0888, w$R_2$ = 0.1400 |
| Largest peak/hole [e·Å$^{-3}$] | 0.43/-0.52 | 0.89/-0.62 |
| Flack X parameter | n/a | n/a |

| Compound | 4.3b | 4.3c |
|---|---|---|
| Identification code | mo_drcd19b_0m_a | mo_dr527_0m_a |
| CCDC number | 2206705 | 2206709 |
| Empirical formula | $C_{40}H_8AlF_{46}N_2O_6P$ | $C_{48}BF_{38}N_2O_2P$ |
| Formula weight | 1544.43 | 1400.28 |
| Temperature [K] | 100.00 | 100(2) |
| Crystal system | monoclinic | tetragonal |
| Space group | $P2_1/n$ | $P\bar{4}$ |
| $a$ [Å] | 14.469(3) | 16.953(3) |
| $b$ [Å] | 18.071(3) | 16.953 |
| $c$ [Å] | 20.513(3) | 7.9194(10) |
| $\alpha$ [°] | 90 | 90 |
| $\beta$ [°] | 106.200(7) | 90 |
| $\gamma$ [°] | 90 | 90 |
| Volume [Å$^3$] | 5150.3(16) | 2276.1(7) |
| $Z$ | 4 | 2 |
| $\rho_{calc}$ [g·cm$^3$] | 1.992 | 2.043 |
| $\mu$ [mm$^{-1}$] | 0.288 | 0.266 |
| $F(000)$ | 3008 | 1360 |
| Crystal size [mm$^3$] | 0.432×0.341×0.271 | 0.387×0.352×0.232 |
| Radiation | Mo-$K_\alpha$ ($\lambda$ = 0.71073 Å) | Mo-$K_\alpha$ ($\lambda$ = 0.71073 Å) |
| 2θ range [°] | 4.03 to 54.18 (0.78 Å) | 4.81 to 54.22 (0.78 Å) |
| Index ranges | -18 ≤ h ≤ 18, -23 ≤ k ≤ 23, -26 ≤ l ≤ 26 | -21 ≤ h ≤ 21, -21 ≤ k ≤ 21, -10 ≤ l ≤ 10 |
| Reflections collected | 238891 | 145653 |
| Independent reflections | 11309, $R_{int}$ = 0.0697, $R_{sigma}$ = 0.0178 | 5013, $R_{int}$ = 0.0570, $R_{sigma}$ = 0.0161 |
| Compl. to θ = 25.242° | 99.9 % | 99.9 % |
| Data/Restraints/Parameters | 11309/0/865 | 5013/0/415 |
| Goodness-of-fit on $F^2$ | 1.147 | 1.111 |
| Final $R$ indexes [$I \geq 2\sigma(I)$] | $R_1$ = 0.0613, w$R_2$ = 0.1559 | $R_1$ = 0.0223, w$R_2$ = 0.0595 |
| Final $R$ indexes [all data] | $R_1$ = 0.0659, w$R_2$ = 0.1584 | $R_1$ = 0.0225, w$R_2$ = 0.0596 |
| Largest peak/hole [e·Å$^{-3}$] | 1.05/-0.44 | 0.23/-0.24 |
| Flack X parameter | n/a | 0.00(2) |

| Compound | 4.4 | 4.5 |
|---|---|---|
| Identification code | mo_dr549_0m_a | mo_drXYZ_0m |
| CCDC number | 2206704 | 2206706 |
| Empirical formula | $C_{24}HB_0F_{18}N_2O_2PSi_0$ | $C_{252}H_{48}B_4Cl_8F_{152}N_8O_8P_4$ |
| Formula weight | 722.24 | 6653.70 |
| Temperature [K] | 104(2) | 100(2) |
| Crystal system | monoclinic | monoclinic |
| Space group | $C2/c$ | $P2_1/n$ |
| $a$ [Å] | 11.4379(7) | 20.9380(12) |
| $b$ [Å] | 9.7012(6) | 13.2369(8) |
| $c$ [Å] | 21.2154(13) | 24.8836(15) |
| $\alpha$ [°] | 90 | 90 |
| $\beta$ [°] | 105.117(2) | 102.075(2) |
| $\gamma$ [°] | 90 | 90 |
| Volume [Å³] | 2272.6(2) | 6744.0(7) |
| $Z$ | 4 | 1 |
| $\rho_{calc}$ [g·cm³] | 2.111 | 1.638 |
| $\mu$ [mm⁻¹] | 0.302 | 0.271 |
| $F$(000) | 1408 | 3264 |
| Crystal size [mm³] | 0.401×0.297×0.122 | 0.146×0.096×0.057 |
| Radiation | Mo-$K_\alpha$ ($\lambda$ = 0.71073 Å) | Mo-$K_\alpha$ ($\lambda$ = 0.71073 Å) |
| 2Θ range [°] | 3.98 to 61.22 (0.70 Å) | 3.85 to 52.92 (0.80 Å) |
| Index ranges | −16 ≤ h ≤ 16, −13 ≤ k ≤ 13, −30 ≤ l ≤ 30 | -26 ≤ h ≤ 26, -16 ≤ k ≤ 16, -31 ≤ l ≤ 31 |
| Reflections collected | 83074 | 277081 |
| Independent reflections | 3507, $R_{int}$ = 0.0625, $R_{sigma}$ = 0.0212 | 13898, $R_{int}$ = 0.0657, $R_{sigma}$ = 0.0218 |
| Compl. to ϴ = 25.242° | 100.0 % | 99.9 % |
| Data/Restraints/Parameters | 3507/0/214 | 13898/0/982 |
| Goodness-of-fit on $F^2$ | 1.114 | 1.010 |
| Final $R$ indexes [$I \geq 2\sigma(I)$] | $R_1$ = 0.0369, w$R_2$ = 0.0949 | $R_1$ = 0.0377, w$R_2$ = 0.0945 |
| Final $R$ indexes [all data] | $R_1$ = 0.0384, w$R_2$ = 0.0961 | $R_1$ = 0.0493, w$R_2$ = 0.1022 |
| Largest peak/hole [e·Å⁻³] | 1.31/-0.45 | 0.44/-0.48 |
| Flack X parameter | n/a | n/a |

| Compound | 4.7 | 4.12 |
|---|---|---|
| Identification code | mo_dr583_0ma | mo_dr618b_2_0m_a |
| CCDC number | 2206710 | 2206708 |
| Empirical formula | $C_{32}H_5B_0F_{18}N_2O_2P$ | $C_{224}H_{24}F_{144}N_{16}O_{16}P_8S_8$ |
| Formula weight | 822.35 | 6434.83 |
| Temperature [K] | 100(2) | 105(2) |
| Crystal system | orthorhombic | orthorhombic |
| Space group | $Pca2_1$ | $Pbca$ |
| $a$ [Å] | 20.4427(9) | 20.4603(16) |
| $b$ [Å] | 15.8379(8) | 12.7893(9) |
| $c$ [Å] | 8.9722(5) | 21.0733(15) |
| α [°] | 90 | 90 |
| β [°] | 90 | 90 |
| γ [°] | 90 | 90 |
| Volume [Å$^3$] | 2904.9(3) | 5514.3(7) |
| $Z$ | 4 | 1 |
| $\rho_{calc}$ [g·cm$^3$] | 1.880 | 1.938 |
| $\mu$ [mm$^{-1}$] | 0.250 | 0.333 |
| $F$(000) | 1616 | 3152 |
| Crystal size [mm$^3$] | 0.343×0.205×0.102 | 0.321×0.267×0.245 |
| Radiation | Mo-$K_\alpha$ (λ = 0.71073 Å) | Mo-$K_\alpha$ (λ = 0.71073 Å) |
| 2θ range [°] | 3.98 to 56.84 (0.75 Å) | 3.87 to 61.09 (0.70 Å) |
| Index ranges | -27 ≤ h ≤ 27, -21 ≤ k ≤ 21, -11 ≤ l ≤ 11 | -29 ≤ h ≤ 29, -17 ≤ k ≤ 17, -28 ≤ l ≤ 28 |
| Reflections collected | 160608 | 369949 |
| Independent reflections | 7244, $R_{int}$ = 0.0657, $R_{sigma}$ = 0.0193 | 7797, $R_{int}$ = 0.0546, $R_{sigma}$ = 0.0140 |
| Compl. to θ = 25.242° | 99.9 % | 99.9 % |
| Data/Restraints/Parameters | 7244/1/496 | 7797/183/509 |
| Goodness-of-fit on $F^2$ | 1.129 | 1.131 |
| Final $R$ indexes [$I \geq 2\sigma(I)$] | $R_1$ = 0.0303, w$R_2$ = 0.0726 | $R_1$ = 0.0523, w$R_2$ = 0.1347 |
| Final $R$ indexes [all data] | $R_1$ = 0.0324, w$R_2$ = 0.0745 | $R_1$ = 0.0540, w$R_2$ = 0.1359 |
| Largest peak/hole [e·Å$^{-3}$] | 0.29/-0.22 | 1.07/-0.36 |
| Flack X parameter | 0.01(3) | n/a |

| Compound | 4.15 | 4.2b |
|---|---|---|
| Identification code | mo_dr520_0m | mo_drcd14_0m |
| CCDC number | 2206702 | 2206704 |
| Empirical formula | $C_{188}H_{72}Al_4F_{184}N_8O_{24}P_4$ | $C_{24}H_8ClF_{10}N_2O_2P$ |
| Formula weight | 6554.33 | 612.74 |
| Temperature [K] | 100(2) | 100(2) |
| Crystal system | monoclinic | monoclinic |
| Space group | $P2_1/n$ | $P2_1/c$ |
| $a$ [Å] | 18.8343(10) | 9.0960(5) |
| $b$ [Å] | 16.6911(9) | 24.5912(13) |
| $c$ [Å] | 19.5959(12) | 10.8962(6) |
| $\alpha$ [°] | 90 | 90 |
| $\beta$ [°] | 114.833(2) | 111.556(2) |
| $\gamma$ [°] | 90 | 90 |
| Volume [Å$^3$] | 5590.7(6) | 2266.8(2) |
| $Z$ | 1 | 4 |
| $\rho_{calc}$ [g·cm$^3$] | 1.947 | 1.795 |
| $\mu$ [mm$^{-1}$] | 0.271 | 0.351 |
| $F(000)$ | 3216 | 1216 |
| Crystal size [mm$^3$] | 0.269×0.201×0.080 | 0.317×0.295×0.276 |
| Radiation | Mo-$K_\alpha$ ($\lambda$ = 0.71073 Å) | Mo-$K_\alpha$ ($\lambda$ = 0.71073 Å) |
| 2Θ range [°] | 3.94 to 51.55 (0.82 Å) | 4.35 to 55.09 (0.77 Å) |
| Index ranges | -23 ≤ h ≤ 23, -20 ≤ k ≤ 20, -23 ≤ l ≤ 23 | -11 ≤ h ≤ 11, -31 ≤ k ≤ 31, -14 ≤ l ≤ 14 |
| Reflections collected | 133775 | 179043 |
| Independent reflections | 10705, $R_{int}$ = 0.0520, $R_{sigma}$ = 0.0229 | 5218, $R_{int}$ = 0.0750, $R_{sigma}$ = 0.0195 |
| Compl. to θ = 25.242° | 100.0 % | 100.0 % |
| Data/Restraints/Parameters | 10705/22360/1948 | 5218/0/361 |
| Goodness-of-fit on $F^2$ | 1.517 | 1.038 |
| Final $R$ indexes [$I \geq 2\sigma(I)$] | $R_1$ = 0.0969, w$R_2$ = 0.3091 | $R_1$ = 0.0343, w$R_2$ = 0.0915 |
| Final $R$ indexes [all data] | $R_1$ = 0.1166, w$R_2$ = 0.3380 | $R_1$ = 0.0406, w$R_2$ = 0.0962 |
| Largest peak/hole [e·Å$^{-3}$] | 0.69/-0.79 | 0.49/-0.38 |
| Flack X parameter | n/a | n/a |

| Compound | 5.4a | 5.3b |
|---|---|---|
| Identification code | mo_dr522_0m_a | mo_dr533_0m_a |
| CCDC number | n/a | n/a |
| Empirical formula | $C_{34}H_{16}Cl_{10}N_4O_6P_2$ | $C_{41}H_{28}AlF_{36}N_2O_7P$ |
| Formula weight | 992.95 | 1402.60 |
| Temperature [K] | 100(2) | 100(2) |
| Crystal system | triclinic | monoclinic |
| Space group | $P\overline{1}$ | $Pc$ |
| $a$ [Å] | 9.3433(7) | 10.2531(5) |
| $b$ [Å] | 12.0911(10) | 11.3200(6) |
| $c$ [Å] | 18.3264(14) | 23.3472(11) |
| $\alpha$ [°] | 100.589(3) | 90 |
| $\beta$ [°] | 98.939(3) | 102.255(2) |
| $\gamma$ [°] | 106.061(3) | 90 |
| Volume [Å³] | 1908.5(3) | 2648.0(2) |
| $Z$ | 2 | 2 |
| $\rho_{calc}$ [g·cm³] | 1.728 | 1.759 |
| $\mu$ [mm⁻¹] | 0.867 | 0.245 |
| $F(000)$ | 992 | 1392 |
| Crystal size [mm³] | 0.275×0.246×0.141 | 0.391×0.363×0.332 |
| Radiation | Mo-$K_\alpha$ (λ = 0.71073 Å) | Mo-$K_\alpha$ (λ = 0.71073 Å) |
| 2Θ range [°] | 3.61 to 54.31 (0.78 Å) | 5.07 to 56.00 (0.76 Å) |
| Index ranges | −11 ≤ h ≤ 11, −15 ≤ k ≤ 15, −23 ≤ l ≤ 23 | −13 ≤ h ≤ 13, −14 ≤ k ≤ 14, −30 ≤ l ≤ 30 |
| Reflections collected | 93840 | 191142 |
| Independent reflections | 8446, $R_{int}$ = 0.0541, $R_{sigma}$ = 0.0230 | 12747, $R_{int}$ = 0.0482, $R_{sigma}$ = 0.0188 |
| Compl. to Θ = 25.242° | 100.0 % | 99.8 % |
| Data/Restraints/Parameters | 8446/0/505 | 12747/10534/1356 |
| Goodness-of-fit on $F^2$ | 1.072 | 1.032 |
| Final $R$ indexes [$I \geq 2\sigma(I)$] | $R_1$ = 0.0332, w$R_2$ = 0.0828 | $R_1$ = 0.0476, w$R_2$ = 0.1329 |
| Final $R$ indexes [all data] | $R_1$ = 0.0369, w$R_2$ = 0.0857 | $R_1$ = 0.0496, w$R_2$ = 0.1359 |
| Largest peak/hole [e·Å⁻³] | 0.49/-0.51 | 0.46/-0.38 |
| Flack X parameter | n/a | 0.026(14) |

| Compound | 5.4b | 5.5 |
|---|---|---|
| Identification code | mo_dr525_0m_a | mo_dr514_0m_a |
| CCDC number | n/a | n/a |
| Empirical formula | $C_{34}H_{10}AlCl_6F_{36}N_2O_7P$ | $C_{11}H_8ClN_2OP$ |
| Formula weight | 1513.09 | 250.61 |
| Temperature [K] | 100(2) | 100(2) |
| Crystal system | triclinic | monoclinic |
| Space group | $P\overline{1}$ | $P2_1/c$ |
| $a$ [Å] | 11.751(3) | 10.0482(19) |
| $b$ [Å] | 13.736(4) | 12.957(2) |
| $c$ [Å] | 16.187(7) | 8.592(3) |
| $\alpha$ [°] | 94.030(18) | 90 |
| $\beta$ [°] | 93.812(15) | 104.401(10) |
| $\gamma$ [°] | 104.565(11) | 90 |
| Volume [Å$^3$] | 2513.0(15) | 1083.5(4) |
| $Z$ | 2 | 4 |
| $\rho_{calc}$ [g·cm$^3$] | 2.000 | 1.536 |
| $\mu$ [mm$^{-1}$] | 0.575 | 0.477 |
| $F$(000) | 1476 | 512 |
| Crystal size [mm$^3$] | 0.347×0.321×0.298 | 0.464×0.262×0.203 |
| Radiation | Mo-$K_\alpha$ ($\lambda$ = 0.71073 Å) | Mo-$K_\alpha$ ($\lambda$ = 0.71073 Å) |
| 2Θ range [°] | 4.09 to 54.43 (0.78 Å) | 4.19 to 55.02 (0.77 Å) |
| Index ranges | $-15 \leq h \leq 15$, $-17 \leq k \leq 17$, $-20 \leq l \leq 20$ | $-13 \leq h \leq 13$, $-16 \leq k \leq 16$, $-11 \leq l \leq 11$ |
| Reflections collected | 113180 | 71240 |
| Independent reflections | 11113, $R_{int}$ = 0.0568, $R_{sigma}$ = 0.0275 | 2488, $R_{int}$ = 0.0409, $R_{sigma}$ = 0.0115 |
| Compl. to θ = 25.242° | 99.9 % | 100.0 % |
| Data/Restraints/Parameters | 11113/4384/1027 | 2488/0/145 |
| Goodness-of-fit on $F^2$ | 1.023 | 1.105 |
| Final $R$ indexes [$I \geq 2\sigma(I)$] | $R_1$ = 0.0449, w$R_2$ = 0.1166 | $R_1$ = 0.0284, w$R_2$ = 0.0797 |
| Final $R$ indexes [all data] | $R_1$ = 0.0530, w$R_2$ = 0.1233 | $R_1$ = 0.0305, w$R_2$ = 0.0809 |
| Largest peak/hole [e·Å$^{-3}$] | 0.80/-0.35 | 0.32/-0.31 |
| Flack X parameter | n/a | n/a |

| Compound | 5.4b | 5.5 |
|---|---|---|
| Identification code | mo_dr525_0m_a | mo_dr514_0m_a |
| CCDC number | n/a | n/a |
| Empirical formula | $C_{34}H_{10}AlCl_6F_{36}N_2O_7P$ | $C_{11}H_8ClN_2OP$ |
| Formula weight | 1513.09 | 250.61 |
| Temperature [K] | 100(2) | 100(2) |
| Crystal system | triclinic | monoclinic |
| Space group | $P\overline{1}$ | $P2_1/c$ |
| $a$ [Å] | 11.751(3) | 10.0482(19) |
| $b$ [Å] | 13.736(4) | 12.957(2) |
| $c$ [Å] | 16.187(7) | 8.592(3) |
| $\alpha$ [°] | 94.030(18) | 90 |
| $\beta$ [°] | 93.812(15) | 104.401(10) |
| $\gamma$ [°] | 104.565(11) | 90 |
| Volume [Å³] | 2513.0(15) | 1083.5(4) |
| $Z$ | 2 | 4 |
| $\rho_{calc}$ [g·cm³] | 2.000 | 1.536 |
| $\mu$ [mm⁻¹] | 0.575 | 0.477 |
| $F(000)$ | 1476 | 512 |
| Crystal size [mm³] | 0.347×0.321×0.298 | 0.464×0.262×0.203 |
| Radiation | Mo-$K_\alpha$ ($\lambda$ = 0.71073 Å) | Mo-$K_\alpha$ ($\lambda$ = 0.71073 Å) |
| 2θ range [°] | 4.09 to 54.43 (0.78 Å) | 4.19 to 55.02 (0.77 Å) |
| Index ranges | $-15 \leq h \leq 15, -17 \leq k \leq 17,$ $-20 \leq l \leq 20$ | $-13 \leq h \leq 13, -16 \leq k \leq 16,$ $-11 \leq l \leq 11$ |
| Reflections collected | 113180 | 71240 |
| Independent reflections | 11113, $R_{int}$ = 0.0568, $R_{sigma}$ = 0.0275 | 2488, $R_{int}$ = 0.0409, $R_{sigma}$ = 0.0115 |
| Compl. to θ = 25.242° | 99.9 % | 100.0 % |
| Data/Restraints/Parameters | 11113/4384/1027 | 2488/0/145 |
| Goodness-of-fit on $F^2$ | 1.023 | 1.105 |
| Final $R$ indexes [$I \geq 2\sigma(I)$] | $R_1$ = 0.0449, w$R_2$ = 0.1166 | $R_1$ = 0.0284, w$R_2$ = 0.0797 |
| Final $R$ indexes [all data] | $R_1$ = 0.0530, w$R_2$ = 0.1233 | $R_1$ = 0.0305, w$R_2$ = 0.0809 |
| Largest peak/hole [e·Å⁻³] | 0.80/-0.35 | 0.32/-0.31 |
| Flack X parameter | n/a | n/a |

| Compound | 5.10 | 5.4a-$O_2C_6Cl_4$ |
|---|---|---|
| Identification code | mo_dr604_0m | mo_dr528_0m_a_sq |
| CCDC number | n/a | n/a |
| Empirical formula | $C_{50}H_{36}AlCl_2F_{36}N_2O_7P$ | $C_{23}H_8Cl_9N_2O_5P$ |
| Formula weight | 1589.66 | 742.33 |
| Temperature [K] | 100(2) | 100(2) |
| Crystal system | triclinic | monoclinic |
| Space group | $P\bar{1}$ | $P2_1/c$ |
| $a$ [Å] | 18.4258(18) | 13.479(7) |
| $b$ [Å] | 19.4339(19) | 14.115(7) |
| $c$ [Å] | 20.124(2) | 17.962(9) |
| $\alpha$ [°] | 63.484(4) | 90 |
| $\beta$ [°] | 87.054(4) | 109.31(2) |
| $\gamma$ [°] | 70.742(4) | 90 |
| Volume [Å$^3$] | 6047.9(11) | 3225(3) |
| $Z$ | 4 | 4 |
| $\rho_{calc}$ [g·cm$^3$] | 1.746 | 1.529 |
| $\mu$ [mm$^{-1}$] | 0.312 | 0.866 |
| $F(000)$ | 3168 | 1472 |
| Crystal size [mm$^3$] | 0.353×0.169×0.093 | 0.201×0.180×0.141 |
| Radiation | Mo-$K_\alpha$ ($\lambda$ = 0.71073 Å) | Mo-$K_\alpha$ ($\lambda$ = 0.71073 Å) |
| 2Θ range [°] | 3.98 to 53.46 (0.79 Å) | 4.31 to 52.84 (0.80 Å) |
| Index ranges | $-23 \leq h \leq 23$, $-24 \leq k \leq 24$, $-25 \leq l \leq 25$ | $-16 \leq h \leq 16$, $-17 \leq k \leq 17$, $-22 \leq l \leq 22$ |
| Reflections collected | 325164 | 157455 |
| Independent reflections | 25685, $R_{int}$ = 0.0698, $R_{sigma}$ = 0.0336 | 6594, $R_{int}$ = 0.0535, $R_{sigma}$ = 0.0167 |
| Compl. to ϴ = 25.242° | 100.0 % | 100.0 % |
| Data/Restraints/Parameters | 25685/6141/2176 | 6594/0/361 |
| Goodness-of-fit on $F^2$ | 1.030 | 1.081 |
| Final $R$ indexes [$I \geq 2\sigma(I)$] | $R_1$ = 0.0657, w$R_2$ = 0.1795 | $R_1$ = 0.0467, w$R_2$ = 0.1174 |
| Final $R$ indexes [all data] | $R_1$ = 0.0913, w$R_2$ = 0.2004 | $R_1$ = 0.0524, w$R_2$ = 0.1223 |
| Largest peak/hole [e·Å$^{-3}$] | 1.03/-0.97 | 0.94/-0.82 |
| Flack X parameter | n/a | n/a |

| Compound | 5.13 |
| --- | --- |
| Identification code | mo_dr635_0m_a |
| CCDC number | n/a |
| Empirical formula | $C_{43}H_{34}AlAuClF_{36}N_2O_7PS$ |
| Formula weight | 1697.15 |
| Temperature [K] | 105(2) |
| Crystal system | monoclinic |
| Space group | $P2_1/c$ |
| $a$ [Å] | 12.6053(10) |
| $b$ [Å] | 28.802(2) |
| $c$ [Å] | 15.7850(13) |
| $\alpha$ [°] | 90 |
| $\beta$ [°] | 91.694(3) |
| $\gamma$ [°] | 90 |
| Volume [Å$^3$] | 5728.4(8) |
| $Z$ | 4 |
| $\rho_{calc}$ [g·cm$^3$] | 1.968 |
| $\mu$ [mm$^{-1}$] | 2.862 |
| $F(000)$ | 3304 |
| Crystal size [mm$^3$] | 0.715×0.254×0.188 |
| Radiation | Mo-$K_\alpha$ ($\lambda$ = 0.71073 Å) |
| 2Θ range [°] | 3.83 to 56.77 (0.75 Å) |
| Index ranges | $-16 \leq h \leq 16$, $-38 \leq k \leq 38$, $-21 \leq l \leq 21$ |
| Reflections collected | 310277 |
| Independent reflections | 14307, $R_{int}$ = 0.0721, $R_{sigma}$ = 0.0243 |
| Compl. to $\theta$ = 25.242° | 99.9 % |
| Data/Restraints/Parameters | 14307/6171/1221 |
| Goodness-of-fit on $F^2$ | 1.209 |
| Final $R$ indexes [$I \geq 2\sigma(I)$] | $R_1$ = 0.0563, w$R_2$ = 0.1429 |
| Final $R$ indexes [all data] | $R_1$ = 0.0614, w$R_2$ = 0.1455 |
| Largest peak/hole [e·Å$^{-3}$] | 1.92/-1.80 |
| Flack X parameter | n/a |

| Compound | 6.1b | 6.2b |
|---|---|---|
| Identification code | | |
| CCDC number | 2286220 | 2286219 |
| Empirical formula | $C_4H_{3.33}Cl_{0.33}N_{0.67}O_{0.33}P_{0.33}$ | $C_6H_{4.50}Br_{0.50}Cl_{0.50}NO_{0.50}P_{0.50}$ |
| Formula weight | 88.21 | 171.77 |
| Temperature [K] | 107(2) | 100(2) |
| Crystal system | triclinic | triclinic |
| Space group | $P\bar{1}$ | $P\bar{1}$ |
| $a$ [Å] | 6.6299(13) | 7.3725(6) |
| $b$ [Å] | 8.7021(18) | 8.2385(6) |
| $c$ [Å] | 10.980(2) | 11.9756(10) |
| $\alpha$ [°] | 84.671(8) | 88.692(3) |
| $\beta$ [°] | 76.550(8) | 72.181(4) |
| $\gamma$ [°] | 68.754(7) | 65.925(3) |
| Volume [Å³] | 574.2(2) | 627.88(9) |
| $Z$ | 6 | 4 |
| $\rho_{calc}$ [g·cm³] | 1.531 | 1.817 |
| $\mu$ [mm⁻¹] | 0.454 | 3.600 |
| $F$(000) | 272 | 340 |
| Crystal size [mm³] | 0.360×0.209×0.209 | 0.418×0.250×0.077 |
| Radiation | Mo-$K_\alpha$ ($\lambda$ = 0.71073 Å) | Mo-$K_\alpha$ ($\lambda$ = 0.71073 Å) |
| 2Θ range [°] | 5.02 to 57.75 (0.74 Å) | 5.45 to 59.52 (0.72 Å) |
| Index ranges | $-8 \leq h \leq 8$, $-11 \leq k \leq 11$, $-14 \leq l \leq 14$ | $-9 \leq h \leq 10$, $-11 \leq k \leq 11$, $0 \leq l \leq 16$ |
| Reflections collected | 29152 | 3563 |
| Independent reflections | 2985, $R_{int}$ = 0.0527, $R_{sigma}$ = 0.0290 | 3563, $R_{int}$ = 0.0799, $R_{sigma}$ = 0.0390 |
| Compl. to Θ = 25.242° | 99.8 % | 100.0 % |
| Data/Restraints/Parameters | 2985/0/154 | 3563/0/163 |
| Goodness-of-fit on $F^2$ | 1.102 | 1.169 |
| Final $R$ indexes [$I \geq 2\sigma(I)$] | $R_1$ = 0.0449, w$R_2$ = 0.1164 | $R_1$ = 0.0747, w$R_2$ = 0.2099 |
| Final $R$ indexes [all data] | $R_1$ = 0.0483, w$R_2$ = 0.1193 | $R_1$ = 0.0845, w$R_2$ = 0.2178 |
| Largest peak/hole [e·Å⁻³] | 0.81/-0.30 | 1.65/-1.43 |
| Flack X parameter | n/a | n/a |

| Compound | 6.3b | 6.4b |
|---|---|---|
| Identification code | | |
| CCDC number | 2286221 | 2286223 |
| Empirical formula | $C_4H_{2.67}ClN_{0.67}O_{0.33}P_{0.33}$ | $C_4H_{2.33}Br_{0.33}ClN_{0.67}O_{0.33}P_{0.33}$ |
| Formula weight | 111.17 | 137.48 |
| Temperature [K] | 100(2) | 100(2) |
| Crystal system | monoclinic | monoclinic |
| Space group | $P2_1/n$ | $P2_1/c$ |
| $a$ [Å] | 10.559(2) | 8.145(2) |
| $b$ [Å] | 10.1604(17) | 7.2314(18) |
| $c$ [Å] | 12.195(3) | 24.956(7) |
| $\alpha$ [°] | 90 | 90 |
| $\beta$ [°] | 96.641(9) | 95.630(11) |
| $\gamma$ [°] | 90 | 90 |
| Volume [Å$^3$] | 1299.6(4) | 1462.9(7) |
| $Z$ | 12 | 12 |
| $\rho_{calc}$ [g·cm$^3$] | 1.705 | 1.873 |
| $\mu$ [mm$^{-1}$] | 0.818 | 3.461 |
| $F(000)$ | 672 | 808 |
| Crystal size [mm$^3$] | 0.607×0.102×0.098 | 0.359×0.156×0.142 |
| Radiation | Mo-$K_\alpha$ ($\lambda$ = 0.71073 Å) | Mo-$K_\alpha$ ($\lambda$ = 0.71073 Å) |
| 2θ range [°] | 4.83 to 55.97 (0.76 Å) | 5.03 to 56.99 (0.74 Å) |
| Index ranges | $-13 \le h \le 13$, $-13 \le k \le 13$, $-16 \le l \le 16$ | $-10 \le h \le 10$, $-9 \le k \le 9$, $-33 \le l \le 33$ |
| Reflections collected | 57956 | 32927 |
| Independent reflections | 3104, $R_{int}$ = 0.0767, $R_{sigma}$ = 0.0334 | 3675, $R_{int}$ = 0.0847, $R_{sigma}$ = 0.0470 |
| Compl. to θ = 25.242° | 99.7 % | 99.8 % |
| Data/Restraints/Parameters | 3104/0/172 | 3675/0/181 |
| Goodness-of-fit on $F^2$ | 1.083 | 1.235 |
| Final $R$ indexes [$I \ge 2\sigma(I)$] | $R_1$ = 0.0373, w$R_2$ = 0.1005 | $R_1$ = 0.0643, w$R_2$ = 0.1443 |
| Final $R$ indexes [all data] | $R_1$ = 0.0408, w$R_2$ = 0.1045 | $R_1$ = 0.0699, w$R_2$ = 0.1463 |
| Largest peak/hole [e·Å$^{-3}$] | 0.49/-0.64 | 1.04/-0.90 |
| Flack X parameter | n/a | n/a |

| Compound | 6.4c | [6.2c]•[H][C₄H₃S] |
|---|---|---|
| Identification code | | |
| CCDC number | 2286222 | 2286225 |
| Empirical formula | $C_{4.67}H_{1.17}Al_{0.17}Br_{0.17}Cl_{0.33}F_6N_{0.33}O_{0.83}P_{0.17}$ | $C_{40}H_{13}BBrCl_0F_{20}N_2OPS$ |
| Formula weight | 224.02 | 1071.27 |
| Temperature [K] | 170(2) | 109(2) |
| Crystal system | triclinic | monoclinic |
| Space group | $P\bar{1}$ | $P2_1/n$ |
| $a$ [Å] | 10.721(2) | 13.721(3) |
| $b$ [Å] | 10.9535(18) | 12.602(4) |
| $c$ [Å] | 18.322(3) | 26.097(7) |
| α [°] | 83.352(7) | 90 |
| β [°] | 83.003(8) | 101.811(10) |
| γ [°] | 82.547(7) | 90 |
| Volume [Å³] | 2106.7(7) | 4417(2) |
| $Z$ | 12 | 4 |
| $\rho_{calc}$ [g·cm³] | 2.119 | 1.611 |
| $\mu$ [mm⁻¹] | 1.365 | 1.134 |
| $F$(000) | 1300 | 2104 |
| Crystal size [mm³] | 0.495×0.318×0.144 | 0.264×0.229×0.140 |
| Radiation | Mo-$K_\alpha$ (λ = 0.71073 Å) | Mo-$K_\alpha$ (λ = 0.71073 Å) |
| 2θ range [°] | 3.77 to 54.52 (0.78 Å) | 4.43 to 56.03 (0.76 Å) |
| Index ranges | −13 ≤ h ≤ 13, −14 ≤ k ≤ 14, −23 ≤ l ≤ 23 | −18 ≤ h ≤ 18, −16 ≤ k ≤ 16, −34 ≤ l ≤ 34 |
| Reflections collected | 85673 | 173466 |
| Independent reflections | 9370, $R_{int}$ = 0.0572, $R_{sigma}$ = 0.0345 | 10568, $R_{int}$ = 0.0651, $R_{sigma}$ = 0.0306 |
| Compl. to θ = 25.242° | 99.9 % | 99.9 % |
| Data/Restraints/Parameters | 9370/10348/1193 | 10568/0/607 |
| Goodness-of-fit on $F^2$ | 1.059 | 1.021 |
| Final $R$ indexes [$I$ ≥2σ($I$)] | $R_1$ = 0.0462, w$R_2$ = 0.1191 | $R_1$ = 0.0351, w$R_2$ = 0.1010 |
| Final $R$ indexes [all data] | $R_1$ = 0.0558, w$R_2$ = 0.1272 | $R_1$ = 0.0387, w$R_2$ = 0.1038 |
| Largest peak/hole [e·Å⁻³] | 0.79/-0.50 | 0.76/-0.62 |
| Flack X parameter | n/a | n/a |

| Compound | [6.3c]•[H][C₆H₄Cl] | [6.4c]•[H][Ph] |
|---|---|---|
| Identification code | | |
| CCDC number | 2286224 | 2286226 |
| Empirical formula | $C_{42}H_{12.76}BCl_3F_{20}N_2OP$ | $C_{6.29}H_{2.43}B_{0.14}Br_{0.14}Cl_{0.86}F_{2.86}$ $N_{0.29}O_{0.14}P_{0.14}$ |
| Formula weight | 1089.40 | 186.28 |
| Temperature [K] | 100(2) | 100(2) |
| Crystal system | monoclinic | triclinic |
| Space group | $P2_1/n$ | $P\overline{1}$ |
| $a$ [Å] | 8.008(2) | 10.788(5) |
| $b$ [Å] | 37.037(12) | 11.793(5) |
| $c$ [Å] | 13.589(4) | 19.843(8) |
| α [°] | 90 | 104.334(16) |
| β [°] | 94.474(10) | 105.131(17) |
| γ [°] | 90 | 93.651(17) |
| Volume [Å³] | 4018(2) | 2338.7(17) |
| $Z$ | 4 | 14 |
| $\rho_{calc}$ [g·cm³] | 1.801 | 1.852 |
| $\mu$ [mm⁻¹] | 0.402 | 1.377 |
| $F(000)$ | 2151 | 1280 |
| Crystal size [mm³] | 0.312×0.185×0.095 | 0.368×0.260×0.194 |
| Radiation | Mo-$K_\alpha$ (λ = 0.71073 Å) | Mo-$K_\alpha$ (λ = 0.71073 Å) |
| 2θ range [°] | 4.40 to 55.93 (0.76 Å) | 3.67 to 56.56 (0.75 Å) |
| Index ranges | −10 ≤ h ≤ 10, −48 ≤ k ≤ 48, −17 ≤ l ≤ 17 | −14 ≤ h ≤ 14, −15 ≤ k ≤ 15, −26 ≤ l ≤ 26 |
| Reflections collected | 179022 | 169149 |
| Independent reflections | 9640, $R_{int}$ = 0.0596, $R_{sigma}$ = 0.0235 | 11592, $R_{int}$ = 0.0714, $R_{sigma}$ = 0.0392 |
| Compl. to θ = 25.242° | 99.9 % | 99.8 % |
| Data/Restraints/Parameters | 9640/649/764 | 11592/59/716 |
| Goodness-of-fit on $F^2$ | 1.106 | 1.076 |
| Final $R$ indexes [$I \geq 2\sigma(I)$] | $R_1$ = 0.0500, w$R_2$ = 0.1244 | $R_1$ = 0.0401, w$R_2$ = 0.1043 |
| Final $R$ indexes [all data] | $R_1$ = 0.0561, w$R_2$ = 0.1280 | $R_1$ = 0.0427, w$R_2$ = 0.1064 |
| Largest peak/hole [e·Å⁻³] | 0.95/-0.67 | 0.70/-0.79 |
| Flack X parameter | n/a | n/a |

# Danksagung

In diesem Abschnitt meiner Arbeit würde ich mich gerne bedanken und meine Wertschätzung zeigen für alle Menschen, die mich während meiner Promotionszeit unterstützt haben und auf verschiedensten Wegen zur Fertigstellung dieser Arbeit beigetragen haben.

Als erstes muss ich mich natürlich bei meinem Doktorvater, mittlerweile *Professor* Dr. Lutz Greb, bedanken für das ermöglichen meiner Doktorarbeit über ein faszinierendes Thema mit hervorragender Betreuung, guten Ratschlägen, aber auch wissenschaftlicher Freiheit eigenen Ideen nachzugehen. Danke für das immerwährende Interesse und die Begeisterung, die mir besonders Motivation gegeben haben. Dankbar bin ich auch für die Möglichkeit, dass ich einen Teil dieser Arbeit in den USA durchführen konnte.

Für die Übernahme des Koreferats möchte ich mich bei PD Dr. Joachim Ballmann bedanken.

Vielen Dank an meine Korrekturleser, Dr. Rezisha Maskey, Nils Ansmann, Christoph Bendel, Lukas Sigmund, Lennart Stoess und Paul Jansen, die das zum Teil relativ kurzfristig noch übernommen haben.

Für finanzielle Unterstützung in Form eines Kekulé-Stipendiums möchte ich mich beim Fonds der chemischen Industrie, und beim DAAD für ein Stipendium zur Unterstützung meines Auslandaufenthaltes bedanken.

Bei Prof. Dr. Dr. Hans-Jörg Himmel möchte ich mich bedanken für die Eingliederung der Arbeitsgruppe Greb in den eigenen Arbeitskreis während der ersten Jahre meiner Promotion und die gemeinsamen Arbeitskreisseminare.

Danke auch an alle aktuellen Mitglieder und Alumni des AK Himmels, die den Arbeitsalltag und die Zeit nach der Arbeit mit unzähligen Veranstaltungen sehr unterhaltsam gemacht haben und für eine großartige Arbeitsatmosphäre gesorgt haben.

Allen Mitgliedern der etwaigen analytischen Einrichtungen der chemischen Institute möchte ich für die Übernahme unzähliger Messungen mit großer Sorgfalt danken. Mein Dank gilt auch den anderen Mitarbeitern des Insituts, inklusive der Feinmechaniker (auch denen im Zentralbereich), Schlossern, Elektrikern, Glasbläsern und Reinigungskräften, die alles am laufen halten. Vielen Dank auch an Karin, Silke und Ute, die mich bei etlichen administrativen und bürokratischen Angelegenheiten unterstützt haben. Danke auch an Marion und Maik für die Unterstütung bei Problemen im Laboralltag.

Bei meinen Bachelor- und Forschungsstudenten Till Kalkuhl, Nils Ansmann, Clara Douglas und Linghua Zhang bedanke ich mich für die wissenschaftlichen Beiträge zu dieser Arbeit und hoffe, dass ihr während der Zeit Spaß hattet.

Insbesondere möchte ich mich bei allen Mitgliedern des AK Greb bedanken, die mich die letzten Jahre im Labor und außerhalb unterstützt und für viel Spaß gesorgt haben. Durch euch wurden alle AK-Unternehmungen (Edersee, AK-Wochenenden, Weihnachtsmarkt, Mittagspausen, Kaffeepausen, Skiseminare, etc.) zu einem großen Vergnügen.

Dazu gehören natürlich die Alumnis, Nina, Fabian, Debbie, Yael und Rezi, die besonders in den Anfängen meiner Zeit im AK Greb dafür gesorgt haben, dass die Chemie gestimmt hat (sowohl im Labor, als auch bei etlichen FABs und Unternehmungen).

Danke an die Originalmitglieder des Labor -1.06, Rezi und Lukas für einen lustigen Laboralltag mit guten Unterhaltungen und fragwürdiger Musikauswahl. Lukas, wir kennen uns schon seit Beginn des Studium und es hat immer Spaß gemacht mit dir, von Übungsblättern im ersten Semester bis zu den Diskussionen über die Doktorarbeit! Genau so danke an meinen anderen Mitstreiter Philipp, der es über Umwege doch in den AK Greb geschafft hat.

Heiko und Thaddäus, mit euch habe ich zusammen (quasi) die Promotion hier angefangen. Vielen Danke für unzählige Unterhaltungen, ob wissenschaftlich oder nicht, und Unternehmungen, ich hatte immer Spaß dabei.

Thank you to the Postdocs that have come and gone during my time in the group, Marcel, Ravi and Avijit, I have enjoyed talking and learning from you and wish all the

best for your future endeavors (i.e. as Prof. Schorpp, Prof. Yadav and maybe soon Prof. Maiti).

Danke natürlich auch an alle Neuankömmlinge und Jungdoktorand*innen Nils, Paul, Christoph, Lennart , Coco, Lijun, Valentin und Senta. Es hat mich gefreut mit euch zusammen arbeiten zu können, mal mehr, mal weniger hart. Danke an CB für die Idee mit der Dartscheibe, und meine etwaigen Gegenspieler, Paul, CB, TT, Lennart, Valentin und der Rest. Danke auch an die Masteranden Paul, Andreas und Arne, mein Laborkollege während meiner letzten Monate im Labor, viel Glück euch bei eurer (vielleicht) anstehenden Promotion und macht nicht zuviel Blödzinn.

Of course I also have to give my appreciation to all the people in the Rad lab, who made my time at MIT so enjoyable. So thank you to Alex (Prof. Radosevich) for welcoming me to his working group and guiding me during my time there. Thank you also to my office mates Shicheng, Quinton and Roberto, my fellow visiting student from Europe, Aisling, as well as the rest of the group, Myles, Siraj, Marissa, Soohyun, Gear, Nico, Ashton, Bora, Lilly and Philip. I have greatly enjoyed not only working together with and learning from you, but also our non-scientific talks and get-togethers at the Muddys after work.
Thank you also to the Annie, Steven, Dekai, Vincent, Janis, Leo and all the other visiting students at MIT for all the fun after-work and weekend activities, as well as enjoying all the free food together.

*Last but not least*, möchte ich mich bei meinen Eltern und meiner Familie für die bedingungslose Unterstützung während der Promotionszeit, aber auch über die Jahre hinweg bedanken.

# Eidesstattliche Versicherung

**GESAMTFAKULTÄT FÜR MATHEMATIK, INGENIEUR-
UND NATURWISSENSCHAFTEN**

**COMBINED FACULTY OF MATHEMATICS, ENGINEERING
AND NATURAL SCIENCES**

RUPRECHT-KARLS-
UNIVERSITÄT
HEIDELBERG

**Eidesstattliche Versicherung gemäß § 8 der Promotionsordnung für die Gesamtfakultät
für Mathematik, Ingenieur- und Naturwissenschaften der Universität Heidelberg /
Sworn Affidavit according to § 8 of the doctoral degree regulations of the Combined
Faculty of Mathematics, Engineering and Natural Sciences at Heidelberg University**

1. Bei der eingereichten Dissertation zu dem Thema / The thesis I have submitted entitled

   .....................................................................................................................

   .....................................................................................................................

   handelt es sich um meine eigenständig erbrachte Leistung / is my own work.

2. Ich habe nur die angegebenen Quellen und Hilfsmittel benutzt und mich keiner unzulässigen Hilfe
   Dritter bedient. Insbesondere habe ich wörtlich oder sinngemäß aus anderen Werken übernommene
   Inhalte als solche kenntlich gemacht. / I have only used the sources indicated and have not made
   unauthorised use of services of a third party. Where the work of others has been quoted or
   reproduced, the source is always given.

3. Die Arbeit oder Teile davon habe ich wie folgt/bislang nicht[1] an einer Hochschule des In- oder
   Auslands als Bestandteil einer Prüfungs- oder Qualifikationsleistung vorgelegt. / I have not yet/have
   already[1] presented this thesis or parts thereof to a university as part of an examination or degree.

   Titel der Arbeit / Title of the thesis: ...........................................................................

   Hochschule und Jahr / University and year: ...........................................................................

   Art der Prüfungs- oder Qualifikationsleistung / Type of examination or degree: ...........................

4. Die Richtigkeit der vorstehenden Erklärungen bestätige ich. / I confirm that the declarations made
   above are correct.

5. Die Bedeutung der eidesstattlichen Versicherung und die strafrechtlichen Folgen einer unrichtigen oder
   unvollständigen eidesstattlichen Versicherung sind mir bekannt. / I am aware of the importance of
   a sworn affidavit and the criminal prosecution in case of a false or incomplete affidavit.

Ich versichere an Eides statt, dass ich nach bestem Wissen die reine Wahrheit erklärt und nichts
verschwiegen habe. / I affirm that the above is the absolute truth to the best of my knowledge and that
I have not concealed anything.

.........................................................        .........................................................
Ort und Datum / Place and date                                   Unterschrift / Signature

[1] Nicht Zutreffendes streichen. Bei Bejahung sind anzugeben: der Titel der andernorts vorgelegten Arbeit, die
Hochschule, das Jahr der Vorlage und die Art der Prüfungs- oder Qualifikationsleistung. / Please cross out what is
not applicable. If applicable, please provide: the title of the thesis that was presented elsewhere, the name of the
university, the year of presentation and the type of examination or degree.

The German text is legally binding.

XXXV